INVESTIGATING THE RESPECTIVE ROLES OF SOX9 AND PAR1 IN PANCREATIC DUCTAL ADENOCARCINOMA INITIATION AND IMMUNE EVASION

by

Patrick G. Schweickert

A Dissertation

Submitted to the Faculty of Purdue University

In Partial Fulfillment of the Requirements for the degree of

Doctor of Philosophy

Department of Biological Sciences

West Lafayette, Indiana

May 2020

THE PURDUE UNIVERSITY GRADUATE SCHOOL
STATEMENT OF COMMITTEE APPROVAL

Dr. Andrea Kasinski, Chair

Department of Biological Sciences

Dr. Stephen Konieczny, Major Professor

Department of Biological Sciences

Dr. Claudio Aguilar

Department of Biological Sciences

Dr. James Fleet

Department of Nutrition Science

Approved by:

Dr. Janice Evans

Dedicated to my wife, family, and the late Bo Mach

ACKNOWLEDGMENTS

I would first like to thank my parents, Richard Schweickert and Carolyn Jagacinski, for being a constant source of support and guidance. When I tell people both of my parents are psychologists, they often give me a curious look and ask what type of psychoanalyses or mind tricks they used on me growing up. While I'm sure they leaned into their understanding of positive reinforcement and conditioning to help raise me, I always reply, "they're not really those kinds of psychologists." And while to this day I'm still not entirely sure what mathematical psychology really is (sorry Dad), I will say having two science-oriented parents undoubtedly helped shape my way of thinking and instilled in me a reflexive predisposition to view things logically and objectively. Our dinner conversations frequently revolved around the latest highlights and headlines in *Science Magazine* covering broad topics from space science and physics to biology and anthropology, which was a constant reminder of the vastness of our universe and the many curiosities it contains.

To my wife, Connie, I want to thank you for standing by my side through all of this. Obtaining my PhD was by no means easy and by nature the type of studies I undertook were frequently arduous and often unsuccessful. You put up with my absence during long weekends and late nights after which I frequently came home disheartened simply to say, "it didn't work". But through all of this you've stood by my side and given me the space, time, and encouragement I needed to get through it. I know it's been a longer road than we expected, and in the time it's taken me to finish my degree you've tried out multiple careers, gone back to school yourself, graduated, and found your niche. We've both grown a lot since this journey started and I'm excited to see where we go from here.

To the members of the Konieczny lab, Dan DiRenzo, Dave Hess, Anju Karki, Chunjing Qu, Brad Jakubison, and Yi Yang, you've been like a family. It's been great spending time with you in and outside of work. It's important to let off steam and have a group you can joke around with but also talk seriously about project pitfalls and difficulties. I especially want to thank Dan and Dave for teaching me some important techniques early on. I'd also be remised if I didn't acknowledge the infamous and lengthy game nights with Brad and Yi, I'm confident we'll find a way to make those happen again even though we'll be on opposite coasts.

Finally, of course, I owe multitudes to my advisor Dr. Stephen Konieczny. I'll never forget his first words to me when I showed up at his office looking for a position as a laboratory technician, "I'm not sure why I agreed to meet with you." This may sound a little harsh, but it's quite the opposite and reveals Steve's character perfectly. He wasn't looking for a technician, he hadn't posted an open position, but I had emailed him out of the blue having just finished my undergraduate studies but being unsure what to do next. Steve had a fully staffed lab at the time and really didn't need the extra help, but he hired me anyway seeing that I was looking for some added experience and needed a little more time to decide if I was ready to tackle graduate school. Looking back, I see his first words as a reflection of Steve's leadership and mentoring style. The lab didn't really need a technician, hence his initial statement. If he was purely focused on his lab's productivity, the money and resources needed to take on another lab member might've gone to something else. However, knowing Steve now it's hard to see the situation playing out any other way. He's a true mentor through and through and I don't think there's any scenario where he would leave a student rudderless. I've observed countless occasions where he's helped students find their way and the high number of undergraduate researchers that pass through our lab is just another indication of his priorities as a teacher. Even into my graduate career Steve always put mentorship first. Another perfect example of this was when I asked to take on an academic internship at Eli Lilly and Company. This was no small request, I was supposed to be nearing the end of my studies but had been working on a project that had no clear conclusion in sight, yet I was asking to step away for six months full-time. Many advisors would have baulked at my request, and to make matters worse, Steve had been planning to retire within the year, but if he agreed to let me leave it was unlikely that I'd finish my research and graduate within that timeline. But once again, Steve put his student's needs first, letting me take the internship opportunity and keeping his lab running even though he should've been relaxing in his well-earned retirement. On top of all of this, Steve's training is excellent. He teaches objectivity and independence, giving each student ownership of their project and allowing them to make critical decisions on what directions should be pursued. He's also a big proponent in following the data even when it leads in unexpected directions, something he himself did early on when he completely switched fields from muscle research to pancreatic development based on where his own discoveries took him. All in all, I've learned so much as a trainee in Steve's lab, not only scientifically, but also as a teacher and mentor, and I know these lessons will serve me well in any future endeavor.

TABLE OF CONTENTS

LIST OF TABLES

LIST OF FIGURES

LIST OF ABBREVIATIONS

ADM	Acinar-To-Ductal Metaplasia
AMY	Amylase
APC	Activated Protein C
APM	Antigen Processing Machinery
BCC	Basal Cell Carcinoma
CAR T	Chimeric Antigen Receptor T Cell
CCK	Cholecystokinin
CDCL	Clonally Derived Cell Line
ChIP	Chromatin Immunoprecipitation
CHO	Chinese Hamster Ovary
CRISPR	Clustered Regularly Interspaced Short Pallendromic Repeats
crRNA	Crispr RNA
CSC	Cancer Stem Cell
CTL	Cytotoxic T Lymphocyte
DAB	3,3'-Diaminobenzidine
DAPI	4',6-Diamidino-2-Phenylindole
DC	Dendritic Cell
DEG	Differentially Expressed Gene
DMBA	Dimethylbenzathracene
DOX	Doxycycline
DSB	Double-Strand Break
ECM	Extracellular Matrix
ELISA	Enzyme-Linked Immunosorbent Assay

EMT	Epithelial Mesenchymal Transition
FBS	Fetal Bovine Serum
FDA	Food and Drug Administration
FDR	False Discovery Rate
GEM	Genetically Engineered Mouse
GFP	Green Fluorescent Protein
GS	Glutamine Synthetase
GSEA	Gene Set Enrichment Analysis
GTP	Guanosine Triphosphate
HA	Hemagglutinin
HDR	Homology-Directed Repair
HMG	High Mobility Group
IDAA	Indel Detection by Amplicon Analysis
IDR	Irreproducible Discovery Rate
Indel	Insertions Or Deletions
IPMN	Intraductal Pancreatic Mucinous Neoplasm
KC	*LSL-Kras^{G12SD}; Mist1^{CreER}*
KO	Knockout
KPC	*LSL-Kras^{G12SD}; LSL-Trp53^{R172H} Mist1^{CreER}*
LC-MS/MS	Liquid Chromatography With Tandem Mass Spectrometry
LDH	Lactate Dehydrogenase
mAb	Monoclonal Antibody
MCN	Mucinous Cystic Neoplasm
MDA	Mutation Detection Assay
MDSC	Myeloid-Derived Suppressor Cell

MGI	Mouse Genome Informatics
MHC-I	Major Histocompatibility Class I
MMP1	Metalloprotease-1
MOI	Multiplicity Of Infection
NHEJ	Non-Homologues End-Joining
NSG	NOD SCID Gamma
PAM	Protospacer Adjacent Motif
PanIN	Pancreatic Intraepithelial Neoplasia
PAR1	Protease Activated Receptor 1
PBS	Phosphate Buffered Saline
PCR	Polymerase Chain Reaction
PDAC	Pancreatic Ductal Adeno Carcinoma
PGE2	Prostaglandin E_2
PIC	Protease Inhibitor Cocktail
QC	Quality Control
RiP	Reads Within Peaks
RNP	Ribonucleoprotein
RT-qPCR	Real Time-Quantitative Polymerase Chain Reaction
SOX9	SRY-Related High Mobility Group Box 9
SSD	Standardized Standard Deviation
TAM	Tumor-Associated Macrophages
TCR	T Cell Receptor
TF	Tissue Factor
TME	Tumor Microenvironment
Tregs	Regulatory T Cell

TSS	Transcription Start Site
VTE	Venous Thromboembolism
WT	Wild Type
ZFN	Zinc Finger Nuclease

ABSTRACT

Pancreatic ductal adenocarcinoma (PDAC) is a poorly immune responsive, treatment refractory disease, representing the fourth leading cause of cancer deaths in the United States. A lack of significant improvements in patient prognoses over the last few decades highlights the necessity for a more basic understanding of how PDAC develops and progresses. To this end, the research outlined here investigates the contributions of SOX9 and PAR1 in PDAC initiation and tumor immune evasion, respectively.

SOX9 is a developmental transcription factor important for proper pancreas development that is restricted to only a small subset of cells in the adult organ. However, SOX9 is aberrantly expressed in precancerous lesions of the pancreas and throughout PDAC development. Using genetically engineered mouse models we demonstrated that PDAC precursor lesions cannot form in the absence of SOX9 and conversely formed at an accelerated rate when SOX9 was ectopically expressed. Surprisingly deletion of SOX9 in primary mouse PDAC cell lines had no impact on tumor growth in subcutaneous allograft experiments, indicating that although SOX9 expression is necessary for PDAC initiation, it is dispensable in many cases for tumor maintenance and growth. Research investigating the transcriptional changes induced by SOX9 prior to lesion formation is ongoing to identify additional downstream factors critical for disease initiation.

Previous research has shown that PDAC tumors frequently display low levels of immune infiltration, which is a major limitation for the use of immune-based therapeutics and is generally an unfavorable prognostic factor. We show that in primary mouse tumor cells ablation of the thrombin receptor PAR1 caused a significant increase in the infiltration of tumor targeting $CD8a^{+}$ T cells which in turn were found to eliminate PAR1 knockout tumors. When $PAR1^{KO}$ and PAR1 expressing PDAC tumor cells were co-injected into wild type mice, cells lacking PAR1 were preferentially targeted and eliminated by the immune system, indicating that PAR1 provides cell autonomous protection during an active anti-tumor adaptive immune response. Furthermore, we identified a previously underappreciated association between PAR1-mediated expression of *Csf2* and *Ptgs2*, and PDAC tumor immune evasion. Together these findings provide novel insights into the mechanisms and drivers of PDAC initiation and immune evasion.

CHAPTER 1. INTRODUCTION

1.1 Anatomy and physiology of the pancreas

The pancreas is located behind the stomach and adjacent to the duodenum and serves dual functions as both an endocrine and exocrine organ. The endocrine cells of the pancreas form small clusters called islets of Langerhans (Figure 1.1), with each islet consisting of five endocrine cell types: glucagon-producing α-cells, insulin-producing β-cells, somatostatin-producing δ-cells, pancreatic polypeptide-producing γ-cells, and ε-cells that produce ghrelin, a protein that stimulates hunger (Da Silva Xavier, 2018). These cells function together to regulate blood glucose homeostasis through the release of their respective hormones. Insulin secretion leads to cellular absorption and storage of glucose, while glucagon conversely promotes gluconeogenesis and glycogenolysis. Somatostatin helps regulate both insulin and glucagon secretion to avoid excessive release of either hormone, and finally pancreatic polypeptide can inhibit glucagon release and functions as a satiety hormone (Abdulreda et al., 2016; Tan and Bloom, 2013). Of note, approximately 50% of the cells in a human islet are insulin-producing β-cells, and loss of these cells due to autoimmunity, or the development of resistance to their insulin signaling, can lead to hyperglycemia and diabetes mellitus (American Diabetes Association, 2010; Pan and Wright, 2011).

Despite their importance, islets only comprise a small portion of the pancreas while the majority of the tissue, 85% by mass, is made up of exocrine cells that function to synthesize, store, and secrete digestive enzymes that are released into the duodenum to aid in nutrient breakdown (Moini, 2019). In fact, the exocrine pancreas has the highest protein synthesis rate of any mammalian organ and secretes 1.5-2 L of digestive juices per day (Bhagavan et al., 2015; Pandol, 2010). This extreme level of protein output is accomplished by pancreatic acinar cells which possess a pronounced endoplasmic reticulum to help meet this demand (Kubisch and Logsdon, 2008). Acinar cells are polarized epithelial cells that group together to form acini (acinus, singular) consisting of 15-100 cells organized concentrically around a central lumen (Figure 1.1) (Paniccia and Schulick, 2017). To avoid self-proteolysis, many of the digestive proteins generated by acinar cells are inactive proenzymes packaged and stored in zymogen granules that localize at the acinar cell apical pole (Grady et al., 1998; Xuequn Chen, 2018). Following a meal, acinar cells

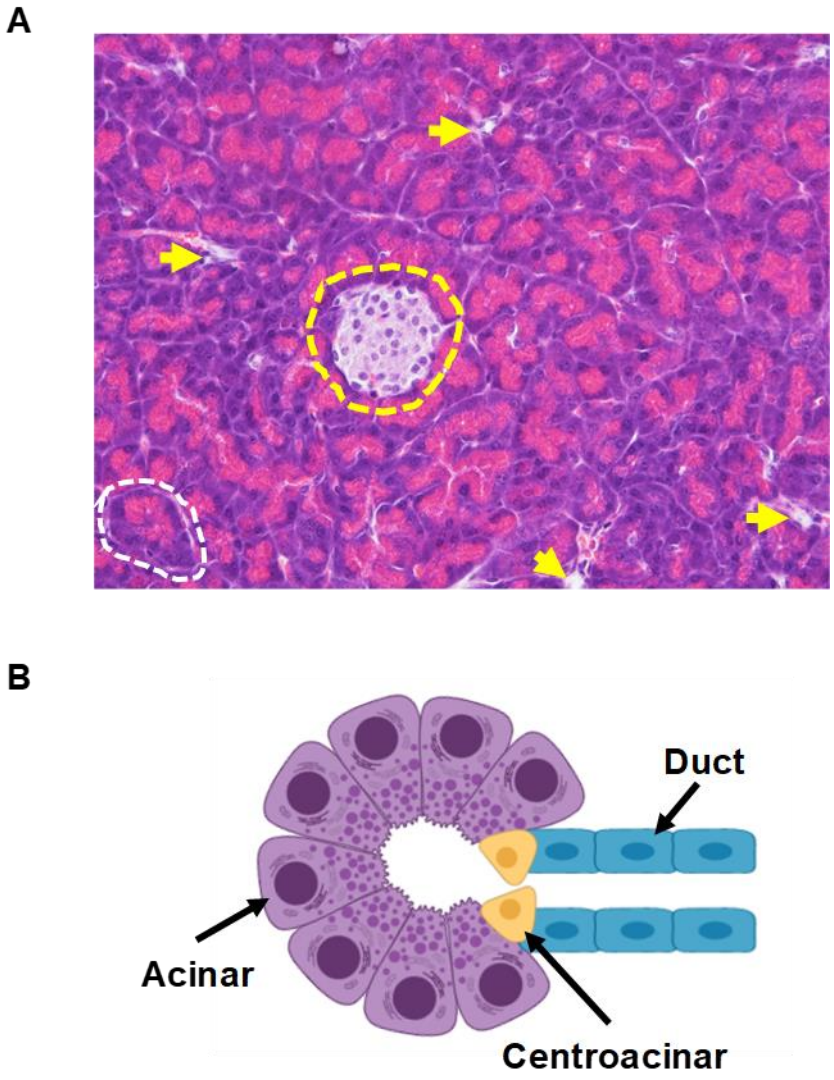

Figure 1.1 Cellular composition of the pancreas.

(A) Hematoxylin and eosin staining of a healthy mouse pancreas section. The yellow dotted line marks an islet of Langerhans, while the yellow arrows indicate pancreatic ducts and the white dotted line marks an acinus. **(B)** A diagram showing the cellular organization of the exocrine pancreas, with acinar cells organized around a central lumen that feeds into a pancreatic duct with centroacinar cells marking the delineation between the acinus and duct.

are stimulated by secretagogues such as acetylcholine and cholecystokinin (CCK) causing the release of their zymogens into the central lumen and subsequent ductal network, ultimately transporting them to the duodenum (Case, 1978). Proenzymes are finally activated in the duodenum starting with the hydrolysis of trypsinogen into trypsin by the brush-boarder glycoprotein peptidase enterokinase located on the intestinal surface (Pandol, 2010). Once activated, trypsin then catalyzes the activation of the remaining proenzymes. As referenced above, ductal cells are the second major cell type of the exocrine pancreas and form a network of branched tubes connecting acini to the duodenum (Figure 1.1). Duct cells are cuboidal or columnar epithelial cells that in addition to transporting pancreatic juices also secrete bicarbonate to neutralize stomach acidity and mucins (Grapin-Botton, 2005; Lee and Muallem, 2008). Finally, a specialized subset of ductal cells called centroacinar cells make up the final pancreatic exocrine cell type. These cells are localized at the center of acini at the duct terminus (Figure 1.1), and while their role is still under investigation some studies indicate that they may function as adult pancreas progenitor cells, though this still remains a matter of debate (reviewed in: (Beer et al., 2016)).

1.2 Diseases of the exocrine pancreas

Diseases of the exocrine pancreas include exocrine pancreatic insufficiency, pancreatitis, and pancreatic ductal adenocarcinoma. Exocrine pancreatic insufficiency develops when the pancreas is unable to secrete sufficient digestive enzymes for proper metabolism. This occurs when pancreatic function is reduced by more than 90% causing maldigestion, and as a result malnutrition (Pezzilli et al., 2013; Struyvenberg et al., 2017). Exocrine pancreatic insufficiency can have many causes including ductal obstruction, decreased pancreatic stimulation, acid-mediated inactivation of pancreatic enzymes, or loss of pancreatic parenchyma due to surgical resection or as a consequence of other diseases such as pancreatitis or pancreatic ductal adenocarcinoma (Domínguez-Muñoz, 2011). Indeed, chronic pancreatitis is one of the leading causes of exocrine pancreatic insufficiency (Falconi et al., 2010) and exocrine pancreatic insufficiency has been shown to be an independent risk factor for mortality in patients with chronic pancreatitis (de la Iglesia-Garcia et al., 2018).

As the name implies, pancreatitis is a condition of pancreatic inflammation and can present in either an acute or chronic form, the major defining criteria being that chronic pancreatitis results

in permanent damage in the form of fibrosis, calcification, and/or ductal abnormalities (Sarner and Cotton, 1984). While the pancreas can recover from bouts of acute pancreatitis, recurrent episodes can eventually develop into chronic pancreatitis (Klöppel and Maillet, 1992; Mitchell et al., 2003; Yadav et al., 2012). Heavy and prolonged alcohol consumption is a major cause of both acute and chronic pancreatitis and is associated with 30% (Forsmark et al., 2016) and 60-70% (Steer et al., 1995) of cases respectively. Of note, chronic pancreatitis only arises in 10% of heavy alcohol users, indicating that additional unknown risk factors must coincide for chronic pancreatitis to occur (Herreros-Villanueva et al., 2013). While the mechanisms of alcohol-induced pancreatitis are still being investigated, metabolism of alcohol by the pancreas has been shown to reduce acinar cell zymogen granule and lysosomal membrane integrity, which could result in intracellular exposure of trypsinogen to lysosomal cathepsin B (Apte et al., 2010). Because cathepsin B has been shown to convert trypsinogen to trypsin (Lindkvist et al., 2006), this could lead to premature digestive enzyme activation and pancreatic autodigestion. Indeed evidence has suggested that autodigestion is a component of pancreatitis (Geokas and Rinderknecht, 1974; Hofbauer et al., 1998; Lerch and Gorelick, 2000), especially supported by the link between mutations in the trypsin-1 gene, *PRSS1*, and a rare form of hereditary pancreatitis (Whitcomb et al., 1996). Additionally, apical zymogen exocytosis is blocked during pancreatitis causing abnormal enzyme release into the paracellular space, further contributing to the state of autodigestion and inflammation (Braganza et al., 2011; Gaisano and Gorelick, 2009). Alcohol has also been shown to activate pancreatic stellate cells, cells surrounding acini that regulated extracellular matrix turnover (Apte et al., 2006). Once activated pancreatic stellate cells adopt a myofibroblast-like phenotype and are responsible for the high level of fibrosis characteristic of chronic pancreatitis (Apte et al., 2006). In terms of prognosis, mortality due to acute pancreatitis is relatively rare, occurring in roughly 2-5% of cases (Wu et al., 2008). However organ failure can be common in more severe cases (Zhu et al., 2003) with infection being a major risk factor for death (Gloor et al., 2001). For chronic pancreatitis the mortality rate has been reported to be 4-fold higher than that of the general population (Nøjgaard et al., 2010), with a death rate of roughly 50% within 20 years of diagnosis in cases of alcohol-induced chronic pancreatitis (Ammann, 2006). The incidence of pancreatic cancer is also higher in patients with chronic pancreatitis, making pancreatitis a strong risk factor for the development of pancreatic cancer, though only 3.8-5% of patients with chronic pancreatitis develop pancreatic cancer (Bansal and Sonnenberg, 1995; Nøjgaard et al., 2010; Raimondi et al., 2010).

Pancreatic ductal adenocarcinoma (PDAC) is the most common form of pancreatic cancer, accounting for 93% of all cases, with the remining 7% arising from pancreatic endocrine cells (American Cancer Society, 2019). Despite having a relatively low incidence (56,770 estimated new cases in 2019 for the Unites States), PDAC is the fourth leading cause of cancer deaths in men and women in the Unites States due to its extremely high mortality rate, with a five year survival rate of only 9% (Siegel et al., 2019). In fact, despite strong efforts to better understand and treat PDAC, little progress has been made to improve patient prognosis and the mortality rate is actually increasing (American Cancer Society, 2019; Siegel et al., 2019). PDAC is particularly difficult to treat because disease progression is often asymptomatic, and as a result the majority of cases (80%) are diagnosed at advanced stages when the tumor has already begun to metastasize (American Cancer Society, 2019). Indeed, early detection is associated with a more favorable prognosis due to the increased chance for surgical resection (Hartwig et al., 2013; Takeda et al., 2017). Unfortunately, no good biomarkers or screening methods have been identified for early detection of PDAC in the general population, though research in this area is ongoing (Becker et al., 2014; Kunovsky et al., 2018). However, some studies have shown that screening and maintaining surveillance of patients at high risk for PDAC, based on hereditary and genetic factors, can increase the chance of detecting tumors at a resectable stage (Canto et al., 2018; Vasen et al., 2016). Many at risk factors for PDAC have been identified including modifiable factors such as use of tobacco or alcohol, diet, obesity, chronic pancreatitis, diabetes mellitus, and certain abdominal surgeries and infection, as well as genetic risk factors including hereditary breast and ovarian cancer syndrome, Lynch Syndrome, familial adenomatous polyposis, Peutz-Jeghers Syndrome, familial atypical multiple mole melanoma syndrome, hereditary pancreatitis, cystic fibrosis, and ataxia-telangiectasia (reviewed in: (Becker et al., 2014)). Nonetheless, the strongest risk factor for PDAC is increased age with a median age at presentation of 70 years, the highest of any cancer (Bekkali and Oppong, 2017; Olson and Kurtz, 2013).

As mentioned above, early detection of PDAC is particularly important because it increases the chance for surgical resection, the only curative treatment currently available (Hackert and Büchler, 2013; Hartwig et al., 2013). However, only a small percentage (<20%) of patients present with resectable tumors, and, despite some patients achieving long term survival, the median postoperative survival is only 20-22 months with a 5-year survival of only 20% due to high rates of tumor recurrence (Van den broeck et al., 2009; Griffin et al., 2015; Hidalgo, 2010). As such,

achieving an R0 resection, which means histologically free margins are detected, is one of the most important prognostic factors for long term survival post-surgery (Adamska et al., 2017; Van den broeck et al., 2009; Neoptolemos et al., 2001). Adjuvant chemotherapy with gemcitabine, a nucleoside analog, plus 5-fluorourociel, a thymidylate synthetase inhibitor, is the current standard of care post-resection and has been shown to increase median survival (Neoptolemos et al., 2017). The importance of neoadjuvant therapy is still being studied, but recent findings have shown that in cases of locally advanced PDAC its use can lead to tumor downsizing and downstaging, increasing the potential for resection once the initial treatment has completed (Hackert, 2018; Seufferlein and Ettrich, 2019).

For patients with unresectable tumors chemotherapy or chemoradiotherapy have been shown to significantly increase overall survival, though even using these regimens median overall survival is less than one year (Adamska et al., 2017). Current first-line therapy for advanced PDAC includes gemcitabine in combination with albumin-bound paclitaxel or a multidrug combination (irinotecan, oxaliplatin, fluorouracil, and leucovorin) called FOLFIRINOX, both achieving significant improvements in patient outcome reaching median overall survival of 8.7 (Goldstein et al., 2015) and 11.1 (Conroy et al., 2011) months respectively. However, these combination drug therapies are also associated with increased adverse events and toxicity, meaning only patients in good performance status are eligible for their use (Adamska et al., 2017). In general, PDAC represents a highly radio- and chemoresistant form of cancer as illustrated by its relatively poor survival outcomes. This is likely due to several factors including the presence of treatment resistant cancer stem cells (Hermann et al., 2007; Li et al., 2007), cancer cells that have undergone epithelial mesenchymal transition (EMT) (Arumugam et al., 2009), changes in gene expression and signaling pathways leading to acquired resistance, and influences from the tumor microenvironment (Long et al., 2011) including reduced drug delivery due to poor vascular integrity (Provenzano et al., 2012).

1.3 Pancreatic ductal adenocarcinoma pathology

PDAC tumors most commonly occur in the head of the pancreas, the region closest to the duodenum (Bosman et al., 2010), and are composed primarily of dense stroma, accounting for roughly 90% of the total tumor volume (Xie and Xie, 2015). The epithelial PDAC cells, therefore, form only a small part of the total tumor and have a characteristically duct like phenotype (Figure 1.2). Similar to other cancers, it is thought that PDAC progresses from premalignant lesions of the pancreas, specifically: pancreatic intraepithelial neoplasia (PanIN), intraductal pancreatic mucinous neoplasm (IPMN), or mucinous cystic neoplasms (MCNs) (Pittman et al., 2017), though MCN are quite rare and pose a very low risk of becoming malignant (Crippa et al., 2008; Distler et al., 2014). IPMN are grossly visible mucinous lesions that occur within the pancreatic ductal system and are detectable by advanced imaging techniques (Shi and Hruban, 2012). If found early IPMN can either be monitored or surgically resected depending on the assessed risk of malignant progression (Tanaka et al., 2012). However, most IPMN are benign and only a small percentage (10%) are associated with invasive carcinoma, while the remaining 90% of PDAC cases likely originate from PanIN lesions (Patra et al., 2017). Unfortunately, because PanINs are asymptomatic, microscopic lesions (Distler et al., 2014), they are imperceptible by gross observation and therefore poor candidates for image-based early detection or surgical resection.

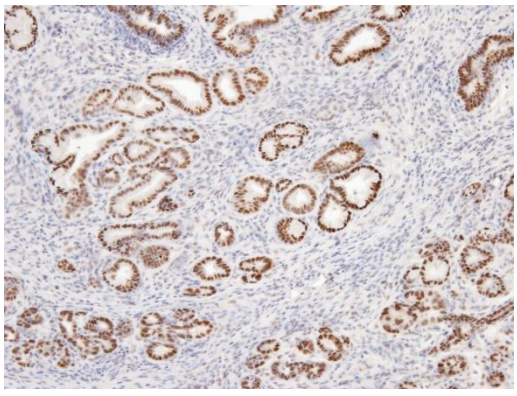

Figure 1.2 PDAC histology

DAB staining of a mouse PDAC tumor. SOX9 staining (brown) marks the epithelial PDAC cells which are reminiscent in structure to pancreatic ducts and form only a small part of the total cellular composition of the tumor.

Based on clinical observations and studies using genetically engineered mouse (GEM) models a stepwise progression pattern has been proposed for the development of PanIN into PDAC (Figure 1.3). PanIN lesions are classified into three grades based on increasing levels of atypia, dysplasia, and nuclear abnormalities: PanIN-1 (A/B), PanIN-2, and PanIN-3 (Hruban et al., 2000, 2001, 2008). It is important to note that PanIN-1 lesions are detectable in 40% of adults without invasive carcinoma and are therefore relatively common, while PanIN-3 lesions are observed in <5% of adults, but are present in 30-50% of patients with PDAC, supporting a progression of PanIN-3 to frank carcinoma (Hruban et al., 2004). Indeed phylogenetic analysis of patient PanIN and PDAC samples has largely supported an evolutionary model wherein PanINs progress to PDAC, though it is thought that this transition is slow, potentially taking place over several years (Makohon-Moore et al., 2018; McCarthy et al., 2001). Additionally, mutations in the proto-oncogene *KRAS* are present in >90% of PDAC cases (Witkiewicz et al., 2015), and are observed at a similar frequency in all grades of PanIN (Kanda et al., 2012). Based on this finding and subsequent GEM studies, it appears that most instances of PDAC are first initiated by a *KRAS* driver mutation, most typically occurring at codon G12, inhibiting GTPase activity and causing constitutive KRAS activation (Eser et al., 2014). As PanINs progress from low to high grade lesions additional inactivating mutations in tumor suppressor genes are often observed including mutations in *CDKN2A*, *TP53*, *SMAD4*, and/or *BRCA2* (Hruban et al., 2008).

Interestingly, while PDAC cells have many duct-like characteristics, the PDAC cell of origin has been an area of much debate. The first mouse models to mimic PDAC development expressed oncogenic $Kras^{G12D}$ from common pancreatic progenitor cells using a CRE *LoxP* system and produced PanIN and invasive metastatic tumors that faithfully replicated the human condition (Hingorani et al., 2003). Subsequent studies used lineage restricted expression of oncogenic *Kras* to determine the neoplastic capacity of specific terminally differentiated pancreatic cell types. These studies revealed acinar cells to be particularly susceptible to PanIN and PDAC formation (Grippo et al., 2003; Guerra et al., 2007; Habbe et al., 2008; Kopp et al., 2012; De La O et al., 2008; Morris et al., 2010b; Shi et al., 2009), while duct cells remained relatively incalcitrant (Brembeck et al., 2003; Kopp et al., 2012; Ray et al., 2011). However, more recent studies have gone on to show that under the right conditions, such as $Kras^{G12D}$ expression combined with either loss of *Trp53* (Lee et al., 2018) or chronic pancreatitis (Shi et al., 2019), duct cells can give rise to PDAC and in some instances PanIN. It is worth noting that pancreatitis, a prominent risk factor

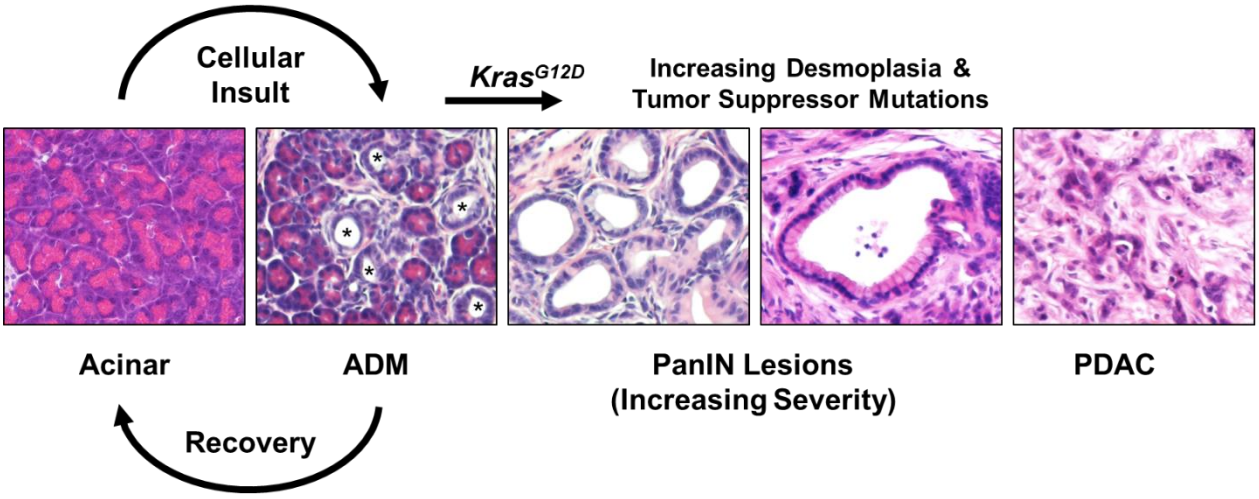

Figure 1.3 Model of PDAC pathogenesis

A diagram and histological representations from mouse models of the stages of PDAC pathogenesis. Healthy acinar cells when exposed to a cellular insult, such as pancreatitis, undergo acinar-to-ductal metaplasia (ADM), as marked by the asterisk in the second panel. Under normal circumstances ADMs recover and redifferentiate into acinar cells. However, in the presence of oncogenic KRAS, often *Kras*^{G12D}, ADMs progress to form PanIN lesions. PanINs progress through various grades of severity, often accumulating mutations in tumor suppressors, before eventually giving rise to PDAC.

for PDAC, also accelerates lesion formation in acinar restricted models of PDAC progression (Guerra et al., 2007; Kopp et al., 2012), and has even been shown to promote PanIN formation from oncogenic *Kras* expressing endocrine cells (Friedlander et al., 2009). While these studies indicate that there may be multiple paths to PDAC formation, acinar cells have been shown to be particularly susceptible to *Kras* induced transformation.

This finding is perhaps not surprising as acinar cells exhibit a high level of plasticity and are capable of transdifferentiating into a dedifferentiated/duct-like state following tissue injury or stress, a process called acinar-to-ductal metaplasia (ADM) (reviewed in: (Puri et al., 2014; Storz, 2017). In mouse models ADM lesions appear transiently following experimentally induced acute pancreatitis, but recover within a weeks' time to repopulate the acinar cell compartment (Fendrich et al., 2008; Jensen et al., 2005; Karki et al., 2015; Murtaugh and Keefe, 2015; Zhou and Melton, 2018). ADM has been observed in human pancreata (Zhu et al., 2007), and in GEM models ADM develops prior to PanINs in $Kras^{G12D}$ expressing mice (Kopp et al., 2012; Morris et al., 2010b; Zhu et al., 2007). These data support a model wherein ADM appears transiently following tissue injury, but in the presence of oncogenic KRAS, ADM persists and is unable to redifferentiate, eventually forming PanINs, thus making ADM the earliest precursor lesion to PDAC (Figure 1.3) (Hruban et al., 2008; Storz, 2017).

It is important to note that while *Kras* mutations are nearly ubiquitous with late stage PanINs and PDAC, acinar cells are largely resistant to KRAS transformation. In GEM studies where $Kras^{G12V}$ was expressed starting at postnatal day 60, as opposed to during development as some models have done, no lesions were detected within a one-year longitudinal study. This was even the case when the tumor suppressors p16 and Trp53 were additionally deleted. However, all $Kras^{G12V}$expressing mice developed late stage PanINs and occasional PDAC if challenged with chronic pancreatitis (Guerra et al., 2007, 2011). These results indicate that while oncogenic *Kras* may be the driving mutation of PDAC initiation, its presence alone is insufficient to induce acinar cell transformation. One possible explanation for this is that while mutations in codon 12 of *Kras* greatly reduces GTP hydrolysis, causing prolonged KRAS activation, external stimuli are still required to reach a threshold of KRAS activity necessary for transformation to occur (reviewed in: (di Magliano and Logsdon, 2013)). Thus, the presence of the inflammatory environment produced by chronic pancreatitis might promote KRAS activation to a level necessary for PanIN lesion formation.

Although oncogenic KRAS alone is unable to induce acinar cell transformation, its presence is required for lesion formation and the maintenance of established PDAC cells. Using a GEM model with doxycycline inducible $Kras^{G12D}$ expression, Collins et al. showed that removal of doxycycline, to turn off $Kras^{G12D}$ expression, triggered a striking regression of established PanINs and PDAC. Removal of mutant KRAS caused low-grade PanIN lesions to redifferentiate into acinar cells restoring normal pancreas parenchyma, while delayed removal of mutant KRAS resulted in PanIN regression largely due to apoptosis, rather than redifferentation. Notably, when $Kras^{G12D}$ was turned off in these experiments it was accompanied by a clearance of surrounding stromal cells, signifying that KRAS activity is not only critical for maintaining PanIN and PDAC, but also contributes to sustaining the surrounding microenvironment (Collins et al., 2012) This points to a possible system of feedback and crosstalk wherein inflammatory signals from the stroma cause KRAS activity to increase past a critical threshold needed to induce transformation, which in turn supports a persistent inflammatory microenvironment (di Magliano and Logsdon, 2013).

1.4 Acinar cell reprogramming during PDAC initiation

Acinar and duct cells originate from a common progenitor, however during development acinar cell identity is determined, and later maintained, by the expression of lineage restricted transcription factors including PTF1A, RBPJL, NR5A2, GATA6, and MIST1 (Cleveland et al., 2012). Of these, the basic helix-loop-helix transcription factor PTF1A is perhaps the most critical, as its absence during development leads to pancreatic agenesis (Cleveland et al., 2012; Krapp et al., 1998; Sellick et al., 2004). In the adult organ PTF1a functions as a protein complex with RBPJL and maintains expression of the digestive enzymes necessary for acinar cell function, including amylase, elastase, and carboxypeptidase (Beres et al., 2006; Cleveland et al., 2012; Hoang et al., 2016; Krapp et al., 1996; Rose et al., 2001), with several of these enzymes being coregulated by NR5A2 (Hale et al., 2014; Holmstrom et al., 2011). Similarly, MIST1, itself a downstream target of PTF1A, works together with PTF1A to coregulate genes critical for key acinar cell processes, including protein synthesis and secretion (Jiang et al., 2016b).

As mentioned earlier, when exposed to stress, such as pancreatitis inflammation, acinar cells undergo ADM and adopt a ductal/progenitor-like phenotype that, in the presence of oncogenic KRAS, can progress to form PanINs and eventually PDAC. During this transition the acinar cell transcriptional network is silenced, including loss of key transcription factors and digestive enzymes (von Figura et al., 2014; Karki et al., 2015; Molero et al., 2012; Shi et al., 2013). As acinar cells lose their differentiation status, they also become more susceptible to KRAS-driven transformation. This has been demonstrated in several GEM studies examining the effects of transcription factor ablation on acinar cell homeostasis. In *Mist1* knockout mice, for example, acinar cells display defects in cell organization, and over time acquire duct-like lesions similar to ADM (Pin et al., 2001). When $Kras^{G12D}$ is introduced, *Mist1* null acinar cells form both more and higher grade PanIN lesions compared to mice with intact *Mist1* expression (Shi et al., 2009). Similarly, loss of *Nr5a2* in adult mice blocked acinar cell redifferentiation following experimentally induced acute pancreatitis, and when *Nr5a2* was deleted in $Kras^{G12D}$ expressing cells PanIN lesion formation was again accelerated (von Figura et al., 2014; Flandez et al., 2014). This same pattern has been observed in *Gata6* (Martinelli et al., 2013, 2016) and *Ptf1a* (Hoang et al., 2016; Krah et al., 2015; Sakikubo et al., 2018) gene deletion studies, wherein transcription factor ablation produced spontaneous ADM formation and, if coupled with oncogenic KRAS expression, increased PanIN formation. These results emphasize both the importance of these transcription factors in preserving acinar cell identity, and the fragility of this transcriptional network, as loss of even one of these interconnected factors provokes dedifferentiation and thus increased susceptibility to neoplastic transformation.

The concept that differentiation factors may serve a protective role by restraining transformation and tumorigenesis has been further examined in both cell culture and GEM experiments. Recently, Krah et al. developed a mouse model with acinar lineage-specific doxycycline inducible expression of *Ptf1a,* allowing for temporal control of transgenic *Ptf1a* expression, even when the endogenous gene was silenced. Using this system, they not only showed that forced expression of *Ptf1a* could prevent PanIN formation in $Kras^{G12D}$ expressing cells, even when acute pancreatitis was used to exacerbate lesion formation, but remarkably found that reactivation of *Ptf1a* in already established PanINs caused lesions to redifferentiate back into acinar cells (Krah et al., 2019). Indeed, even in PDAC cell lines acinar cell transcriptional programming can be partially re-established through expression of *Ptf1a, Mist1,* or the Ptf1a/Mist1

binding partner *E47* (Jakubison et al., 2018; Kim et al., 2015; Krah et al., 2019). In these studies, PDAC cells regained expression of digestive enzymes and protein processing genes and showed a decrease in malignant properties such as proliferation and soft agar colony-forming capability. Consistent with these findings, the reactivation of developmental signaling pathways during acinar cell dedifferentiation and subsequent regeneration, such as Hedgehog, Wnt, TGFβ, and Notch, has also been shown to contribute to PDAC initiation and maintenance, though studies indicate that the precise dosage and timing of these signals may be critical to their ability to impact disease progression (reviewed in: (Morris et al., 2010a).

Interestingly, ADM lesions not only resemble ducts histologically, but also express some ductal markers including *Krt19, Muc1*, and the transcription factors *Hnf6* and *Sox9* (Storz, 2017). However, *Hnf6* expression, which comes on early during the ADM transition, tapers off as lesions progress to PanIN and PDAC (Pekala et al., 2014; Prévot et al., 2012), unlike the other factors mentioned above. Despite this, evidence suggests that Hnf6 may be an initiating factor for ADM. Prèvot et al. showed that forced expression of *Hnf6* in an acinar-derived cell line produced transcriptional changes like those found in ADM, including the upregulation of the ductal genes *Sox9, Krt19, Opn,* and *Hnf1β*, and the downregulation of acinar cell-specific genes *Mist1, Ptf1a, Amylase, Elastase,* and *Carboxypeptidase*. Additionally, ectopic expression of *Hnf6* in otherwise normal mouse pancreata caused ADM, while in pancreatitis experiments *Hnf6-null* mice maintained acinar cell integrity and were largely protected from ADM, indicating that HNF6 is critical for ADM. Despite these results, *Hnf6-null* mice nevertheless did produce PanINs when exposed to the carcinogen DMBA, perhaps in part because *Sox9* expression was still induced even in the absence of HNF6 (Prévot et al., 2012). Indeed, in a pivotal study by Kopp et al., SOX9 was revealed to be a critical gatekeeper in the transition from ADM to PanIN. While ADM could still form in the absence of SOX9, deletion of *Sox9* from acinar cells completely ablated PanIN formation, even when pancreatitis was induced in combination with oncogenic KRAS expression (Kopp et al., 2012). Taken together, these studies show that acinar reprogramming is an important initiating event in PDAC development and indicate that both loss of acinar-specific transcription factors, and the expression of SOX9 are critical rate limiting steps in disease progression. However, the exact mechanisms by which these transcriptional changes promote neoplastic transformation has yet to be fully explained.

1.5 SOX9

SOX9 is an HMG-box protein, specifically a member of the SOX transcription factor family subset, which all share sequence similarity to the first *Sox* gene ever discovered: *Sry*, or sex-determining region on the Y chromosome (reviewed in: (Lefebvre et al., 2007). There are 20 *Sox* genes in total subdivided into eight groups, SOX9 being a member of the *Sox* E group along with SOX8 and SOX10. All Sox proteins share considerable identity in their DNA binding HMG-box domain, while only members in the same group show similarities outside this region, typically at a high degree (~70-95% identity). Sox E proteins possess a strong transactivation domain, along with a DNA-dependent dimerization domain unique to the Sox E group. The transactivation domain of SOX9 has been shown to directly interact with the coactivator and histone acyltransferases CBP/p300 to upregulate target gene transcription (Lefebvre et al., 2007). However, SUMOylation of SOX E proteins has also been shown to inhibit this interaction in favor of GRG4 recruitment, resulting in target gene inhibition. Thus, SOX9 can act as both an activator or repressor depending on the context (Lee et al., 2012).

SOX proteins bind DNA through their HMG-Box domain which makes contact with the minor groove of DNA causing it to bend to varying degrees, the importance of which has yet to be determined (Lefebvre et al., 2007). This interaction has been shown to have some sequence specificity, consisting of 5'-AGAACAATGG-3' for SOX9 based on random oligonucleotide selection *in vitro* (Mertin et al., 1999). However, in practice SOX proteins typically show very little preference for their consensus sites, making it nearly impossible to predict putative targets based solely on genome sequence analysis (Lefebvre et al., 2007). Additionally, SOX proteins on their own display very weak DNA binding affinity, 100-10,000-fold weaker than most transcription factors based on *in vitro* analysis, thus supporting a model wherein SOX proteins must form hetero- or homodimers with other transcription factors in order to stably bind DNA and alter transcription (Kamachi et al., 2000; Lefebvre et al., 2007). This model of partner dependent gene regulation is further supported by the fact that SOX proteins show tissue dependent patterns of gene regulation, meaning the same SOX protein can regulate alternative gene targets based on the cell type in which it is expressed, likely due to differences in the availability of specific binding partners (Kamachi et al., 2000). Indeed, SOX proteins often play critical roles in development and cell determination contingent on the tissue type in which they are expressed. For example,

heterozygous mutations in the SOX9 DNA binding domain can lead to campomelic dysplasia, a disease characterized by defects in skeletal development and often associated with XY sex reversal (Lefebvre and Smits, 2005). Based on the presentation of this disease, it has since been demonstrated that SOX9 regulates several target genes necessary for chondrocyte development and maturation, and is thus required for chondrogenesis (Lefebvre and Dvir-Ginzberg, 2017; Lefebvre and Smits, 2005). Likewise, an essential role for SOX9 in male sex determination and the development of Sertoli cells was also discovered, wherein SOX9 and SF1 heterodimerize and upregulate anti-Müllerian hormone gene expression, promoting phenotypically male genital development (De Santa Barbara et al., 1998). Furthermore, it has been shown that *Sox9* mutations in the region necessary for homodimerization causes campomelic dysplasia, but not XY sex reversal, further exemplifying the context and partner dependent functionality of SOX proteins (Bernard et al., 2003). Given its ability to regulate highly specialized, cell-type specific targets critical for development and differentiation, and its capacity to remodel chromatin, SOX9 has been proposed to function as a pioneer factor, though whether it is a true master pioneer factor, or merely contributes pioneer functionality remains unclear (Adam et al., 2015; Liu et al., 2018). Indeed, because SOX9 displays tissue specific patterns of gene regulation generalizations about it is functionality between tissue types is difficult and it is best studied on an individual basis in the exact context of interest.

SOX9 expression is also critical for the proper function and maintenance of several other cell types including hair follicle, mammary, neural crest, and intestinal stem cells, as well as retinal, neural, and pancreatic progenitors (Sarkar and Hochedlinger, 2013). Indeed, though SOX9 expression is restricted to ductal and centroacinar cells in the adult pancreas, mouse studies show that all pancreatic cells originate from a common SOX9 positive progenitor pool starting as early as E9.5, and even haploinsufficiency of SOX9 during development leads to pancreatic hypoplasia, indicating that SOX9 is not merely a marker for this cell population, but is in fact critical for its expansion (Seymour, 2014). SOX9 also maintains duct cell integrity in the adult pancreas, as ablation of *Sox9* causes ductal dilation, the formation of cysts, and loss of duct cell primary cilia presumably due to down regulation of the putative SOX9 target gene *Pkd2* (Shih et al., 2012).

SOX9 is overexpressed in several cancer types including colorectal, lung, prostate, brain, breast, and PDAC (Matheu et al., 2012), and in most cases SOX9 expression correlates with poor prognosis (Ruan et al., 2017), though a few studies have found that SOX9 expression can inhibit

tumorigenesis. For example, in a study using melanoma cells, it was found that SOX9 expression actually decreases following melanocyte transformation and overexpression of SOX9 in the transformed cells caused a reduction in cell proliferation and tumorigenicity (Passeron et al., 2009). Alternatively, a study using colorectal carcinoma cells found SOX9 expression repressed claudin-7, altering cell polarity and inhibiting tumorigenesis (Darido et al., 2008). As mentioned earlier, SOX9 is aberrantly expressed early during PDAC initiation, becoming readily detectable in ADM lesions, and its expression is required for neoplastic transformation in *Kras*^{G12D} expressing mice (Kopp et al., 2012). Several putative upstream regulators of *Sox9* have been identified in this context, including HNF6 as mentioned earlier (Prévot et al., 2012). NFATc1 and NFATc4, two factors aberrantly expressed during ADM, were also shown to function upstream of *Sox9* in response to EGFR stimulation (Chen et al., 2015a; Hessmann et al., 2016). Both factors directly bound the *Sox9* promoter, and their presence was necessary for EGFR dependent induction of *Sox9* expression. Additionally, in the absence of *Nfatc1*, *Kras*^{G12D} expressing transgenic mice no longer exhibited persistent ADM lesions following acute pancreatitis, and instead recovered normally, though whether this is a SOX9 dependent phenotype remains to be determined (Chen et al., 2015a). Using an established PDAC cell line, *Sox9* expression was synergistically upregulated by co-activation of hedgehog and EGFR, further establishing a link between EGFR signaling and *Sox9* expression (Eberl et al., 2012). Furthermore, a positive feedback loop between SOX9 and the hedgehog effector Gli1 has also been identified *in vitro* (Deng et al., 2015). Notch and Wnt/β-catenin, two developmental signaling pathways reactivated during PDAC progression and critical for early lesion formation (De La O et al., 2008; Mazur et al., 2010; Thomas et al., 2014; Zhang et al., 2013), have also been shown to control *Sox9* expression, and inhibition of β-catenin prevented induction of SOX9 and subsequent lesion formation in a 3D culture progression model (Shih et al., 2012; Wang et al., 2019b). Tsuda et al. showed that PDX1, a pancreas developmental transcription factor re-expressed during ADM/PanIN formation, was recruited to the *Sox9* promoter by Brg1 to directly regulate *Sox9* expression in isolated acinar cells. Loss of Brg1 thus prevented induction of *Sox9* expression *in vivo*, precluding ADM/PanIN formation. Indeed, forced expression of *Sox9* restored lesion formation even in the absence of Brg1, indicating that this phenotype was indeed SOX9 dependent (Tsuda et al., 2018). Similarly, Prxx1b, an isoform of Prrx1 that is upregulated during ADM, was shown to directly bind the *Sox9* promoter and induce *Sox9* expression in isolated PDAC cell lines (Reichert and Takano, 2013). NF-κB, which has been shown to promote ADM

(Liou et al., 2013), also directly regulated *Sox9* expression in a PDAC tumor cell line (Sun et al., 2013), and interestingly, the tumor suppressor p27 has been shown to repress *Sox9* (Jeannot et al., 2015). Loss of or suppression of p27 during PDAC initiation may therefore promote *Sox9* expression. Together these studies find SOX9 to be a common target of several signaling pathways and transcription factors that are upregulated during PDAC initiation and progression. However, a unified model taking into account the intersection and signal cross talk between these pathways as it pertains to *Sox9* expression during ADM and PanIN formation has yet to be determined. Additionally, why SOX9 expression is necessary for PanINs to form remains to be determined.

In addition to playing a critical role in PDAC initiation, SOX9 contributes to malignant qualities in frank PDAC as well. As both a marker of pancreatic progenitors, expression of SOX9 during early lesion formation and in PDAC is perhaps more a sign of dedifferentiation than ductal conversion. This is fitting as expression of SOX9 in PDAC cells is associated with increased stemness properties and the presence of cancer stem cells (CSCs) (Deng et al., 2015; Eberl et al., 2012; Higashihara et al., 2017; Schultz et al., 2016; Sun et al., 2013) Indeed, separate studies found that shRNA knockdown of *SOX9* in PDAC cells reduced stem cell properties including sphere formation and xenograft tumor growth (Eberl et al., 2012; Higashihara et al., 2017) and Deng et al.(2015) showed that SOX9 expression promotes PDAC CSC through stabilization of Gli1 by nonconical means via physical sequestering a Gli1 targeting ubiquitin ligase (Deng et al., 2015).

In summary, previous studies indicate that SOX9 operates in a highly context dependent manner, often functioning to maintain stem and progenitor cell populations or conversely, to promote cell type specific differentiation programs as is the case for chondrocytes and Sertoli cells (Lefebvre et al., 2007). Indeed, SOX9 is necessary for proper pancreas development and to upholding duct cell integrity. However, during ADM/PanIN formation SOX9 becomes aberrantly expressed, potentially being upregulated by several signaling pathways and transcription factors acting in concert. This upregulation of SOX9 during ADM is necessary for $Kras^{G12D}$ driven neoplastic transformation to occur, making SOX9 a critical gatekeeper of PDAC initiation. Likewise, in established PDAC cells SOX9 enhances cancer stem cell properties and was necessary for tumorigenesis in a PDAC xenograft model. However, despite the wealth of research on the impact of SOX9 on PDAC initiation and progression, the mechanism(s) by which SOX9 promotes PDAC initiation remain to be determined.

1.6 PAR1

Cancer is often associated with hypercoagulation, a phenomenon observed as far back as 1823 when it was first reported by Jean-Baptiste Bouillaud (Bouillaud and Bouillaud, 1823) and later corroborated in 1865 by Armand Trousseau (Trousseau, 1865). Indeed, venous thromboembolism (VTE), a condition where blood clots form in deep veins, is common in cancer patients and is the second leading cause of cancer deaths (Noble and Pasi, 2010). Of particular relevance is the finding that pancreatic cancer has one of the highest risks of VTE compared to other cancers (Horsted et al., 2012). It is also important to note that while the chance of VTE is increased in cancer patients, so too is the risk of cancer increased in patients with idiopathic VTE, indicating a two-way association between coagulation and cancer (Murchison et al., 2004; Noble and Pasi, 2010). Indeed, experimental studies have shown that many factors within the coagulation cascade can promote malignancy and metastasis (Sharma et al., 2019).

Mechanistically, several cancer associated components can promote coagulation including mucins and hypoxia (Razak et al., 2018) which are known to be strongly associated with PDAC (Jonckheere et al., 2010; Koong et al., 2000). However, tumor cell expression of the procoagulant protein tissue factor (TF) may offer a more direct explanation for PDAC associated hypercoagulation. Under normal physiological conditions TF is expressed by sub-endothelial cells and is sequestered from components in the blood stream. However, upon loss of vascular integrity due to injury or breach TF is exposed to factors in the blood, thus initiating the coagulation cascade which culminates in thrombin protease-mediated platelet activation and cleavage of fibrinogen to generate a crosslinked fibrin clot (Figure 1.4) (Butenas, 2012). TF is also expressed in PanIN and PDAC epithelium and correlates with histological grade and disease prognosis, but is absent from normal pancreatic tissue (Kakkar et al., 1995; Khorana et al., 2007; Nitori et al., 2005). In PDAC components of the coagulation cascade are detected extravascularly thus enabling tumor cell TF to directly contact hemostatic factors typically confined to the blood stream (Wojtukiewicz et al., 2001).

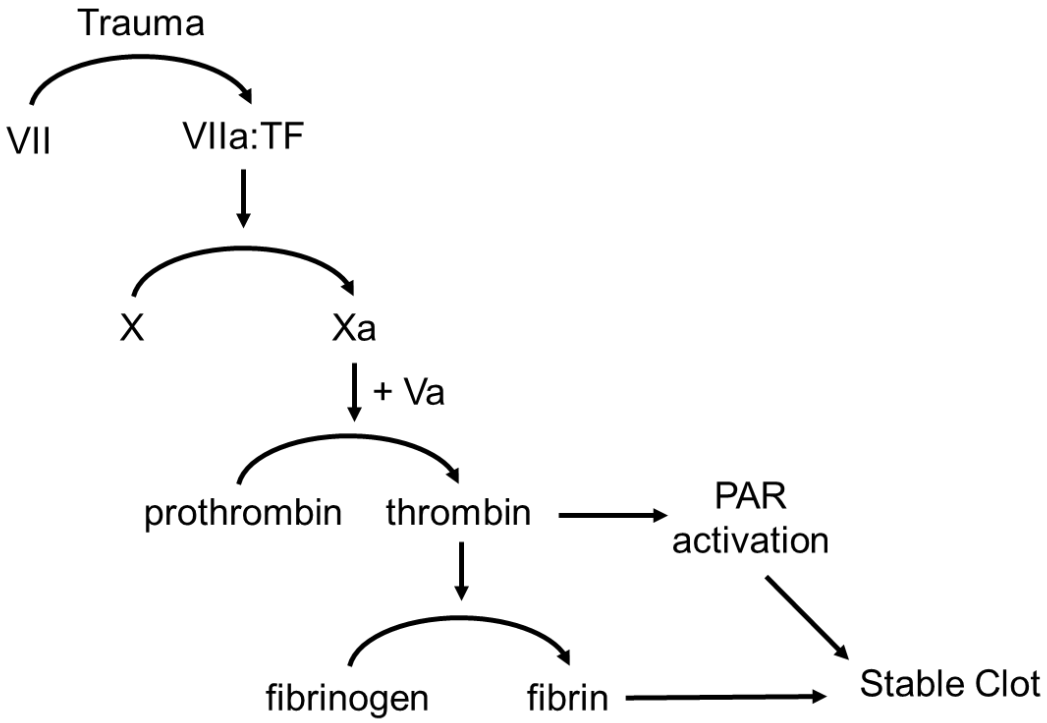

Figure 1.4 Simplified diagram of the extrinsic coagulation cascade.

Blood vessel damage allows Factor VII to come in contact and form an active enzymatic complex with tissue factor (TF). In turn the VIIa:TF complex activates Factor X through enzymatic cleavage. Xa and its co-factor Va activate prothrombin to thrombin, which in term cleaves fibrinogen to its insoluble form, fibrin, and activates PAR receptors on the endothelium and platelets to ultimately form a stable blood clot.

Both TF expression and subsequent thrombin activation have been shown to impact tumor growth and metastasis in PDAC and other cancers (Sharma et al., 2019; Yang et al., 2019b). Indeed, reduction of tumor cell TF by shRNA or systemic reduction of prothrombin decreased PDAC tumor growth and metastasis in syngeneic allograft studies (Yang et al., 2019b). Though thrombin has many targets as a serine protease, and therefore its effect on tumor growth may be multifaceted, one target of interest for its impact on tumor malignancy is the protease activated receptor PAR1. PAR1 is a seven transmembrane G protein-coupled receptor encoded by the gene *F2R* and is one of four PAR family proteins (reviewed in: (Soh et al., 2010). PARs are unique in their mode of activation, wherein proteolytic cleavage of the N-terminal extracellular tail exposes a new N-terminal domain capable of binding to residues within PAR's second extracellular loop, thus acting as a tethered ligand creating conformational changes that enable intracellular G-protein interaction and activation (Figure 1.5) (Soh et al., 2010). Once activated PAR1 can signal through multiple heterotrimeric G-proteins including $G\alpha_i$, $G\alpha_q$, and $G\alpha_{12/13}$ which can produce cytoskeletal rearrangements through Rho activation, and increased cell motility, proliferation, and secretion among other affects (for a comprehensive list of PAR1 affects in specific cell types see (Steinhoff et al., 2005)). Because PAR1 protein activation is irreversible, as a result of permanent N-terminus cleavage, once activated PAR1 is internalized and degraded by the lysosome, while an inactive pool of PAR1 is constantly cycled between endosomes and the cell surface to ensure rapid post-activation cellular resensitization (Soh et al., 2010). Thrombin activates PAR1 by binding with high affinity to a hirudin-like domain in the extracellular tail, however other proteases such as FXa, activated protein C (APC), trypsin, elastase, and matrix metalloprotease-1 (MMP1) are also capable of activating PAR1 (Heuberger and Schuepbach, 2019). In some instances these proteases, such as APC or elastase, target PAR1 at non-canonical cleavage sites thus creating alternative tethered ligands that exert biased signaling through more restricted downstream pathways (Zhao et al., 2014). For example, elastase has been shown to preferentially signal through the $G\alpha_i$/MAPK pathway (Mihara et al., 2013).

PAR1 is expressed in many tissues and cell types including platelets (human, but not mouse), endothelial cells, fibroblasts, monocytes, T cells, and smooth muscle cells, as well as some cancers, most notably PDAC, melanoma, and breast cancer (Steinhoff et al., 2005). PAR1 activation on endothelial cells and platelets contributes to hemostasis by affecting endothelial barrier permeability and platelet pseudopodia extrusion and aggregation (Ossovskaya and Bunnett, 2004).

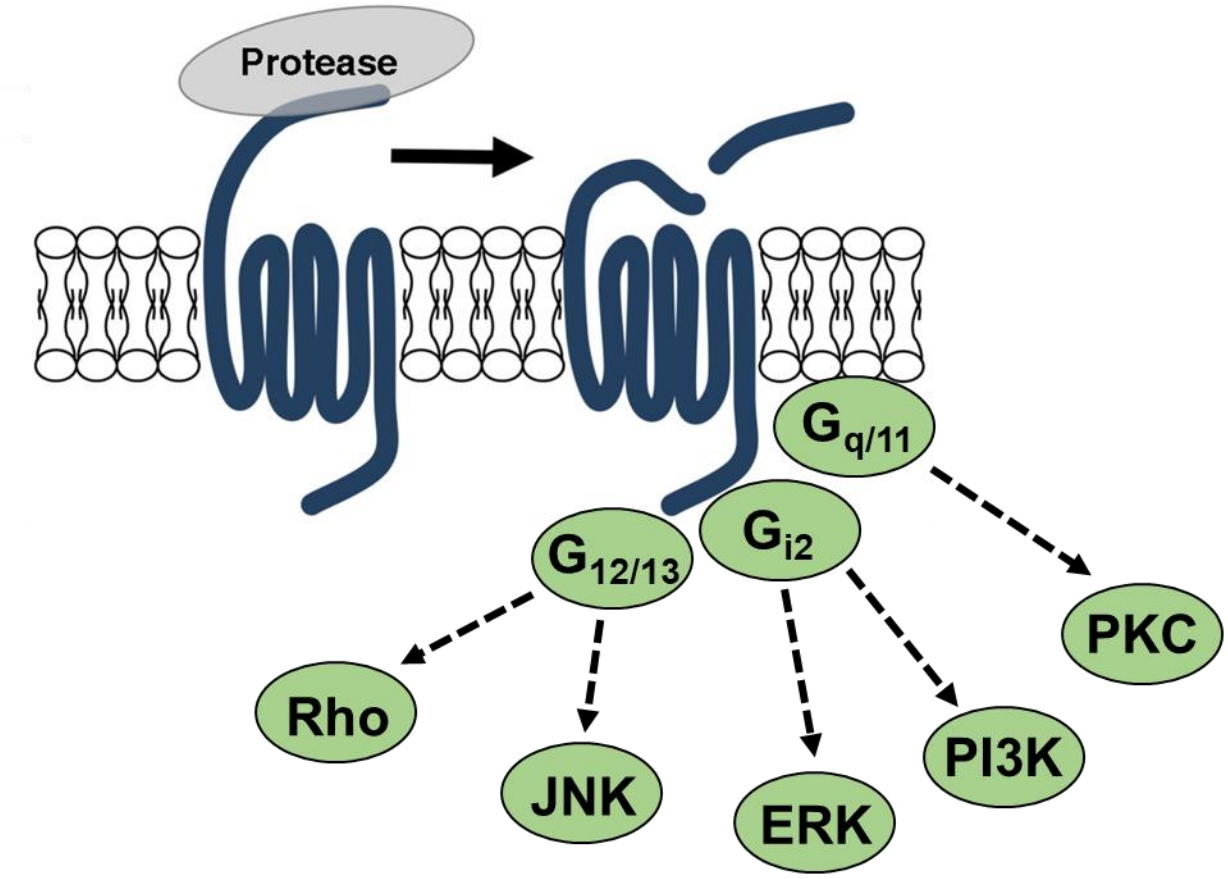

Figure 1.5 Mechanisms of PAR1 activation and signaling.

Protease activated receptors (PARs) are activated by irreversible enzymatic cleavage of their extracellular tail, thus revealing a new N-terminal peptide sequence that acts as a tethered ligand to activate PAR signaling. PAR activation produces a conformational change enabling G-proteins to interact and signal through several different downstream pathways. Image adapted from (Macfarlane et al., 2001) and (Nieman, 2016).

Additionally as a component of the coagulation cascade and wound healing process PAR1 signaling plays a role in inflammation and inflammatory diseases and can stimulate the release of proinflammatory cytokines such as IL-6 and IL-8 (Heuberger and Schuepbach, 2019; Ossovskaya and Bunnett, 2004; Steinhoff et al., 2005). In cancer cells PAR1 expression has been shown to promote proliferation, cell survival, angiogenesis, and metastasis (Arora et al., 2007; Han et al., 2011), and ectopic expression of PAR1 caused transformation of NIH3T3 cells as determined by anchorage independent growth (Martin et al., 2001). However, occasional studies have found instances where PAR1 expression has limited cancer cell malignancy, perhaps highlighting the complexity of a system wherein PAR1 can be expressed by multiple cell types within the tumor environment and can exhibit alternative downstream affects depending on what proteases trigger its activation. For example, Tantivejkul et al. found PAR1 to be highly expressed in prostate cancer cells and showed that PAR1 activation in culture by either thrombin, or a synthetic peptide that mimics the tethered ligand formed by thrombin cleavage of PAR1, enhanced cell survival as demonstrated by decreased doxetaxel-induced apoptosis (Tantivejkul et al., 2005). However, Adams et al. later showed that genetic ablation of PAR1 greatly increased spontaneous tumor growth in a genetic mouse model of prostate cancer, and found that treatment of mouse prostate cancer cells in culture with peptides mimicking APC activation of PAR1 induced apoptosis (Adams et al., 2018). While these studies initially seem to report discordant results, further examination reveals the intricacies of this biological system. Adams et al. reported increased apoptosis upon APC induced PAR1 signaling, however APC is known to cleave PAR1 at noncanonical sights creating biased signaling. When the same cells were treated with peptides mimicking thrombin activation of PAR1, no negative impact on cell survival was detected, and thus these results do not dispute Tantivejkul et al.'s findings. Additionally, though Adams et al. found ablation of PAR1 promoted tumor growth and therefore showed that PAR1 expression suppresses tumorigenesis, these studies were performed in PAR1-null mice, wherein PAR1 is completely absent from all cells. Due to the limitations of that model individual contributions of PAR1 expression on tumor cells versus stromal cells cannot be assessed, and further experiments are needed to determine if targeted ablation of PAR1 from specific cell types produces any distinct phenotypes.

In regards to PDAC, PAR1 expression correlates with differentiation status in human PDAC cell lines, with PAR1 being highly expressed in undifferentiated PDAC cells (Rudroff et al., 2002). Though the reason for aberrant PAR1 expression in this context is unknown, as PAR1 is absent from normal pancreas epithelium but is upregulated in PDAC stroma and tumor cells (Queiroz et al., 2014; Yang et al., 2019b), studies have shown that PAR1 is repressed by p53 (Salah et al., 2008) and activator protein (AP)-2α (Tellez et al., 2003), two factors shown to be lost or mutated in PDAC human samples (Fauquette et al., 2007; Lu and Zeng, 2017). Additionally, mutant gain of function p53 actually increased PAR1 expression (Salah et al., 2008) as did oncogenic RAS (Ellis et al., 1999), again aligning with mutations frequently observed in PDAC. Further *in vitro* analysis found that PAR1 activation enhanced PDAC cell adhesion to extracellular matrices in a β1 integrin dependent manner (Kanemaru et al., 2012), which is of relevance as knockdown of β1 integrin in PDAC cells reduced both metastasis and primary tumor growth in an orthotopic xenograft model (Grzesiak et al., 2011).

In vivo studies have also been performed examining the contribution of stromal and tumor cell PAR1 to PDAC tumor growth. Queiroz et al. showed that when PDAC cells were orthotopically implanted in PAR1-null mice tumor growth, angiogenesis, and myeloid cell recruitment were reduced and tumors showed increased sensitivity to gemcitabine, indicating a role for stromal PAR1 in PDAC progression (Queiroz et al., 2014). Further studies from the same group showed that shRNA knockdown of PAR1 in PDAC cells reduced metastasis, but actually enhanced primary tumor growth in a syngeneic mouse allograft tumor model (Tekin et al., 2018). However, results from our lab conflict with these findings, as shRNA knockdown and CRISPR/Cas9 mediated ablation of PAR1 in two murine PDAC cell lines, similar to those used by Tekin et al., massively reduced primary tumor growth and tail vein-induced pulmonary metastasis in syngeneic allografts (Yang et al., 2019b). Additionally, we found no reduction in tumor growth when our PAR1 expressing PDAC cells were injected into PAR1-null mice, seemingly indicating a lack of stromal PAR1 contribution in our model. Notably, tumor growth was restored in our studies when PAR1 was re-expressed in our PAR1-knockout tumor cells from a doxycycline inducible transgene, greatly reducing the likelihood that our findings are attributed to an experimental artifact or off-target affect. Unfortunately, the reasons for the discrepancies between these studies remains unclear but may in part be due to heterogeneity between the tumor cell lines used or subtle differences in the mutational drivers. Further analysis of transcriptional

changes downstream of PAR1 activation in our model indicated enrichment in immune related transcripts. Upon further investigation we found that PAR1-null PDAC cells readily formed tumors in immunocompromised mice, and that specific ablation of $CD8a^+$ T cells could rescue PAR1-null tumor growth in wild type mice (Yang et al., 2019b). These findings indicate a previously unrecognized role of tumor cell PAR1 in immune evasion, however the mechanism by which PAR1 expressing PDAC cells avoid detection and/or clearance by cytotoxic lymphocytes requires further investigation.

PAR1 has gained attention as a potential therapeutic target for cancer as more studies support its involvement in tumor malignancy (Liu et al., 2017b). Several PAR1 targeting therapeutics are in development, including small molecules such as the FDA approved vorapaxar, an inhibitor that binds the PAR1 tethered ligand site to prevent proteases from binding and activating the receptor, as well as peptide-based inhibitors such as the class of lapidated pepducins that interfere with PAR/G-protein interactions (Flaumenhaft and De Ceunynck, 2017). However, while preclinical trials using pepducins have shown efficacy in limiting tumor growth in animal xenograft models (Boire et al., 2005; Cisowski et al., 2011; Yang et al., 2009), no clinical trials are yet underway to investigate PAR1 inhibition as a cancer therapeutic. Still, once additional PAR1 targeting drugs gain FDA approval for indications currently being tested, such as myocardial infarction and coronary artery disease, their use as cancer therapeutics will likely be more closely evaluated.

1.7 PDAC Immune Evasion

Historically cancer treatment has relied heavily on chemo- and radiotherapeutic strategies to target and kill cancer cells. However, the immune system is naturally capable of detecting and eliminated tumor cells, a property that has recently gained attention with the advent of immune checkpoint blockade and chimeric antigen receptor T (CAR T) cell therapies which rely on immune cells to target and eradicate cancer (Hargadon et al., 2018; Miliotou and Papadopoulou, 2018). Classical anti-tumor immunity is achieved through the cancer-immunity cycle (reviewed in (Chen and Mellman, 2013), wherein dendritic cells (DCs) within the tumor microenvironment capture tumor associated antigens released by dying tumor cells and present these antigens to T cells in the surrounding lymphoid organs causing effector T cell priming, expansion, and activation in an antigen-specific manner. Effector $CD8^+$ cytotoxic T cells are then trafficked to the tumor site

where they infiltrate the tumor microenvironment. These $CD8^+$ T cells, through their T cell receptor (TCR), then recognize tumor associated antigens presented on the cancer cell surface by major histocompatibility class I (MHC-I) molecules and kill tumor cells displaying these antigens. This in turn increases the release of tumor antigens into the microenvironment and increases the antitumor immune response cycle.

Nevertheless, many tumors overcome the immune system's constraints and continue to progress and metastasize even in patients with healthy immune systems. A study using GEM to examine immune cell composition during the progression of PDAC from low grade preinvasive lesions to advanced disease found that while leukocytes were present even at early stages, most immune cells were immunosuppressive in nature consisting primarily of myeloid-derived suppressor cells (MDSCs), tumor-associated macrophages (TAMs), and regulatory T cells (T regs), with extremely low levels of antitumor $CD8^+$ T cells, the majority of which were found to be in an inactive naïve state (Clark et al., 2007). Indeed, higher levels of $CD4^+$ and $CD8^+$ T cell infiltration in PDAC is associated with prolonged survival (Carstens et al., 2017; Ino et al., 2013), yet PDAC is often comprised of an immunosuppressive milieu and is largely considered a poorly immunogenic cancer, allowing it to subvert immune detection and subsequent activation.

Generally speaking, tumor immune evasion can be attributed to three basic mechanisms: 1) the expression of inhibitory contact dependent factors such as PDL1 and CTLA4, 2) secretion of factors that are either directly immunosuppressive or lead to the generation of an immunosuppressive microenvironment through recruitment of additional cell types, and/or 3) low tumor cell immunogenicity through loss or lack of neoantigens and/or low MHC-I expression (Figure 1.6) (Amedei et al., 2014; Martinez-Bosch et al., 2018). The first of these mechanisms involves the expression of cell surface checkpoint proteins such as PDL1 that inhibit T cell activation by binding receptors on the T cell surface. PDAC patients with PDL1 positive tumors indeed show significantly poorer prognosis and have lower levels of $CD8^+$ T cell infiltration (Nomi et al., 2007). However, despite the success of PD1/PDL1 blockade therapy in other solid tumors, PDAC has proven to be largely refractory to this treatment strategy (Macherla et al., 2018). This is likely due to the lack of infiltrating $CD8^+$ T cells within the PDAC tumor microenvironment, which has been demonstrated to impact sensitivity to checkpoint blockade treatment (Li et al., 2018; Tumeh et al., 2014). The second of these evasive strategies is the creation of an immunosuppressive microenvironment, something that is commonly observed in PDAC, which

displays low levels of infiltrating cytotoxic lymphocytes but high levels of immunoinhibitory TAMs, MDSCs, and Tregs. Indeed, PDAC cells have been shown to secrete suppressive cytokines such as TGF-β, IL10, and PGE_2 as well as chemokines such as CCL5 and CSF2 which recruit Tregs and MDSCs respectively (Bayne et al., 2012; Bellone et al., 1999; Looi et al., 2019; Markosyan et al., 2019). Finally, in addition to shaping an immunosuppressive microenvironment, PDAC tumor cells are considered to be poorly immunogenic and therefore do not elicit a strong cytotoxic immune response. This may in part be due to the low mutational burden observed in PDAC compared with other cancers, thus providing very few tumor-specific neoantigens for cytotoxic lymphocyte detection (Evans et al., 2016; Knudsen et al., 2017). To test the impact of antigen presentation on tumor growth Evans et al. (2016) showed that depletion of $CD4^+$ and $CD8^+$ T cells had no effect on tumor volume or subject survival when syngeneic PDAC cells were injected subcutaneously in C57BL/6 mice, indicating that these PDAC cells were not eliciting a detectable cytolytic immune response. However, when the same cells were engineered to express a strong antigen, in this case ovalbumin, the tumor cells were completely eliminated in a $CD8^+$ T cell dependent fashion (Evans et al., 2016). These results support the concept that PDAC cells are inherently nonimmunogenic due to a lack of high quality neoepitopes for detection by cytotoxic $CD8^+$ T cells. Taken as a whole these studies reveal that PDAC can employ multiple mechanisms of immune evasion, many of which are complex and multi-faceted in nature and involve a high level of cross-talk within the tumor microenvironment.

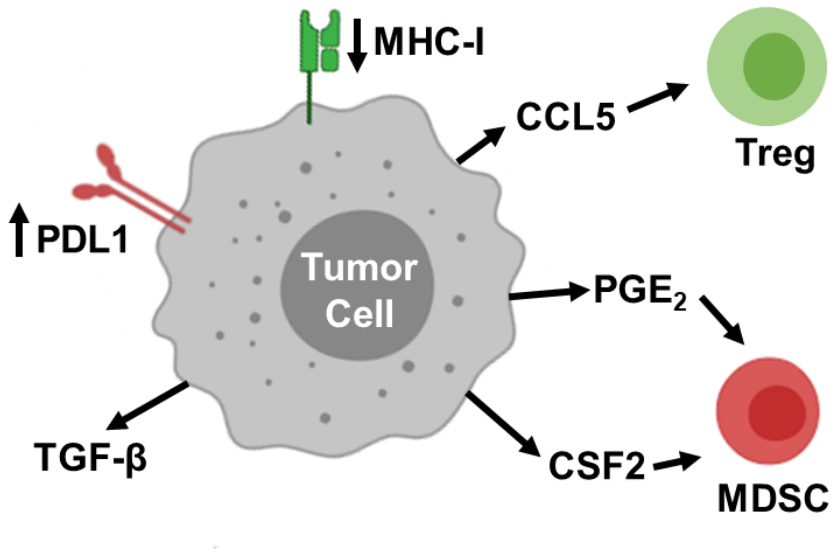

Figure 1.6 General mechanisms of tumor immune evasion.

Tumor cells can use many strategies to evade an antitumor immune response, including the expression of inhibitory checkpoint protein ligands such as PDL1, downregulation of MHC-I molecules, the secretion of immunosuppressive factors such as TGF-β, or the secretion of factors that reshape the tumor microenvironment by promoting the accumulation of immunosuppressive cells such as MDSCs or Tregs.

CHAPTER 2. MATERIALS AND METHODS

2.1 Animal use ethics statement

Use of all animals and experimental procedures were approved by the Purdue University Animal Care and Use Committee (PACUC) under protocol #1110000037.

2.2 Mouse strains

Mist1^{CreER}, *Elastasepr-CreER*, *LSL-Kras*^{G12D}, *LSL-Trp53*^{R172H}, *Sox9*^{fl}, and *Z/Sox9* (*iSox9*) genetically engineered mouse models have been described previously (Akiyama et al., 2002; Habbe et al., 2008; Hingorani et al., 2003, 2005; Scott et al., 2010; Shi et al., 2009, 2013). The *LSL-HA-Sox9* mice were generated as follows. The mouse *Sox9* coding region was amplified by PCR from WT C57BL/6 pancreas cDNA and a human influenza hemagglutinin (HA) tag sequence was added in-frame upstream of the *Sox9* start codon. The *HA-Sox9* sequence was then inserted into a *pCAG-LoxP-CAT-LoxP-LacZ* vector, replacing *LacZ* and enabling Cre recombinase mediated *Sox9* expression. The vector backbone was then removed by enzymatic digestion and the isolated *LSL-HA-Sox9* DNA was used for pronuclear injection by the Purdue University Transgenic Mouse Core Facility to generate founder lines.

2.3 Genotyping

Mouse tail clippings were taken during weaning at postnatal day 21 and digested in 500 μl of 0.2 mg/mL Proteinase K in tail lysis buffer (100 mM Tris-HCl, pH 8.5, 10 mM EDTA, 200 mM NaCl, 0.2% SDS) overnight at 56 °C. Samples were then vortexed and centrifuged for 10 minutes at maximum speed to remove debris. Supernatants were transferred to a new microfuge tube and DNA was precipitated by the addition of 500 ul isopropanol. Samples were mixed then centrifuged again as before. DNA pellets were washed once more in 70% ethanol, centrifuged again, then air dried before a final resuspension in 100 μl TE buffer (10 mM Tris-HCl, pH 8.0, 1 mM EDTA). PCR was performed using Mango Taq reagents from Bioline (BIO-21083, Bioline, Taunton, MA).

Reactions consisted of 1 µl isolated tail DNA, 7.5 µl 2X PCR buffer (40% v/v 5X Mango Taq DNA Reaction Buffer (BIO-21083, Bioline, Taunton, MA), 3 mM $MgCl_2$, 0.02% gelatin, 0.4 mM dNTPs, and 0.02% IGEPAL), 1 µl of 10 mM forward and reverse primer stocks, 5.35 µl water, and 0.15 µl *Taq* polymerase.

PCR thermocycler settings were as follows:

Mist1^{CreER}

1. 96 °C – 5 minutes
2. 96 °C – 30 seconds
3. 59 °C – 90 seconds
4. 72 °C – 1 minute [Repeat steps 2-4 36 times]
5. 72 °C – 5 minutes
6. 16 °C – Hold

Elastasepr-CreER; LSL-Kras^{G12D}*; LSL-Trp53*^{R172H}*, LSL-HA-Sox9*

1. 96 °C – 5 minutes
2. 96 °C – 30 seconds
3. 65 °C – 90 seconds
4. 72 °C – 1 minute [Repeat steps 2-4 36 times]
5. 72 °C – 5 minutes
6. 16 °C – Hold

Sox9^{fl}

1. 94 °C – 5 minutes
2. 94 °C – 30 seconds
3. 56.4 °C – 90 seconds
4. 72 °C – 1 minute [Repeat steps 2-4 36 times]
5. 72 °C – 5 minutes
6. 16 °C – Hold

Z/Sox9 (*iSox9*)

1. 95 °C – 10 minutes
2. 95 °C – 45 seconds
3. 55 °C – 45 seconds
4. 72 °C – 45 minutes [Repeat steps 2-4 36 times]
5. 72 °C – 1- minutes
6. 16 °C – Hold

Table 2.1 Mouse genotyping primers

Mouse Strain	Forward (5'-3')	Reverse (5'-3')	Product Size (bp)
Mist1^{CreER}	GGTTTAAGCAAATTGTCAAGTACGG	GAAGCATTTTCCAGGTATGCTCAG	550
Elastasepr-CreER	AGGCAAATTTTGGTGTACGG	GAGGCGTATAAAGAGGGTTCC	800
LSL-Kras^{G12D}	TCTGAATTAGCTGTATCGTCAAGG	GTCGAGGGACCTAATAACTTCGTA	500
LSL-Trp53^{R172H}	AGCTAGCCACCATGGCTTGAGTAAGT	CTTGGAGACATAGCCACACTG	250
Sox9^{fl}	AGACTCTGGGCAAGCTCTGG	GTCATATTCACGCCCCATT	250 WT 300 floxed
Z/Sox9 (*iSox9*)	GGCGTTAACTCGGCGTTTCAT	CGGTTAACGCCTCGAATCAGC	750
LSL-HA-Sox9	CCCCCTGAACCTGAAACATA	TACTGGTCTGCCAGCTTCCT	450

2.4 Tamoxifen administration

Tamoxifen was used to activate *LSL* containing transgenes combined with either the *Mist1*^{CreER} or *Elastasepr-CreER* models. Tamoxifen (cat # T5648, Sigma, St. Louis, MO) solution was prepared one day prior to use at a concentration of 20 mg/ml in corn oil (cat # C8267, Sigma, St. Louis, MO). Corn oil was heated at 42 °C for 30 minutes prior to tamoxifen addition to aid solubility. The tamoxifen solution was then shaken at 37 °C for 4-6 hours until fully dissolved. Mice were administered 200 µl tamoxifen (4 mg total) by oral gavage using a 22-gauge, 1.5 inch animal feeding needle with 1.25 mm ball tip (7920, Popper, New Hyde Park, NY). In most instances mice were dosed on two consecutive days.

2.5 Caerulein induced acute pancreatitis

Caerulein (cat # C9026-1MG, Sigma, St. Louis, MO) was dissolved in sterile PBS at 10 µg/mL on the day of the procedure and stored at 4 °C when not in use. Mice were injected intraperitoneally with 200 µl of caerulein solution once hourly for eight hours on two consecutive days.

2.6 Subcutaneous and orthotopic tumor growth

For all subcutaneous tumor growth assays tumor volume was measured every 2-4 days using calipers. Tumor volume was calculated using the equation Volume = (Length x Width^2)/2. Subcutaneous allograft studies using KC and KPC cells were performed using 8-12 week old WT C57BL/6 mice. Mice were typically injected in the intrascapular region unless otherwise specified, and this area was shaved prior to injection. Cells were dissociated by trypsin, washed, and finally resuspended in sterile PBS prior to injection. Mice were anesthetized using isoflurane and depending on the experimental conditions were injected with 0.25-1x10^6 cells per animal in 200 µl PBS.

Panc-1 xenograft studies were performed by the Purdue University Center for Cancer Research Molecular Discovery and Evaluation core. Panc-1 cells were trypsinized, washed, and resuspended in serum free media at 1x10^7 cells/mL. This cell suspension was then mixed with an equal volume of Matrigel just prior to injection. Immunocompromised mice were injected in the

flank with 200 µl of Matrigel/cell suspension mix equating to $1x10^6$ cells per mouse and tumor volume was measured over time.

For orthotopic pancreas injections cells were again resuspended in PBS, but for these studies mice were injected with $5x10^4$ cells in 20 µl PBS using a 0.3 cc syringe with a 30G needle. Prior to injection mice were anethsatized with isoflurane and shaved on their left side. During the procedure mice were kept under isoflurane and placed on a heating pad. The shaved region was sterilized with 70% ethanol and betadine solution and an incision was made along the left side of the abdomen just below the ribs exposing the peritoneal cavity. The spleen was then gently pulled outward using sponge forceps exposing the pancreas. Cells were injected slowly into the tail of the pancreas taking care to slowly remove the needle after injection to avoid any cell leakage. The spleen and pancreas were then returned to their original location and the body wall incision was closed using absorbable sutures. The skin was then sealed with wound clips and sterilized with betadine. Finally, mice were injected intramuscularly with 50 µl of 0.03 mg/mL buprenorphine (Buprenex Injection, NDC 12496-07575) immediately following the procedure and again on the following day. Where applicable doxycycline chow (cat #TD.08541, Envigo, Indianapolis, IN) was used and was initiated 1-2 days prior to tumor cell injection.

2.7 Immune cell depletion

Lymphocyte depletion was accomplished by intraperitoneal injection of monoclonal antibodies targeting CD8a (clone 2.43), CD4 (clone GK1.5), or NK1.1 (clone PK136) cell surface markers. Antibodies were received as a gift from Bennet D. Elzey. Dosages for injection were determined by titration experiments and varied for each antibody used. Mice were injected twice weekly starting one day prior to tumor cell injection.

Macrophage depletion was performed using mannosylated liposomal clodronate (SKU CLD-8914, Encapsula Nano Sciences, Bentwood, TN). Mice were injected retro-orbitally with 100 µl of either clodronate or control liposomes, equivalent to 25 mg/kg body weight, every 5 days starting one day prior to tumor cell injection. The site of tumor cell injection was also injected with 50 µl of liposome solution on the day prior to tumor cell injection to deplete any resident macrophages from the area.

2.8 RNA extraction and RT-qPCR analysis

RNA isolation and purification were performed using the E.Z.N.A. Total RNA Kit I from Omega Bio-TEK (SKU R6834-01, Omega Bio-Tek, Norcross, GA) according to the manufacturer's instructions. For tissue culture samples cells were collected in the provided lysis buffer using a cell scraper and then passed through homogenizer columns (SKU RHCR001, Omega Bio-Tek, Norcross, GA) prior to initiating the RNA isolation protocol. For mouse pancreas samples mice were euthanized by CO_2 for standard RNA isolation or by cervical break for RNA-Seq sample isolation, as this shortened the time between euthanization and RNA stabilization in order to better preserve the RNA integrity. Pancreata were then homogenized in the provided lysis buffer with a Tissue Tearor rotor-stator for 20-30 seconds and RNA was isolated according to the manufacture's instruction.

cDNA was prepared using the iScript cDNA Synthesis Kit (cat# 1708890, Bio-Rad, Hercules, CA) according to the manufacturer's instructions. For most applications 1 µg of RNA was used as starting material in a 20 µl total reaction volume and samples were further diluted to 50 µl total volume after cDNA synthesis was complete.

RT-qPCR was performed using KAPA SYBR FAST reagent (cat# KK4602, KAPA Biosystems, Cape Town, South Africa). A single reaction consisted of 2 µl cDNA, 10 µl SYBR reagent, 1 µl of 10 µM primer mix (containing forward and reverse primers), and 7 µl water. Samples were then run on a LightCycler 96 thermocycler (Roche, Basel, Switzerland) using the following parameters: 95 °C for 10 seconds, 56 °C for 10 seconds, 72 °C for 10 seconds for 40 cycles. Relative expression was then determined using the ΔΔCt method.

Table 2.2 Mouse RT-qPCR primers (5' to 3')

Gene	Forward	Reverse
18s	TGTCTCAAAGATTAAGCCATGC	GCGACCAAAGGAACCATAAC
Actg1	AAGAGGGGTATCCTGACCCT	GAACAGAACCCTGCGTCATC
Alcam	AAAAGTCGCTGTCCCCCTAA	GTACCATCCAAGGCCTGGTC
Amy	CAGAGACATGGTGACAAGGTG	ATCGTTAAAGTCCCAAGCAGA
Atf4	CGGCTATGGATGATGGCTT	GCATCGAAGTCAAACTCTTTCAG
BC107364	GAAAACCGGACAACCAGACC	GTGCTGGCAAAACCTGATCC
Bcl3	CCGCAGGGTCATTGATATCTT	CAGGAAGGCAGGTGTAGATG
Bub1	CTTCGAGACTCGGGGTTAGG	TGGGCTTCAAACATGCGAAA

Gene	Forward	Reverse
Cblc	GGAAGCATCCTGCAAACCAT	GTCTGAGTCCTCTGACACTTG
Ccl2	TGCAAGGTGTGGATCCATTT	CCTTGGAATCTCAAACACAAAGT
Cldn6	TCTCTTTTGCAGGCTCGGATA	CAGACCAGTAGAGGCCATGA
Csf2	TGCCTGTCACGTTGAATGAAG	GTGAAATTGCCCCGTAGACC
Ctrb1	TAATGACATCACCCTGCTGAA	ATCATCACATCGGTGATCTTG
Ech1	GAGAGCCCCCGAGGAAGTC	CATTCCACCAACTCCCTCCAGAAA
Eif2ak3	ACGAGTCCGGATTTTAACTGA	TGTGGAGAGCCATGTTCCT
Errfi1	CCGCTCCCTTGGGGGAAT	GGGACTCGAATATCCTGAGCA
Fblim1	GCTTCCCACAAAGACACCTG	GGGAGAGAGCATCCTCCATT
FoxM1	TGCCAAGATGTTGACACTCC	AGCGTTAAGCAGGAACTGGA
Fxyd3	TTGACATGCAAGAGGTTGTTC	ACAGAGAATCCCTGCACAAAT
Gpx1	GCTCATTGAGAATGTCGCGT	TCTTGCCATTCTCCTGGTGT
Hfe2	GGGAAACATCACAGAAGTACCC	GGACTGGCCCATACCTATCC
Hmgn2	CCAAAACAGACCAGGCACAGAA	CCTTCCCCCACCCAGTAAT
Ido1	GCGTCAAGACCTGAAAGCAT	CCACAAAGTCACGCATCCTC
Ido2	CCAAATCCTCTGGAAGCACT	AGGCATCCTGTACACGTGAG
Il34	TCTTGCTGTAAACAAAGCCCC	GTACATTGCATCAAGGACCCC
K19	CCTCCCGAGATTACAACCACT	AGGCGTGTTCTGTCTCAAACT
Kcnn4	CATCTCCAAGATGCACATGATCC	GGCTAGAAAACACAGGAGCAG
Kif11	AGGTCTTCCATTTTTCCAGCGAA	TCACACAGCAGTCCCCTTTT
Mapk3	GATCCGACAGATGAGCCAGT	ATCCAAAAGGACAGGGGTGT
Mindy1	CAAGTGGACCAGCAGCAG	TTGTTCGCACAGGTTGAACT
Mist1	TGGTGGCTAAAGCTACGTGT	CATAGCTCCAGGCTGGTTTT
Myob5	GAACTGGGACCGGTCTGG	CCTTGTGTACCGGGTGTAGA
Notch2	ACTGCCTGCCAGGTTTTGAA	CCATAGCCTCCGTTTCGGTT
Pafah1b3	TGTCGGCTTTACAGGGGG	CTGTCCGCTACAAACCGATG
Prune1	CGGAGTGCCGGATTACGC	GAGGCCTGGAATCCTGCAAA
Ptf1a	TTCTTTGCCCAGCACTTCAC	TTAAGTCCACTCCATGGCCC
Ptgs2	TTCTTTGCCCAGCACTTCAC	TTAAGTCCACTCCATGGCCC
Rbpj	TCCATCGGCGGGGAAGTT	TTCCAACCACTGCCCATAAGA
Rnf44	GCGGACAGTTCTTAAAGGGC	GGGCTCACAACCCGGC
RPLP0	AGAACTGCTGCCTCACATCC	CAATGGTGCCTCTGGAGATT
Sgpp2	TGGTTGTGATATGGGTTTTGGT	CTCACAACGGGAGGAAAGGA
Siglec15	CGGAACCTCGACCCTAGC	GGACCAGGTGATCTAGTCGG
Sox9	GAAGCTGGCAGACCAGTACC	CGCCTTGAAGATAGCATTAGG
Tgfb1	CGCAACAACGCCATCTATGA	ACTGCTTCCCGAATGTCTGA
tubd1	CATAAGGAGCGAGCGCATTT	GGGTCACCGAAGGGTTATGT
Usp4	AGCAAGAATCTGAGGCCTGT	ATGGTGGTGAAGAGCTCGAT

Vmp1	GACCGGAAGTGACGCGA	GAACTGAAGAGGGGTCTGTGA

2.9 RNA-Seq

RNA integrity was assessed by the Purdue Genomics Core Facility using an Agilent Bioanalyzer and samples with an RNA integrity number above 7 were used for next generation sequencing (NGS). The iSox9 RNA-Seq was performed by BGI (Hong Kong) at a depth of > 80 M reads per sample at a read length of 100 bp using a 200 bp insert size on an Illumina Hiseq200 using four biological replicates per group. Raw reads were then analyzed by the IUPUI bioinformatics core using mouse reference genome build mm9. Final differential gene expression was determined using EdgeR v2.11 (Robinson et al., 2010) and an FDR $\leq$ 0.05. Due to the relatively low number of DEGs identified no fold-change cut-off was applied. The KPC cell thrombin/PAR1^{KO} RNA-Seq library preparation and sequencing were performed by the Purdue Genomics core facility. NGS was performed using paired-end 2x100 bp reads using a HiSeq2500 instrument at a depth of > 70 M reads per sample. Raw sequencing results were then analyzed for quality, aligned to genome build mm10 and differential gene expression was determined using EdgeR at an FDR $\leq$ 0.01 and $\geq$ 2 fold-change in expression.

2.10 ChIP-Seq

The SimpleChIP kit (cat #9003S, Cell Signaling Technology, Danvers, MA) was used for chromatin preparation and the manufacturer's guidelines were largely followed with slight modifications. KC mouse pancreas samples were excised at 4-5 weeks post caerulein induced acute pancreatitis and 150 mg of tissue was used for chromatin isolation. Tissue was finely minced using a razor and suspended in 6 mL PBS containing EDTA-free protease inhibitor cocktail (PIC). Formaldehyde from a freshly opened ampule was then added to reach a finale concentration of 1.5% formaldehyde, and samples were rocked at room temperature for 20 minutes. The formaldehyde was then quenched with 0.6 mL of 10x glycine provided in the SimpleChIP kit and samples were mixed for 5 minutes at room temperature followed by a centrifugation step at 1500 RPM for 5 minutes at 4 °C. The supernatant was then discarded, and the pellet was washed once in 6 mL PBS + PIC and centrifuged as before. The pellet was then resuspended in 5 mL PBS + PIC and samples were transferred to a Dounce homogenizer and disaggregated with 15 strokes

using pestle “A” and then 15 strokes using pestle “B”. Samples were again pelleted at 1500 RPM for 5 minutes at 4 °C and then resuspended in 6 mL of ice-cold 1x buffer A + DTT + PIC (provided in the SimpleChIP kit). Samples were incubated on ice for 10 minutes and mixed by inversion every 3 minutes followed a centrifugation step at 3000 RPM for 5 minutes at 4 °C. Pellets were then resuspended in 6 mL of ice-cold 1x buffer B + DTT and centrifuged again at 3000 RPM for 5 minutes at 4 °C. Pellets were then resuspended in 0.6 mL buffer B + DTT and 3 µl of MNase (provided in SimpleChIP kit) was added and mixed by inversion. Samples were digested at 37 °C for 35 minutes and mixed by inversion every 4 minutes as previously optimized. Digestion was stopped by the addition of 60 ul of 0.5 M EDTA and samples were placed on ice for 1-2 minutes before being centrifuged at 16000 x g for 1 minute at 4 °C. Pellets were then resuspended in 600 µl of ChIP buffer + PIC (provided in SimpleChIP kit) and incubated on ice for 10 minutes. Samples were then sonicated on ice using a Vibra Cell probe sonicator on setting 40 with 20 seconds on and 30 seconds rest for 2 pulses. Samples were then centrifuged at 9,400 x g for 10 minutes at 4 °C and the supernatant was subsequently used as chromatin material for immunoprecipitation. Chromatin fragmentation and concentration was then determined by reverse crosslinking a 50 µl aliquot according to the manufacturer’s instruction. Finally, 10-13 µg of chromatin was immunoprecipitated using an equal concentration of SOX9 antibody (cat #ab185230, Abcam, Cambridge, UK) according to the manufacturer’s instruction.

Samples were then sent to Quick Biology (Pasadena, CA) for final QC, library preparation, and sequencing. The ChIP-Seq library was prepared using a KAPA Hyper Prep Kit (KAPA Biosystems, Wilmington, MA) using 10 ng of DNA as input. Final library quality and quantity was analyzed by Agilent Bioanalyzer 2100 and Life Technologies Qubit3.0 Fluorometer. 150 bp paired end reads were sequenced on Illumina HighSeq 4000 (Illumnia Inc., San Diego, CA). NGS data was then analyzed by first trimming reads using Trimmomatic to reach a minimum read length of 20 bp and a phred score of ≥ 28. Reads were then aligned to the mouse genome build mm9 using Bowtie2, and then filtered using Samtools with a minimum MAPQ 30 setting. Peaks were finally called using MACS2 under default settings in paired-end mode. ChIP-Seq quality was assessed using ChIPQC and overlapping peaks were determined using Bedtools intercept function. Additionally, significant peaks were also identified based on the irreproducible discovery rate (Li et al., 2011) using the top 120,000 peaks per sample as inputs.

Table 2.3 ChIP-qPCR mouse primers (5' to 3')

Closest Gene	Forward	Reverse
Cnot	AACATCCCGGCTTCTCATT	GCTCACTGCTCCGAGACC
Gm16062	GGGTGACGTCAAAACTGACA	CTCCCAGAATCCAGAGGAAA
Rnf44	GTCTGGGCACACTACCTTCC	AGCTCTCCCCCTGACAGC
Ptgcd2/Mrps27	AGGGGCCGAAACACTGTAG	GAGCGCACCAAGTGGAAG
Nmral1	CCTAACAGAGCCCGTTCAGA	GTGAAGGGAGGAACCATCAG
Tardp	GATGCTAGCAGGCTCTTCG	GTGGCCGTTCTGTCCTTC
Nphp4	AGTCAGCGTGTGTTGGAGTC	TGTCCGTAAGAATCAATATGCAG
Sept11	AAGAAAGCCACAGGAAGGAA	ACCGTGATCCTGGTCAGC
Por	TTTAGAAGGGGAGCAAAAGC	GCGGTCCTGTAGGTCTCTGA
Sulf2	TCACGCCTAATTGCGGGCTGGTGT	CCCATGGGCACGGGAAGTGTGG
Cea1	ACATACTCCGAGCAGCAAGG	TGGAGTAAACCCCACCTCTG
SOMa	GCAAATGAAGCTAAACAACCTCAC	TTCCCTTGTCGGGTCAATTTCTCT
Mia	TACCTGGACCCTCCAGAGAC	AGGCCAGACGTTGAGTGTTT

2.11 Immunohistochemistry and Immunofluorescence staining

Tissue samples were first fixed in 10% neutral buffered formalin for a minimum of 24 hours then dehydrated in a tissue processor in the following conditions: 70% ethanol for 1 hour, 95% ethanol for 1 hour, 100% ethanol for 1 hour, 100% ethanol for 2 hours, 100% ethanol for 2 hours, xylenes for 1 hour, xylenes 1.5 hours, xylenes 1.5 hours, hot paraffin wax 2 hours, hot paraffin wax 3 hours. Samples were then embedded in paraffin blocks that could be sliced using a microtome and adhered to glass slides. Paraffin slides were then deparaffinized and rehydrated using a series of dunk tanks consisting of three xylene tanks, two 100% ethanol tanks, two 95% ethanol tanks, one 70% ethanol tank, one 50% ethanol tank, and two tanks of water with slides being submerged for 2 minute incubations in each tank. Cell culture staining was achieved by plating cells on glass coverslips and fixing cells in 10% neutral buffered formalin for 15 minutes before staining.

Hematoxylin and eosin staining were achieved by submerging slides in hematoxylin (cat # HHS16-500ML, Sigma, St. Louis, MO) for 2 minutes, followed by a wash step where slides were dipped 30+ times in a 3 L beaker of tap water. Slides were then submerged in 0.25% ammonia water (cat # 26123-10, Electron Microscopy sciences, Hatfield, PA) for 30 seconds, washed in tap

water once again, then submerged in eosin solution (cat # 1931492, Lerner Laboratories, defunct) for 2 minutes. Slides were then immediately dehydrated using a series of dunk tanks consisting of two 95% ethanol tanks, two 100% ethanol tanks, and two xylene tanks and mounted with VectaMount (SKU H-5000, Vector Laboratires, Burlingame, CA).

For nuclear staining on tissue sections (e.g. SOX9) antigen retrieval was performed using a citric acid based unmasking solution (SKU H-3300-250, Vector Laboratories, Burlingame, CA) and a 2100-Retriever (Cat #62706, Electron Microscopy sciences, Hatfield, PA). Slides were then washed with water and each tissue section was traced with a hydrophobic pen (SKU H-4000, Vector Laboratories, Burlingame, CA). The following steps were then performed at room temperature with five PBS washes between each step. Tissue samples were permeabilized with 0.1% triton X-100 in water for 20 minutes. For 3,3'-diaminobenzidine (DAB) staining endogenous peroxidases were blocked with 3% H_2O_2 in tap water for 5 minutes. Slides were then blocked for 1 hour with a blocking solution (SKU BMK-2202, Vector Laboratories, Burlingame, CA) containing 4 drops/mL of an avidin blocking solution (SKU SP-2001, Vector Laboratories, Burlingame, CA). Primary antibody was then prepared in a staining diluent (SKU BMK-2202, Vector Laboratories, Burlingame, CA) along with 4 drops/mL of a biotin blocking solution (SKU SP-2001, Vector Laboratories, Burlingame, CA) and slides were incubated for 1 hour. Secondary antibodies were diluted 1:200 in antibody staining diluent and slides were incubated for 10 minutes. If applicable tertiary antibodies were applied 1:200 for 10 minutes as well. For immunofluorescence staining 4',6-diamidino-2-phenylindole (DAPI) was added at 1:500 for 10 minutes and slides were finally mounted with VECTASHIELD Anti-fade mounting medium (SKU H-1000, Vector Laboratories, Burlingame, CA). For DAB staining an avidin/biotin-based peroxidase reagent (SKU PK-7100, Vector Laboratories, Burlingame, CA) was added and slides were incubated for 1 hour. Slides were then developed by eye using a DAB substrate solution (SKU SK-4105, Vector Laboratories, Burlingame, CA), followed by counter staining with hematoxylin (SKU H-3404-100, Vector Laboratories, Burlingame, CA). Slides were finally dehydrated using a series of dunk tanks consisting of two 95% ethanol tanks, two 100% ethanol tanks, and two xylene tanks and mounted with VectaMount (SKU H-5000, Vector Laboratires, Burlingame, CA). Imaging was performed on an epifluorescence microscope.

2.12 Immunoblots

Immunoblots were performed as described previously (Karki et al., 2015). Briefly protein lysates were isolated using ice cold RIPA buffer containing sodium vanadate as well as protease inhibitor and phosphatase inhibitor cocktails 2 and 3. For pancreas samples tissue was homogenized in RIPA buffer using a roto-stator, while samples from cultured cells were briefly sonicated. Debris was removed by centrifugation at 4 °C for 10 minutes at 5000 RPM. Protein concentrations were assessed using the Bio-Rad protein assay (cat # 5000006, Bio-Rad, Hercules, CA) according to the manufacturer's instructions. Samples were diluted in Laemmli sample loading buffer (cat # 1610747, Bio-Rad, Hercules, CA) and heated in a 95 °C sand bath for 5 minutes before loading in a 12% SDS polyacrylamide gel. Gel electrophoresis was performed at 30 mA for approximately 90 minutes or until sample loading dye had exited the gel chamber. The gel was then transferred to a PVDF membrane (cat # 1620177, Bio-Rad, Hercules, CA) at 300 mA for 1 hour with a cooling block added to prevent overheating. Membranes were then blocked overnight in 5% non-fat dry milk in TBS-T. The next day primary antibody was added at the required dilution in fresh 5% milk/TBS-T solution and rocked at room temperature for 1 hour. Membranes were then washed with TBS-T three times for 5 minutes each with rocking. A peroxidase conjugated secondary antibody was then added at 1:5000 dilution in 5% milk/TBS-T solution for one hour followed again by a TBS-T wash step. Finally, membranes were coated in ECL reagent (cat #32106, Thermo Scientific, Waltham, MA) and imaged on a Bio-Rad ChemiDoc Touch Imagine System.

Table 2.4 IHC/immunoblot antibody list

Antibody	Provider	Cat #
GAPDH	Abmion	AM4300
GFP	Abcam	ab13970
HSP90	Santa Cruz	sc-7947
SMA	Santa Cruz	sc-32251
RFP	Rockland	600-401-379

2.13 Cell culture

All cell lines were maintained at 37 °C with 5% CO_2. Panc-1 cells were cultured in high glucose DMEM containing L-glutamine and supplemented with 10% FBS and 1% penicillin/streptomycin. MiaPaCa2 cells and primary mouse cell lines (KC, KPC1, KPC2, and subsequent knockout and viral rescue lines) were cultured in RPMI 1640 containing L-glutamine and supplemented with 10% FBS and 1% penicillin/streptomycin. Cells were dissociated with trypsin and passaged every 2-3 days. Panc-1 and MiaPaCa2 cells were obtained from ATCC, while primary mouse cell lines were isolated in house and have been described previously (Jakubison et al., 2018; Yang et al., 2019b).

CHO cells were maintained in a proprietary DMEM-based medium with or without 8mM glutamine (Cat.G7512, Sigma-aldrich, St. Louis, MO) depending on the experimental conditions. Cells were cultured in shake flasks in temperature and CO_2-controlled incubators with shaking. Cells were passaged every 3-4 days

2.14 Generation of knockout cell lines

KPC2 knockout cell lines were generated using a modified CRISPR/Cas9 system that generates DNA double stranded breaks using Fok1 dimerization, analogous to the zinc finger nuclease gene editing technology, and thus requires dual guides for gene targeting and reducing the risk of off-target effects (see (Tsai et al., 2014). Guide RNA design was performed using the ZiFiT Targeter webtool (http://zifit.partners.org/ZiFiT/) and guides with the fewest potential off-target binding sites as identified using CasOT (Xiao et al., 2014) were selected. Guides were typically targeted to early coding exons where possible. Oligo design and vector cloning into the pSQT1313 vector (cat #53370, Addgene, Watertown, MA) were performed as clearly outlined in Tsai et al., (2014) supplemental material (Tsai et al., 2014). Cells were then transfected using X-tremeGene 9 transfection reagent (cat #6365787001, Roche, Basel, Switzerland) according to the manufacturer's instructions in a 6 cm dish format with 1.87 μg pSQT1601 (expressing Fok1-dCas9) (cat #53369, Addgene, Watertown, MA), 625 ng pSQT1313 (containing dual guide targeting inserts) (cat #53370, Addgene, Watertown, MA), and 150 ng linear puromycin marker. Cells were treated with 2 μg/mL puromycin starting on the following day. Two days post transfection cells were transferred to 4-5 150 cm dishes and puromycin selection was maintained until colonies

emerged and could be isolated using cloning rings. Individual colonies were then extracted and expanded in the absence of puromycin. The presence of insertions or deletions was then assessed using a polyacrylamide gel electrophoresis-based method (see (Zhu et al., 2014)) and confirmed by either immunoblot or ELISA.

For gene editing experiments performed at Eli Lilly, Cas12a protein from *Acidaminococcus sp.* was purchased from IDT (cat #1076159, IDT, Carolville, IA). IDT has since discontinued this version of Cas12a and released a newly optimized Cas12a V3 (cat #1081069, IDT, Carolville, IA) with improved editing efficiency and stability based on IDT internal research. Cas12a crRNAs were designed using Benchling webtools (www.benchling.com). All crRNAs had a 20 nucleotide guide sequence and targeted 5'-TTTV PAM sites. crRNAs were purchased from IDT along with IDT's electroporation enhancer (cat #1076301, IDT, Carolville, IA).

ZFNs targeting Gene A were designed and validated through the Sigma-Aldrich CompoZr Custom ZFN service (cat #SAFCZFN-1KT, Sigma-Adrich, St. Louis, MO). ZFN mRNA for transfection was generated by *in vitro* transcription from the provided plasmids. mRNA integrity was assessed prior to transfection by gel electrophoresis.

CRISPR/Cas12a transfections were carried out according to the manufacturer's instructions for ribonucleoprotein delivery (cat #1076159, IDT, Coralville, IA), but scaled up for use with a nucleofector 2b system (Lonza, Slough U.K.). ZFN transfections using CompoZr Custom ZFNs (Sigma-Aldrich, St. Louis, MO) were performed in accordance with Lilly internal operating procedure. All transfections of antibody expression vectors were performed using Lilly internal procedures and were followed by glutamine synthetase selection.

Bulk transfected cultures were sorted into single cell suspensions in 384 well plates using a MoFlo XDP Cell Sorter (Serial # 2216, Beckman Coulter, Atlanta, Georgia). Sorting was done under the most stringent conditions using a method demonstrated to yield single cell deposition in each well (Krebs et al., 2015). After outgrowth, cells were consolidated into 96 well plates and maintained in deep-well plates until knockout clonally derived cell lines were identified.

The Surveyor Mutation Detection assay (cat #706021, IDT, Carolville, IA) was used according to the manufacturer's protocol. Capillary electrophoresis was additionally used to confirm indel frequencies using a Caliper LabChip GXII with a HT DNA extended range LabChip (cat #760517, Perkin Elmer, Waltham, MA) and high sensitivity reagent kit (cat #CLS760672, Perkin Elmer, Waltham, MA). Indel detection by amplicon analysis (IDAA) was performed

according to the guidelines in Lonowski et al.'s protocol (Lonowski et al., 2017). Fragment analysis was performed by GeneWiz LLC and results were analyzed using Peak Scanner 2 (ThermoFisher, Waltham, MA). Sanger sequencing to confirm indels was performed by GeneWiz LLC following Topo-TA cloning (ThermoFisher, Waltham, MA) of PCR amplicons containing the target sites.

Mouse *Sox9* CRISPR guides and cloning oligos

Target site 1: TGGGGCTGGGGGCGCCAGAC

Left oligo 1: GCAGTGGGGCTGGGGGCGCCAGACGTTTTAG

Left oligo 2: AGCTCTAAAACGTCTGGCGCCCCCAGCCCCA

Target site 2: GGCTGGTTCGCCCTGTCCCT

Right oligo 1: GGCAGGGCTGGTTCGCCCTGTCCCT

Right oligo 2: AAACAGGGACAGGGCGAACCAGCCC

Mouse *Ptgs2* CRISPR guides and cloning oligos

Target site 1: ACTGTCAATCAAATATGATC

Left oligo 1: GCAGACTGTCAATCAAATATGATCGTTTTAG

Left oligo 2: AGCTCTAAAACGATCATATTTGATTGACAGT

Target site 2: TGCACTATGGTTACAAAAGC

Right oligo 1: GGCAGTGCACTATGGTTACAAAAGC

Right oligo 2: AAACGCTTTTGTAACCATAGTGCAC

Mouse *Csf2* CRISPR guides and cloning oligos (for clone #4, 15, & 18)

Target site 1: CCAAGGCCGGGTGACAGTGA

Left oligo 1: GCAGCCAAGGCCGGGTGACAGTGAGTTTTAG

Left oligo 2: AGCTCTAAAACTCACTGTCACCCGGCCTTGG

Target site 2: CAAAGAAGCCCTGAACCTCC

Right oligo 1: GGCAGCAAAGAAGCCCTGAACCTCC

Right oligo 2: AAACGGAGGTTCAGGGCTTCTTTGC

Mouse *Csf2* CRISPR guides and cloning oligos (for clone #21)

Target site 1: GGCTGTAGACCACAATGCCC

Left oligo 1: GCAGGGCTGTAGACCACAATGCCCGTTTTAG

Left oligo 2: AGCTCTAAAACGGGCATTGTGGTCTACAGCC

Target site 2: GCTCACCCATCACTGTCACC

Right oligo 1: GGCAGGCTCACCCATCACTGTCACC

Right oligo 2: AAACGGTGACAGTGATGGGTGAGCC

2.15 Transductions

Lentiviral particles were purchased from VectorBuilder for the expression of mouse *Csf2, Ptgs2, Siglec15, Il34,* and *Tgfb1*. Vector expression was driven by the EF1A promoter and included a neomycin selection marker. VectorBuilder CMV-EGFP:T2A:Puro-EF1A-mCherry containing lentiviral particles were used as controls [note: KPC2 cells did not express genes driven by the CMV promoter following lentiviral transduction]. shRNAs targeting mouse *Sgpp2* were purchased from Sigma in the pLKO.1-CMV-Neo vector (Clone ID: TRCN00000798, TRCN00000799, TRCN00000800, TRCN00000801, TRCN00000802, Sigma, St. Louis, MO) along with a nontargeting control vector. Based on knockdown efficiency TCRN00000798, TCRN00000801, and 50:50 mix of both particles was used to generate stable lines for the allograft experiments. A previously validated shRNA targeting human *Sox9* (Eberl et al., 2012) (Clone ID: TCRN0000020386, Sigma, St. Louis, MO) was cloned into the pLKOpuro.1 expression vector and lentiviral particles for transduction were isolated from transfected HEK293 cell supernatants by ultracentrifugation.

Cells were transduced in 12 well plates at an MOI of 1 with 10 μg/mL polybrene. The following day cells were transferred to a 6 well plate and transduced cells were selected using 250 μg/mL Geneticin G418 (cat #10131-035, Gibco, Waltham, MA), or fluorescence activated cell soring was used based on mCherry expression for the control expression vector. After a week of selection, passaging cells as needed, the transduced cell lines were assessed by RT-qPCR and used for subsequent experiments.

2.16 Soft agar colony formation assay

In a 6 well plate a 0.5% agarose base layer was prepared by dissolving 1% agarose in water using a microwave and combining this solution with an equal volume of 2x concentrate of DMEM with 20% FBS and 2% penicillin/streptomycin in order to achieve a final concentration of 0.5% agarose, 1x DMEM with 10% FBS and 1% penicillin/streptomycin. One mL of 0.5% base agarose was plated per well and allowed to cool at room temperature for 15 minutes. Using the same method as the base layer a 0.4% agarose and media solution was prepared and mixed with $5x10^3$ cells before plating at 1 mL/well. The top layer was again allowed to cool and then 500 µl of media was added to the top of each well. Media was replaced every 5-7 days for 4 weeks, then cells were stained with 0.005% crystal violet, imaged using a gel imager, and the colonies were enumerated using ImageJ (Schindelin et al., 2012).

2.17 Cell proliferation assay

Cell proliferation was determined using the CyQUANT cell proliferation assay (cat #C7026, Thermo Scientific, Waltham, MA) according to the manufacturer's instructions. Briefly, 1000 or 5000 cells were seeded on black flat clear bottom 96 well plates in 4-5 plates per assay. One plate was harvested per time point starting approximately 2-4 hours after plating. For each time point media was blotted on a paper towel and cells were washed once with 100 µl sterile PBS. Plates were again blotted dry, wrapped in parafilm and stored at -80 °C until all plates could be analyzed together. Wells were then treated with CyQUANT reagent and the fluorescence intensity was measured on a plate reader and used to the determine cell number and proliferation rates.

2.18 *In vitro* thrombin treatment

Once cells reached 50-60% confluency they were serum starved overnight. MiaPaCa2 cells were starved using serum free media while KPC2 cells were grown in 1% FBS containing media. The next day 1 U/mL thrombin was added to the media and cells were harvested accordingly. KPC2 cells were treated with bovine thrombin (cat #BT-1002a, Enzyme Research Lab, South Bend, IN), while MiaPaCa2 cells were treated with human thrombin (cat #HT-1002a, Enzyme Research Lab, South Bend, IN).

2.19 Transwell migration assay

Transwell assays were performed using 8 μm 24 well plate inserts (cat #662638, Greiner Bio-one, Monroe, NC). Cells were pre-treated with 1 U/mL thrombin or an equivalent volume of vehicle in serum free media containing 0.1% BSA for 1 hour prior to transwell seeding. Cells were dissociated using TrypLE reagent (cat #12604013, Gibco, Waltham, MA), washed twice in 0.1% BSA media, and $1x10^5$ cells were plated on the upper chamber in 100 μl 0.1% BSA media with 1 U/mL thrombin or vehicle equivalent while the lower chamber was filled with 600 μl 2% FBS media. Cells were incubated for 12 hours at 37 °C with 5% CO_2. Transwells were then fixed and stained using the differential Quik Modified Giemsa (cat #24606-250, Polysciences Inc., Warrington, PA) staining reagent and cells that did not migrate were then wiped away using a sterile cotton swab. The stained transwell inserts were then removed using a razorblade and mounted on coverslips in order to image and quantify cell migration by microscopy.

2.20 *In vitro* cytotoxic lymphocyte (CTL) assay

Mice were injected with $5x10^5$ $PAR1^{KO}$ or $5x10^4$ B16 cells into the hock and primed cytotoxic T lymphocytes (CTLs) were then harvested from the popliteal lymph node 18 days later. CTLs were expanded in culture using a bryostatin 1/ionomycin treatment strategy as outlined specifically in Kmieciak et al. 2011 (Kmieciak et al., 2011). Viable CTLs were then purified using Ficoll (cat #175446-02, GE Healthcare, Chicago, IL), and co-cultured with KPC or $PAR1^{KO}$ cells at various effector to target cell ratios and cytotoxicity was evaluated by lactate dehydrogenase (LDH) release (cat #C20300, Thermo Scientific, Waltham, MA).

2.21 ELISA

Briefly, cells were serum starved overnight in 1% FBS containing media, then 1 U/mL thrombin or vehicle equivalent was added and media was collected 48 hours later. Cell debris was removed by centrifugation at 1500 RPM for 10 minutes. If not used immediately conditioned media was frozen at -80 °C until use. ELISA's were subsequently performed according to the manufacturers instructions (Mouse GM-CSF Quantikine ELISA kit cat #MGM00, R&D Systems, Minneapolis, MN; Prostaglandin E_2 Express ELISA Kit cat #500141, Cayman Chemical, Ann Arbor, MI).

2.22 Tumor cell dissociation for flow cytometry

The tumor dissociation protocol was adapted and modified from Pasut et al. (2012) (Pasut et al., 2012). Tumor samples between 10-100 mm^3 were excised and placed in ice cold PBS until all samples were harvested. Tumors were then finely minced with a razor blade and resuspended in 1 mL digestion buffer (2 U/mL Collagenase B, cat #11088815001, Roche, Basel, Switzerland; 2 U/mL Dispase II in 10 mM NaAc (pH 7.5), 5 mM CaAC buffer, cat #D4693-1G, Sigma, St. Louis, MO; 50 mM HEPES pH 7.4; 150 mM NaCl; 1 ug/mL DNase I; bring volume to 1 mL/sample with PBS). The tissue was then incubated in a 37 °C water bath and mixed by pipetting every 15 minutes for 45 minutes or until samples were well digested. 1 mL 20% FBS in PBS was then added to the digestion mix and samples were passed through a 70 μm filter and spun at 1000 RPM for 5 minutes at 4 °C. The supernatant was then transferred to a new tube and centrifuged as before. Pellets from both centrifugation steps were combined and resuspended in 500 μl red blood cell lysis buffer (150 mM NH_4Cl, 10 mM $KHCO_3$, 0.1 mM Na_2EDTA in water, pH 7.2-7.4) and allowed to sit at room temperature for 2 minutes. This was then quenched using 3 mL of 10% FBS in PBS. Samples were passed through a 40 μm filter and centrifuged at 1000 RPM for 5 minutes at 4 °C. The supernatant was then discarded, and pellets were resuspended in 5 mL of 5% FBS in PBS and centrifuged a final time at 2000 RPM for 5 minutes at 4 °C. Pellets were resuspended in MACS buffer (1 mM EDTA, 2% FBS in PBS) and stained for flow cytometry.

2.23 Flow cytometry

Cell suspensions in MACS buffer ($1x10^6$-$1x10^8$ cell/stain) were blocked with a 1:100 dilution of Fc block (cat #553142, BD Biosciences, San Jose, CA) for 20 minutes on ice. Cells were then stained for 30 minutes on ice and protected from light with fluorescently-conjugated antibodies at 1:400 dilution each and a 1:1000 dilution of live/dead stain (cat #L34955, Thermo Scientific, Waltham, MA) where appropriate. Cells were then washed with 2 mL MACS buffer and centrifuged for 5 minutes at 1800 RPM. This wash step was repeated, and cells were finally resuspended in 500 µl MACS buffer and transferred to a 35 µm filter cap tube before being analyzed on a BD LSRFortessa flow cytometer. Compensation controls were set up using UltraComp eBeads (cat # 01-2222-42, Thermo Scientific, Waltham, MA). Final analysis was performed using FlowJo.

Table 2.5 Antibodies used for flowcytometry

Antibody	Provider	Clone ID
CD45	BioLegend	30-F11
CD3	BioLegend	17A2
CD8a	BioLegend	53-6.7
CD4	eBiosciences	RM4-5
CD11b	BioLegend	M1/70
Ly6C	BioLegend	HK1.4
Ly6G	Invitrogen	1A8-Ly6g
F4/80	BioLegend	BM8
Nk1.1	eBiosciences	PK136
CD49b	eBiosciences	DX5
PDL1	BioLegend	10F.9G2
H-2kb	BioLegend	AF6-88.5

2.24 Terminal studies in shake flasks

Seventeen day shake flask terminal studies were performed for titer analysis. Cells were cultured in temperature and CO_2-controlled incubators with shaking and were regularly fed on predetermined days. Titers were measured on days 10, 14 and 17 using a Cedex Bio HT (Roche, Indianapolis, IN) or Octet Red 96 (FortéBio, Menlo Park, CA). Supernatants from day 17 were kept and antibody was isolated by protein A capture for titer and product quality analysis.

2.25 LC-MS/MS shotgun proteomics analysis

Antibody titers for proteomic analysis were isolated by protein A capture, while whole cell lysates for the detection of Gene A were generated using sonication-based cell disruption. The shotgun proteomics experiment was performed by Ning Wang at Eli Lilly as previously described by Huang (Huang et al., 2017). Briefly, aliquots containing 0.2 mg proteins were mixed with 5.0 µL of 1 M tris-HCl buffer, pH 8, and digested by 1.6 µL of 2.5 mg/mL recombinant bovine trypsin (Eli Lilly and Company, Indianapolis, IN) at 37 ºC overnight, followed by reduction with 2 µL of 50 mg/mL dithiothreitol (DTT) (Thermo Fisher Scientific, Rockford, IL) at 90 ˚C for 10 min. Each sample was then centrifuged at 13,000 g for 2 min and the supernatant was mixed with 5 µL of 10% formic acid in water. The LC-MS/MS experiment was performed on a Waters Acquity UPLC (Milford, MA) coupled to a Thermo Scientific Q Exactive Plus mass spectrometer (Bremen, Germany). The tryptic digests were injected onto a Waters Acquity UPLC CSH C18 (2.1×50 mm, 1.7 µm particle size) column, which was maintained at 60 °C. Mobile Phase A comprised of 0.1% formic acid in water and Mobile Phase B 0.1% formic acid in acetonitrile. Separation was achieved by starting at 0% B and maintaining it for 2 min, ramping it up linearly to 10% B over 23 min, to 20% B over 57 minutes, to 30% over 30, followed with multiple zig-zag wash cycles. Data-dependent MS/MS was performed as follows: the first event was the survey positive mass scan (m/z range of 230 – 1500) followed by 10 HCD events (28% NCE) on the 10 most abundant ions from the first event. The dynamic exclusion duration of 60 s was used with a single repeat count.

2.26 LC-MS/MS peptide mapping

40 µg of Pro-A captured sample was first dried down and then mixed with 10 µL of 6 M guanidine•HCl (Thermo Fisher Scientific, Rockford, IL), 250 mM tris-HCl buffer, pH 8. The samples were then reduced by 1 µL of 50 mg/mL DTT at 37 °C for 45 minutes and alkylated by 3 µL of 50 mg/mL iodoacetamide (Sigma-Aldrich, St.Louis, MO) solution in the dark at room temperature for 30 minutes. Additional 1 µL of 50 mg/mL DTT and 169 µL of 50 mM tris buffer, pH 8, was then added. The reduced and alkylated samples were digested by a mixture of 5 µL of 0.1 µg/µL Lys-C (Wako, Richmond, VA) and 10 µL of 0.1 µg/µl trypsin (Promega, Madison, WI) at 37°C for 3 hours and the digestion was quenched with 1 µL of 50% trifluoroacetic acid (TFA) in water before LC-MS/MS analysis. 30 µL of each tryptic digest was injected onto a Waters Acquity UPLC BEH C18 (2.1×150 mm, 1.7 µm particle size) column. The LC-MS experiment was performed on a Waters Acquity UPLC coupled to a Thermo Scientific Orbitrap Elite mass spectrometer. The flow rate was set at 250 µL/min and the column temperature was maintained at 60 °C. Mobile Phase A comprised of 0.05% TFA in water and Mobile Phase B 0.04% TFA in acetonitrile. Separation was achieved by starting at 0% B and maintaining it for 2 min, ramping it up linearly to 40% B over 80 min, and followed by multiple zig-zag wash cycles at a flow rate of 400 µL/min. The MS instrument was operated in positive mode with a source voltage of 4 kV, an S-Lens RF level of 60, a capillary temperature of 350 ºC, a sheath gas flow rate of 35, and an auxiliary gas flow rate of 10. Data-dependent MS/MS was performed as follows: the first event was the survey positive mass scan (m/z range of 130 – 2000) followed by 5 CID events (35 V collision energy) on the 5 most abundant ions from the first event. Resolution was set at 120,000 and 30,000 for survey scans and MS/MS events, respectively.

2.27 Statistical methods

RT-qPCR, proliferation assays, and tumor mass data were analyzed by two-tailed unpaired Student's *t*-test. When multiple comparisons were made a standard ANOVA followed by either Dunnett's or Tukey's test was used as indicated. Tumor growth over time was analyzed using repeated measures ANOVA. All data are presented as mean ± SEM. * $p < 0.05$; ** $p < 0.01$; *** $p < 0.001$; *** $p < 0.0001$; n.s. – not significant.

CHAPTER 3. SOX9 IS CRITICAL FOR PDAC INITIATION, BUT IS NOT REQUIRED FOR LATE STAGE TUMOR MAINTENANCE

3.1 Introduction

When exposed to cellular stress, such as inflammation from pancreatitis, acinar cells display a high level of plasticity and undergo a process termed acinar-to-ductal metaplasia (ADM) (reviewed in: (Puri et al., 2014; Storz, 2017). During this transition critical transcription factors necessary for maintaining acinar cell identity are silenced, while ductal and progenitor cell defining factors become expressed. The formation of ADM lesions is a transient process in the maintenance of pancreatic homeostasis, and acinar cell redifferentiation and repopulation typically occurs once the inciting cellular insult subsides. However, transgenic mouse models indicate that ADM lesions persist in the presence of oncogenic KRAS and give rise to premalignant pancreatic intraepithelial neoplasia (PanIN), which over time can progress to PDAC. Loss of acinar identity is therefore one of the earliest steps in PDAC initiation, and research has demonstrated that changes in the transcriptional programming of acinar cells is a critical phase in this process. Indeed, loss of acinar cell-specific transcription factors such as *Mist1* (Shi et al., 2009) or *Ptf1a* (Krah et al., 2015) hastens PanIN formation in PDAC mouse models, while forced expression of either factor can limit disease progression (Direnzo et al., 2012; Jakubison et al., 2018; Krah et al., 2019; Shi et al., 2013). Remarkably, transgenic mouse studies that allowed for conditional deletion of *Sox9* in the acinar cells of the adult pancreas while simultaneously inducing $Kras^{G12D}$ expression revealed that aberrant expression of the transcription factor SOX9 is required for ADM to progress into PanIN lesions. Indeed, lesions did not form in the absence of SOX9, even when pancreatitis induced inflammation was used to exacerbate disease progression (Kopp et al., 2012). Conversely, lesion formation is accelerated when *Sox9* is ectopically expressed in the acinar cell compartment (Kopp et al., 2012). These striking results reveal SOX9 to be a pivotal gatekeeper in PDAC initiation, and one of the few known factors required for disease progression. However, why and how SOX9 promotes PanIN formation has not been fully elucidated and requires further research.

SOX9 is a master regulator crucial for the proper development and maintenance of several cell types, including pancreatic progenitor cells, chondrocytes, and Sertoli cells among many others (Lefebvre et al., 2007; Sarkar and Hochedlinger, 2013). Given SOX9's role in

differentiation, and the diverse and highly specialized nature of the tissues in which it is expressed, it is not surprising that SOX9 regulates distinct gene networks based on its cellular context. It is believed that differences in SOX9's tissue-dependent gene regulation patterns are in part dictated by its interactions with cell type specific DNA binding partners, which also help overcome SOX9's inherently weak DNA binding affinity (Kamachi et al., 2000; Lefebvre et al., 2007). However, this means SOX9's role in each tissue must be examined on an individual basis, as generalizations about target gene regulation may not hold true for all cell types. Adding to this difficultly is the finding that *in vivo* SOX9 binds to a poorly defined DNA consensus sequence, making it impractical to identify putative gene targets *in siloco* based on sequence data alone (Lefebvre et al., 2007). For this reason, further investigation into SOX9's transcriptional network to identify potential gene targets critical for PDAC initiation requires both *in vivo* models and omics based experimental approaches to capture the tissue and context dependent nature of SOX9's activity.

My research has therefore focused on understanding how SOX9 promotes PanIN formation and determining if SOX9's role in PDAC progression extends beyond disease initiation and into tumorigenesis and tumor maintenance. As a transcription factor SOX9's primary function is to regulate the expression of gene networks. Accordingly, it stands to reason that SOX9 promotes PDAC initiation through the transcriptional regulation of specific gene targets that in turn perform tasks or enhance signals critical for cellular transformation. However, as described earlier, SOX9's specific gene regulatory activity is highly dependent on its cellular context. This makes it difficult to glean insight into the precise functionality of SOX9 in PDAC progression based on any prior research in other cell types. Instead it is best to examine SOX9's activity in as close to its endogenous environment as possible. Therefore, to identify SOX9 regulated gene targets critical for PDAC initiation I utilized *in vivo* models to mimic early events in PDAC progression and transcriptomic approaches to identify SOX9-dependent gene regulatory events. Additionally, to assess the role of SOX9 in established PDAC cells, I examined the effects of SOX9 ablation of allograft tumor growth in various primary mouse PDAC cell lines.

3.2 Results

3.2.1 SOX9 is critical for PanIN formation

PDAC shares many characteristics with pancreatic duct cells. However, studies using genetically engineered mice (GEM) indicate that pancreatic acinar cells are particularly susceptible to malignant transformation and can give rise to metastatic disease, implicating these cells as a likely origin of PDAC (Grippo et al., 2003; Guerra et al., 2007; Habbe et al., 2008; Kopp et al., 2012; De La O et al., 2008; Morris et al., 2010b; Shi et al., 2009). Though all cells in the pancreas arise from SOX9 positive progenitors, SOX9 is excluded from pancreatic acinar cells and is restricted to duct and centroacinar cells in the adult organ (Seymour, 2014). Indeed, SOX9 expression is absent in acinar cells of the adult pancreas but is aberrantly expressed in acinar-derived premalignant ADM and PanIN lesions, as well as frank PDAC (Figure 3.1). Importantly, similar expression patterns have been observed in patient tissue samples as well (Kopp et al., 2012).

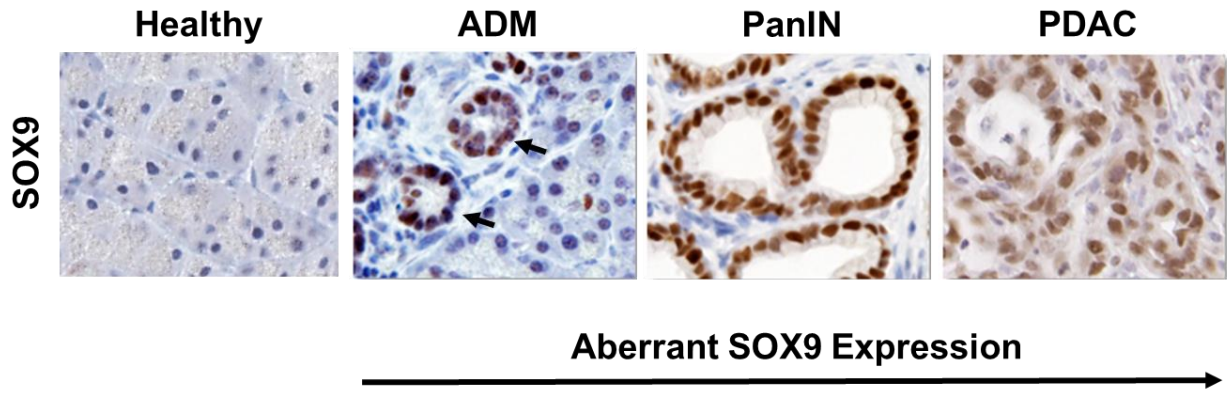

Figure 3.1 SOX9 is aberrantly expressed during PDAC pathogenesis.

DAB staining for SOX9 on mouse tissue sections, showing that SOX9 is absent from healthy acinar cells but readily detected in ADM lesions (black arrows), PanIN and PDAC cells.

Previous research has indicated that the forced expression of transcription factors critical for maintaining acinar cell identity and differentiation status can delay or even revert PanIN formation. Therefore, to determine if expression of SOX9 could conversely accelerate lesion formation a transgenic mouse model was used to ectopically induce expression of a *Sox9* transgene in pancreatic acinar cells. Initial effort was put towards generating a novel Cre recombinase inducible transgenic mouse line that could express an HA-tagged mouse *Sox9* transgene (Figure 3.2A). Though these mice were eventually developed and did show Cre recombinase dependent *Sox9* expression (Figure 3.2BC), prior to their full characterization our lab obtained a previously established *LSL-Sox9-IRES-GFP* expressing transgenic mouse line (Figure 3.3AB) as a gift from Dr. Kathryn Cheah, referred to as inducible SOX9 or iSOX9 mice. The iSOX9 mice had been previously employed by others to examine the role of SOX9 in neural stem cell maintenance (Scott et al., 2010), prostate cancer development (Thomsen et al., 2011) and chondrogenesis (Leung et al., 2011) and so we decided to use this more characterized line for our studies. iSox9 mice were crossbred with a *LSL-Kras*^{G12D}*; Mist1*^{CreER} (KC) mouse line to enable acinar cell-specific, tamoxifen inducible expression of oncogenic KRAS and SOX9. PanIN lesions form gradually in KC mice, and relatively few lesions were observed when pancreata were harvested at 8 weeks post transgene induction. However, pancreata from iSOX9 expressing KC mice displayed a dramatic and significant increase in PanIN lesions. These lesions stained positively for GFP indicating that they originated from iSOX9 expressing cells (Figure 3.4AB). Additionally, ectopic expression of SOX9 in the absence of KRAS^{G12D} delayed tissue recovery from caerulein-induced pancreatitis (Figure 3.5). These findings show that forced expression of SOX9 can exacerbate lesion formation, especially in the presence of oncogenic KRAS.

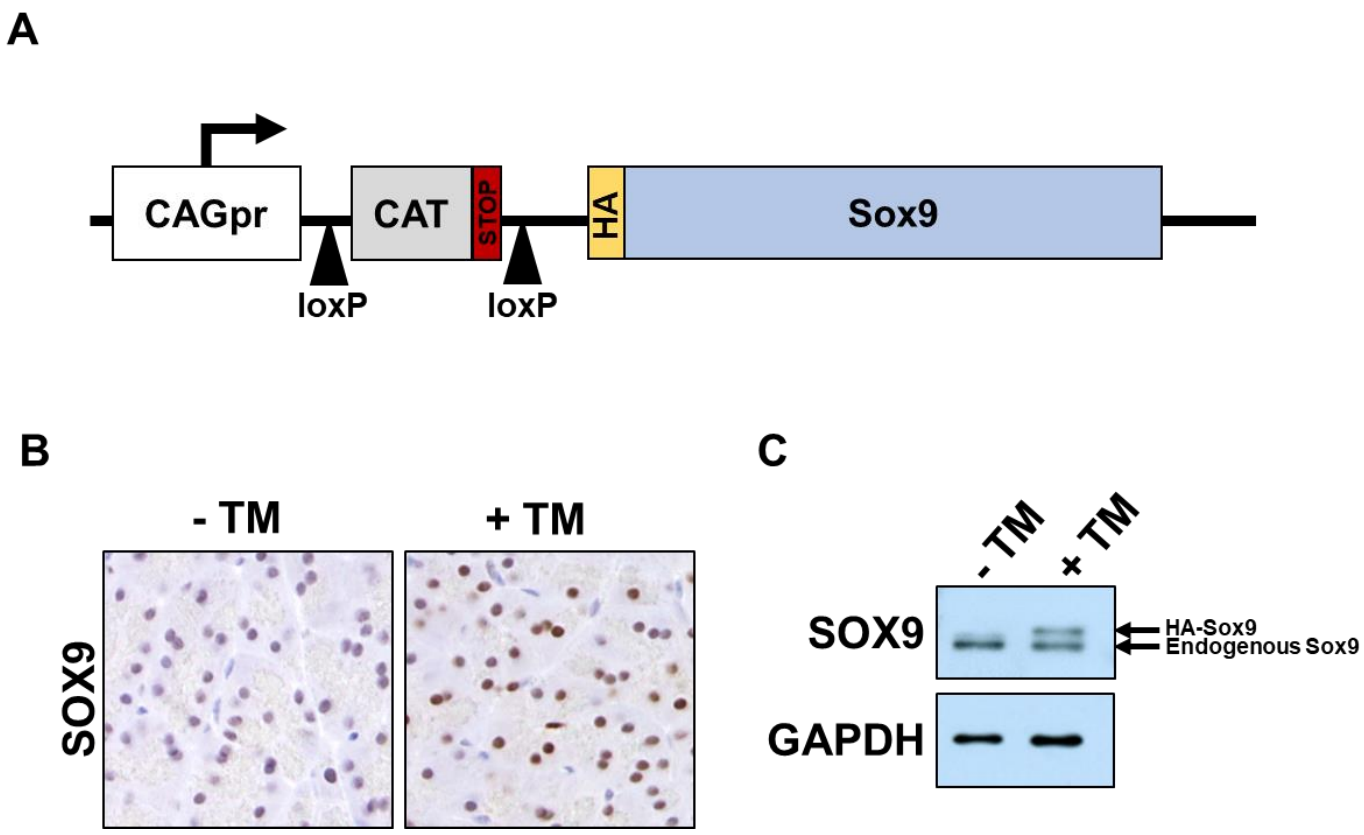

Figure 3.2 Design and expression of the *LSL-HA-msSox9* mouse line.

(A) A diagram of the *LSL-HA-msSox9* vector which is driven by a CAG promoter and has a C-terminal HA tag. **(B)** SOX9 staining of pancreas sections taken from *Mist1*^{CreER}*; LSL-HA-msSox9* mice 72 hours after treatment with tamoxifen (TM) or vehicle. Brown staining shows SOX9 positive acinar cells only in the tamoxifen treated animal. **(C)** Immunoblot data from the pancreas samples shown in **(B)** indicating that HA-tagged SOX9 is only detected in the tamoxifen treated group. Note that endogenous SOX9 appears at a lower molecular weight and is detectable in both samples due to its expression in pancreatic duct cells.

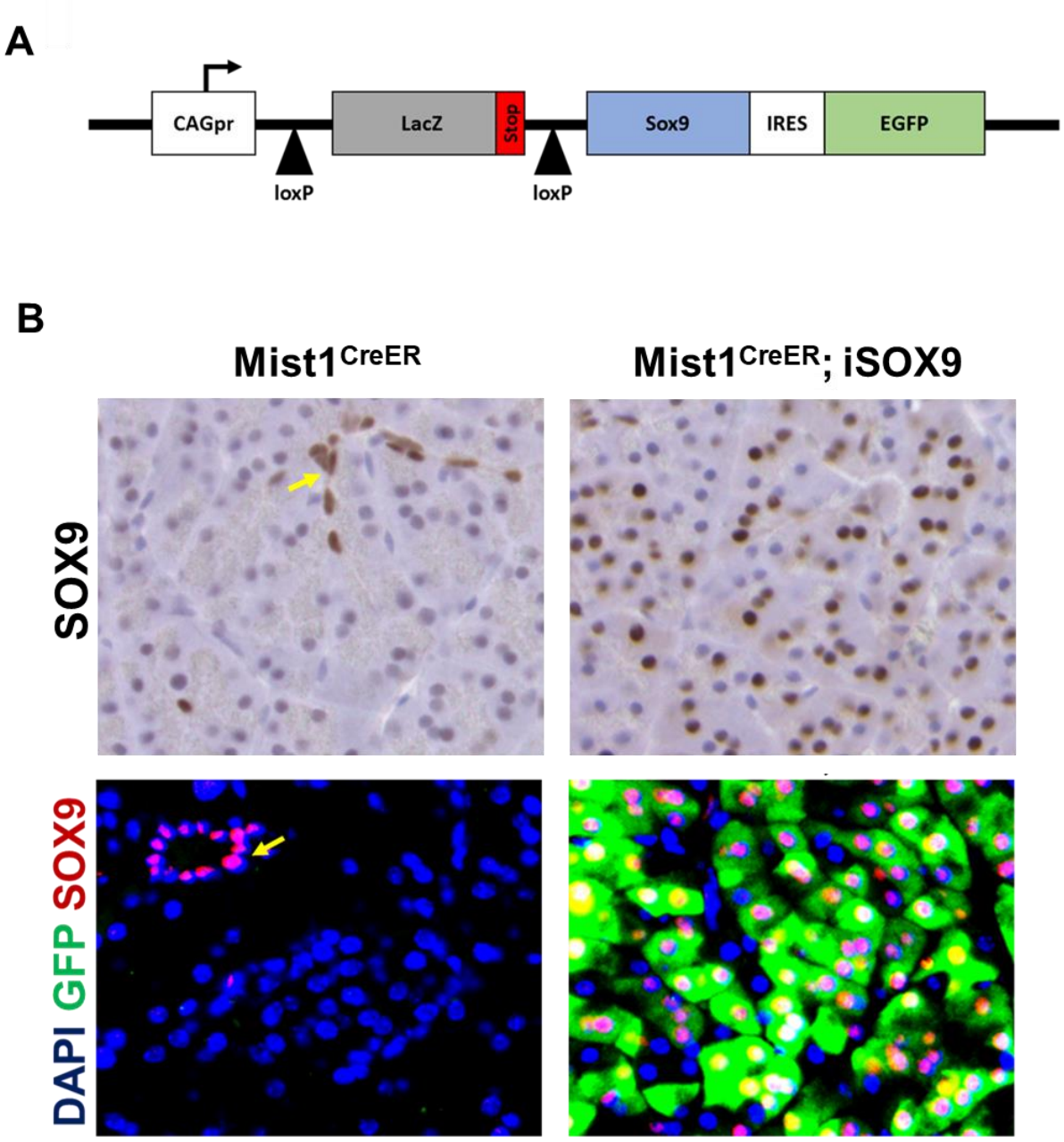

Figure 3.3 Diagram and expression results of the iSOX9 mouse model.

(A) Schematic showing the design of the iSOX9 transgene which contains the full length mouse *Sox9* sequence and will coexpress SOX9 and EGFP from the CAG promoter following Cre recombinase mediated recombination of the upstream loxP sites. **(B)** SOX9 (top) and immunofluorescence staining (bottom) of mouse pancreas sections 72 hours post tamoxifen treatment showing widespread ectopic coexpression of SOX9 and EGFP in the iSOX9 mouse model. The yellow arrow marks a SOX9 positive duct in the Mist1^{CreER} control sample.

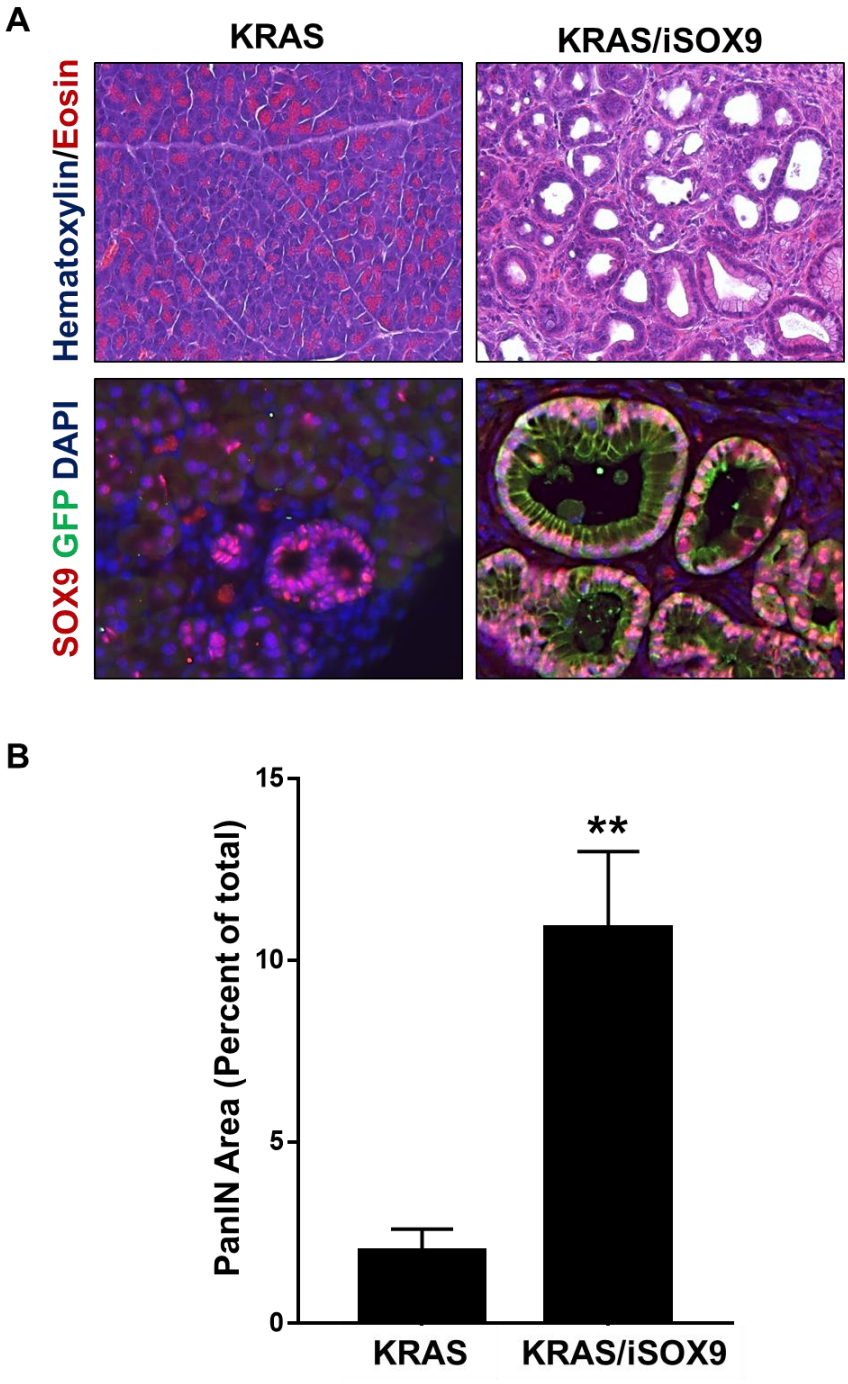

Figure 3.4 SOX9 accelerates PanIN lesion formation in KRAS^{G12D} expressing mice.

(A) Upper: Histology from mouse pancreata showing that forced expression of SOX9 through the iSOX9 transgene accelerates PanIN formation in the presence of oncogenic KRAS^{G12D} (KRAS). Lower: GFP/SOX9 co-staining indicating that PanIN lesions arise from iSOX9 expressing cells (samples taken 8 weeks post *Kras*^{G12D} activation). **(B)** Quantification of lesions in A based on alcian blue staining of mucinous PanIN lesions as a percentage of total tissue area. (n = 4 mice/group; ** $p < 0.01$)

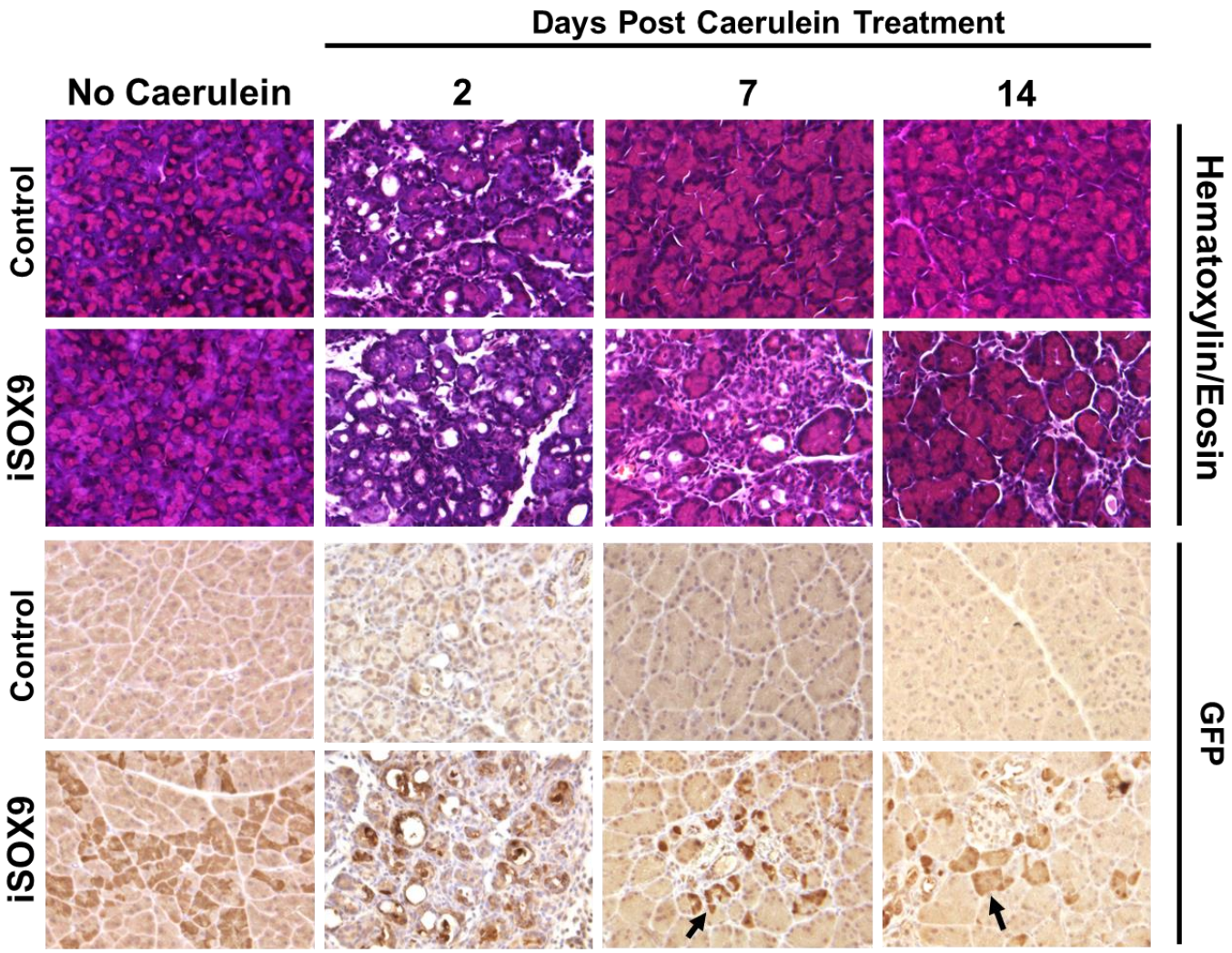

Figure 3.5 iSOX9 expression delays recovery from acute pancreatitis.

Tissue sections from Mist1^{CreER} (Control) and Mist1^{CreER}; iSOX9 (iSOX9) mice. Six-week-old mice were dosed with tamoxifen to activate the iSOX9 transgene one week prior to the initiation of caerulein-induced pancreatitis treatment. Hematoxylin and eosin staining shows severe tissue damage at 2 days post treatment in both groups. Control pancreata were largely recovered within 7 days while areas of damage were still present in the iSOX9 group. GFP staining indicates that lesions remaining at 7 days post treatment arise from iSOX9 expressing cells (black arrow) and further shows that many of these cells return to a phenotypically normal state within 14 days of caerulein treatment (black arrow)

To determine if SOX9 not only accelerates disease progression, but is actually required for PanIN formation, a *Sox9* floxed (*Sox9*$^{fl/fl}$) mouse model (Akiyama et al., 2002) was used to prevent SOX9 expression in the acinar cell compartment. To achieve this goal *Sox9*$^{fl/fl}$ mice were bred with KC mice to generate *LSL-Kras*^{G12D}*; Mist1*^{CreER}*; Sox9*$^{fl/fl}$ (KC/ΔSOX9) mice. These animals were then dosed with tamoxifen between 6-8 weeks of age in order to activate acinar-cell specific Cre recombinase activity, causing simultaneous deletion of *Sox9* and expression of oncogenic *Kras* exclusively in pancreatic acinar cells. Mice were also treated with caerulein to induce acute pancreatitis (AP) as a method to predictably induce PanIN formation in KC mice within 3-4 weeks (Carrière et al., 2009). Remarkably, histology from KC/ΔSOX9 pancreata resembled untreated control tissue, while tissue from KC mice displayed widespread lesion formation and desmoplasia (Figure 3.6). Furthermore, all PanIN lesions identified in the KC/ΔSOX9 samples stained positively for SOX9 (Figure 3.6) indicating they originated from cells that failed to properly delete *Sox9*. Thus, it appeared that KRAS^{G12D} activity induced PanIN formation only if SOX9 was present. However, due to the imperfect penetrance of *Sox9* deletion it was not possible to extend these findings to determine the impact of SOX9 on PDAC development and survival. Indeed, SOX9 positive tumors developed readily in *LSL-Kras*^{G12D}*; LSL-Trp53*^{R127H}*; Elastasepr*^{CreER}*; Sox9*$^{fl/fl}$ mice (Figure 3.7). Taken as a whole the results of our experiments indicate that SOX9 is aberrantly expressed prior to the development of PanINs during PDAC initiation, and that SOX9 is not only required for PanIN formation but can accelerate disease progression if ectopically expressed along with oncogenic KRAS in pancreatic acinar cells.

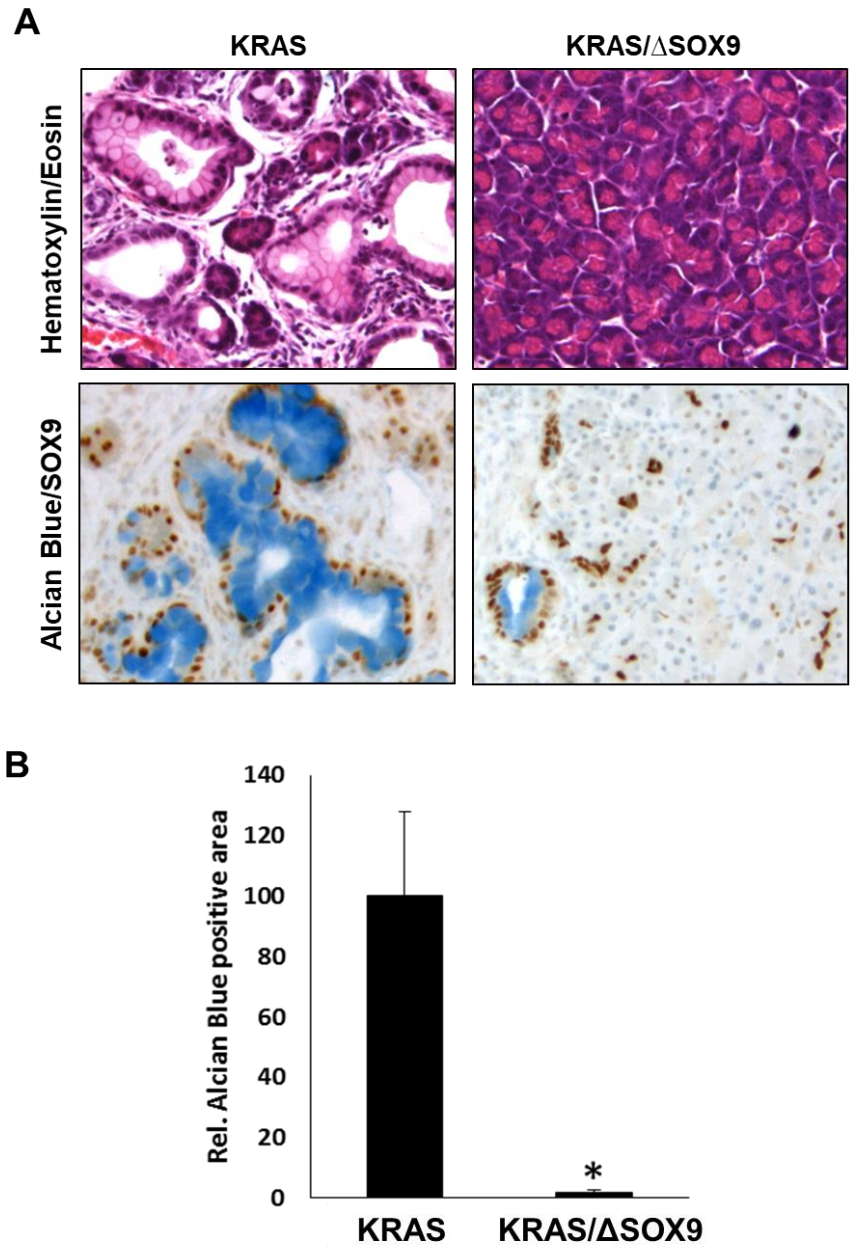

Figure 3.6 SOX9 is required for PanIN formation.

(A) Pancreas histology from $KRAS^{G12D}$ expressing mice with either endogenous SOX9 expression (KRAS) or genetic deletion of SOX9 (KRAS/ΔSOX9). Samples were taken 26 days post caerulein induced acute pancreatitis. Alcian blue staining (lower panel) marks PanIN lesions which also stain positively for SOX9, even in the ΔSOX9 samples (brown stain). **(B)** Quantification of the relative alcian blue positive areas (n = 4-5 mice/group), * $p < 0.05$

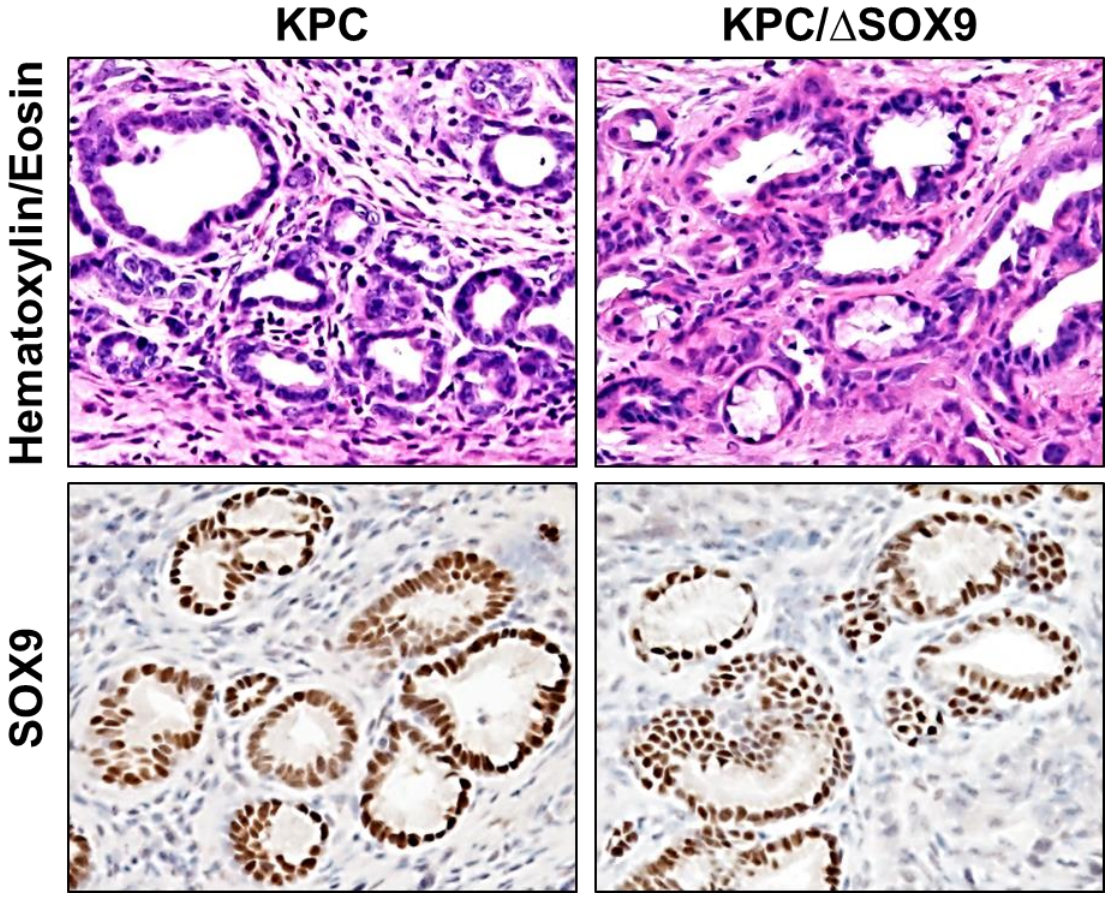

Figure 3.7 Cells that escape SOX9 deletion give rise to high grade lesions and PDAC.

KPC and KPCΔSOX9 mice both exhibit high grade PanIN lesions and develop PDAC tumors. SOX9 staining indicates PanIN and PDAC epithelial cells from KPCΔSOX9 mice still express SOX9 (brown stain).

3.2.2 SOX9 promotes malignant properties in human Panc-1 cells but is not required for tumor growth and maintenance in syngeneic allograft models

It is clear that SOX9 plays a critical role in the early stages of PDAC initiation, specifically contributing to the development of premalignant PanIN lesions. However, whether SOX9 is also important for the progression and maintenance of established PDAC cells remains to be fully determined. To this end, *SOX9* expression was knocked-down using shRNA in Panc-1 cells, which are a commonly used human PDAC cell line (Figure 3.8AB). Reduction of SOX9 expression significantly decreased Panc-1 cell proliferation and soft agar colony formation (Figure 3.8CD). Additionally, xenograft tumor growth was also significantly reduced upon *SOX9* knockdown (Figure 3.8E), despite the finding that SOX9 expression was largely indistinguishable between experimental and control tumors by the study's end point (Figure 3.9A-C). Because a heterogenous pooled cell population was used for this study, the "re-expression" of SOX9 in the knockout tumors may have been the result of selective pressure within the tumor that provided a survival advantage to cells retaining high levels of SOX9 expression. Panc-1 is not a very aggressive PDAC cell line, forming tumors gradually over a long period in xenograft studies, and because they are of human origin, they must be grown in immunocompromised mice for all tumor growth studies. Therefore, to further study SOX9's role in established tumor cells the initial study was repeated using aggressive syngeneic KPC cell lines. This allowed allograft tumor growth experiments to be performed in immunocompetent mice and, because CRISPR/Cas9 was used to ablate SOX9 expression for these studies, this eliminated the risk that SOX9 expression might "re-emerge" during the course of the study. The KPC2 cell line was examined first. Of note, copy number variant analysis by qPCR (Haurogné et al., 2007) showed no signs of *Sox9* gene amplification in the KPC2 cells (Figure 3.10). $SOX9^{KO}$ cells were generated using a modified CRISPR/Cas9 system (Tsai et al., 2014) targeting a region within exon 1 of *Sox9*, roughly 80 nucleotides from the start codon (Figure 3.11A). Loss of SOX9 was confirmed by immunoblot, immunofluorescence staining, and RT-qPCR (Figure 3.11B-D). Surprisingly allograft tumor growth was highly variable in the $SOX9^{KO}$ cell lines (Figure 3.12A), as some lines were nontumorigenic, while others grew far more aggressively than the KPC2 parental cells. This appears to have been due to heterogeneity within the original KPC2 parental cell population, which was generated from a mouse PDAC tumor, and was not related to expression of SOX9 as confirmed by immunohistochemistry analysis of tumor sections (Figure 3.12B). Indeed, subclones

isolated from the original KPC2 cell line displayed variable allograft tumor growth similar to that observed in the SOX9^{KO} cells (Figure 3.13A). A subcloned version of the KPC2 cell line (KPC2c1) was generated for future studies that faithfully replicated the tumor growth pattern of the parental

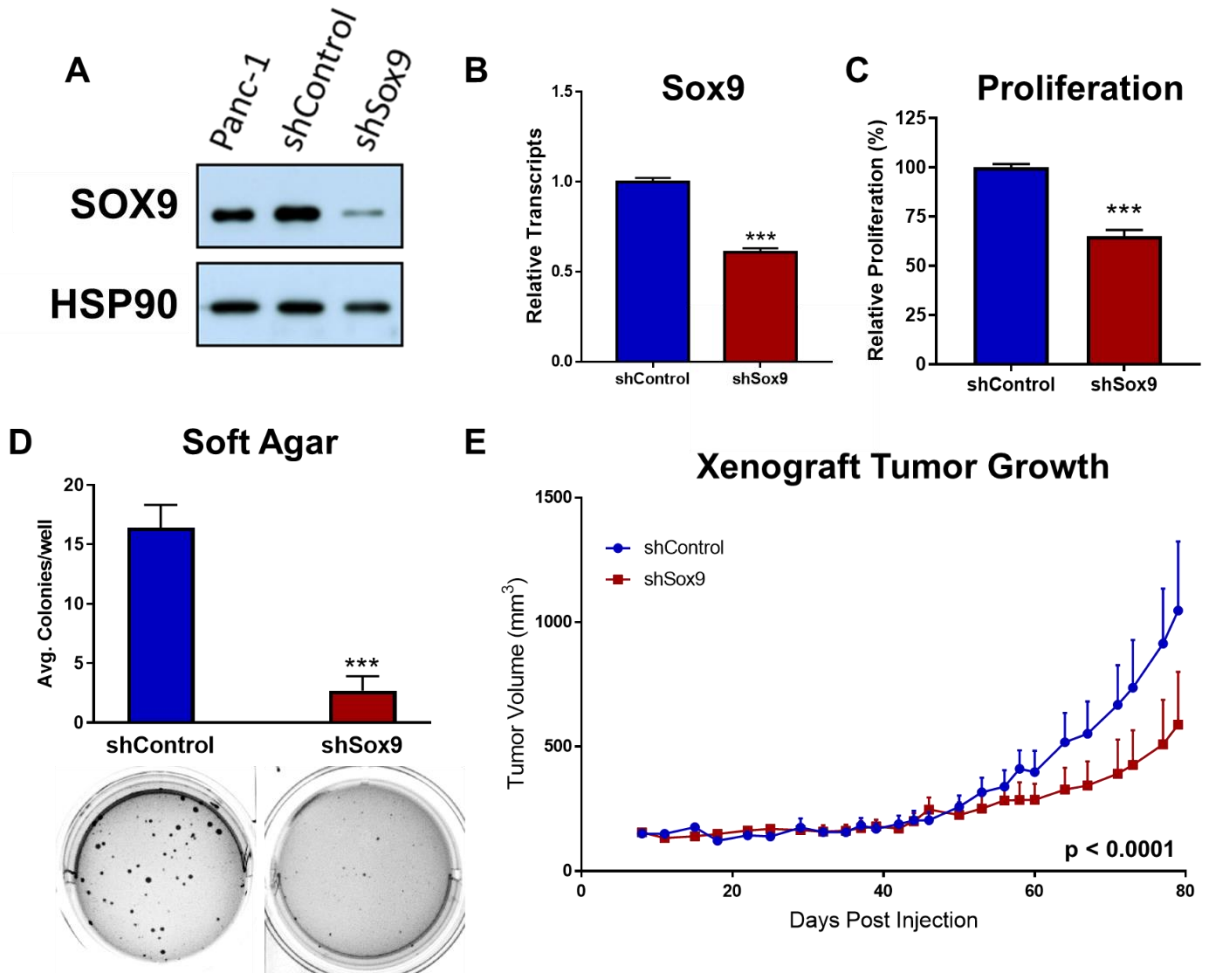

Figure 3.8 SOX9 knockdown reduces tumorigenic properties in PDAC cells

(A) Immunoblot showing a reduction of SOX9 expression in Panc-1 cells transduced with a *SOX9* targeting shRNA. **(B)** *SOX9* transcripts are significantly reduced in shSOX9 expressing cells (n = 3/group). **(C)** Cell proliferation is significantly decreased following SOX9 knockdown (n = 3/group). **(D)** SOX9 knockdown drastically reduces soft agar colony formation in Panc-1 cells (n = 5/group). **(E)** Xenograft tumor growth is significantly impaired in shSOX9 Panc-1 cells compared to controls (n = 10/group, RM-ANOVA). *** $p < 0.001$

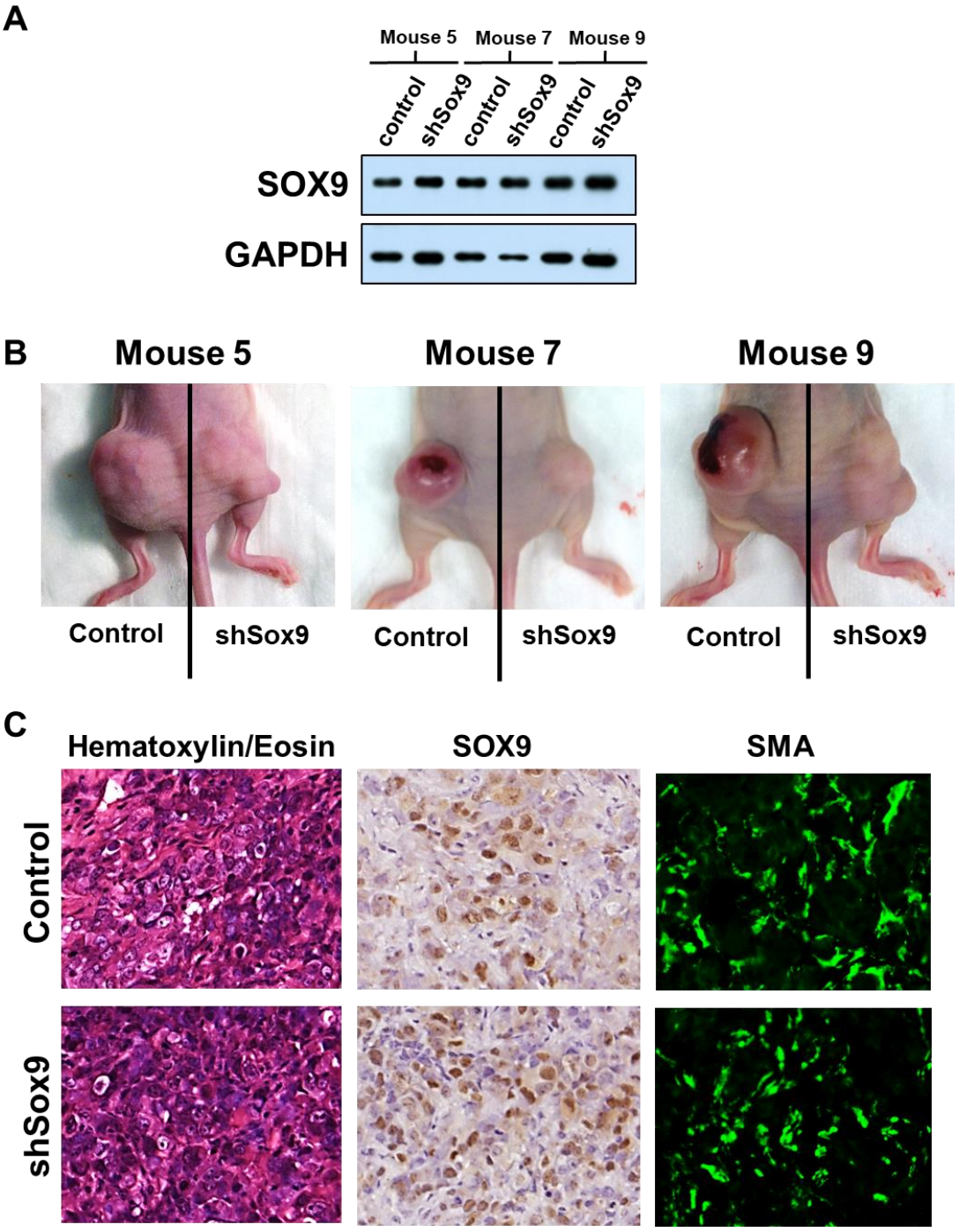

Figure 3.9 SOX9 expression is still detectable in shSOX9 expressing Panc-1 xenograft tumors.

(A) Immunoblot showing SOX9 expression levels from the control (shControl) and shSOX9 Panc-1 xenograft tumor described in Figure 3.8 E. **(B)** Images of the tumors analyzed in (A) prior to excision. **(C)** Control and shSOX9 Panc-1 xenograft tumor histology

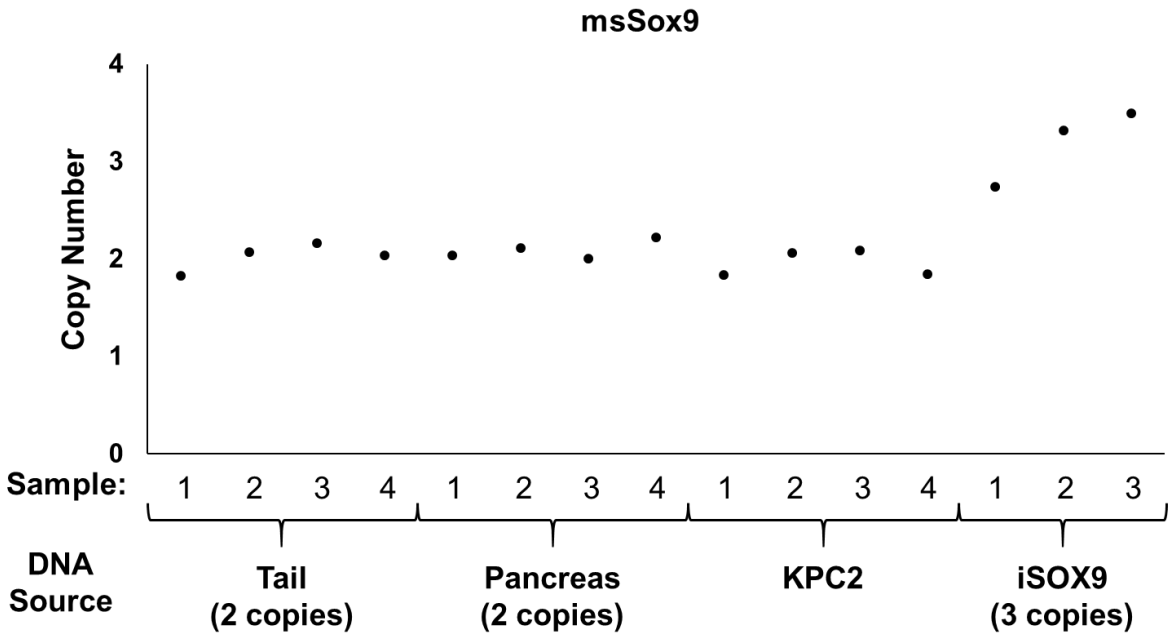

Figure 3.10 KPC2 *Sox9* copy number variant analysis.

Sox9 copy number analysis was performed on KPC2 cells by qPCR and compared to DNA samples where the *Sox9* allele copy number was known, specifically WT C57BL/6 tail and pancreas DNA and iSOX9 tail DNA.

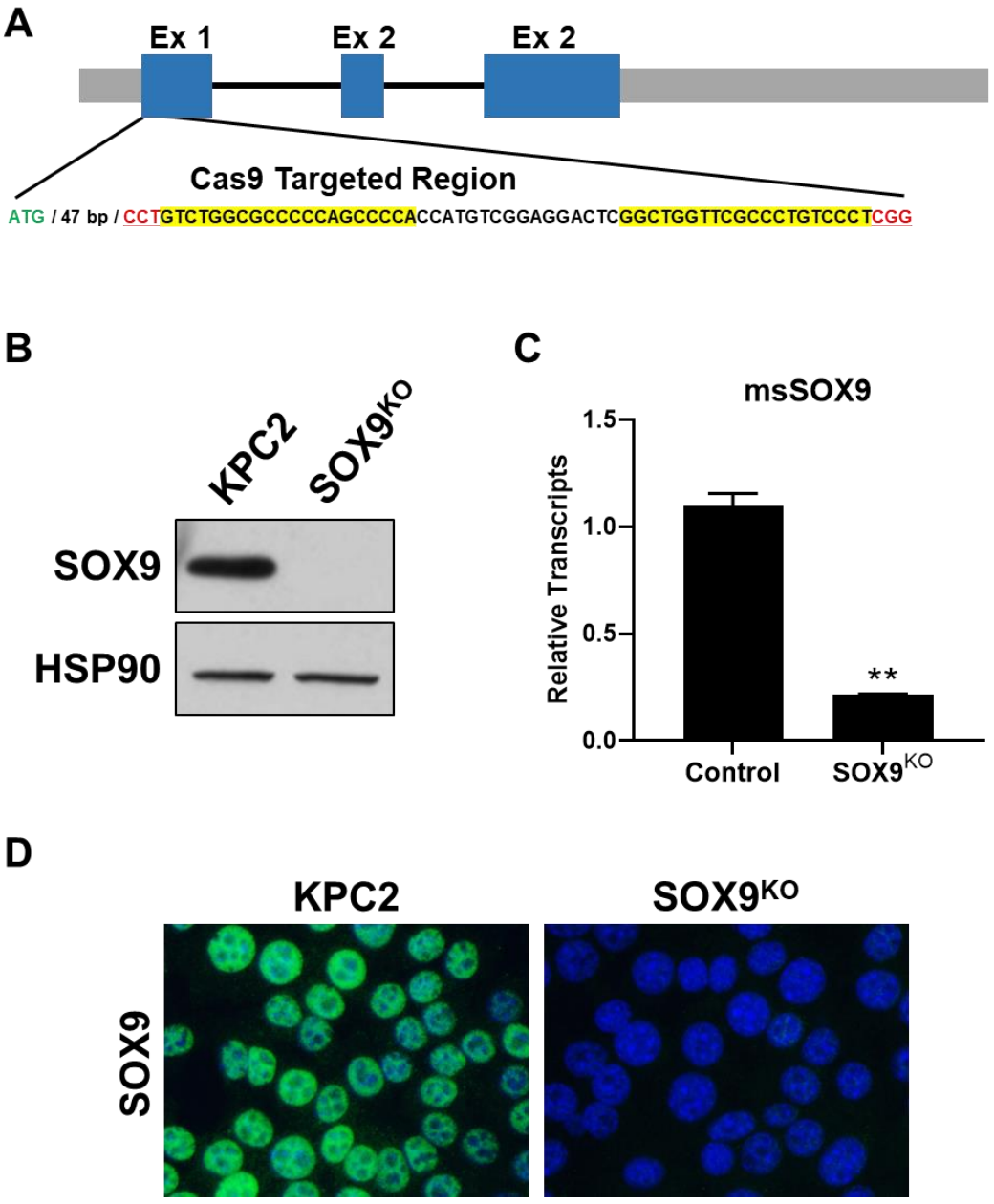

Figure 3.11 Generation of KPC2 SOX9^{KO} cells.

(A) A diagram showing the Cas9 targeting location within exon 1 of the mouse *Sox9* gene. The start codon is marked by green text, PAM sites are red and gRNA binding sites are highlighted in yellow. The dual Cas9 system used targets and cleaves DNA between the two gRNA binding sites. **(B)** A representative immunoblot showing ablation of SOX9 protein from one of the KPC2 SOX9^{KO} cell lines. **(C)** RT-qPCR data showing a reduction in *Sox9* transcripts in SOX9^{KO} cells (n = 3/group, ** $p < 0.01$). **(D)** Immunofluorescence staining showing SOX9 is uniformly lost from SOX9^{KO} cells.

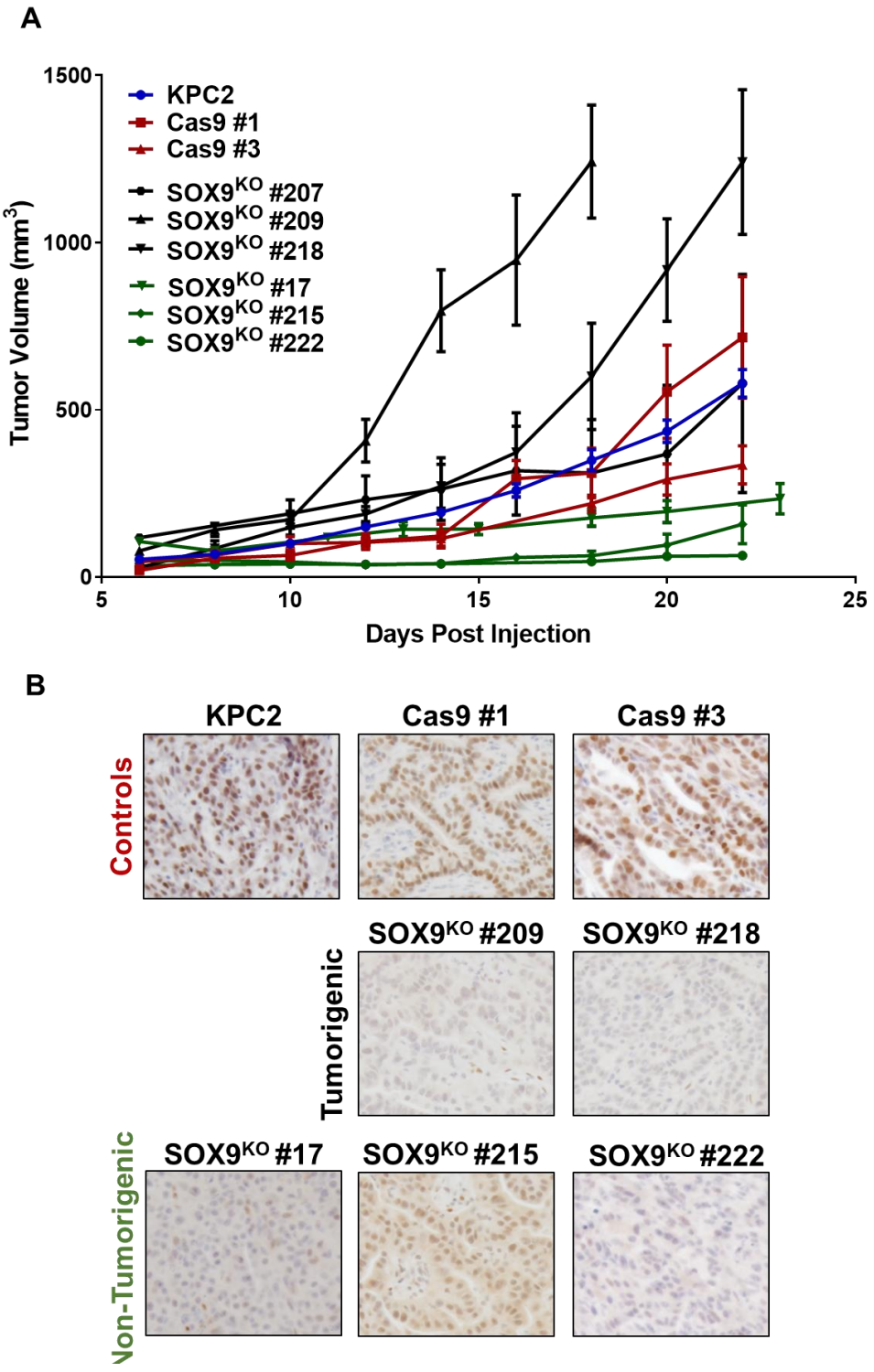

Figure 3.12 KPC2 SOX9^{KO} allograft tumor growth is highly variable.

(A) Subcutaneous allograft tumor growth data for the KPC2 parental cells, Cas9 controls transfected without gRNAs, and six SOX9^{KO} cell lines. **(B)** SOX9 DAB staining on tissue sections from allograft tumor samples.

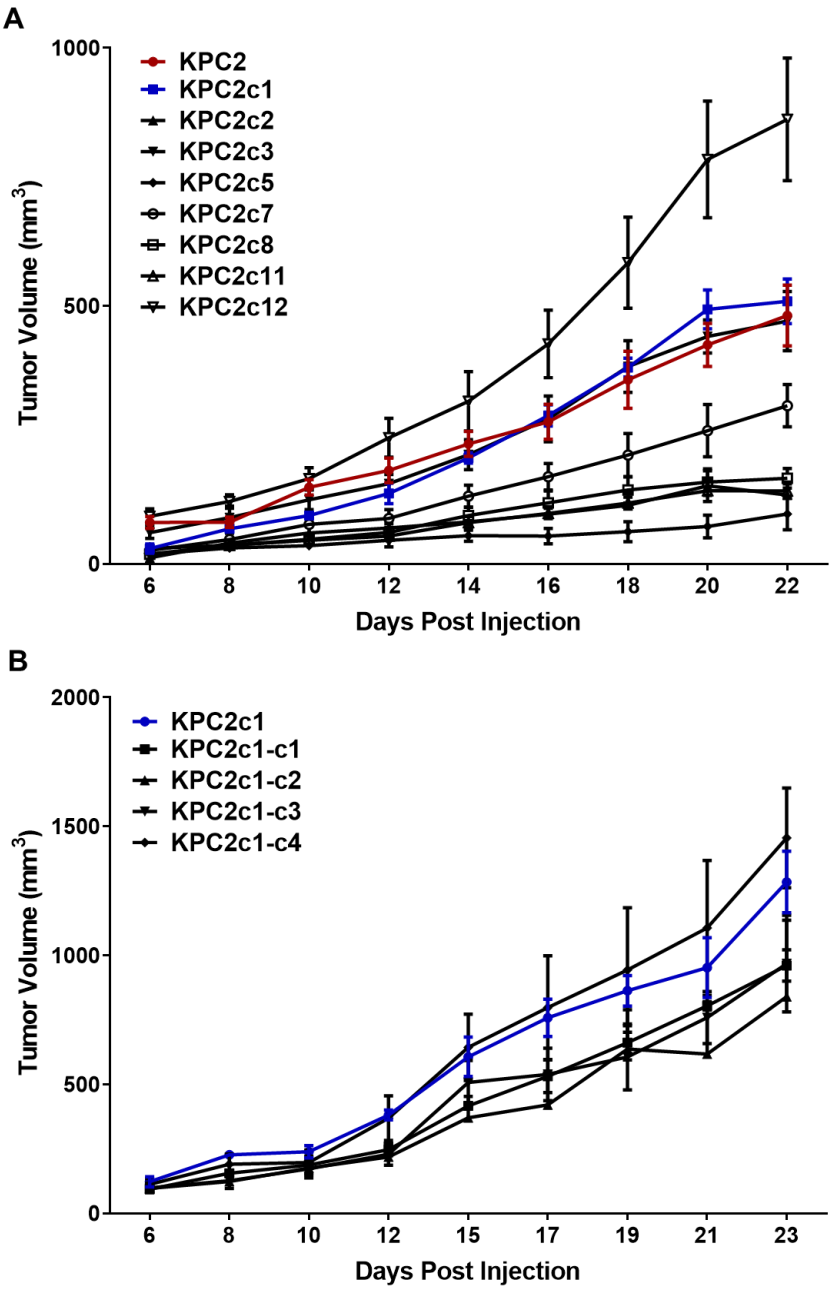

Figure 3.13 KPC2 subclones have variable tumorigenic capacity.

(A) Subcutaneous allograft tumor growth data from clonally derived cell lines isolated from the parental KPC2 cell line. **(B)** Allograft tumor growth data from clonally derived cell lines isolated from a tumorigenic KPC2 subclone (KPC2c1).

cell line, even when subcloned further (Figure 3.13B). The underlying reason for the drastic variability in the tumorigenic capacity of the KPC2 cells remains unknown and is a thought-provoking subject for additional analysis. Interestingly, *Foxm1* expression was negatively correlated with tumor growth in the SOX9^{KO} cell lines (Figure 3.14). FoxM1 is a downstream target of oncogenic KRAS known to regulate genes involved in proliferation, stem cell self-renewal, epithelial-to-mesenchymal transition (EMT), angiogenesis, and metastasis that has been well studied in PDAC and other cancers (Huang et al., 2014). Whether variability in the expression of *FoxM1* has a causal effect on the differences in tumorigenicity observed here remains unknown, especially given the counterintuitive finding that high levels of *Foxm1* are associated with less aggressive tumor growth, though at this time it is unknown whether *Foxm1* is primarily expressed by tumor or stromal cells. Despite the irregularity in KPC2 tumor growth, the results clearly indicate that aggressive KPC2 PDAC cells can still form tumors in the absence of SOX9, as half of the SOX9^{KO} cell lines formed tumors equal to or larger than the controls.

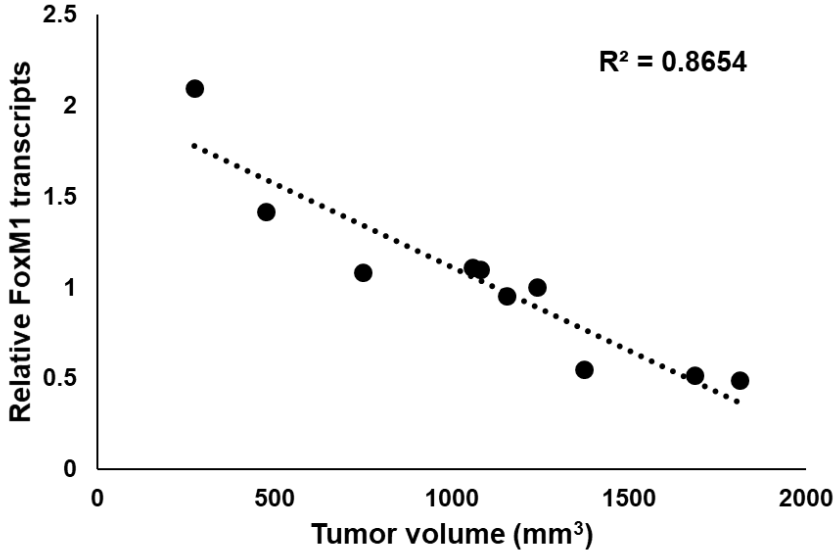

Figure 3.14 FoxM1 expression is negatively correlated with SOX9^{KO} cell tumor growth.

RT-qPCR was performed on total RNA samples isolated from SOX9^{KO} allograft tumors, and *Foxm1* expression was plotted relative to final tumor volume.

Introduction of a doxycycline inducible human *SOX9* transgene had no effect on tumor growth when expressed into a nontumorigenic SOX9^{KO} cell line but suppressed tumorigeneses in one of the aggressively tumorigenic SOX9^{KO} cell lines (Figure 3.15A-C). Human *SOX9* was used in this instance because it differed from mouse *Sox9* in the CRISPR/Cas9 target sequence, reducing the risk that the transgene could be disrupted should any residual CAS9 expression remain from the original cell line generation process, though later analysis showed no expression of CAS9 protein in the final SOX9^{KO} cell lines. Human SOX9 shares > 95% homology with mouse SOX9 so it seems unlikely that cross species differences could account for the negative impact on tumor growth. However, the human *SOX9* transgene was expressed at levels far above that of endogenous KPC2 SOX9 (Figure 3.15C), and SOX9 has been well documented to function in a dose-dependent manner (Prévostel and Blache, 2017; Seymour et al., 2008; Yang et al., 2019b) and can negatively impact tumor growth in some types of cancer, such as melanoma (Passeron et al., 2009). Therefore, sustained high level expression of SOX9 could suppress KPC2 tumorigenesis although further evaluation is necessary to determine if this is the case.

Ablation of SOX9 from a KC cell line produced similar results to those obtained with the KPC2 cells, with 2/3 cell lines showing no change in tumor growth (Figure 3.16). Again, this experiment was performed prior to subcloning the parental KC cell line, likely accounting for the variability. Finally, *Sox9* was also deleted in KPC1 cells, which displayed far less variability in allograft tumor growth compared to the other primary cell lines used and clearly showed no impact of SOX9 loss on tumor growth (Figure 3.17). Taken together, these results indicate that loss of SOX9 had no detectable impact on tumor growth and maintenance in established KC and KPC PDAC cell lines, and that over expression of SOX9 may even be detrimental. However, reduction in SOX9 expression by shRNA did reduce malignant properties of Panc-1 cells, including soft agar colony formation and xenograft tumor growth. My findings point to a nuanced role for SOX9 in PDAC development past the stage of PanIN formation, wherein cellular context, and perhaps SOX9 expression levels, determine the importance and influence of SOX9 on tumor growth. However, these findings ultimately show several instances wherein SOX9 is dispensable for tumor growth.

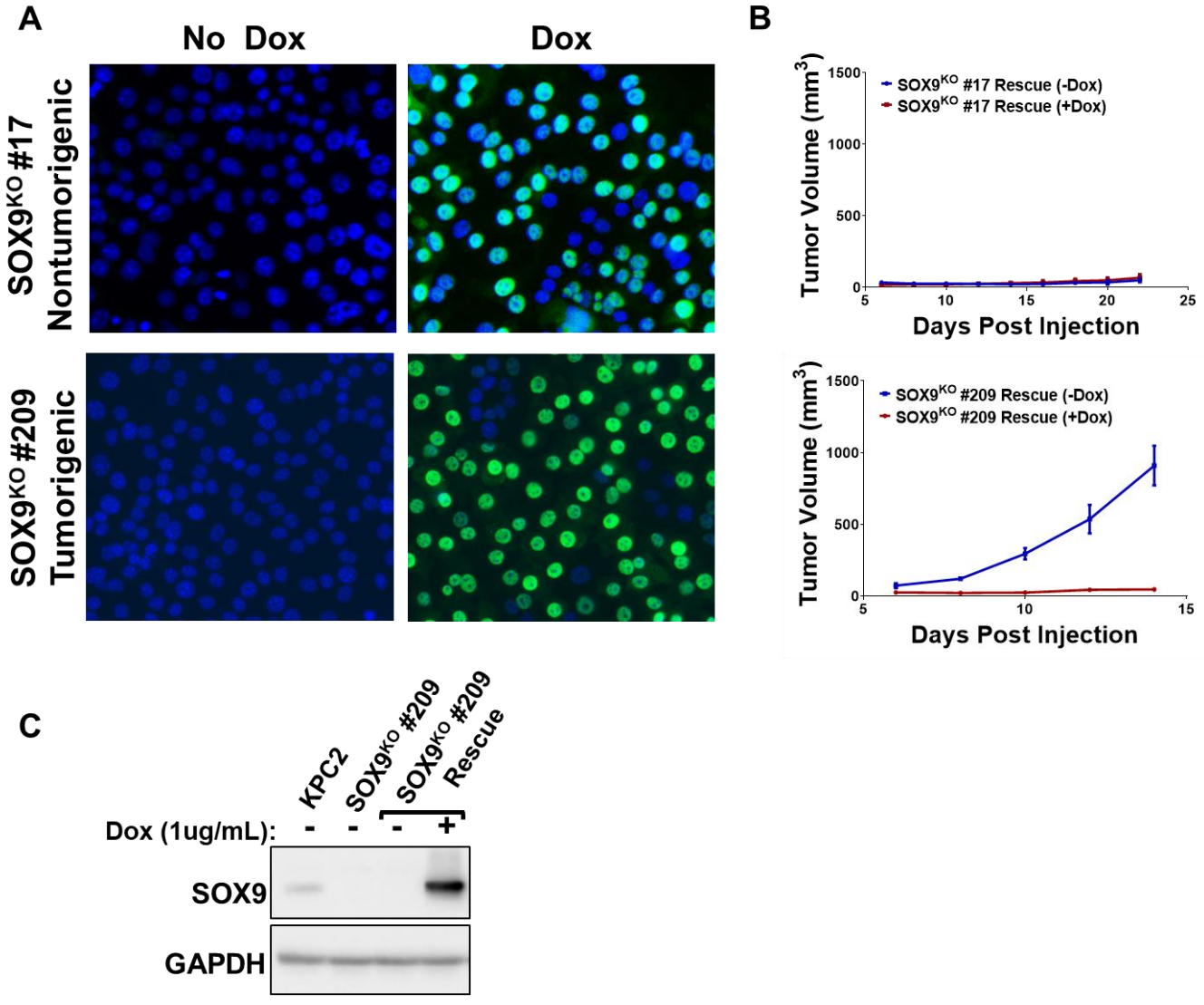

Figure 3.15 Generation and analysis of doxycycline inducible SOX9 rescue cell lines.

(A) SOX9 immunofluorescence staining of stable cell lines generated from nontumorigenic and tumorigenic $SOX9^{KO}$ cell lines. Transgenic human SOX9 expression was detected 24 hours post treatment with 1 μg/mL doxycycline. **(B)** Tumor growth curves from subcutaneous allograft experiments analyzing tumorigenesis in mice fed either control or doxycycline chow to activate the human SOX9 transgene (n = 4-5 mice/group).

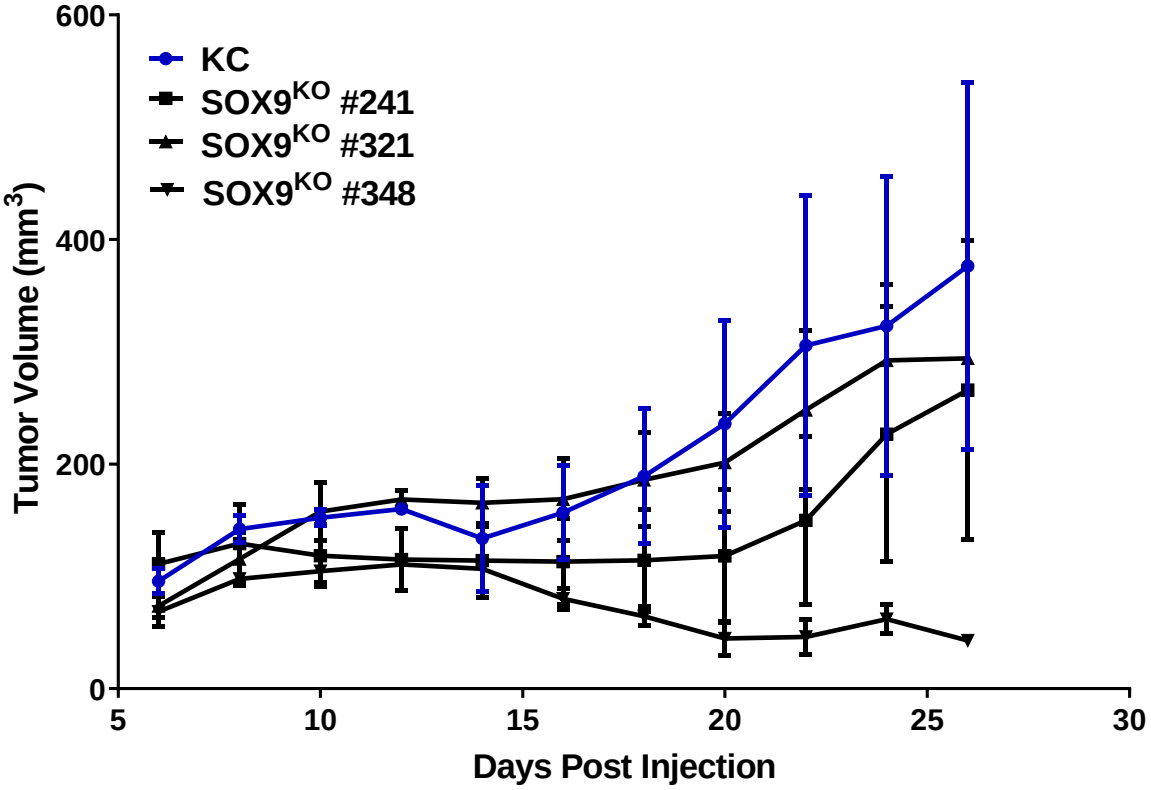

Figure 3.16 KC SOX9^{KO} cell allograft tumor growth.

Tumor growth curve of the parental KC cells and three KC SOX9^{KO} cell lines.

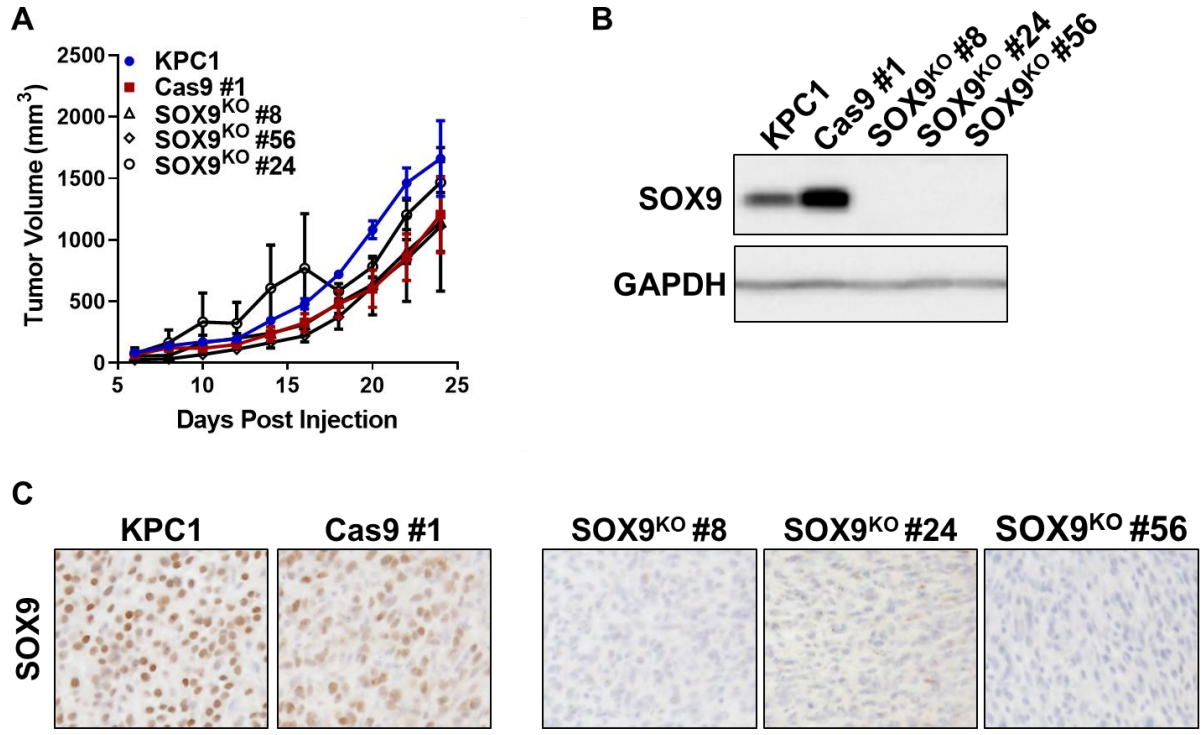

Figure 3.17 KPC1 SOX9^{KO} cell allograft tumor growth and analysis.

(A) Tumor growth curve for subcutaneous allografts from KPC1 parental, Cas9 control, and three KPC1 SOX9^{KO} tumor cell lines. **(B)** SOX9 immunoblot of tumor protein lysates. **(C)** SOX9 DAB staining of tissue sections from allograft tumors.

3.2.3 Omics approaches to analyzing aberrant SOX9 expression

As a transcription factor, SOX9 regulates the expression of specific gene targets in order to manipulate aspects of cellular identity and differentiation. Therefore, an analysis of the transcriptional network controlled by SOX9 as it relates to early stages of PanIN formation can provide novel insight into the mechanism of SOX9 dependent PDAC initiation. Because SOX9 expression is activated early after pancreatic injury, even prior to lesion formation, experiments were undertaken to examine the consequences of ectopic SOX9 expression on gene regulation in pancreatic acinar cells. These experiments recapitulated one of the earliest events in PDAC pathogenesis and allowed the effects of SOX9 on gene regulation to be isolated and studied more closely. Briefly, Mist1^{CreER}/iSOX9 mice were utilized to induce acinar cell expression of the *Sox9* transgene. High integrity RNA was then harvested 72 h post transgene activation and used for RNA-Seq analysis comparing these samples to pancreas RNA from Mist1^{CreER} control animals. EdgeR analysis identified 427 differentially expressed genes (DEGs) at an FDR $\leq$ 0.05 with no fold change cutoff (Figure 3.18A, Appendix A). Within the list of DEGs, seven previously published SOX9 regulated genes (*Col11a2, Ceacam1, Sulf2, Mia, Nedd9, Top2a* and *Ptgds*) (Bi et al., 1999; Kadaja et al., 2014; Kolanczyk et al., 2011; Liu et al., 2017a; Shi et al., 2015; Wilhelm et al., 2007; Zalzali et al., 2008) were upregulated upon SOX9 induction, serving as internal validation of our results. Interestingly, four of these genes (*Ceacam1, Sulf2, Nedd9, Top2a,* and *Mia*) have been independently shown to be upregulated in PanIN and/or PDAC samples (El Fitori et al., 2005; Gill et al., 2014; Pei et al., 2018; Simeone et al., 2007; Xue et al., 2013).

MetaCore network analysis was performed on the RNA-Seq results and showed significant enrichment in categories related to cell adhesion, cytoskeletal components, and blood vessel growth and development (Figure 3.18B), and a similar theme was present in results from KEGG pathway analysis (Figure 3.18C). A network of previously published directly interacting factors within the RNA-Seq was also produced by MetaCore analysis and revealed some of the interconnectivity within the dataset (Figure 3.19). The RNA-Seq data was then cross referenced with previously published microarray and RNA-Seq datasets that had identified transcriptional differences between normal pancreata and pancreas samples with widespread ADM or PanIN lesions. ADM RNA-Seq data was taken from a study wherein conditional deletion of *Ptf1a* caused

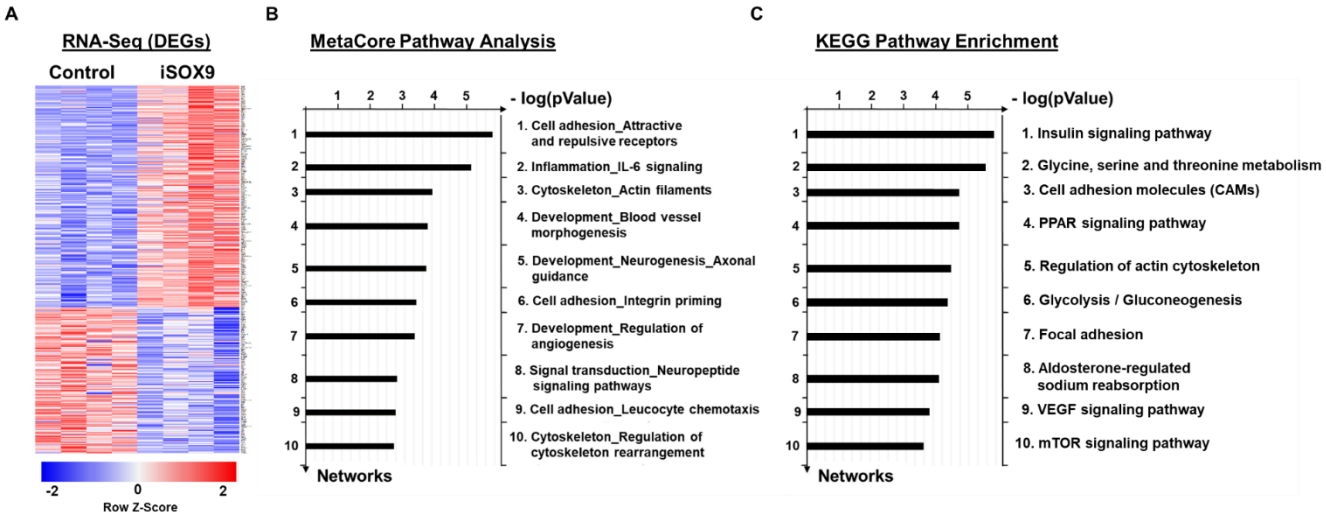

Figure 3.18 RNA-Seq identifies SOX9 dependent changes in acinar cell transcriptional networks.

(A) A heatmap of the 427 differentially expressed genes identified by edgeR comparing transcripts from Mist1^{CreER} (control) and Mist1^{CreER}; iSOX9 (iSOX9) mouse pancreas samples. **(B, C)** Top 10 enriched categories from MetaCore and KEGG pathway analysis of the RNA-Seq dataset.

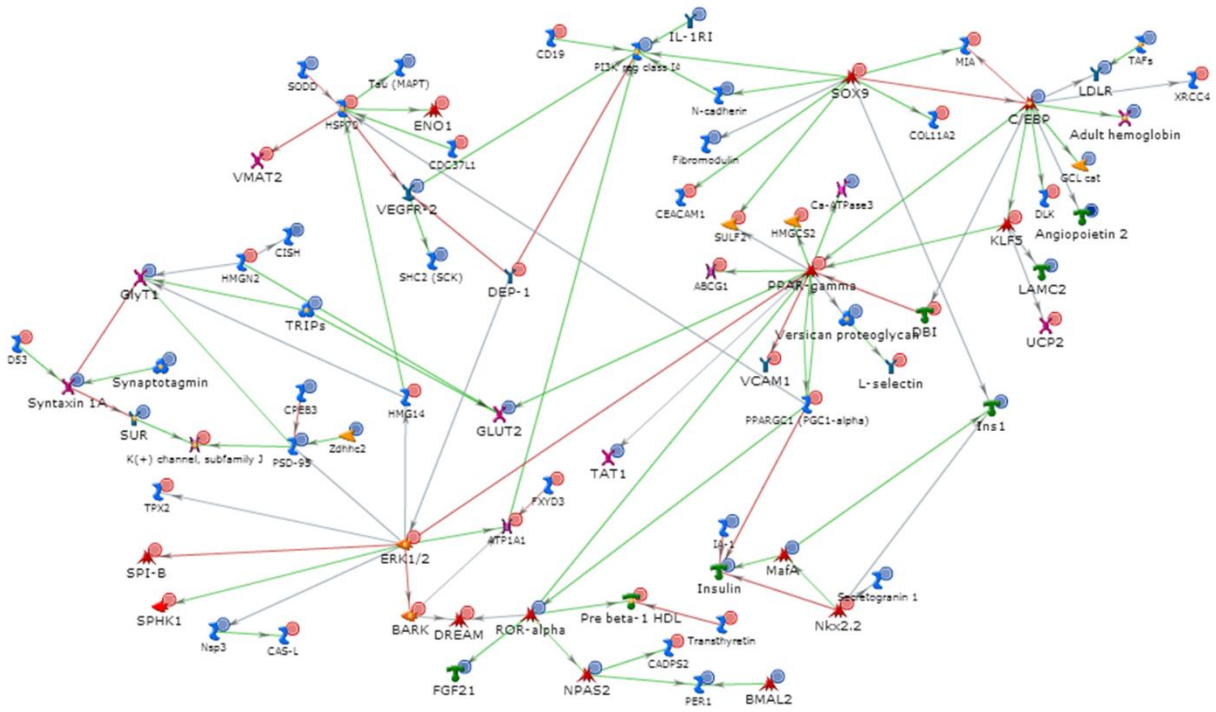

Figure 3.19 MetaCore iSOX9 analysis direct interaction network.

A network map showing direct interactions between DEG encoded proteins from the iSOX9 RNA-Seq based on MetaCore's curated data from previous publications. Red circles indicate factors upregulated in the RNA-Seq, while blue circles were downregulated. Green lines show positive regulation or activation, while red lines show negative or inhibitory interactions.

ADM lesions to form (Krah et al., 2015), while PanIN microarray data was from an analysis of KC mice (Ling et al., 2012). Out of the 427 DEGs identified in the iSOX9 RNA-Seq 105 genes were commonly up or downregulated in one or both additional datasets (Appendix B). This included previously identified direct SOX9 targets *Sulf2, Mia, Top2a,* and *Nedd9,* along with additional genes previously implicated in PDAC malignancy such as *Fxyd3, Vcam1*, and *Klf5* (He et al., 2018; Kayed et al., 2006; Li et al., 2019; Tempia-Caliera et al., 2002). This group of overlapping DEGs thus provides an even narrower list of DEGs worth further exploration that are regulated by ectopic expression of SOX9 and that show altered expression following ADM/PanIN formation.

Of note, while no changes in well characterized duct or acinar cell specific transcripts were detected within the DEGs, and morphologically iSOX9 tissue was indistinguishable from control samples, DEG analysis using Enrichr (Kuleshov et al., 2016) identified our lab's previously published *Mist1* knockout microarray dataset (Direnzo et al., 2012) as the top hit within the transcription factor perturbation category (Table 2.1). This indicates a small but seemingly significant overlap (31 genes total, 23 of which showed consistent upregulated in both the $Mist1^{KO}$ and iSOX9 datasets) between the iSOX9 transcriptional changes and those observed in $Mist1^{KO}$ pancreata, perhaps pointing to a more subtle level of SOX9 induced dedifferentiation. This is especially interesting as *Mist1* expression was unchanged in the iSOX9 mice. Indeed, even after prolonged ectopic expression of SOX9 using both the iSOX9 and *LSL-HA-SOX9* mouse models there was no evidence of ductal reprogramming based on analysis of classical transcriptional markers including *Mist1* (Figure 3.20). However, prominent central lumen dilation was observed when the iSOX9 transgene was expressed in $Mist1^{CreER/CreER}$ ($MIST1^{KO}$) mice (Figure 3.21), whose pancreatic acinar cells are known to be more susceptible to transdifferentiation (Shi et al., 2013).

Table 3.1 Enrichr transcription factor perturbations analysis of the iSOX9 DEGs

Term	P-value	Adj. P-value	Odds Ratio
BHLHA15 KO MOUSE GSE34232 CREEDSID GENE 172 UP	1.47E-15	2.87E-12	5.95
ESRRB MUT MOUSE GSE8434 CREEDSID GENE 1047 DOWN	7.71E-10	7.55E-07	3.94
MYC ACTIVATION MOUSE GSE4356 CREEDSID GENE 752 DOWN	4.19E-08	2.73E-05	5.10
ESRRA KO MOUSE GSE16623 CREEDSID GENE 2159 DOWN	1.36E-07	6.68E-05	4.24
GFI1B OE MOUSE GSE33709 CREEDSID GENE 452 UP	2.21E-07	8.67E-05	3.77
GFI1B OE MOUSE GSE33709 CREEDSID GENE 772 DOWN	2.36E-07	7.70E-05	3.75
GATA3 KO MOUSE GSE39864 CREEDSID GENE 1162 UP	5.03E-07	1.41E-04	3.46
NFE2L2 KO MOUSE GSE18344 CREEDSID GENE 965 DOWN	5.84E-07	1.43E-04	3.21
AIRE KO MOUSE GSE30129 CREEDSID GENE 1676 UP	6.67E-07	1.45E-04	3.53
PPARD KO MOUSE GSE16048 CREEDSID GENE 81 DOWN	2.41E-06	4.73E-04	4.05

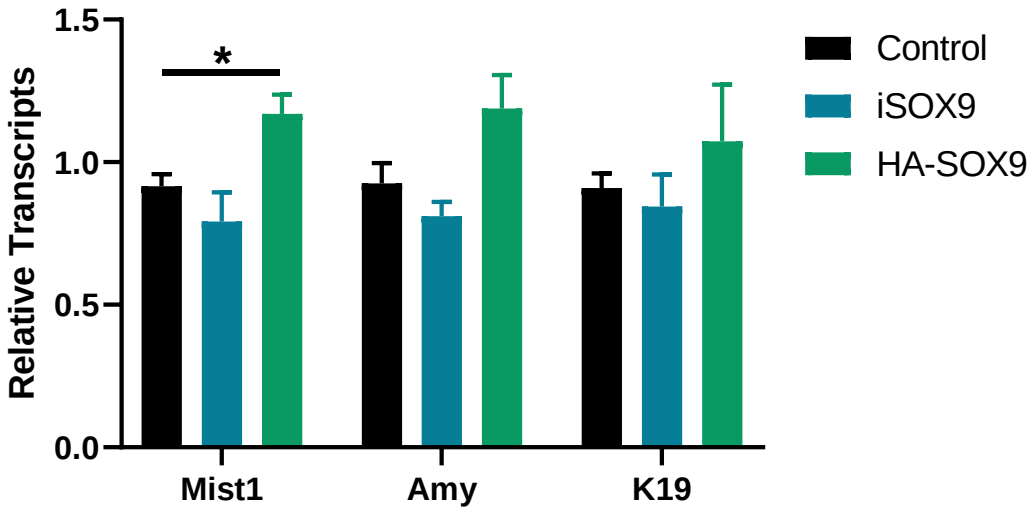

Figure 3.20 Prolonged ectopic expression of SOX9 in pancreatic acinar cells does not alter transcription of classical acinar and ductal genes.

RT-qPCR analysis of total pancreas RNA samples from *Mist1*^{CreER} (Control), *Mist1*^{CreER}*; iSOX9* (iSOX9), or *Mist1*^{CreER}*; LSL-HA-SOX9* (HA-SOX9) 6 weeks after transgene activation. (n = 3-5/group, * $p < 0.05$)

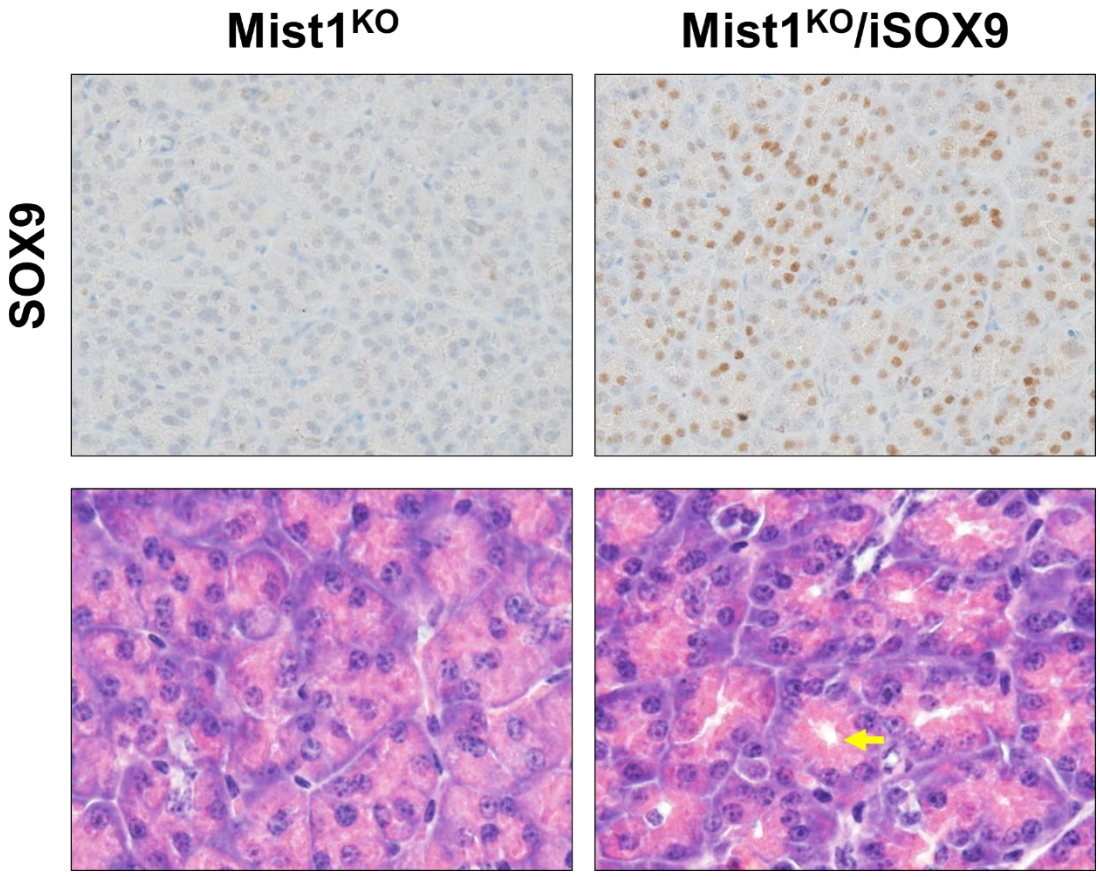

Figure 3.21 iSOX9 mice have pronounce central lumen dilation in the absence of MIST1.

Upper panel shows SOX9 staining of $Mist1^{KO}$ and $Mist1^{KO}$/iSOX9 pancreas sections. The lower panel shows the presence of dilated central lumens (yellow arrow) in the iSOX9 expressing pancreas tissue.

To further map the SOX9 regulatory network as it relates to PDAC initiation and provide a useful complement for the RNA-Seq results, a ChIP-Seq experiment was performed. As mentioned earlier, SOX9 is known to function in a context dependent manner, often requiring specific co-factors for proper gene regulation. A major advantage to ChIP-Seq in this instance is that it can be used to identify genes regulated by endogenous SOX9 within actual ADM/PanIN lesions, thus allowing SOX9's activity to be examined in a more relevant cellular environment. This has the potential to uncover novel SOX9 regulated targets not identified in the RNA-Seq experiment, wherein ectopic expression of SOX9 alone does not cause ADM or PanIN formation. KC mice treated with caerulein to induce acute pancreatitis were used for this study so that ADM and PanIN lesions were widespread (Figure 3.22).

Extensive optimization was undertaken in order to produce samples fit for ChIP-Seq. This required testing multiple fixation and fragmentation methodologies in order to produce samples that displayed good enrichment, considered in this case to be > 4-fold signal compared to a non-specific negative control locus, with the majority of the chromatin sample falling between 100-300 bp in size, and a final DNA quantity after immunoprecipitation of ≥ 10 ng. Both probe-based and Covaris Adaptive Focused Acoustics-based sonication methods were tested in various buffers, but ultimately enzymatic digestion using micrococcal nuclease (MNase) provided the best combination of fragmentation and signal enrichment, so this method was used for the final ChIP-Seq perpetration.

A SOX9 antibody meeting ENCODE's recommendations for ChIP-Seq was used for immunoprecipitation (Figure 3.23A). However, because of SOX9's tissue specific functionality, finding positive SOX9 bound loci for ChIP optimization proved quite difficult as no previous SOX9 ChIP-Seqs have been performed using mouse pancreas samples, with the closest study using human embryonic stem cell derived pancreas progenitor cells (Shih et al., 2015). Additionally, although *Ceacam1*, *Sulf2*, and *Mia* were identified in the iSOX9 RNA-Seq and were upregulated in PanIN samples, primers designed to the previously published SOX9 binding sites of these genes (Kadaja et al., 2014; Xie et al., 1999; Zalzali et al., 2008) showed no SOX9-dependent enrichment over a mock IP (IgG) or when compared to a negative control loci (Figure 3.23B). Given these difficulties a bioinformatics-based approach was used to identify loci that were likely to be bound by SOX9 regardless of the cellular context, referred to as "universal" SOX9 target loci from here on. Because SOX9 is important for a diverse range of biological processes, for example hair

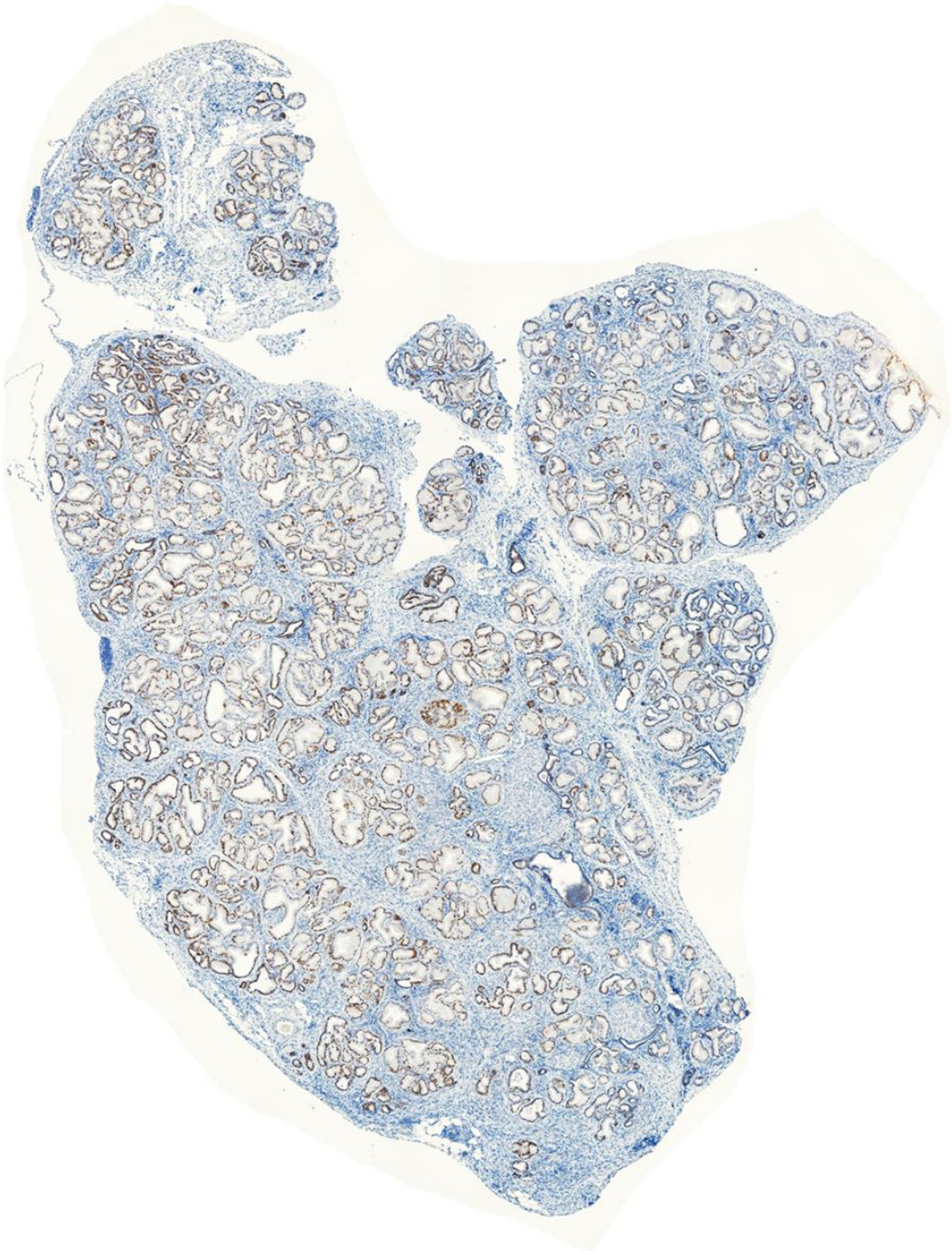

Figure 3.22 KC pancreas tissue has widespread SOX9 positive lesion formation

SOX9 DAB staining of an entire tissue section from a KC mouse pancreas taken 4 weeks after caerulein induced pancreatitis.

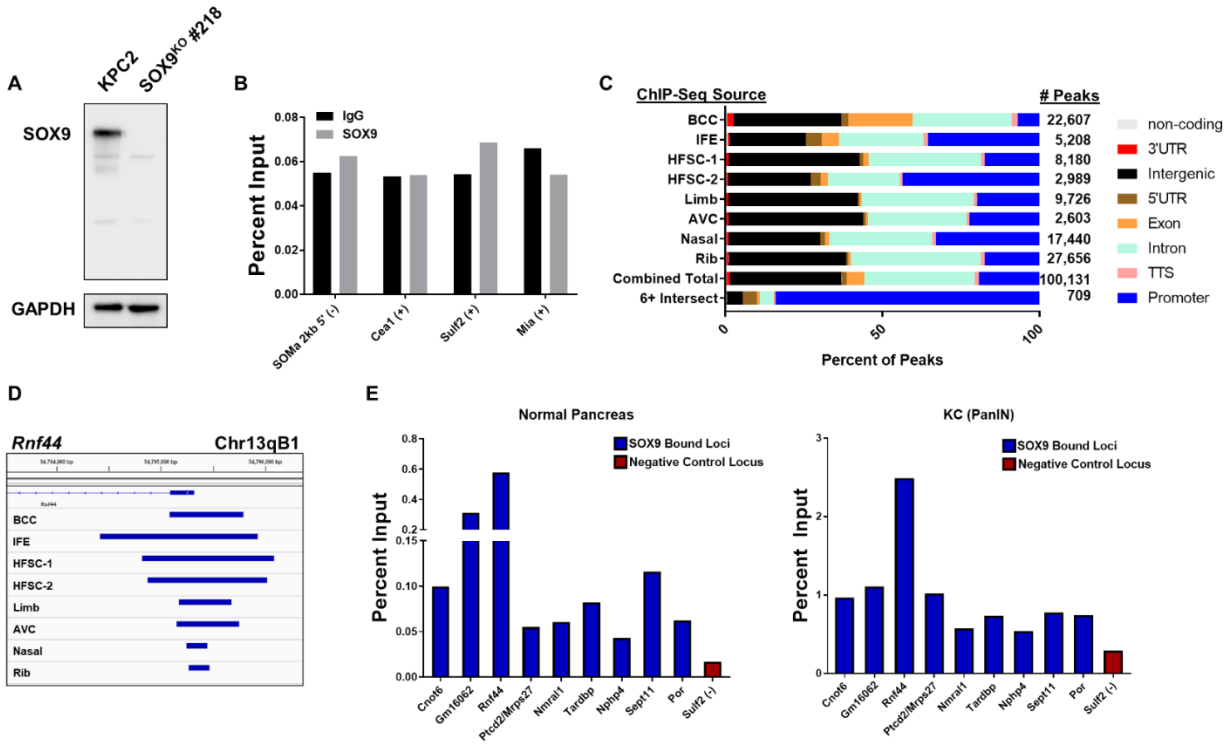

Figure 3.23 SOX9 ChIP showed enrichment in regions commonly identified in previously published SOX9 ChIP-Seq datasets.

(A) Immunoblot showing specificity of the SOX9 antibody used for ChIP based on the low level of background signal and loss of signal in the $SOX9^{KO}$ cell lysate. **(B)** SOX9 ChIP performed on pancreas samples showed no enrichment of IgG for SOX9 binding sites associated with *Ceacam1* (Cea1), *Sulf2*, and *Mia*. The SOMa 2kb 5' negative control loci was used as a comparison and was identified in a previous publication (Mead et al. 2013). **(C)** Peak number and distribution from previously published SOX9 ChIP-Seq experiments. The combined total shows the distribution of all peaks together and the 6+ intersect shows the location of peaks found to commonly overlap within 6 or more tissue types. **(D)** An example of a "universal" SOX9 target showing peak enrichment (blue bars) in multiple datasets within the *Rnf44* promoter. **(E)** ChIP results from normal and KC post-acute pancreatitis pancreas samples. The promoter region of *Sufl2* was used as a negative control (red bar) as it showed no SOX9 enrichment in earlier studies (see **B**), and promoters identified by bioinformatics analysis were used as positive controls (blue bars).

growth, sex determination, and cartilage formation (Jo et al., 2014), several SOX9 ChIP-Seq experiments investigating the role of SOX9 outside the pancreas have already been published. By accessing these publicly available datasets it was possible to identify loci that showed SOX9 binding across multiple ChIP-Seq experiments from a diverse array of cell types. For this analysis eight SOX9 ChIP-Seqs from four publications (Garside et al., 2015; Kadaja et al., 2014; Larsimont et al., 2015; Ohba et al., 2015) were used to identify ChIP-Seq peaks that were present in a minimum of 6 datasets (Figure 3.23CD). This provided a list of 709 loci that we used as "universal" SOX9 targets. Interestingly, annotation of these 709 loci using Homer (Heinz et al., 2010) revealed a disproportionate amount to be located in gene promoter regions (+/- 2Kb from TSS) compared to the distributions of the original datasets (Figure 3.23CD). Of note, previous research has established SOX9 dependent gene regulation through its binding to enhancer regions as a common mechanism of action (Akiyama et al., 2002; He et al., 2016; Kadaja et al., 2014; Lefebvre et al., 1997; Mead et al., 2013; Ohba et al., 2015) and as a result it has been proposed that SOX9 may function as a pioneer factor (Adam et al., 2015). Additionally, some research indicates that SOX9 may have two different modes of DNA associations binding indirectly to highly active promoter/TSS regions by interacting with transcriptional machinery and binding directly to regulate gene expression of tissue specific gene targets at enhancer sites (Ohba et al., 2015). Further analysis of the 709 loci using GREAT (McLean et al., 2010) identified 454 proximal genes associated with these genomic regions. However, when these genes were compared to the DEGs identified in our iSOX9 RNA-seq only five genes were present in both lists: *Fam20b, Pafah1b3, Sulf2, Ube2c,* and *Utp18*, with only *Sulf2* being identified as a putative SOX9 target (Kadaja et al., 2014). Primers were designed to nine loci from the "universal" SOX9 target list and all loci showed enrichment in both normal pancreas, which was presumed at the time to be due to SOX9 positive duct cells, and KC mouse PanIN samples (Figure 3.23E).

ChIP-Seq was then performed on two different KC pancreas samples. This identified 8,708 and 4,773 peaks from the individual samples, with 2,839 peaks showing a direct overlap between samples, and 2,296 common peaks identified based on an irreproducible discovery rate (IDR) of < 0.01 (Figure 3.24). Surprisingly, only a small portion of the target regions identified by IDR analysis were within significantly identified peaks identified by MACS, and as a result often showed very poor overall signal enrichment over background. Quality control analysis, however, indicated relatively poor sample enrichment based on the percent of reads within peaks (RiP),

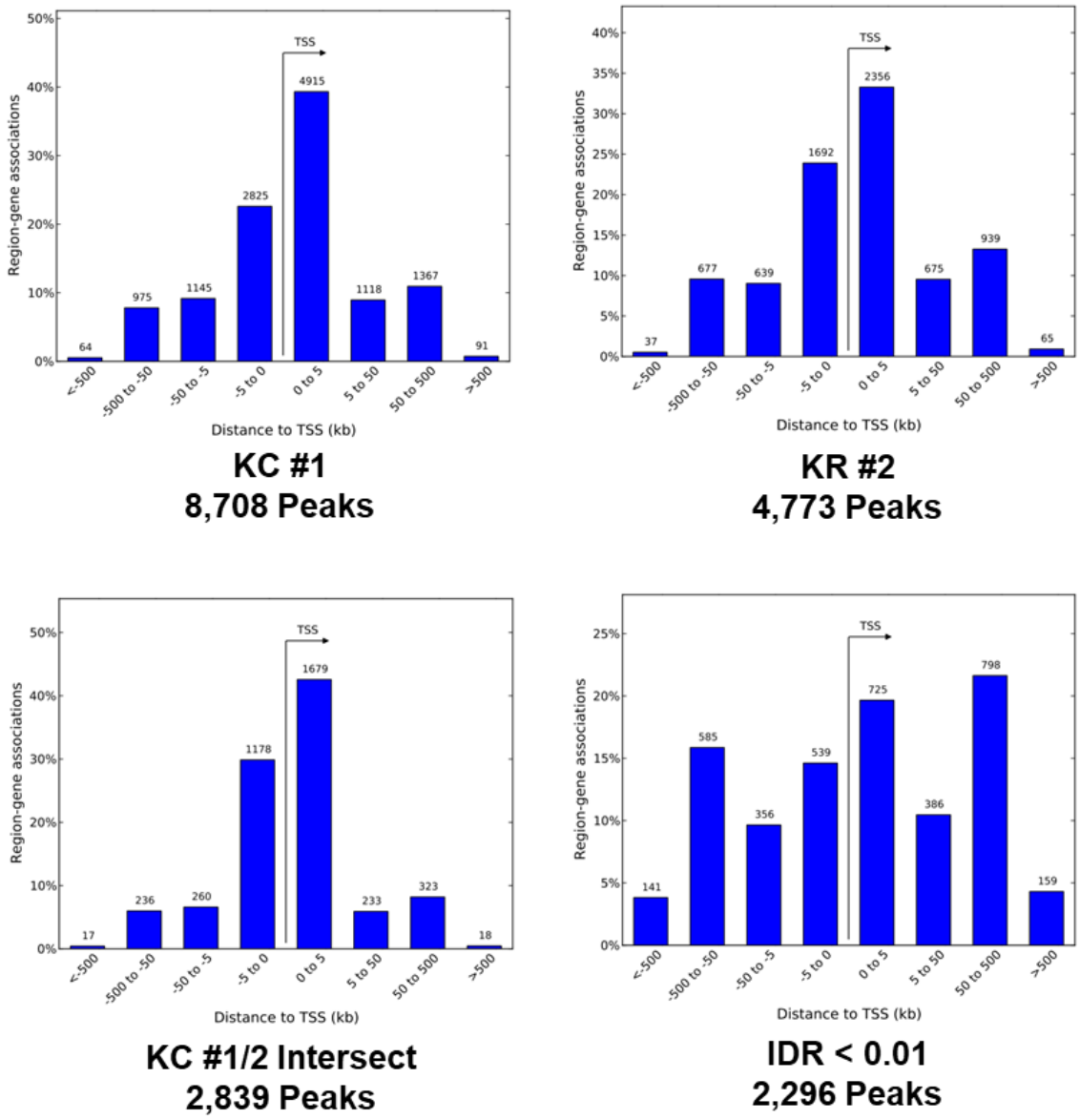

Figure 3.24 KC SOX9 ChIP-Seq peaks are disproportionally located close to TSS/Promoter regions.

ChIP-Seq peak distribution from GREAT analysis shows the majority of peaks within the two KC ChIP-Seq datasets are within 5 Kb of TSS regions. This distribution is shifted when peaks are identified based on IDR < 0.01.

Table 3.2 ChIPQC analysis of SOX9 ChIP-Seq data

ID	Reads	SSD	RiP%
KC #1 SOX9	18385498	0.27	1.50
KC #1 Input	15355485	0.25	0.28
KC #2 SOX9	17222508	0.27	0.69
KC #2 Input	15607377	0.25	0.12

which was less than the ideal 5%, and the low standardized standard deviation (SSD), < 1 (Table 3.2). Additionally, overall KC ChIP-Seq peaks were disproportionally located in gene promoters, though this distribution was slightly shifted in the IDR < 0.01 dataset. This is counter to SOX9's typically reported preference for binding to enhancer elements and could indicate a low presence of peaks related to tissue specific SOX9 enhancer activity. Strangely, RT-qPCR analysis of over 20 genes associated with ChIP-Seq peaks, both promoter and enhancer bound as identified by GREAT analysis, showed no change in expression between KC and KC/ΔSOX9 samples (Figure 3.25), seeming to indicate that the targets identified in the ChIP-Seq were not regulated by SOX9. Based on these findings, further validation of the ChIP-Seq was required. It has been reported previously that active promoter regions can create false positive enrichment in ChIP-Seq experiments (Jain et al., 2015). Because the "universal" SOX9 peaks were almost entirely located in gene promoters, this highlighted a risk that the ChIP experiment was optimized around false positive signals commonly present in ChIP-Seq data. To determine if this was the case ChIP was performed using one of the KPC SOX9^{KO} cell lines. Indeed, ChIP from the SOX9^{KO} samples showed similar, if not stronger, enrichment compared to SOX9 expressing KPC control cells (Figure 3.26), indicating that false positive phantom peaks are present in the ChIP data and it should not be used for further analysis. Despite the shortcomings of the ChIP-Seq experiment, the iSOX9 RNA-Seq data has identified a relatively short list of genes that show SOX9 dependent transcriptional regulation with relevance to ADM/PanIN formation, and these targets should be more closely scrutinized in future studies to determine the impact of these genes on PanIN formation.

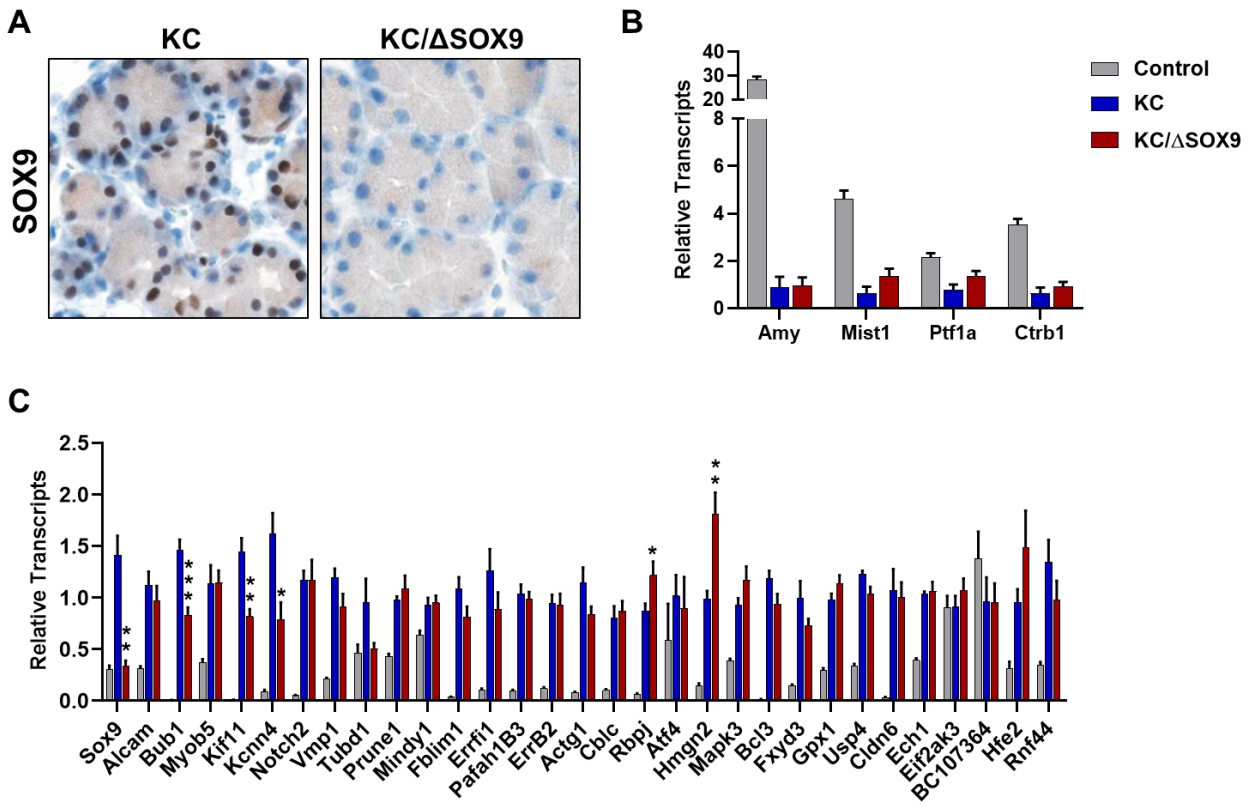

Figure 3.25 Genes with associated SOX9 ChIP-Seq peaks do not show SOX9 dependent expression.

(A) SOX9 DAB staining on tissue sections from KC or KC/ΔSOX9 mice 7 days post acute pancreatitis treatment just before PanIN lesions begin to form. These samples were used to analyze SOX9 dependent changes in gene expression as they relate to lesion formation. **(B)** Analysis of the expression of acinar specific genes associated with SOX9 ChIP-Seq peaks. **(C)** Gene expression profiles for several gene targets identified by the SOX9 ChIP-Seq. (n = 6-7/group, * $p < 0.05$, ** $p < 0.01$, *** $p < 0.001$);
Note - significance was only assessed in comparison of KC and KC/ΔSOX9 samples.

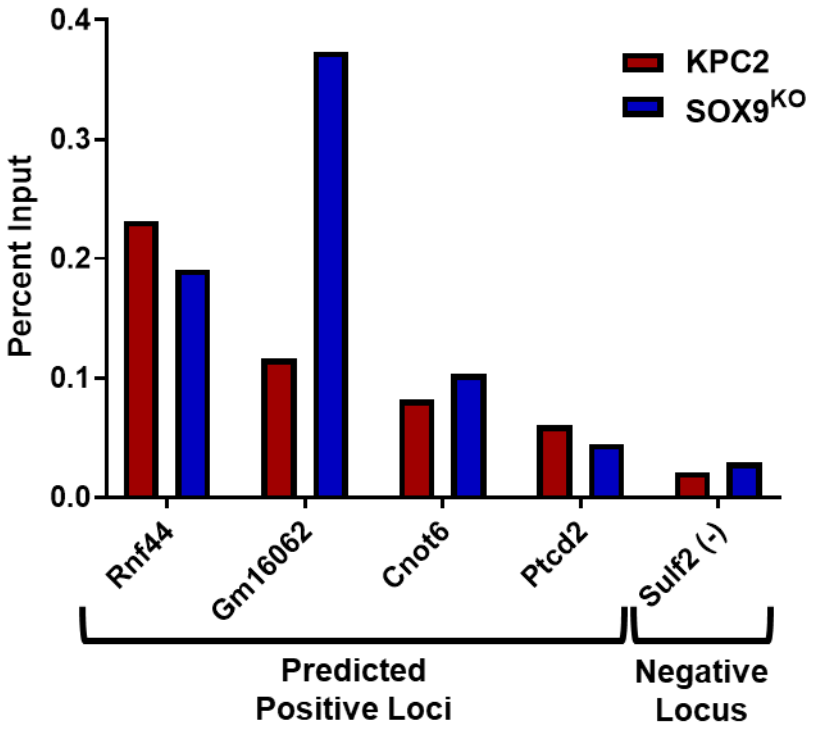

Figure 3.26 False positive peaks show ChIP enrichment in the absence of SOX9

SOX9 ChIP was performed on KPC2-SOX9^{KO} chromatin samples and showed similar enrichment to that of the SOX9 expressing KPC2 cells in loci used for ChIP-Seq optimization.

3.3 Discussion

The data presented here extend and corroborate findings from Kopp et al. (2012) and others (Grimont et al., 2014; Kopp et al., 2012) showing that aberrant SOX9 expression is necessary for PDAC initiation, as our data show that PanIN lesions will not form in the absence of SOX9, even when acute pancreatitis is used to exacerbate lesion formation in $KRAS^{G12D}$ expressing mice. Additionally, ectopic expression of SOX9 greatly accelerated $KRAS^{G12D}$-driven PanIN formation, a process that is normally quite gradual without an inciting cellular insult. However, Kopp et al. (2012) also found that ectopic expression of SOX9 alone caused "ductal reprogramming" within 6 weeks, a type of pre-ADM state wherein acinar transcripts (*Amylase, Mist1*) began to decrease while ductal transcripts (*Krt19*) increased. Additionally, they found that acinar cell morphology began to change after 6 months of transgenic *Sox9* expression as evidenced by central lumen dilation. Using two different inducible SOX9 mouse models, we found no evidence of ductal reprogramming after 6 weeks of prolonged expression. Interestingly, while we did not perform any studies longer than 6 weeks, central lumen dilation was observed when the iSOX9 transgene was expressed in $Mist1^{CreER/CreER}$ ($MIST1^{KO}$) mice, a model known to be more susceptible to transdifferentiation (Shi et al., 2013) Finally, Kopp et al. found that acute pancreatitis caused the formation of pervasive and persistent ductal lesions in mice expressing transgenic *Sox9*. Our studies, on the other hand, showed a milder response, and GFP staining clearly marked iSOX9 expressing acini that were able to recover from injury.

There are a few possible reasons for the discrepancies in these findings. One simple but potentially important difference between our studies and those by Kopp et al. (2012) was the mouse strains used. Kopp et al (2012) maintained mice in a mixed background, while our studies were performed using backcrossed C57BL/6 mice, an inbred line known to be more resistant to tumor formation (Puccini et al., 2013). SOX9 is known to act in a dose-dependent manner (Prévostel and Blache, 2017; Yang et al., 2019a) so differences in the level of transgene expression between the two studies could be a contributing factor. Both studies' transgenic models were controlled by a CAG promoter, but position effects could still influence transgene expression. Recombination efficiency was also similar between the $Mist1^{CreER}$*; iSox9* mice used here and the $Ptf1a^{CreER}$ driven mouse model used for most of Kopp et al (2012)'s experiments, with approximately 60% of the acinar cell population showing signs of recombination in both studies. However, Kopp et al. (2012) also used a constitutively expressed $Ptf1a^{Cre}$ driver to mediate the deletion of SOX9 and activation

of oncogenic *Kras for* many experiments, including those whose results were inconsistent with our findings. The use of $Ptf1a^{Cre}$ in Kopp et al. (2012) is a likely culprit for the differences in our findings. *Ptf1a* is expressed early in pancreatogenesis, around E9.5, and is present in multipotent progenitor cells (Pan and Wright, 2011). This has multiple implications, one being that transgenic *Sox9* would have been expressed during development, rather than in mature and primarily quiescent acinar cells. This may have had some unnoticed effect on acinar cell maturation. More importantly, however, is the more recent finding that *Ptf1a* heterozygosity promotes PanIN and PDAC development in $Kras^{G12D}$ expressing mice by destabilizing acinar cell differentiation status (Krah et al., 2015). PTF1a is a master regulator critical for pancreas development and maintaining acinar cell identity (Cleveland et al., 2012). Because the $Ptf1a^{Cre}$ is a knock-in/knock-out allele, replacing the endogenous *Ptf1a* gene with Cre leads to loss of one *Ptf1a* allele in the Kopp et al. (2012) study, potentially leaving the acinar cell population more susceptible to SOX9 driven ductal reprogramming, resulting in the more extreme phenotypes reported in that study. While these differences may seem subtle, they have important implications regarding the influence of SOX9 on PDAC initiation. Though Kopp et al (2012)'s initial findings place SOX9 in a dominant role, capable on its own of reprograming acinar cells, our study seemingly indicates that SOX9 by itself does not produce these changes, but instead requires an additional disruption to the acinar cell program, as seen in the $Mist1^{KO}$*; iSox9* mice. If Kopp et al. (2012)'s results were exacerbated by the use of a *Ptf1a* heterozygous mouse model, this would actually agree with our findings, supporting the concept that additional destabilization of the acinar cell differentiation program is required for SOX9 induced ductal reprogramming.

Our findings do, however, strongly agree with Kopp et al (2012)'s results regarding the relationship between SOX9 and $KRAS^{G12D}$ driven PanIN formation, showing that SOX9 not only accelerates lesion formation, but is a necessary requirement. Previous studies discovered that oncogenic KRAS alone, when expressed in mature acinar cells, only rarely and gradually gives rise to PanIN lesions, requiring additional perturbations to achieve a threshold of activity high enough for acinar cell transformation to take place (Guerra et al., 2007, 2011; di Magliano and Logsdon, 2013). Additionally, sustained KRAS signaling is necessary for the maintenance of PanIN and PDAC, where cells either redifferentiate or undergo apoptosis when oncogenic KRAS activity is not prolonged (Collins et al., 2012). SOX9 expression has been linked to EGFR signaling and is upregulated upon KRAS activation (Chen et al., 2015a; Collins et al., 2014; Zhou

et al., 2017). Taken together these findings point to a central role for SOX9 in KRAS driven acinar cell transformation, either as a critical downstream effector of KRAS signaling or as a necessary player in a feedback mechanism used to sustain KRAS activity. Grimont et al. (2014) found expression of SOX9 caused upregulation of *ERBB2* transcripts and protein in human PDAC cells, supporting a KRAS signaling feedback model (Grimont et al., 2014). Though we detected no change in *Erbb2* in our iSOX9 RNA-Seq data, *Mapk3*, encoding ERK1 as a component in the ERBB2 signaling pathway, was upregulated in a SOX9 dependent manner, the impact of which requires further analysis. However, Zhou et al. (2017) found no difference in KRAS activation when SOX9 was overexpressed or knocked down in human derived ADM and PDAC cell lines (Zhou et al., 2017), indicating that other mechanisms are likely at play.

While a clear role for SOX9 in PDAC initiation and synergy between SOX9 and KRAS has been delineated, whether SOX9 is required past the point of PanIN formation is less clear. Analysis of human pancreatic cancer cells in our work and previous studies showed that SOX9 expression enhances tumor initiating properties in these cells, and therefore plays an important role in their tumor forming capability (Eberl et al., 2012; Zhou et al., 2017). However, this did not hold true when *Sox9* was deleted in primary mouse KC and KPC cell lines. Indeed, loss of SOX9 had no impact on tumor growth when KC or KPC cells were injected into syngeneic mice, evidenced by unhindered growth of SOX9 negative tumors. This is interesting given the critical role SOX9 plays during disease initiation in these same mouse models. Interestingly, Kopp et al. (2012) observed a drop in the consistency of SOX9 expression from early PanIN lesions to advanced PanIN and PDAC in human tissue samples, with 96% of early PanIN tissue cores exhibiting clear SOX9 staining, while only 72% and 69% of advanced PanIN and PDAC showed SOX9 staining respectively (Kopp et al., 2012). Our results, coupled with Kopp et al (2012)'s observations, support a model wherein SOX9 expression is critical for PDAC initiation but is dispensable, in some cases, as the disease progresses. However, the factors that determine whether SOX9 is necessary or superfluous past the point of transformation remain unknown.

As a transcription factor, we hypothesized that SOX9 promotes lesion formation through the regulation of critical gene targets which in turn carry out specific functions related to transformation and/or dedifferentiation. However, it is important to note that relevant noncanonical functions of SOX9 have also been reported. Deng et al. (2015) showed that SOX9 promoted cancer stem cell properties in several human PDAC cell lines not through its transcriptional activity, but

by binding to and sequestering the GLI1 targeting E3 ubiquitin ligase β-TrCP, thus stabilizing GLI1 protein and amplifying hedgehog signaling (Deng et al., 2015). In addition, it has been shown that SOX9 binds RNA and affects splicing, as SOX9 knockdown in colon cancer cells caused hundreds of splicing changes, while transcription of these alternatively spliced genes remained unchanged (Girardot et al., 2018). These noncanonical mechanisms of SOX9 action should therefore be examined more closely in the context of acinar cell transformation in future studies.

To gain greater insight into the SOX9 regulatory network as it pertains to PDAC initiation we performed RNA-Seq examining the transcriptional differences between normal acinar cells and those ectopically expressing a *Sox9* transgene. This uncovered previously identified SOX9 gene targets related to PDAC progression, as well as a subset of 105 genes that exhibited similar transcriptional changes in ADM and/or PanIN transcriptomics analyses (Krah et al., 2015; Ling et al., 2012). MetaCore pathway analysis identified enriched functional categories related to adhesion, cytoskeletal components, and blood vessel growth and development. Of note, in a comprehensive analysis of SOX9's role in basal cell carcinoma (BCC) Larsimonet et al. (2015) used both RNA-Seq and ChIP-Seq strategies examine the SOX9 regulatory network as it pertained to BCC malignancy. Similar to our results, in their analysis cell adhesion and cytoskeleton/invasion related categories were also identified as areas impacted by SOX9 expression, which they attributed to increased invasiveness (Larsimont et al., 2015). However, despite these similarities, only 28 gene targets were identified in common between our RNA-Seq data and the BCC RNA-Seq, again highlighting the context specific nature of SOX9.

Adopting a similar strategy to Larsimont et al. (2015), we attempted to generate SOX9 ChIP-Seq data as a means to identify SOX9 regulated genes in the precise context of PanIN formation and to complement our RNA-Seq experiment. However, this strategy was unsuccessful largely due to a lack of proper positive control loci that could be used to optimize the ChIP protocol. Indeed, as highlighted above, SOX9 is known to display tissue specific functionality, and as a result commonly regulated SOX9 genes are not well known. We attempted to overcome this obstacle by using a bioinformatics strategy, but inadvertently enhanced the presence of false positive "phantom" peaks in our data. Additionally, due to supply issues midway through our study, we were unable to use the typically accepted and validated SOX9 ChIP-grade antibody (Millipore, AB5535) for our ChIP-Seq, and instead tested six available SOX9 antibodies, identifying one, (Abcam, ab185230) that had peak enrichment similar to AB5535, albeit in false positive loci, and

met ENCODE's guidelines for antibody selection (see Figure 3.23A). ChIP quality is largely at the mercy of the antibody used, so in addition to optimizing our protocol around false positive SOX9 binding sites, the use of an unvalidated antibody may have also contributed to the lack of enrichment in our final dataset. If this study were repeated, SOX9 targets should be validated using $SOX9^{KO}$ or $Sox9^{fl/fl}$ samples prior to performing deep sequencing, and a well characterized and approved ChIP-grade antibody should also be used.

Taken as a whole, the data presented here support a critical role for SOX9 in $KRAS^{G12D}$-driven acinar cell transformation. We find that SOX9 is indeed aberrantly expressed in both premalignant and frank PDAC tissues, and, importantly, we show that ablation of SOX9 prevents lesion formation even when strong disease drivers are present such as oncogenic KRAS and pancreatitis induced inflammation. Indeed, overexpression of SOX9 using a transgenic mouse model accelerates KRAS-mediated transformation, hinting at a synergistic relationship between SOX9 and KRAS signaling that requires closer analysis. However, our results also indicate a more subtle role for SOX9 in acinar reprogramming and PDAC malignancy compared to past reports. We find that ectopic expression of SOX9 alone has minimal impact on acinar cell homeostasis and does not induce ductal reprogramming unless additional disruptive factors are present, such as loss of MIST1 expression. Furthermore, ablation of SOX9 in primary mouse PDAC cell lines had no discernable impact on tumorigenesis in allograft experiments, showing that SOX9 may be dispensable for PDAC maintenance and tumorigenesis. Therefore, SOX9 functions as a gatekeeper at the tipping point of acinar cell transformation but does not induce transformation in the absence of oncogenic KRAS and may not be required once transformation has occurred.

CHAPTER 4. MECHANISMS OF PAR1 DEPENDENT IMMUNE EVASION

4.1 Introduction

Protease activated receptor 1 (PAR1) is a seven transmembrane G protein-coupled receptor uniquely and irreversibly activated through proteolytic cleavage of its cytoplasmic tail by proteases, thrombin being the most well studied of these activating enzymes. PAR1 is found on a wide variety of cell types, including many from the immune lineage (Steinhoff et al., 2005), and it is an important factor in hemostasis (Andersen et al., 1999). However, aberrant expression of PAR1 has also been reported in several cancers including melanoma, breast, and pancreatic ductal adenocarcinoma (PDAC), and has been shown to contribute to tumor cell proliferation and survival as well as angiogenesis and metastasis (Arora et al., 2007; Han et al., 2011).

Indeed, recent work from our lab by Yang et al. (2019) confirmed that PAR1 is largely undetectable in normal pancreas epithelium but is expressed in premalignant PanIN lesions as well as frank carcinoma. Furthermore, CRISPR/Cas9-mediated deletion or shRNA knockdown of PAR1, encoded by the gene *F2r*, in primary mouse cell lines, isolated from *LSL-Kras^{G12D}; LSL-Trp53^{R172H}; Elastasepr^{CreER}* (KPC) PDAC tumors, greatly reduced subcutaneous and orthotopic allograft tumor growth, as well as pulmonary metastasis following tail vein injection. These effects were independent of any changes in *in vitro* cell proliferation or soft agar colony formation and translated to a significant increase in animal survival following orthotopic implantation (Yang et al., 2019b).

It is important to note that these studies utilized syngeneic PDAC tumor cell lines to allow tumor growth studies to be carried out in immunocompetent mice. This strategy is unique in the field and allows for a more complete analysis of the tumor microenvironment's impact on tumor growth without discounting the influence of the immune system. Given that PAR1 has been shown previously to play a role in various inflammatory conditions (Shpacovitch et al., 2008), additional allograft studies were conducted to assess the contribution of the immune system on the tumor forming capacity of PAR1 knockout cells. Remarkably, no difference in tumor growth was detected between the PAR1 knockout and control cells when injected subcutaneously into immunocompromised mice (e.g., NSG), indicating that the impact of PAR1 on PDAC tumor

growth is dependent on its ability to protect tumor cells from immune clearance (Yang et al., 2019b).

My studies have focused on further characterizing the mechanism of PAR1-dependent PDAC immune evasion. I found that the tumor forming capacity of PAR1 knockout cells could be restored by depleting CD8a positive cells in immunocompetent C57BL/6 mice, while depletion of NK1.1 or CD4 expressing cells had no effect. This indicates that PAR1 knockout tumors are cleared by an adaptive, $CD8^+$ cytotoxic T lymphocyte (CTL) response, while PAR1 expressing cells avoid this fate. The mechanism(s) by which PAR1 expression protects KPC tumor cells from an immune challenge is undefined. Therefore, we utilized RNA-Seq data to identify genes regulated by PAR1 activation with protein products that could potentially protect tumor cells from an adaptive CTL response. This analysis identified *Ptgs2*, encoding COX2, and *Csf2* (*Gm-csf*) as candidate targets in the PDAC immune evasion response. Ectopic expression of each of these genes restored tumor growth in PAR1 knockout PDAC cells. Similarly, CRISPR-mediated ablation of *Ptgs2* or *Csf2* in PAR1 expressing PDAC cells greatly attenuated allograft tumor growth, indicating that the presence of PAR1 was not sufficient to maintain tumor growth in the absence of either of these downstream targets. Mechanistically, both CSF2 and prostaglandin E_2 (PGE_2), a major downstream product of COX2 enzymatic activity, are secreted factors known to promote the formation of an immunosuppressive tumor microenvironment. However, PAR1 knockout PDAC cells were preferentially targeted and eliminated from subcutaneous allograft tumors when co-injected with PAR1 expressing "wildtype" (WT) KPC cells, indicating that PAR1 promotes tumor immune evasion through local and not systemic mechanism(s), and therefore does not create a generally immunosuppressive environment capable of supporting PAR1 knockout tumor cell growth. In support of this finding, WT KPC cell tumors grew normally when injected into mice that had already cleared PAR1 knockout tumors and thus were already exposed to common KPC antigens. These findings thus define a novel role for PAR1 in promoting cell intrinsic mechanism(s) of PDAC tumor immune evasion, and although additional research is necessary to fully understand precisely how this is achieved, it highlights PAR1 as a potentially new immuno-oncology therapeutic target.

4.2 Results

4.2.1 Characterization of PDAC cell responses to PAR1 activation *in vitro*

Although our previous data established a strong *in vivo* PAR1-dependent phenotype, only minimal characterization of the direct effects of PAR1 activation on PDAC cells was performed. To begin a more detailed analysis of this pathway, various *in vitro* assays were undertaken based on previously reported PAR1-mediated cellular responses to better understand the impact of PAR1 signaling in PDAC cells. The first step was to track the timing activation and internalization of PAR1 following thrombin treatment. For visualization purposes a previously established KPC-*Par1* knockout cell line ($PAR1^{KO}$ cells) engineered to express a doxycycline inducible Myc-tagged PAR1 transgene (referred to as $Par1^{KO/Tg}$ cells) (Yang et al., 2019b) was used to overcome limitations in direct PAR1 staining due to poor antibody reactivity. Because PAR1 activation involves proteolytic cleavage and is therefore irreversible, once activated, PAR1 is quickly internalized and undergoes lysosomal degradation. Consistent with previous reports of PAR1 cycling (Paing et al., 2006), immunofluorescence staining revealed that PAR1 was largely internalized within 5 minutes of thrombin exposure, showing a more punctate perinuclear expression pattern, and PAR1 was completely undetectable after 45 minutes (Figure 4.1A). The timeframe of rapid internalization corresponded with the activation of known PAR1 downstream signaling pathways (Zhao et al., 2014). *In vitro* both ERK and AKT phosphorylation peaked 5 minutes after thrombin exposure and elevated pERK and pAKT levels were still detectable 2 hours after treatment (Figure 4.1B). Identical signaling patterns were detected in human MIAPaCa2 PDAC cells which others have reported express high levels of PAR1 (Rudroff et al., 2002) (Figure 4.1C). Interestingly, neither cell line showed significant changes in cell proliferation when exposed to thrombin (Figure 4.2), though PAR1 has been reported to enhance proliferation in other cell types (Liu et al., 2017b).

PAR1 signaling can also produce changes in actin organization causing the formation of stress fibers and increased cell motility (Even-Ram et al., 2001; Fujimoto et al., 2013; Hatziapostolou et al., 2008). Indeed, phalloidin staining of the KPC and MIAPaCa2 cells following thrombin treatment revealed distinct cytoskeletal changes, with stress fibers appearing as early as 15 minutes following thrombin exposure (Figure 4.3). Likewise, and consistent with our previous *in vivo* lung metastasis assays (Yang et al., 2019b), thrombin treated KPC cells showed a

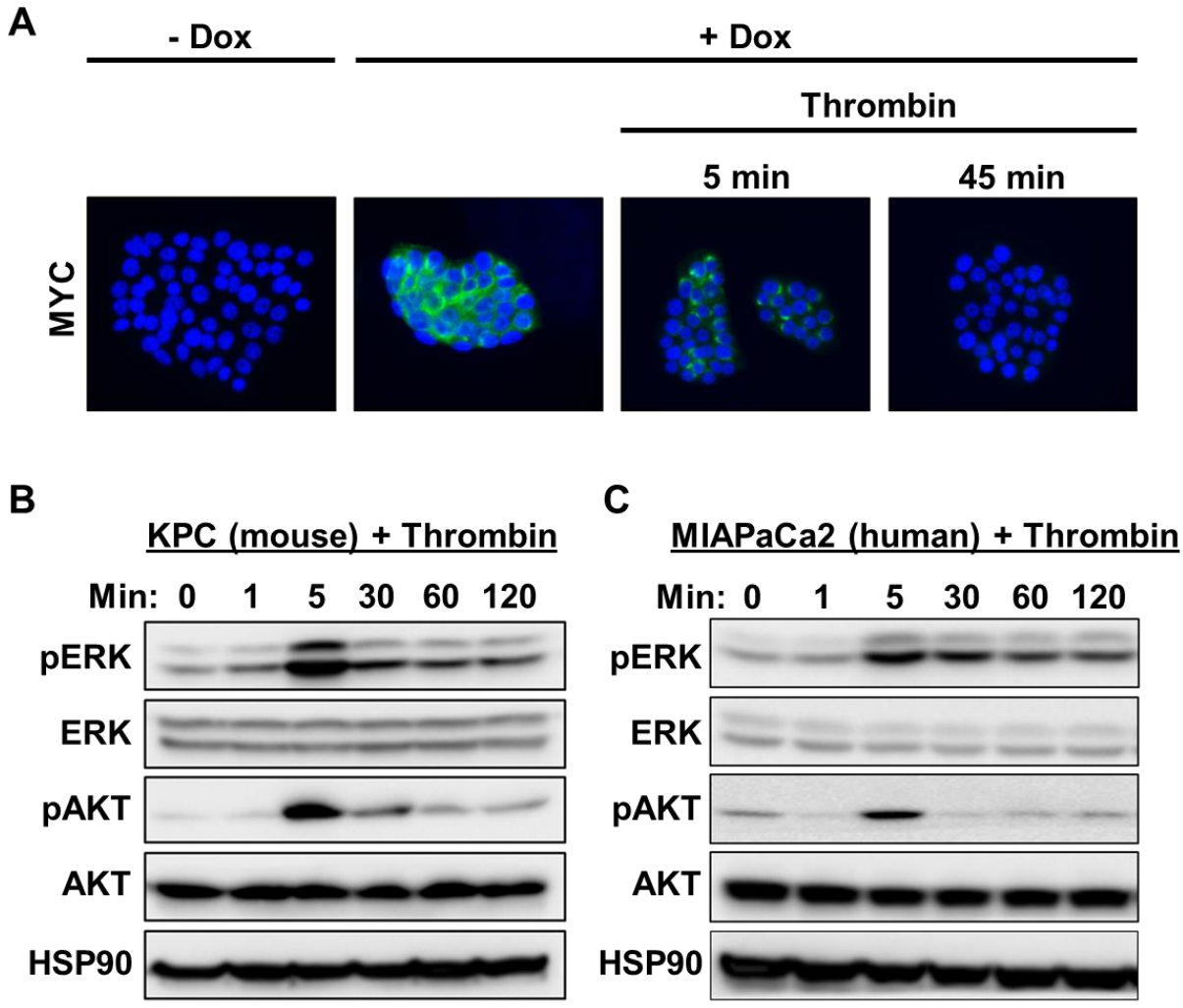

Figure 4.1 Thrombin activates PAR1 *in vitro* within 5 minutes of exposure.

(A) Immunofluorescence staining of KPC cells expressing a doxycycline inducible Myc-tagged PAR1 transgene. PAR1-Myc is absent from untreated cells in culture but appears after treatment with 1 μg/mL doxycycline. Myc staining quickly decreases after exposure to thrombin (1 U/mL). Note that thrombin was not washed from the media and therefore was present for the duration of this experiment. **(B, C)** Immunoblots showing thrombin induced phosphorylation of ERK and AKT in mouse KPC and human MIAPaCa2 PDAC cell lines treated *in vitro*.

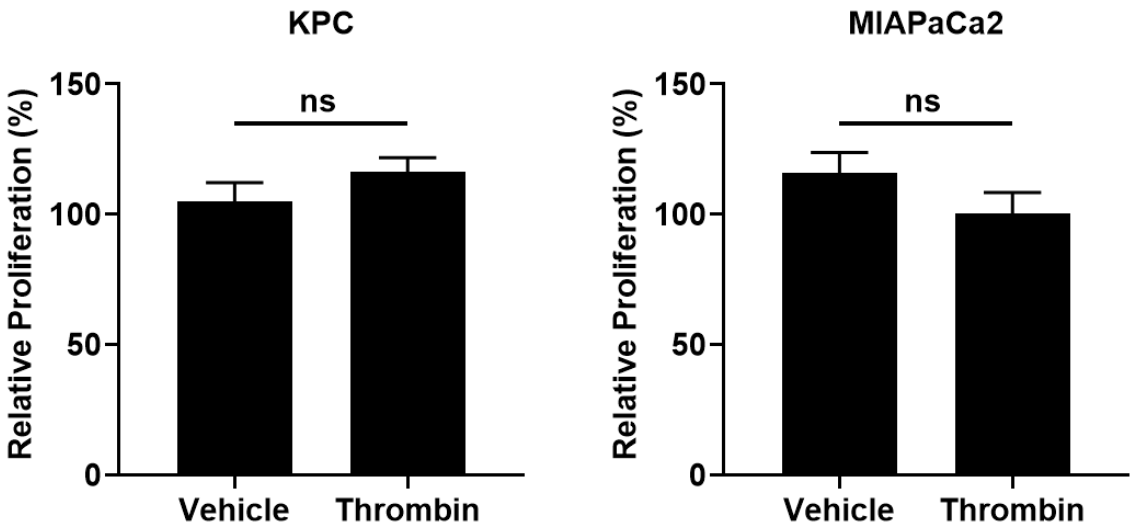

Figure 4.2 Thrombin mediated PAR1 activation does not affect PDAC cell proliferation

The impact of thrombin on the proliferation of KPC and MIAPaCa2 cells was measured using a CyQuant proliferation assay. Data represent the relative proliferation between vehicle and thrombin (1U/mL) treated cells after 5 days in culture, (n = 3/group).

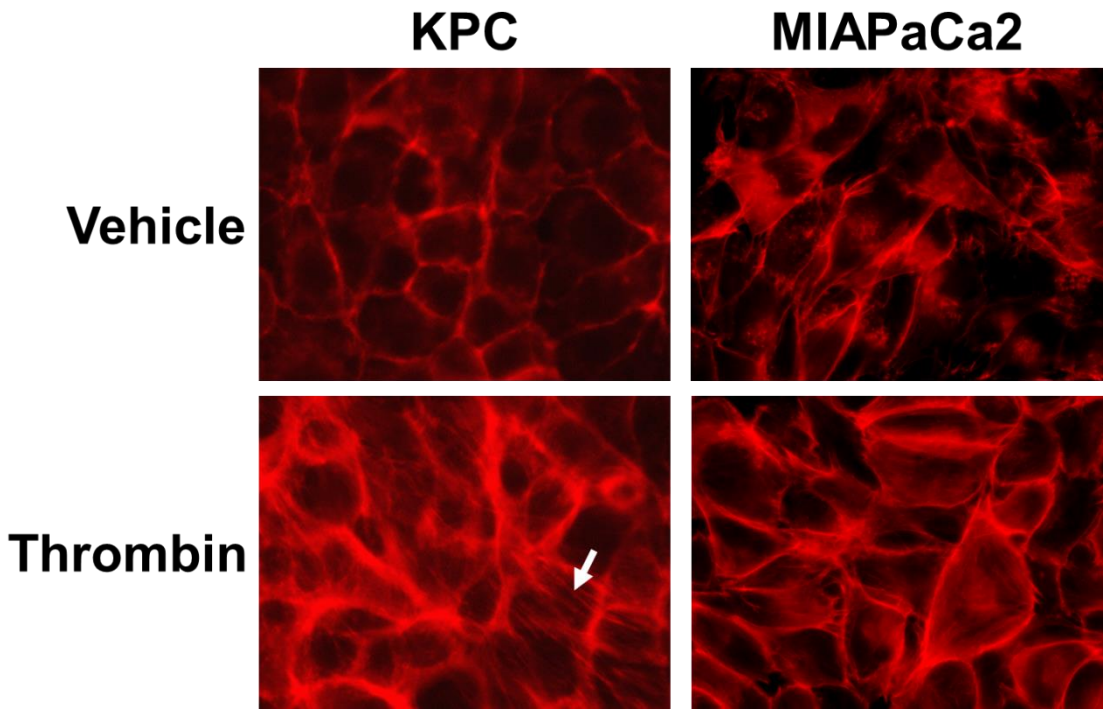

Figure 4.3 Thrombin treatment causes changes in cytoskeletal organization in PDAC cells.

KPC and MIAPaCa2 cells show changes in actin cytoskeletal organization following 1U/mL thrombin treatment including increased cortical actin and the presence of stress fibers (white arrow). Images are of phalloidin staining taken 15 minutes after thrombin treatment.

Significant increase in transwell migration compared to vehicle treated controls (Figure 4.4). As a whole, these results show that PAR1 activation in PDAC cells occurs rapidly following thrombin exposure and produces many of the classically observed phenotypes reported in previous studies of other cell types.

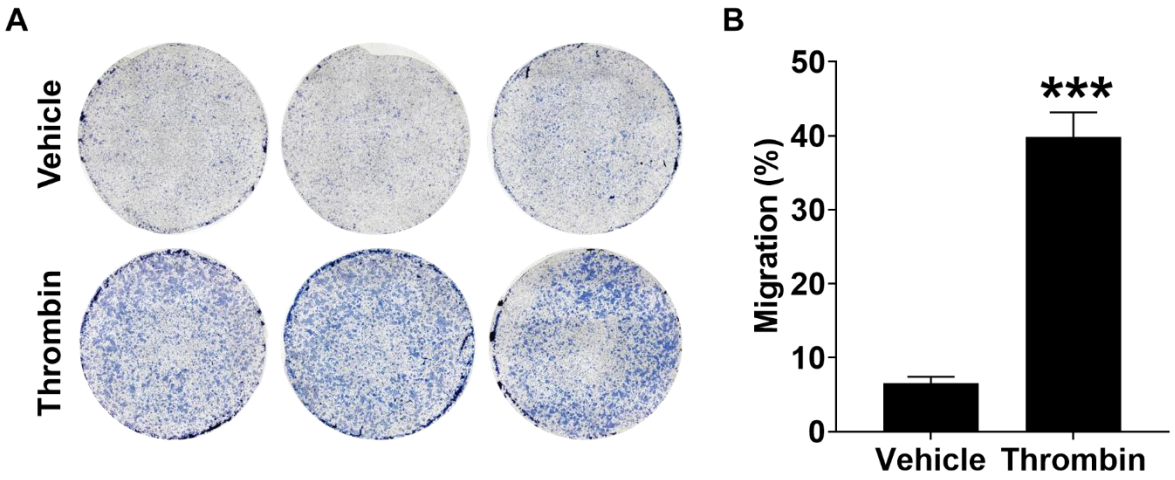

Figure 4.4 KPC cells show increased transwell migration following thrombin treatment.

(A) Transwell inserts stained with modified Giemsa showing differences in KPC cell migration between vehicle and thrombin treated cells. **(B)** Quantification of cell migration relative to total seeded cells based on ImageJ quantification of the stained transwell inserts.
(n = 3/group, ***p < 0.001)

4.2.2 PAR1 protects PDAC cells from clearance by the adaptive immune system

As described earlier, past research from our lab found PAR1 expression to be necessary for PDAC allograft tumor growth in immunocompetent mice (Yang et al., 2019b). This discovery was best exemplified in an experiment utilizing the $PAR1^{KO/Tg}$ cell line. In this study WT C57BL/6 mice were orthotopically injected with $PAR1^{KO/Tg}$ cells and tumor growth was assessed in mice fed either a normal diet or doxycycline containing chow. As predicted, almost no detectable tumors were present in mice fed normal chow and those tumors that did form were quite small. In contrast, mice treated with doxycycline to activate expression of the PAR1 transgene, formed large tumors. I repeated this experiment and achieved nearly identical results to those reported by Yang et al. (2019b). Only one in seven control (-Dox) mice producing a small but detectable tumor, while all doxycycline treated animals had sizable growths (Figure 4.5). While these data indicate that PAR1 is critical for PDAC tumor growth in immunocompetent mice, further experimentation revealed that PAR1 expression was dispensable when PDAC cells were injected into immunocompromised NSG (NOD SCID gamma) mice. In this setting robust tumor growth was observed with both $PAR1^{KO}$ and control KPC cells (Yang et al., 2019b). These findings suggest that PAR1's main role in supporting PDAC tumor growth is providing protection from the immune system. However, the underlying mechanism by which PAR1 controls these events remains to be determined.

Immunocompromised NSG mice are known to be deficient in mature B, T, and NK cells and to possess defective macrophages and dendritic cells. Therefore, additional experiments were necessary to more specifically identify the immune cells responsible for targeting $PAR1^{KO}$ tumor cells *in vivo*. Immune profiling of tumors by flow cytometry revealed significantly more $CD8a^{+}$ T cells in $PAR1^{KO}$ tumors compared to "wildtype" (WT) KPC controls, as well as a decrease in tumor associated macrophages, while no difference was detected in the presence of CD4 positive T cells (Figure 4.6).

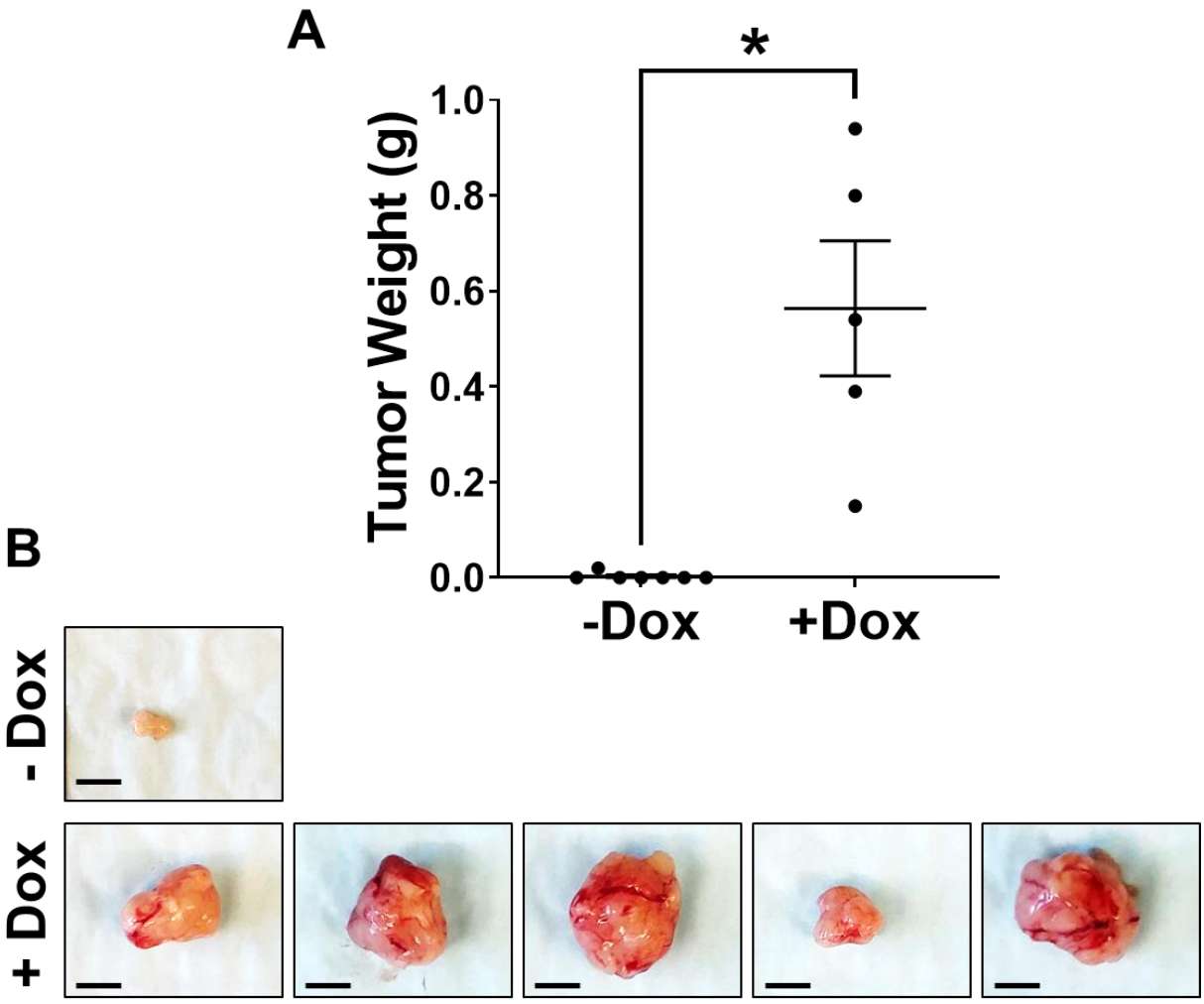

Figure 4.5 Re-expression of PAR1 in KPC-PAR1^{KO} cells rescues orthotopic tumor growth

(A) Quantification of orthotopic tumor weights 21 days post injection**. (B)** Images of gross tumor sections after resection. Scale bar represents 0.05 cm, * $p < 0.05$.

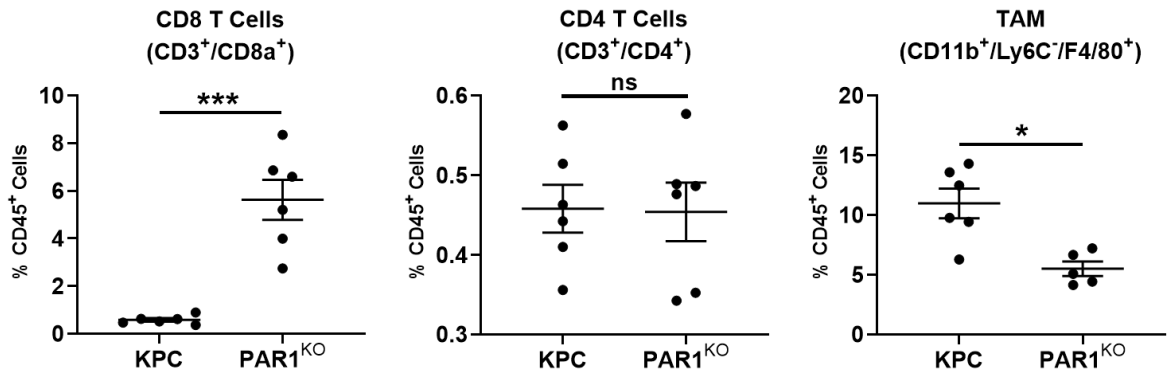

Figure 4.6 PAR1^{KO} tumors have increased CD8a^{+} T cell infiltration and decreased TAMs.
Flow cytometry analysis from subcutaneous allograft tumors harvested 9 days after cell injection profiling CD8 and CD4 T cell and tumor associated macrophage (TAM) population.

To assess the contribution of various T cell subtypes to PAR1^{KO} tumor clearance, monoclonal antibody depletion studies were performed, specifically targeting NK1.1, CD4, and CD8a expressing cells (Figure 4.7A). Although depletion of NK1.1 or CD4 positive cells had no impact on PAR1^{KO} KPC cell tumor growth, tumor forming capacity was restored when CD8a expressing cells were eliminated (Figure 4.7B)

CD8a positive cytotoxic T lymphocytes are members of the adaptive immune system and one of the major host defenses against cancer, capable of recognizing and killing tumor cells based on their antigen presentation (Farhood et al., 2019). My results thus signify that PAR1^{KO} PDAC cells are targeted by an adaptive CD8a T cell mediated response, and alternatively suggests that expression of PAR1 enables PDAC cells to escape this fate by a yet unknown mechanism. While this provides a more specified avenue for further exploration, it is worth noting that depletion of CD8a T cells also positively impacted tumor growth in PAR1-expressing control tumor cells (Figure 4.8AB), revealing that even PAR1 expressing PDAC cells are not completely impervious to CD8a T cell-mediated elimination. This suggests that additional immune cells are involved in the elimination of PAR1^{KO} tumors, as PAR1^{KO} and control KPC cells showed no difference in tumor growth when injected into severely immunocompromised NSG mice (Yang et al., 2019b), while PAR1^{KO} tumors remain significantly smaller than control tumors following CD8a depletion,

and therefore, do not fully regain their full tumor forming capacity by CD8a cell loss alone. Interestingly, histology from these samples revealed a distinct abundance of ductal structures in the $PAR1^{KO}$ tumors compared to the poorly differentiated control KPC allografts (Figure 4.8C), which is consistent with a previous publication finding a positive correlation between PAR1 expression and the differentiation status of human PDAC cell lines (Rudroff et al., 2002). Similar observations have also been made in shPAR1 treated oncogenic KRAS/P53-KO PDAC tumor cell allografts (Tekin et al., 2018), which were attributed in part to PAR1's contribution to epithelial to mesenchymal transition (EMT). Overall these results show that expression of PAR1 protects PDAC cells from elimination by a CD8a-positive cell mediated adaptive immune response.

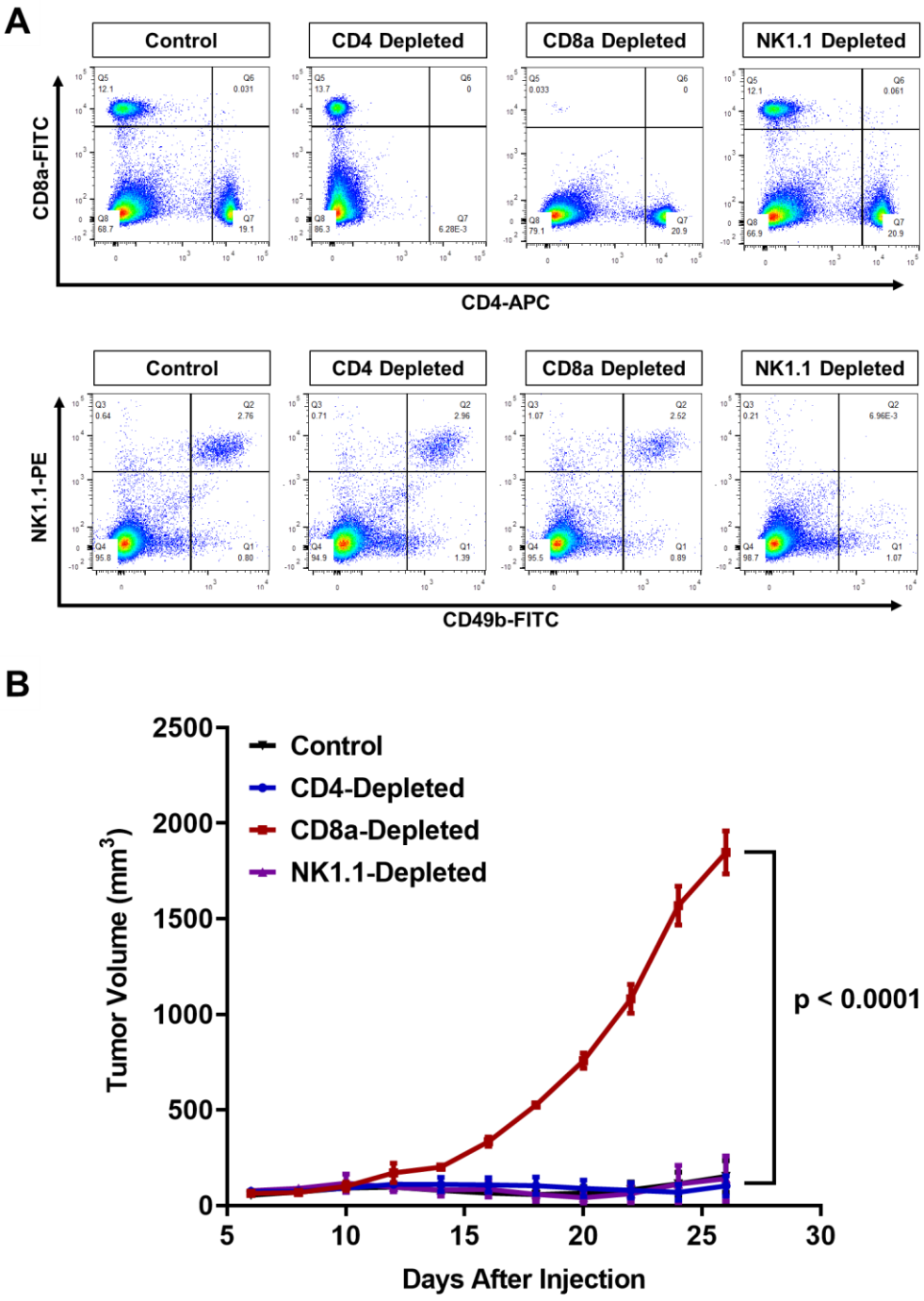

Figure 4.7 KPC-PAR1^{KO} tumor growth is restored upon depletion of CD8a^{+} cells.

(A) Flow cytometry plots of harvested mouse splenocytes showing successful depletion of CD4, CD8a, and NK1.1 expressing cells. **(B)** Allograft tumor growth curve showing that depletion of CD8a expressing cells restores tumor growth in PAR1^{KO} cells. (n = 4/group, RM-ANOVA). Results published previously in Yang et al. (2019b) based on experiments and analysis I performed.

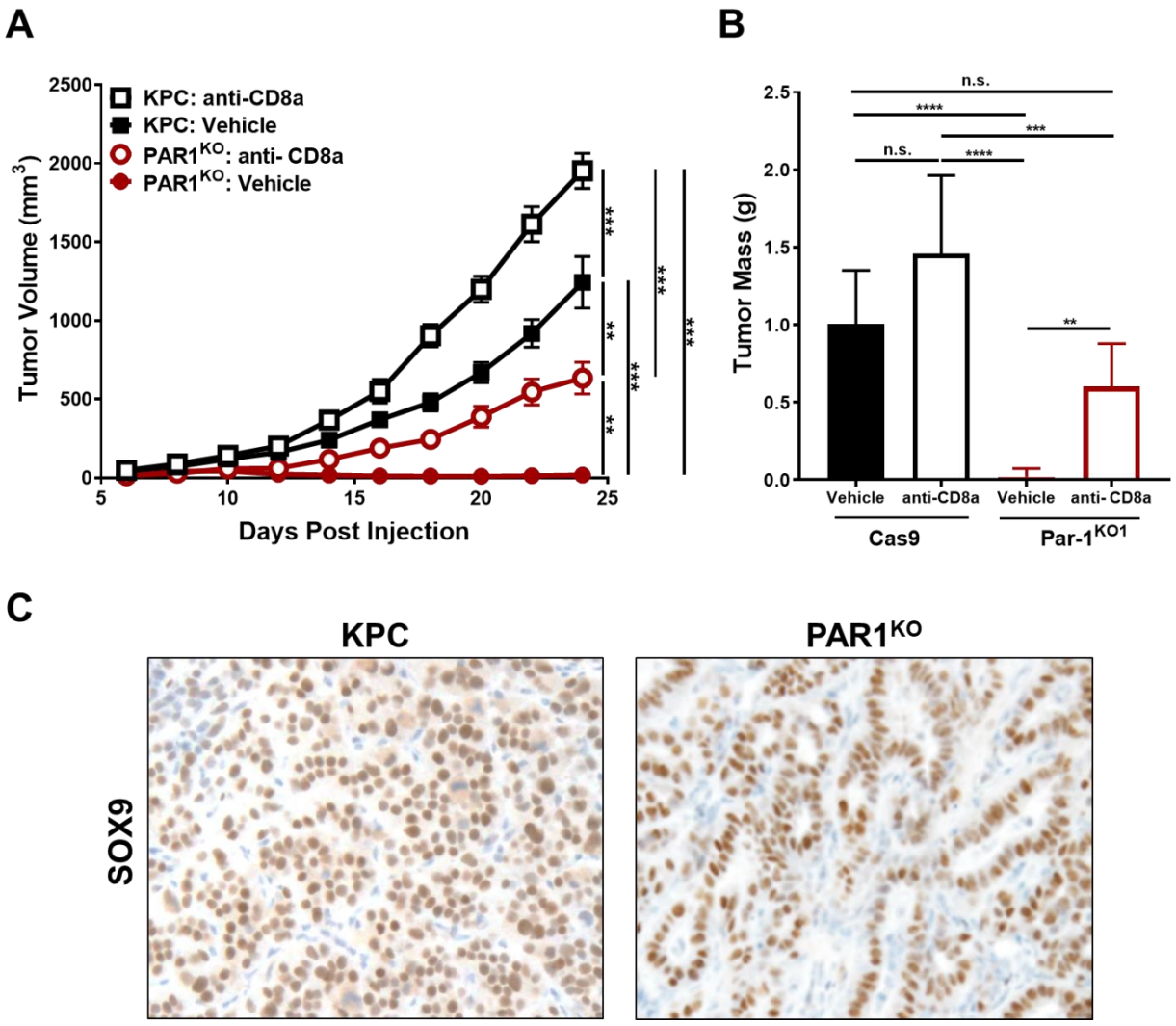

Figure 4.8 Both KPC control and PAR1^{KO} cell tumors have increased growth following CD8a^{+} cell depletion. However, these tumors have distinct histological phenotypes.

(A) Tumor growth curves comparing "wildtype**"** KPC and PAR1^{KO} tumor growth in vehicle and anti-CD8a treated mice. **(B)** Final tumor mass data from the allograft experiment shown in (A). Bars sharing the same letter are not significantly different based on Tukey's post hoc test. **(C)** Histology from anti-CD8a treated tumor samples stained with SOX9 as a general marker for KPC cells. (n = 8 mice/group). (A) and (B) were published previously in Yang et al. (2019b) based on experiments and analysis I performed.

4.2.3 PAR1 expressing PDAC cells escape elimination even in hosts that reject PAR1^{KO} tumor cells

There are many ways for tumors to evade the host immune response. Direct methods such as tumor cell expression of cell surface checkpoint proteins (e.g., PDL1) that can suppress the adaptive immune response or downregulation of MHC-I proteins to avoid cancer cell detection by CTLs. Indirect methods of evasion include the generation of an immune privileged or immunosuppressive microenvironment by reshaping the extracellular matrix (ECM) to prevent immune cell infiltration or by recruitment of immune inhibitory cell types including myeloid-derived suppressor cells (MDSCs) and regulatory T cells (T_{regs}) (Beatty and Gladney, 2015; Mushtaq et al., 2018). To determine if the presence of PAR1-expressing WT KPC cells could provide protection for PAR1^{KO} cells, as might be seen through the creation of an immune privileged microenvironment, allograft experiments were conducted using a mixed cell suspension containing both cell lines. PAR1^{KO} and control KPC cells were first engineered to express tdTomato or GFP, respectively, so that the final tumor cell composition could be assessed by flow cytometry. These cells were then co-injected at equal ratios into C57BL/6 mice (Figure 4.9A). A decrease in the number of PAR1^{KO} cells compared to controls was already detectable 5 days after injection, and by day 25 the tumors consisted almost entirely of control KPC cells with nearly all PAR1^{KO} cells in the tumors eliminated, though the overall tumor size was not reduced (Figure 4.9B-D). Consistent with our previous findings, when CD8a positive cells were depleted PAR1^{KO} cells were able to survive the duration of the study (Figure 4.9E). Although there were fewer PAR1^{KO} cells at the studies end compared to WT KPC cells, this was expected given earlier findings that CD8a depletion boosted both PAR1^{KO} and WT KPC tumor growth, ultimately giving rise to larger WT KPC cell tumors (see Figure 4.8AB). Additionally, and for reasons that remain unclear, analysis of the tumor histology from the study's day 25 end point revealed large areas consisting of only a single fluorescent signal (Figure 4.10), indicating poor intermingling of the labeled cell lines *in vivo*, despite having been injected as a mixed cell suspension and being well dispersed at day 5. Whether this segregation had any impact on the experimental outcome remains unknown.

The preferential targeting of PAR1^{KO} cells in the mixed tumor experiment implies that PAR1-expressing KPC cells can elude an active CTL response, as they persisted even while PDAC cells lacking PAR1 were eliminated from the same tumor. Because the PAR1^{KO} cells are derived

from the control KPC cells it can be reasonably assumed that they share common antigens that can be recognized by the adaptive immune response. Additionally, tumor growth can be entirely restored in the $PAR1^{KO}$ cells through ectopic expression of a PAR1 transgene, further indicating that it is the loss of PAR1 that influences the immune reaction to the $PAR1^{KO}$ cells, rather than the presence of a unique neoantigen. Therefore, to test this further, rechallenge allograft experiments were conducted to determine if PAR1-expressing KPC cells could survive in mice that had previously rejected $PAR1^{KO}$ tumors. These mice should be capable of quickly mounting an immune response to the KPC rechallenge due to the establishment of memory T cells following exposure to common KPC antigens from the initial $PAR1^{KO}$ allograft rejection. Consistent with the mixed tumor study results, KPC cells formed tumors normally when injected into rechallenged mice (Figure 4.11). This supports the hypothesis that PAR1 imbues PDAC cells with a highly effective ability for immune evasion, even in hosts actively mounting a strong anti-tumor immune response against $PAR1^{KO}$ PDAC cells.

4.2.4 $PAR1^{KO}$ cells are more susceptible to CTL mediated killing *in vitro*

In light of the above findings, *in vitro* CTL assays were performed to test whether PAR1 expression enabled direct tumor cell autonomous evasion of CTL killing, in contrast to PAR1 dependent recruitment of suppressive cell types such as MDSCs or effects related to tumor ECM remodeling. Initial experiments found elevated $PAR1^{KO}$ cytotoxicity compared to a non-antigen specific control cell line was detectable after 24 hours in culture, but no difference in cell death was observed between the two lines at a 6-hour time point (Figure 4.12A). The specific cytotoxicity observed was relatively low even at 24 hours, which is longer than typical CTL assays, but did show increasing cell death in relation to the effector:target cell ratio used. Next cytotoxicity was compared between $PAR1^{KO}$ and KPC cells (Figure 4.12B). KPC control cells did show lower levels of cytotoxicity compared to $PAR1^{KO}$ cells, but thrombin treatment had no impact on cytotoxicity. Furthermore, $PAR1^{KO/Tg}$ cells, which have doxycycline inducible PAR1 expression, still showed increased levels of cytotoxicity when treated with both doxycycline and thrombin (data not shown). This finding is perhaps the most confounding as $PAR1^{KO/Tg}$ cells form tumors readily in C57BL/6 mice and should in theory mimic the KPC control cells in any capacity relevant to tumor growth and immune evasion. Additionally, CTLs harvested from mice primed with B16

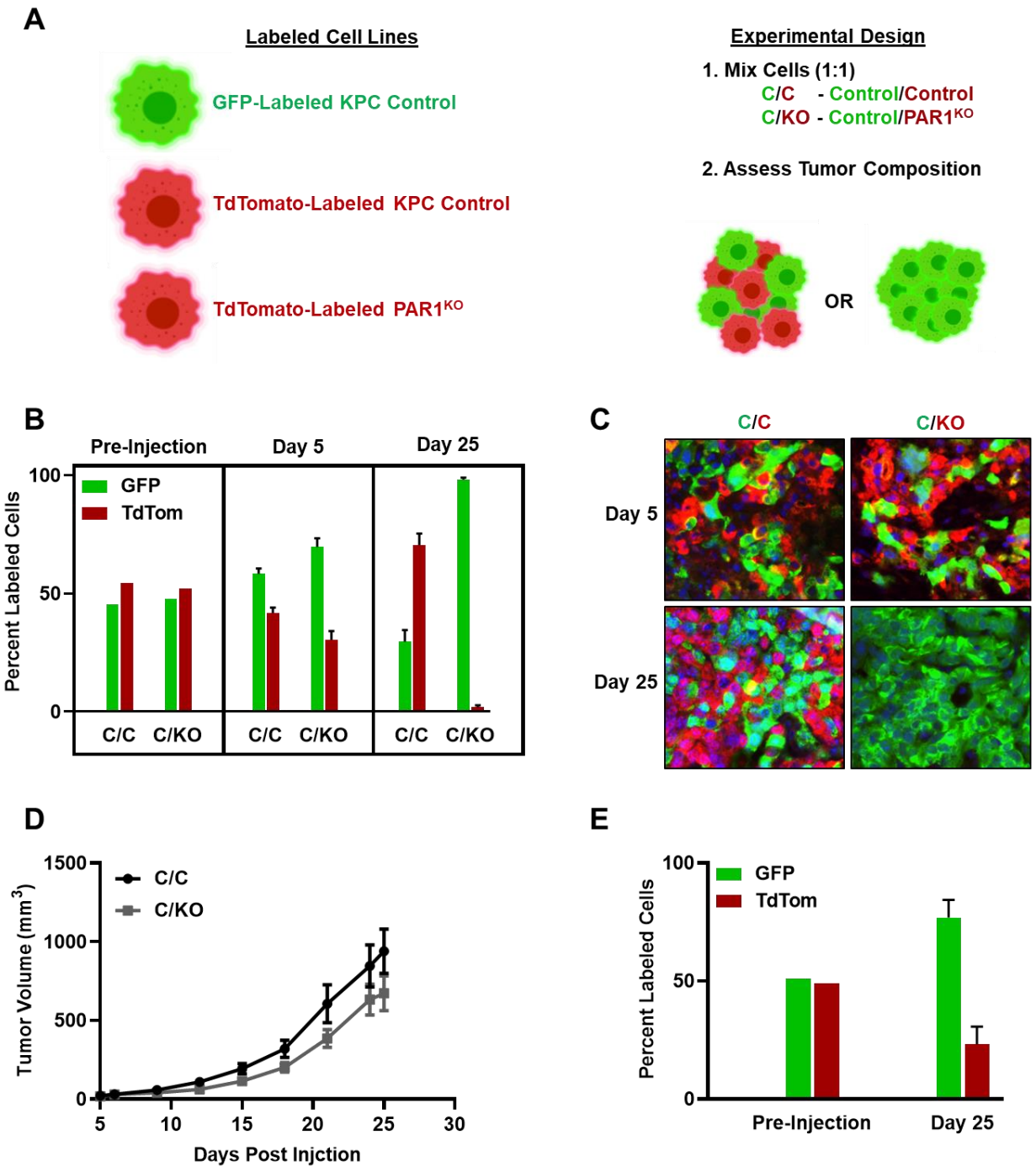

Figure 4.9 PAR1^{KO} cells are preferentially eliminated from mixed tumors.

(A) An overview of the experimental groups and design strategy. **(B)** Quantification of flow cytometry analysis of dissociated mixed tumor samples. **(C)** Immunofluorescence staining of mixed tumor sections showing distribution of GFP and tdTomato labeled cells. **(D)** Tumor growth curve of the data represented in (B) and (C). **(E)** Flow cytometry analysis of GFP labeled WT KPC and tdTomato labeled PAR1^{KO} cell mixed tumors in mice treated with anti-CD8a. (n = 6 mice/group)

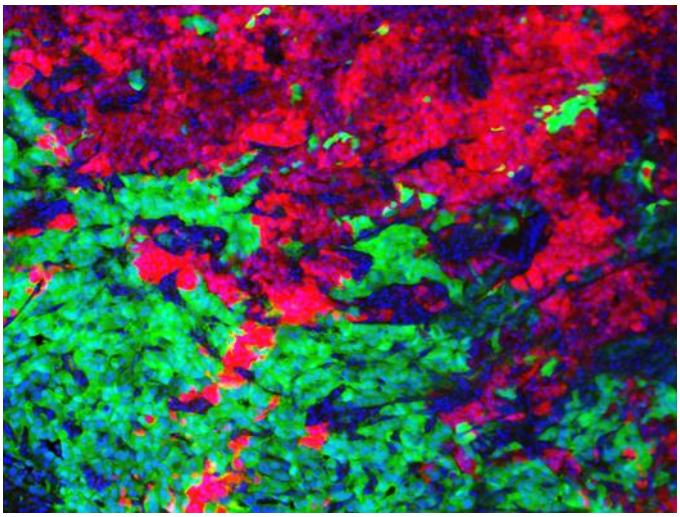

Figure 4.10 Labeled KPC cells are not homogenously distributed in allograft tumors.

Tumors harvested at day 25 post injection showed frequent areas with distinct segregation of GFP and tdTomato labeled cells.

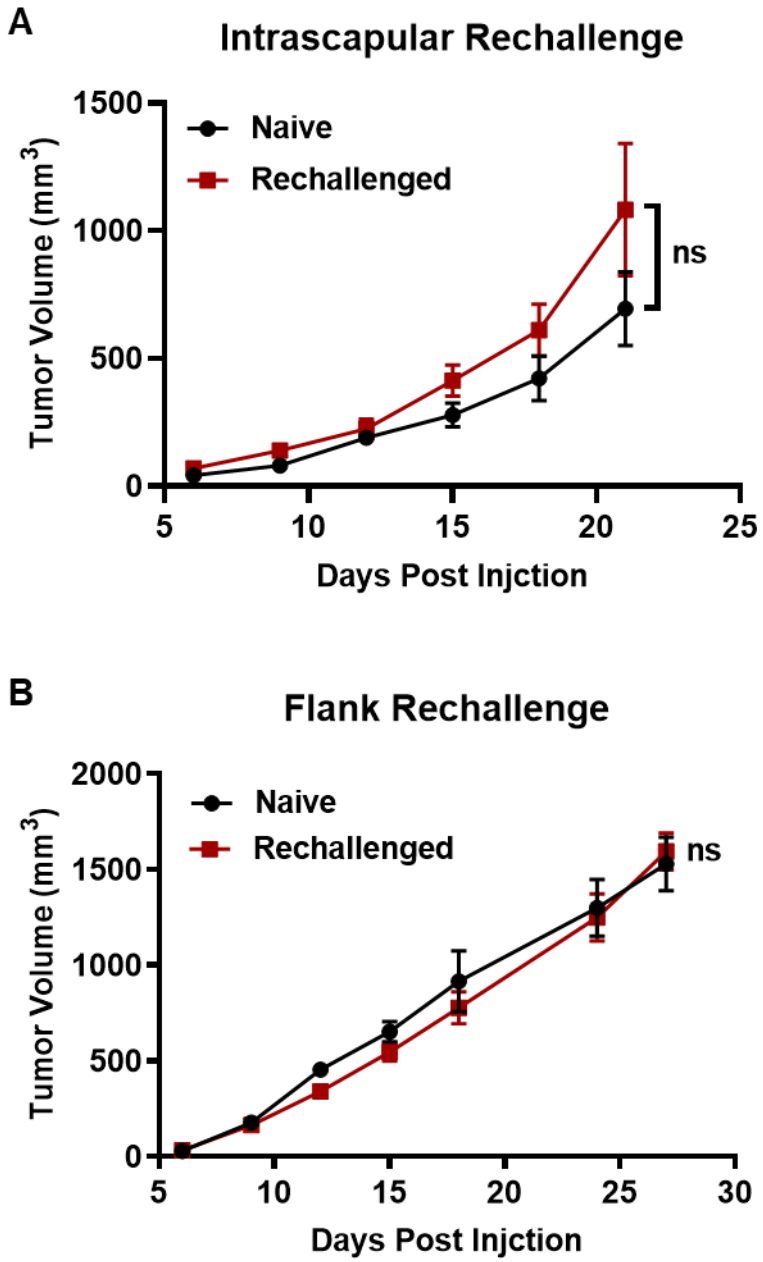

Figure 4.11 WT KPC cells show no difference in tumor growth when injected into mice previously exposed to KPC antigens.

PAR1^{KO} cells were injected into the intrascapular region of WT C57BL/6 mice and mice were left for 36 days so tumors could fully regress. Mice were then rechallenged with WT KPC cells by **(A)** injecting the intracapsular region again or **(B)** injecting the flank and tumor growth was compared that of littermate mice that did not receive the initial PAR1^{KO} injection (naïve group).
(n = 4-8 mice/group)

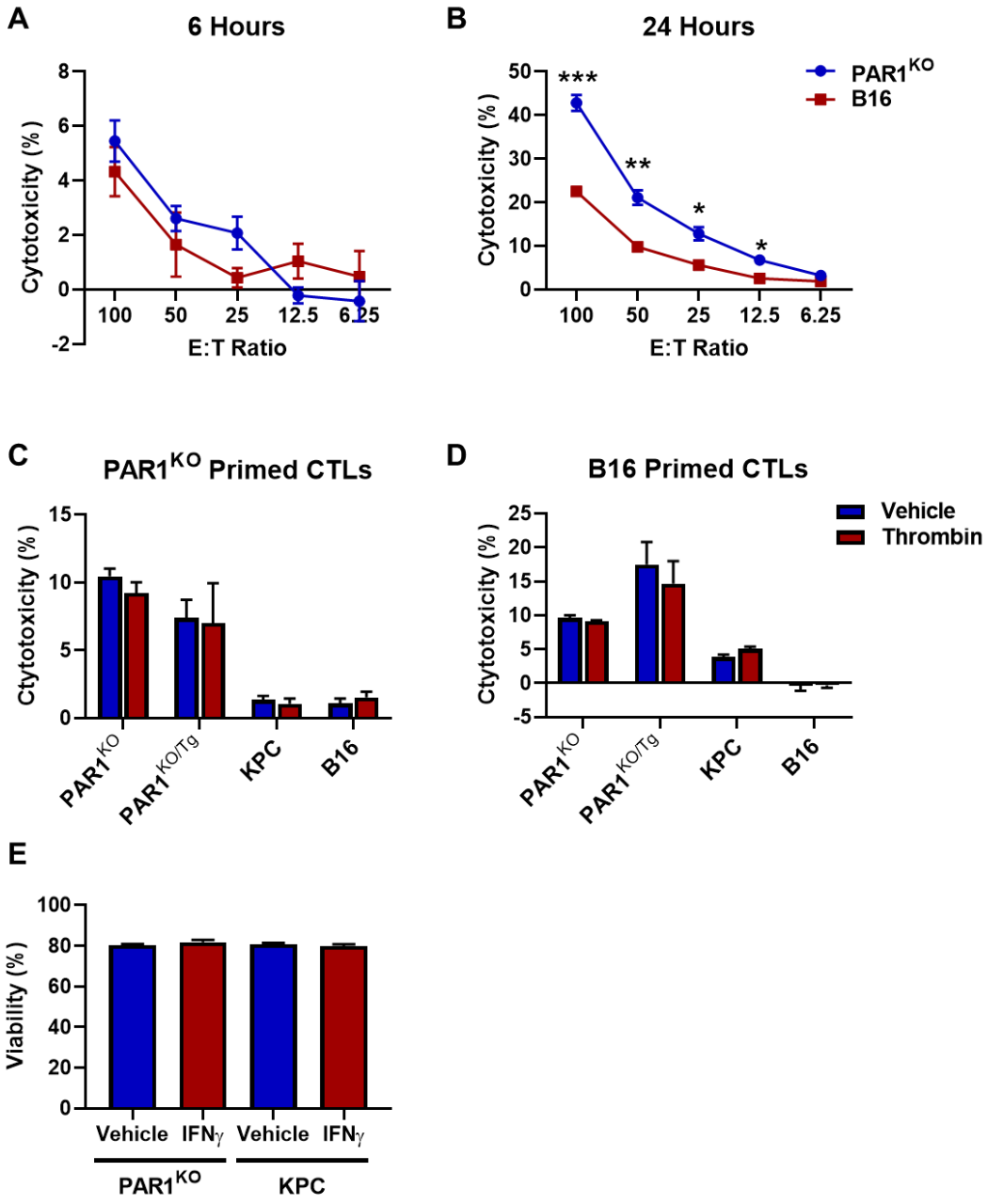

Figure 4.12 PAR1^{KO} cells show high sensitivity to nonspecific CTL mediated killing.

(A, B) Cytotoxicity levels were measured at the indicated time points by LDH release using various effector-CTL to target-tumor cell ratios (E:T). **(C, D)** CTLs isolated from mice primed using PAR1^{KO} or B16 cells were co-cultured with the indicated tumor cell lines at a 50:1 E:T ratio for 24 hours and cytotoxicity was measured by LDH release. All tumor cell lines were pretreated with doxycycline for 24 hours, followed by thrombin or vehicle for 24 hours prior to CTL addition. **(E)** Cell viability measured by flow cytometry based on cell permeability staining 24 hours after treatment with 20 ng/mL IFNγ. (n = 3-4/group)

cells, rather than PAR1^{KO} cells, also killed PAR1^{KO} cells with increased efficiency but were unable to induce cell death in B16 cells (Figure 4.12C). This suggests there is nonspecific cytotoxic activity from the CTLs, since B16 primed CTLs were unable to target B16 cells, but still killed PAR1^{KO} cells without being previously exposed to KPC antigens. As a result, it is unclear whether this iteration of the CTL assay properly tested the capacity of PAR1 expressing cells to escape an adaptive T cell driven immune response and will need to be repeated using other methods of cell priming to achieve cell specific cytotoxicity. However, it does indicate that cells from the PAR1^{KO} background are generally more sensitive to CTL mediated cytotoxic activity in a nonspecific manner and that this is independent of PAR1 expression as evidence by the results from PAR1$^{KO/Tg}$ cells. Of note, IFNγ released by activated CTLs can induce cell death in some tumor cells (Rakshit et al., 2014) and could explain this phenomenon. However, we found no difference in cell viability between PAR1^{KO} and KPC cells after treatment with IFNγ.

4.2.5 RNA-Seq identifies immune related transcripts regulated by PAR1 signaling in PDAC cells

Although PAR1 has been studied previously in the context of inflammation and tumor malignancy, these subjects have been examined separately and research has focused largely on PAR1's expression on immune cells, its involvement in vascular barrier function, or its ability to promote cell autonomous pro-tumorigenic properties such as increased migration and proliferation (Liu et al., 2017b; Shpacovitch et al., 2008; Steinhoff et al., 2005). While these studies provide a useful foundation for PAR1 function, the concept of PAR1-dependent tumor immune evasion is novel and requires examining PAR1 from a previously unexplored perspective. As mentioned earlier, tumors can avoid immune clearance by several means, and it is quite possible that PAR1 invokes multiple tumor-protective mechanisms in parallel. Therefore, to gain a broader insight into the downstream effects of PAR1 signaling in PDAC as a means to identify potential factors involved in tumor immune evasion, Yi Yang from our lab processed and submitted samples for RNA-Sequencing (RNA-Seq) comparing transcriptional changes induced by thrombin treatment in KPC cells (Figure 4.13A). Importantly, KPC-PAR1^{KO} cells were also examined, and showed no transcriptional changes upon thrombin addition, indicating that no other thrombin responsive receptors are active in the KPC cell line (Figure 4.13B). RNA-Seq analysis of our PAR1-expressing KPC cells identified 2,584 differentially expressed genes (DEGs), with 1,051

upregulated and 1,533 downregulated upon thrombin treatment. Gene Set Enrichment Analysis (GSEA) showed thrombin treatment was associated with an undifferentiated cancer gene signature (Figure 4.13C). This is consistent with the histological analysis described earlier in Figure 4.8C. Further evaluation of these DEGs using the mouse genome informatics (MGI) phenotype database showed a strong enrichment for immune related categories (Figure 4.13C). Additionally, KEGG pathway analysis identified significant enrichment in coagulation cascade (adjP = 1.93×10^{-16}), MAPK signaling (adjP = 2.88×10^{-12}), regulation of actin cytoskeleton (adjP = 4.4×10^{-7}), and focal adhesion (adjP = 1.5×10^{-6}) categories which are consistent with known PAR1-mediated cellular responses. The RNA-Seq thus provides a useful and wide-reaching assessment of PAR1 activity in PDAC cells, capturing signatures of known PAR1 regulated events as well as highlighting categories with relevance to a PAR1-immune cell interplay. The RNA-Seq was therefore used as a reference to identify potential mechanisms of PAR1-dependent tumor immune evasion based on changes in gene signatures following PAR1 activation.

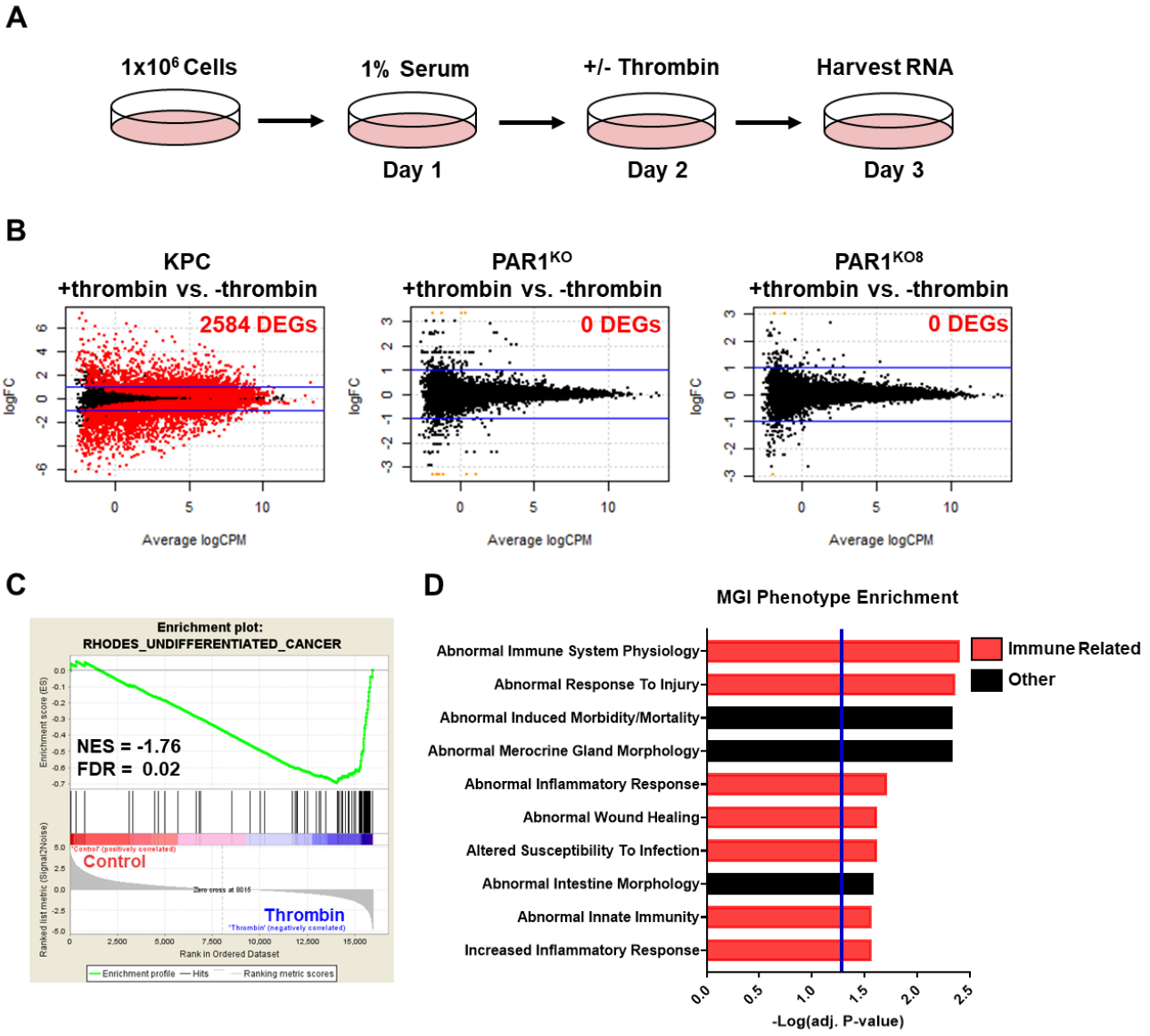

Figure 4.13 RNA-Seq identified thrombin/PAR1 dependent transcriptional changes related to abnormal mouse immune phenotypes.

(A) Experimental design strategy for harvesting RNA-Seq samples. **(B)** MA plots showing transcriptional changes induced by thrombin signaling in WT KPC (KPC) cells, $PAR1^{KO}$ cells and an additional $PAR1^{KO}$ ($PAR1^{KO8}$) cell line. Red dots represent genes with an FDR < 0.01, while the blue lines mark a 2-fold expression threshold cutoff. Orange dots are genes that were only detectable in one group. **(C)** GSEA plot of undifferentiated cancer gene set. NES = normalized enrichment score. **(D)** The top 10 significantly enriched MGI phenotypes based on the KPC ±- thrombin DEGs, blue line represents significance cutoff equivalent to $p < 0.05$. (A, B, & D) were adapted from Yang et al. (2019b). Results in (B) were provided by Nadia Lanman of Purdue University's Bioinformatics Core. Results in (D) are from my own analysis.

4.2.6 PAR1-dependent changes in cell surface molecules do not induce factors important for immune evasion

The labeled control/PAR1^{KO} (C/KO) cell experiment as well as the KPC allograft rechallenge study showed that PAR1 enables KPC cells to avoid elimination both during an active immune response and in hosts previously exposed to common KPC antigens. We hypothesized that this could be achieved through direct tumor-immune cell interactions as might be observed if PAR1 caused increased tumor cell expression of inhibitory checkpoint proteins. These proteins bind co-receptors on effector T cells to suppress T cell function and thus inhibit the immune response. Several checkpoint proteins have been identified to date and the development of checkpoint inhibitors as a cancer immunotherapy is an active research area (Wei et al., 2018). However, our RNA-Seq study showed no thrombin/PAR1-dependent changes in transcripts for most of the well-known inhibitory checkpoint proteins, with no significant change in *Pdl1, Cd276, Siglece,* and *Vista* expression, while *Vtcn1, Hvem, Ceacam1* and *Nox2* were downregulated by thrombin. In addition, transcripts for *Cd80, CD86, Pdl2* (*Pdcd1lg2*), and *Tdo* were undetectable. PDL1 protein expression was also further assessed in thrombin treated KPC cell by flow cytometry, but there was no response to thrombin even when IFNγ was used to induce PDL1 expression (Figure 4.14A). For reasons that remain unclear, the PAR1^{KO} cells had a stronger response to IFNγ treatment than KPC control cells (Figure 4.14B), a result that appeared to be dependent on the expression of PAR1 but independent of PAR1 activation by thrombin. This was also observed in experiments using PAR1$^{KO/Tg}$ cells as well (Figure 4.14C).

Ido1 and *Ido2* gene expression was significantly upregulated in the RNA-Seq upon thrombin treatment. IDO1 and IDO2 have been shown to be immunosuppressive in cancer by catalyzing tryptophan catabolism, the metabolites of which cause effector T cell apoptosis and the accumulation of T_{regs} (Hornyák et al., 2018). However, we were unable to replicate this finding by RT-qPCR. Analysis of RNA from allograft tumor samples showed higher *Ido1* and *Ido2* expression in the PAR1^{KO} tumors compared to control tumors (Figure 4.15). Therefore, no consistent pattern of PAR1-dependent *Ido1* or *Ido2* expression could be identified. *Siglec15* was also significantly upregulated after thrombin treatment in the RNA-Seq and this protein was recently identified as having checkpoint protein-like functionality, and being capable of inhibiting antigen-specific T cell responses (Wang et al., 2019a). *Siglec15* expression was confirmed to by

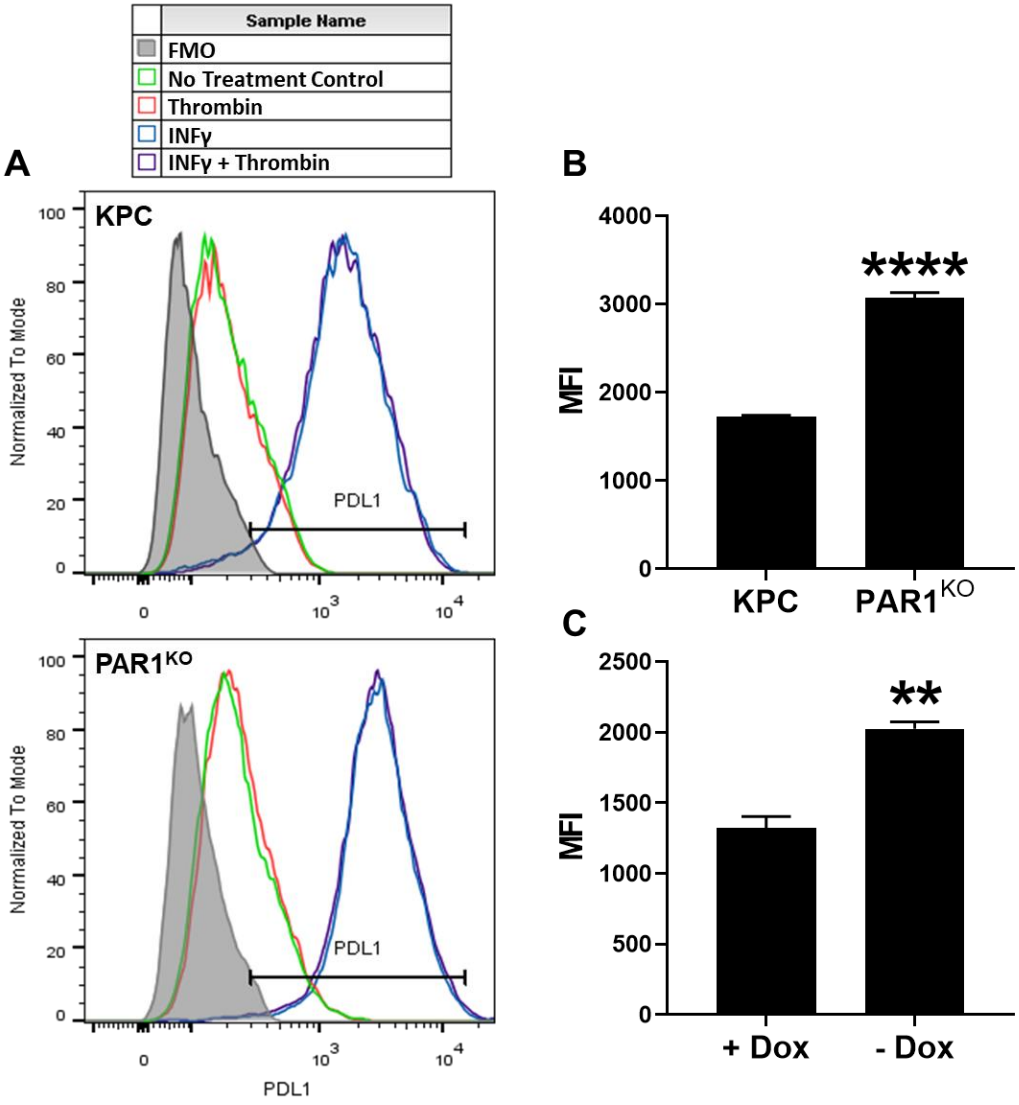

Figure 4.14 Thrombin treatment does not impact PDL1 expression, but IFNγ responsiveness is decreased in PAR1 expressing cells.

(A) Representative flow plots showing PDL1 protein expression in KPC and PAR1^{KO} cells 24 hours after various treatments. **(B)** Quantification of PDL1 expression in IFNγ treated cells. **(C)** Quantification of PDL1 expression in PAR1$^{KO/Tg}$ cells treated with IFNγ and ± doxycycline as a means to induce transgenic PAR1 expression. (n = 3/group, ** $p < 0.01$; **** $p < 0.001$); FMO = fluorescence minus one; MFI = median fluorescence intensity;

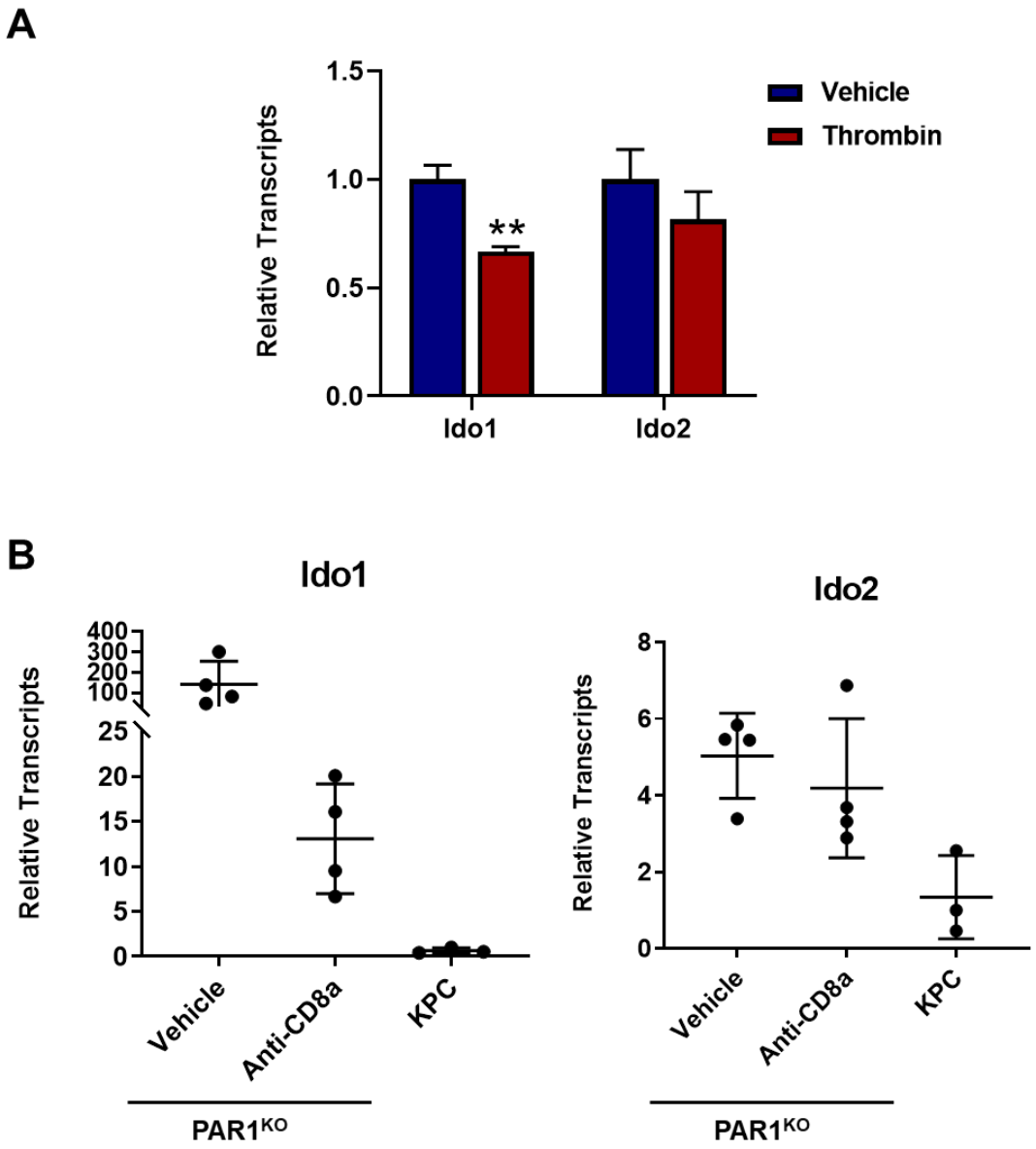

Figure 4.15 *Ido1/2* transcripts are lower in thrombin treated cells *in vitro* and PAR1 expressing tumors.

(A) Analysis of *Ido1* and *Ido2* transcripts from KPC cells treated *in vitro* with thrombin (n = 4/group). **(B)** RT-qPCR analysis of *Ido1* and *Ido2* transcripts using total RNA from subcutaneous allograft tumors. $CD8a^{+}$ cell depleted $PAR1^{KO}$ tumor samples were also analyzed to further confirm that differences in gene expression were due to the presence or absence of PAR1 and not a result of disparities in tumor size or the level of cytotoxic T cell infiltration. ** $p < 0.01$

RT-qPCR and we also observed PAR1-dependent expression in RNA from allograft samples (Figure 4.16AB). Viral transduction was then used to introduce a constitutively active *Siglec15* transgene into the PAR1^{KO} cell line to see if this could restore PDAC tumorigenesis. However, induced *Siglec15* expression had no impact on tumor growth (Figure 4.16CD). Therefore, we currently have no evidence that PAR1 enhances tumor cell immune evasion by upregulating the expression of inhibitory checkpoint proteins.

Cancer cells can also avoid immune clearance through loss of major histocompatibility complex class 1 (MHC-I) molecules to avoid immune detection (Garcia-Lora et al., 2003). MHC-I molecules present fragments of endogenous proteins on a cell's surface for recognition by T cells. CTL T cell receptors (TCRs) then engage with MHC-I and activate T cells to eliminate cells displaying abnormal peptides, such as cancer cells exhibiting neoantigens caused by mutations. Therefore, we tested whether PAR1 signaling decreased MHC-I expression. However, examination of the RNA-Seq data showed no changes in the expression of transcripts encoding the MHC-I molecules *H2-k1, H2-d1, H2l1,* or *B2m.* Nonetheless, several genes linked to antigen processing and MHC-I loading and transport where downregulated in the thrombin treated samples, including *Tap1,* which is essential for proper MHC-1 trafficking (Figure 4.17). MHC-I molecules are unstable until properly loaded with peptide. Loss of the antigen processing machinery (APM) causes a direct decrease in MHC-I cell surface occupancy (Blum et al., 2013). To assess whether PAR1 activation caused changes in MHC-I localization on KPC cells, flow cytometry was performed on cells treated with thrombin *in vitro*. MHC-I was nearly undetectable in both the control and PAR1^{KO} cell lines with or without thrombin treatment (Figure 4.17). MHC-I expression could be induced at a low level using IFNγ, which is a typical cellular response (Zhou, 2009), but thrombin treatment, and therefore PAR1 activation, had no impact (Figure 4.18A). However, just as with PDL1 expression, PAR1^{KO} cells once again had a stronger response to IFNγ treatment, displaying an increased shift in MHC-I expression compared to control KPC cells. This difference in IFNγ response did not appear to be relevant *in vivo*, however, as PAR1^{KO} and control KPC cells showed no difference in MHC-I expression when isolated from subcutaneous allograft tumors (Figure 4.18B). These findings indicate that PAR1 activation does not affect MHC-I presentation, despite evidence present in the RNA-Seq data showing changes in APM transcripts. Additionally, no significant change in the nonclassical NK cell inhibitory MHC-Ib *Qa1* (*H2-t23*) gene expression pattern was detected in the RNA-Seq data.

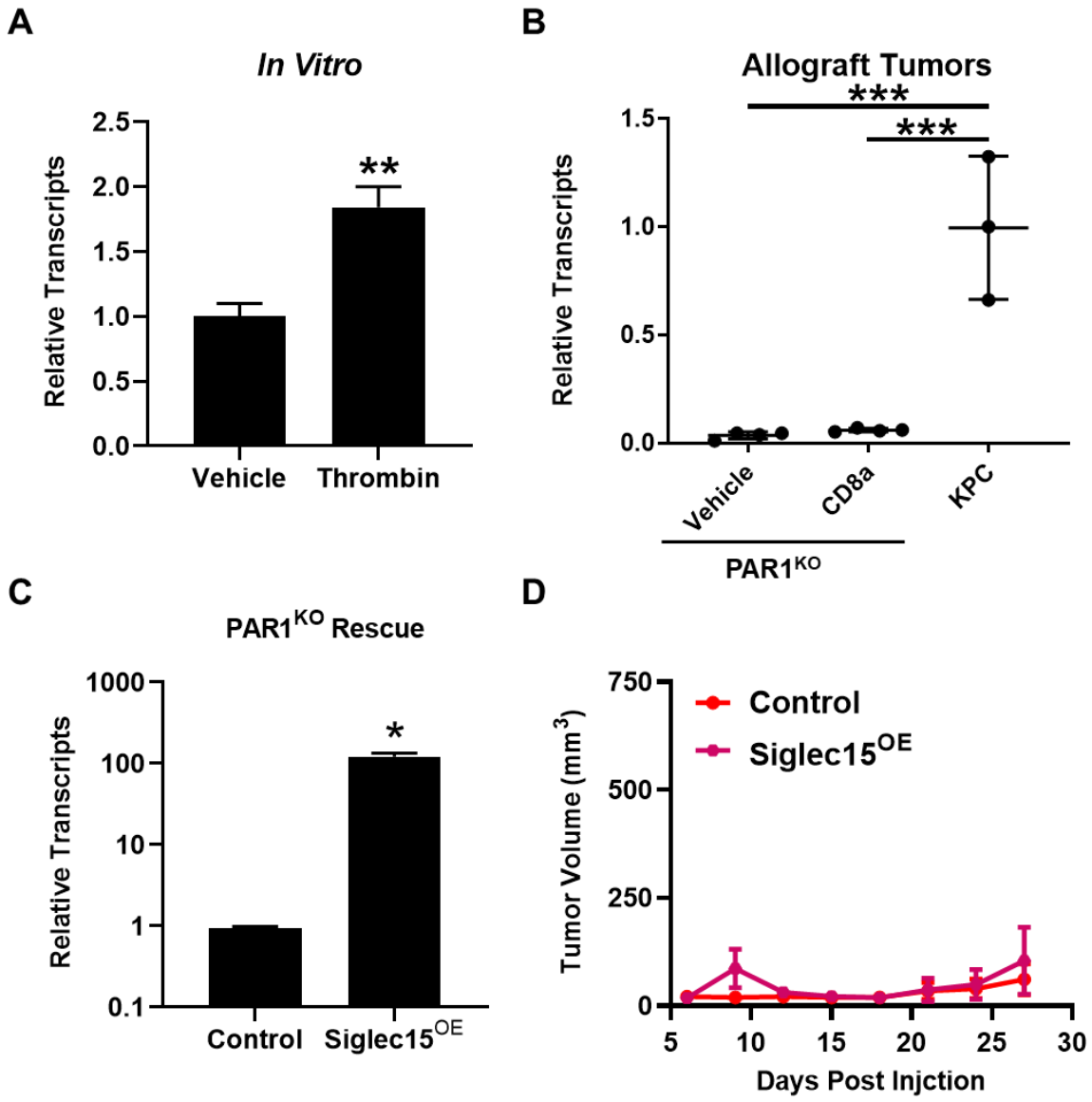

Figure 4.16 Forced expression of the PAR1 downstream target Siglec15 in PAR1^{KO} cells does not restore tumor forming capability.

(A) RT-qPCR analysis of *Siglec15* expression in KPC control cells (n = 4/group). **(B)** *Siglec15* expression patterns in subcutaneous allograft tumor samples. **(C)** RT-qPCR screening results of PAR1^{KO} cells expressing either an mCherry control vector (control) or a constitutively active *Siglec15* expression vector (Siglec15^{OE}) (n = 3/group). **(D)** Allograft tumor growth of PAR1^{KO} control and Siglec15^{OE} cells. (n = 9/group). * $p < 0.05$; ** $p < 0.01$

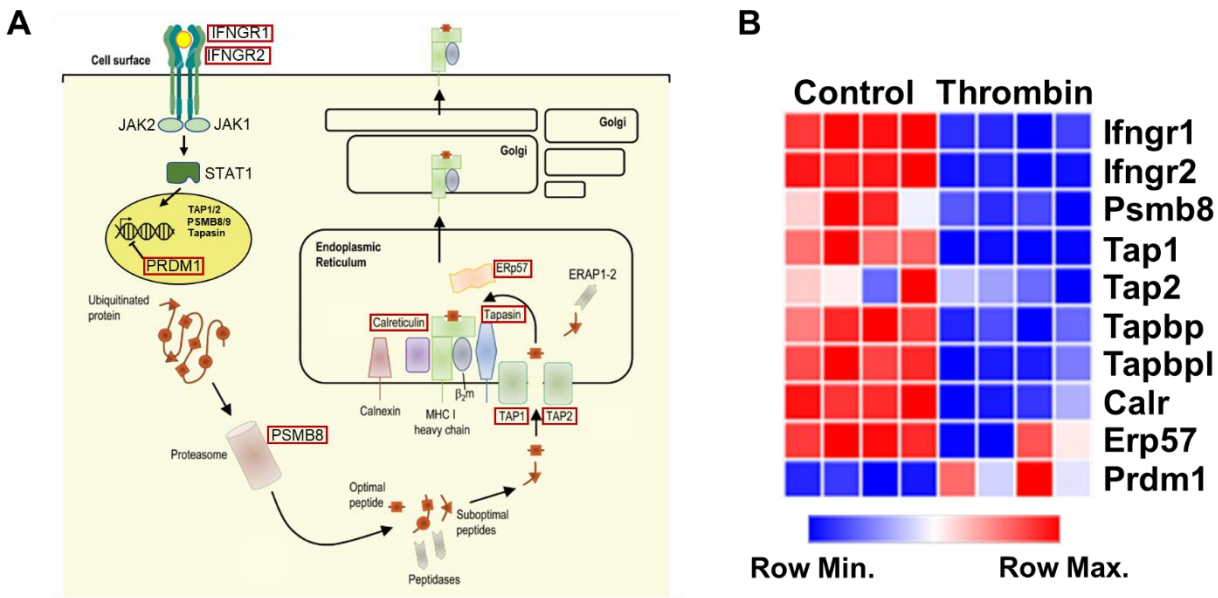

Figure 4.17 Thrombin treatment causes a decrease in transcripts encoding antigen presentation machinery in KPC cells.

(A) A diagram of the MHC-I antigen processing pathway. Red boxes highlight factors with decreased expression in KPC cells upon thrombin treatment. **(B)** RNA-Seq expression results for key components in MHC-I antigen processing pathway. Diagram adapted from (Leone et al. 2013).

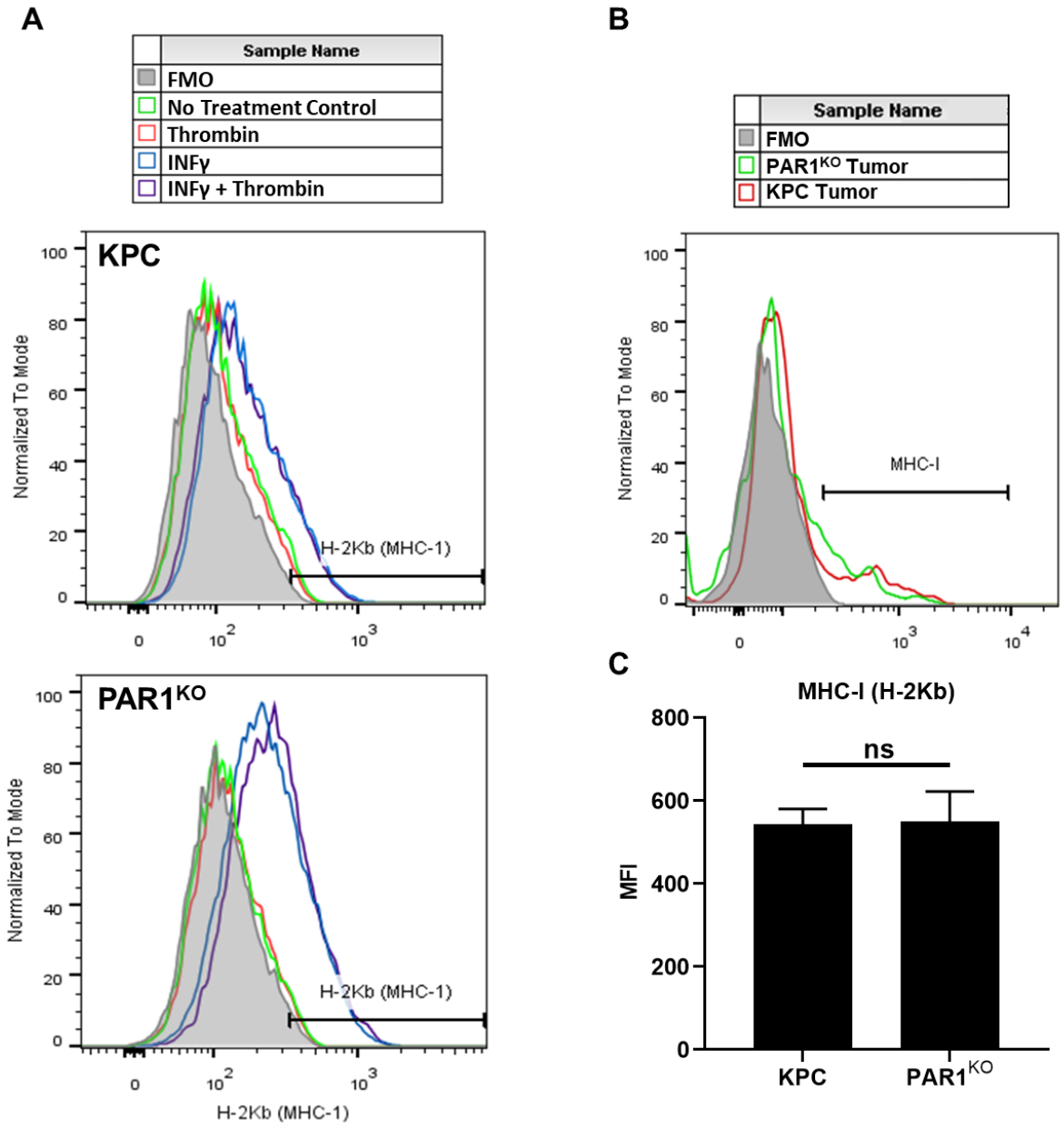

Figure 4.18 MHC-I cell surface occupancy is not impacted by thrombin treatment and was the same in KPC control and PAR1^{KO} allograft tumors.

(A) Representative **f**low plots showing MHC-1 protein H-2Kb expression in KPC control and PAR1^{KO} cells *in vitro*. **(B)** Flow analysis of H-2Kb expression on KPC and PAR1^{KO} tumor cells isolated from subcutaneous allograft tumors harvested 9 days after inoculation. TdTomato-labeled KPC and PAR1^{KO} cells were used in order to identify tumor cells during the flow analysis. **(C)** Quantification of the data presented in (B). (n = 3/group); FMO = fluorescence minus one; MFI = median fluorescence intensity.

In addition to killing tumor cells through secretion of perforin and granzymes, T cells can also activate the FAS death receptor (CD95) on tumor cells as an alternative mechanism of inducing apoptosis. However, cancer cells have been shown to co-opt this system by expressing FASL themselves, causing CTL apoptosis by activating CD95 on infiltrating T cells (Ryan et al., 2005). No expression of *FasL* was detected in our RNA-Seq data regardless of PAR1 activation, eliminating this possibility as a method of immune evasion. *Cd95* was, however, significantly downregulated in the thrombin treated group, but this pattern was not confirmed by RT-qPCR analysis of either *in vitro* or *in vivo* RNA samples. Therefore, it seems unlikely that PAR1-dependent immune evasion is due to modulation of FAS expression or activity.

Adenosine in the TME can impede immune cell activation and infiltration, thus acting as an immunosuppressive metabolite that enhances tumor immune escape (Vigano et al., 2019; Vijayan et al., 2017). There are many ways for adenosine to accumulate in the TME, one being its metabolism from extracellular ATP by cell surface ecto-enzymes expressed on cancer cells. Analysis of the RNA-Seq data indicated that PAR1 activation did not regulate *Nt5e, Cd38,* or*Entpd1* (CD39), the most well studied cell surface enzymes linked to TME adenosine metabolism. Alternative nucleotide processing enzymes were also examined, but no transcripts were detected for *Pap*, *Sahh* did not change, and *Alpl* mRNA expression was significantly decreased after thrombin treatment. The RNA-Seq data thus showed that *in vitro* PAR1 signaling on KPC cells does not upregulate adenosine processing ecto-enzymes. However, it is important to note that adenosine could still accrue in the TME by other means, such as the expression of these enzymes on other cell types within the tumor milieu. Whether PAR1 signaling on PDAC cells can promote the recruitment of these cells to the tumor remains unknown. Taken as a whole, the data outlined here rule out PAR1-dependent changes in the expression of checkpoint proteins, MHC-I, Fas/FasL, and adenosine producing ecto-enzymes as likely mechanisms of KPC cell immune evasion.

4.2.7 PAR1 signaling induces transcription of *Ptgs2* and *Csf2* which are critical for KPC tumorigenesis

Because no relevant changes in the expression of cell surface proteins known to impact tumor immune evasion were identified, secreted factors were next analyzed. PAR1 activation has been previously shown to cause the release of IL6, IL8, VEGF, CCL2, and prostaglandin E2 (PGE_2) in various cellular contexts (Asokananthan et al., 2002; Ortiz-Stern et al., 2012; Zigler et al., 2011). All of these proteins can contribute to tumor immune evasion (David et al., 2016; Fisher et al., 2014; Kudo-Saito et al., 2013; Liu et al., 2015; Yang et al., 2018). While no changes in the expression of *Il6, IL8* homologues, or *Vegf* genes were detected in the RNA-Seq data, *Ccl2* and *Ptgs2,* which encodes COX2, a critical enzyme for the production of PGE_2, mRNA were significantly upregulated in the thrombin treated cells. Further analysis of the RNA-Seq data also showed upregulation of *Csf2 (Gm-csf),* which was previously shown to be induced by thrombin (Shimaya et al., 2012; Wakita et al., 1997). *Tgfb1*, *Il34,* and *Sgpp2* were similarly upregulated transcriptionally and are additional genes of interest relevant to immunosuppression (Baghdadi et al., 2016; Bayne et al., 2012; Pylayeva-Gupta et al., 2012; Rodriguez et al., 2016; Yang et al., 2010). Of these targets, *Sgpp2* was the only one to be downregulated upon thrombin treatment. *Sgpp2* encodes a phosphatase responsible for degrading sphingosine 1-phosphate (S1P), an enzyme that has been linked to the presence of tumor associated macrophages in the TME (Rodriguez et al., 2016). RT-qPCR analysis of both *in vitro* and *in vivo* samples confirmed the RNA-Seq expression profile for all genes except *Ccl2,* which showed no difference *in vivo* between $PAR1^{KO}$ and control tumors (Figure 4.19). *Ccl2* was therefore excluded from further analysis.

Next, to determine if expression of these factors could impact $PAR1^{KO}$ cell tumor growth, stable cell lines were generated by viral transduction to "rescue" target gene expression (Figure 4.20) and tumorigenesis was assessed in immunocompetent C57BL/6 mice. The results from these studies indicated that expression of *Csf2* or *Ptgs2* could independently restore $PAR1^{KO}$ tumor forming capacity, while expression of the other factors had no significant impact on tumor growth (Figure 4.21). *Ptgs2* expression did not fully restore $PAR1^{KO}$ tumorigenesis to control levels. In contrast, *Csf2* expression had a dramatic effect, resulting in expedited tumor growth, severe,

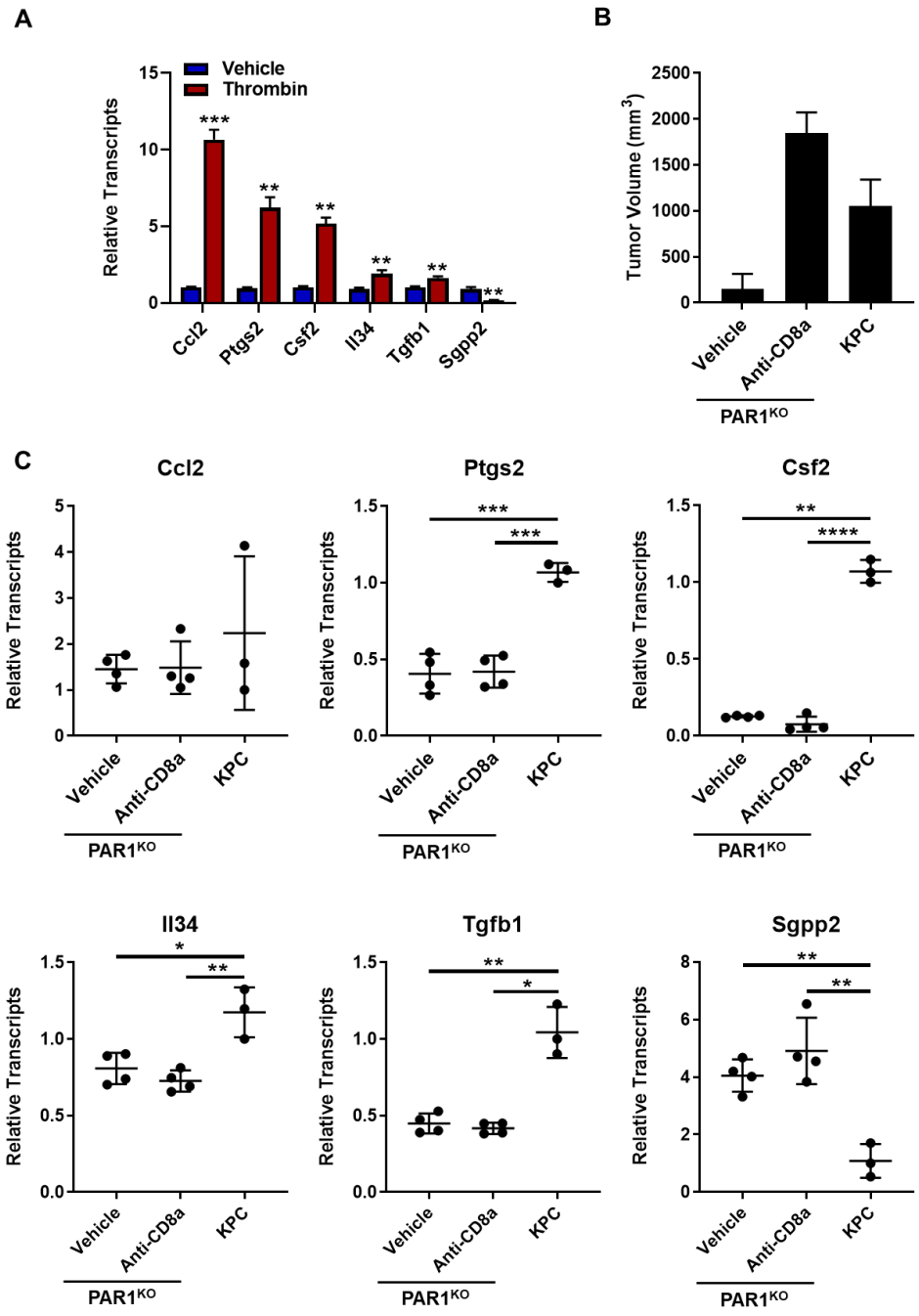

Figure 4.19 PAR1 signaling induces expression of factors that promote immunosuppression.

(A) RT-qPCR results from *in vitro* stimulation of KPC cells with thrombin. (n = 4/group) **(B)** Final tumor volume results from tumor allografts of PAR1^{KO} cells grown in mice treated with vehicle or anti-CD8a monoclonal antibodies or KPC control cells. **(C)** RT-qPCR results using total RNA isolated from the allograft tumors shown in (B).

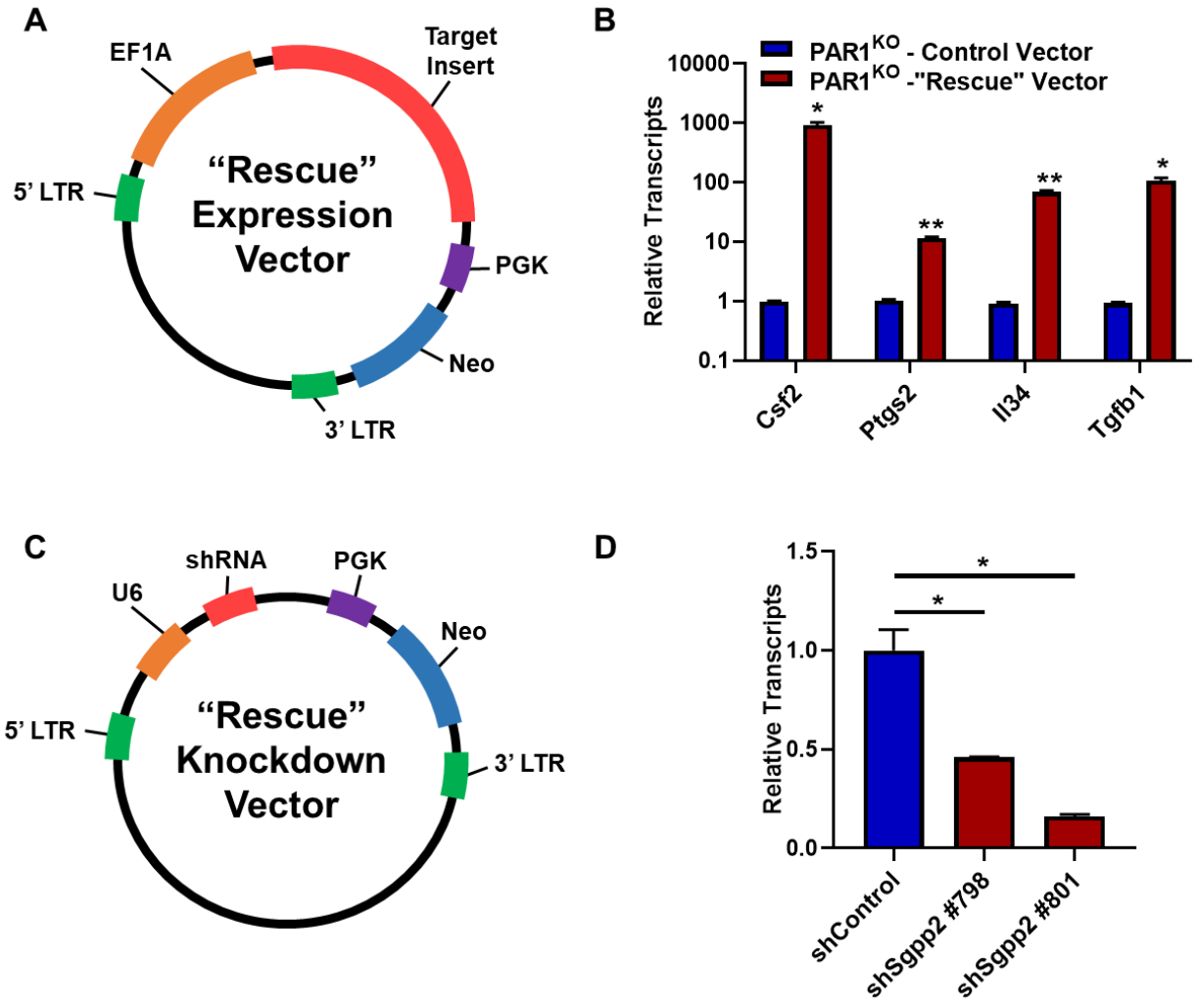

Figure 4.20 PAR1 regulated gene expression patterns were mimicked in PAR1^{KO} cells by viral transduction.

(A) A diagram of the plasmid used to generate lentiviral particles containing genetic material for the various PAR1 downstream targets. **(B)** Separate PAR1^{KO} cell lines were generated expressing a single downstream target transgene. RT-qPCR results confirmed increased target gene expression in each transduced "rescue" cell line compared to cells expressing an mCherry control vector. **(C)** A map of the shRNA expression vector used to generate lentiviral particles to knockdown Sgpp2 expression in the PAR1^{KO} cell line. **(D)** Separate stable lines were made using two different shRNA's targeting Sgpp2. RT-qPCR results show successful knockdown of Sgpp2 in the transduced cells. (n = 3/group, * $p < 0.05$; ** $p < 0.01$)

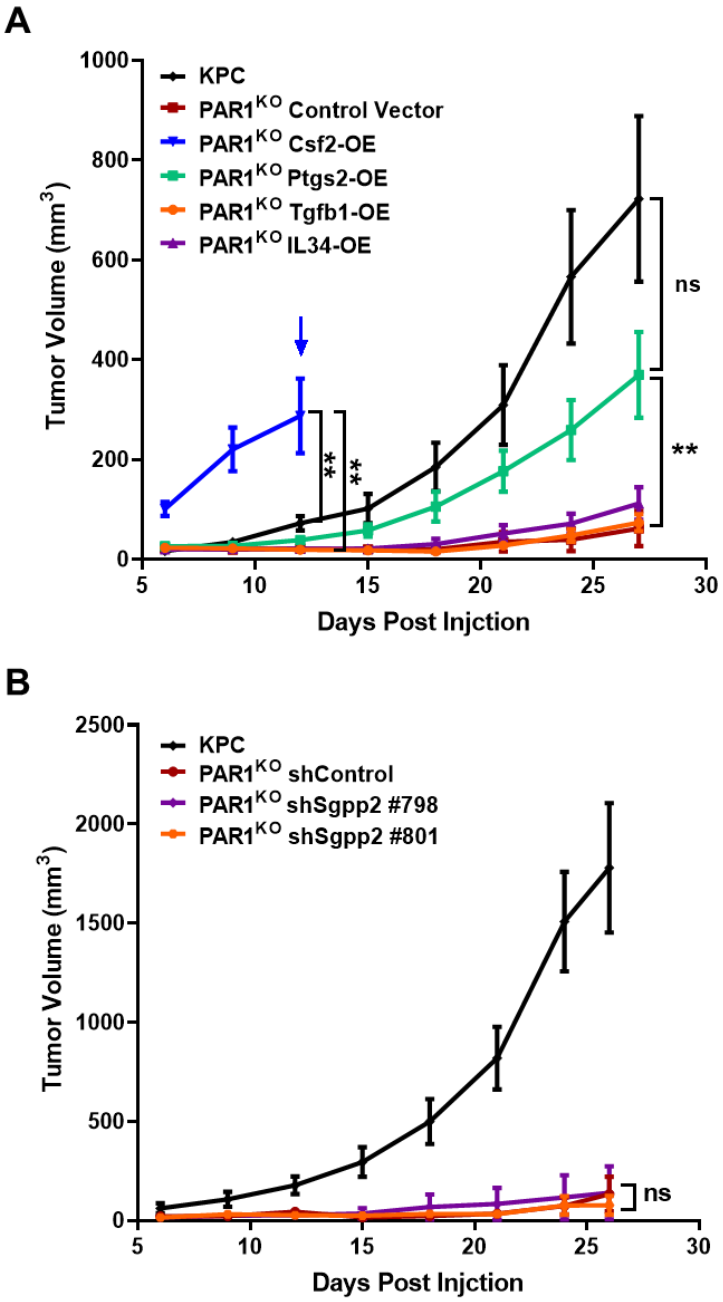

Figure 4.21 *Csf2* and *Ptgs2* restore allograft tumor growth in PAR1^{KO} cells.

(A) Allograft tumor growth data for the PAR1^{KO} "rescue" cell lines. Note the CSF2-OE group was terminated early due to health concerns ad indicated by the blue arrow.
(n = 6-8/group, RM-ANOVA) **(B)** Allograft tumor growth data for the PAR1^{KO} *Sgpp2* knockdown cell lines. (n = 6/group)

splenomegaly, macroscopic pulmonary lesions, and increased animal frailty requiring the early termination of the *Csf2*-expressing cohort. Surprisingly, when these cells were injected orthoptic into the pancreas of C57BL/6 mice tumor growth was only marginally enhanced using the *Ptgs2* or *Csf2* expressing $PAR1^{KO}$ cells resulting in no significant increase in tumor size. (Figure 4.22). Although the number of mice with detectable tumors at the study's end point was significantly increased using *Ptgs2* expressing $PAR1^{KO}$ cells.

Because *Ptgs2* and *Csf2* were capable of restoring $PAR1^{KO}$ tumorigenesis, the importance of these factors for tumor growth in PAR1 expressing control KPC cells was next assessed. *Ptgs2* and *Csf2* knockout cell lines were generated using a CRISPR/Cas9 variant system (Tsai et al., 2014), and loss of CSF2 or PGE_2 was verified by ELISA (Figure 4.23AB). Importantly, ELISA results confirmed that CSF2 and PGE_2 secretion was increased in control cells upon PAR1 activation by thrombin. Allograft experiments using the newly generated knockout KPC lines revealed that ablation of *Csf2* or *Ptgs2* greatly attenuated tumor growth in C57BL/6 mice (Figure 2.23 CD), complementing the $PAR1^{KO}$ "rescue" allograft results. Of note, one of the four $CSF2^{KO}$ cell lines showed no change in tumor growth despite evidence that *Csf2* expression was indeed lost in the final tumor sample. This indicates that *Csf2* is not an absolute requirement for tumorigenesis. Further analysis to identify critical differences between this line and the other $CSF2^{KO}$ cell lines is ongoing. Taken as a whole these data indicate that *Ptgs2* and *Csf2* are critical factors in PDAC tumor growth and their re-expression in $PAR1^{KO}$ cells can restore tumorigenesis.

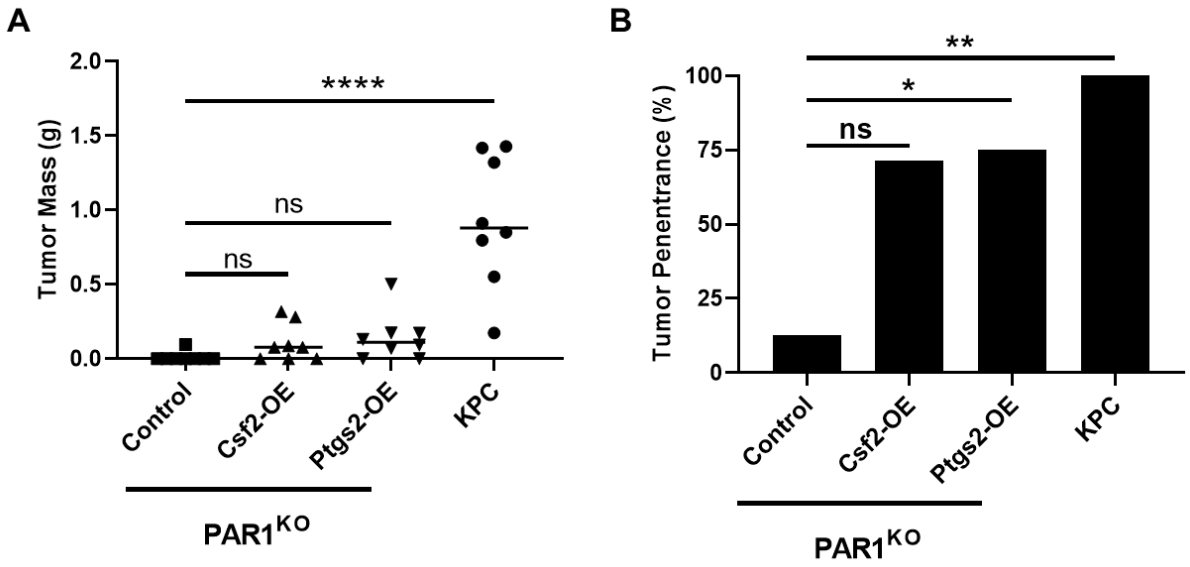

Figure 4.22 PAR1^{KO} *Csf2* and *Ptgs2* "rescue" cells have increased tumor penetrance but produce nominal tumors orthotopically.

(A) Final tumor volume of KPC cells and PAR1^{KO} rescue cells from an orthotopic experiment. **(B)** A graph indicating the percentage of mice with detectable tumors at the studies end, significance was calculated relative to PAR1^{KO} control cells using Fisher's exact text.
Experiment and analysis performed by Yi Yang.

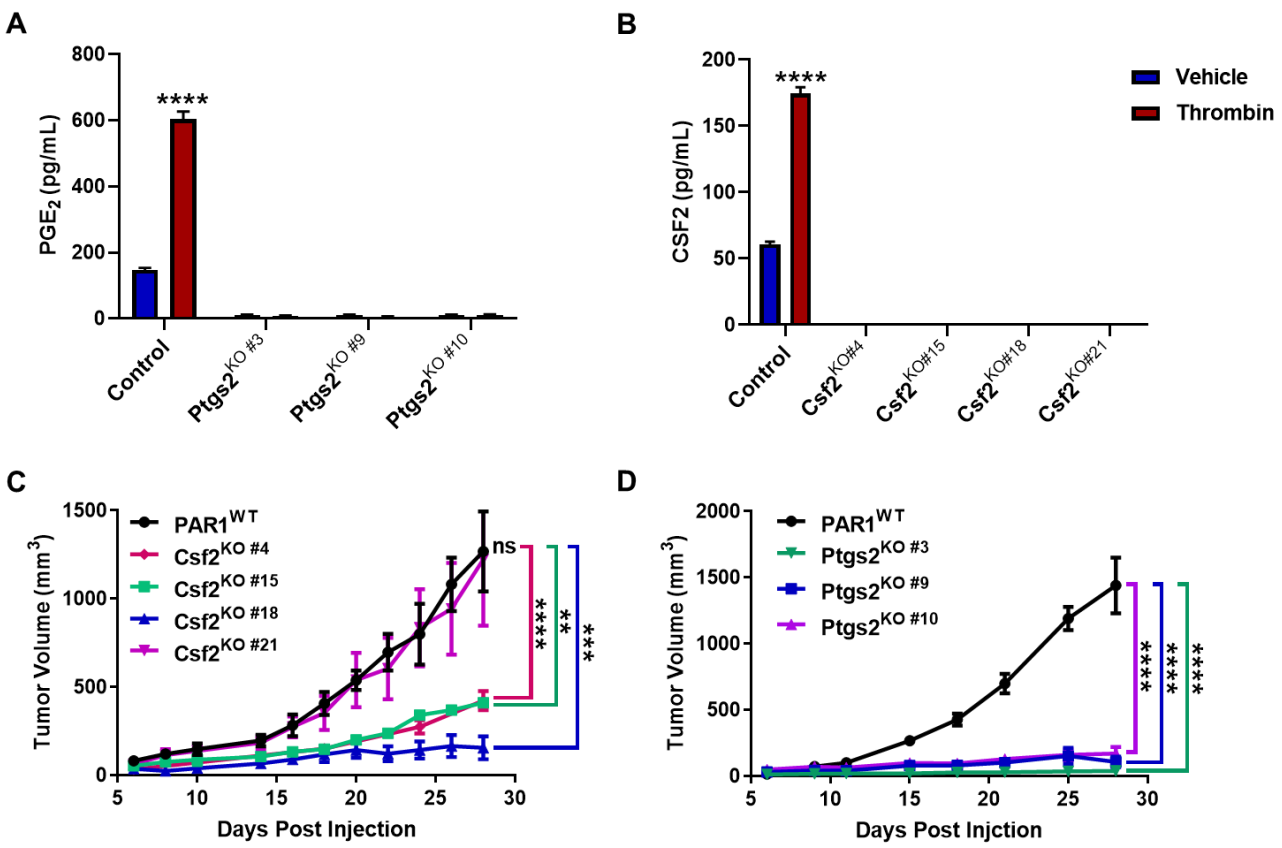

Figure 4.23 Csf2^{KO} and Ptgs2^{KO}cells overall show decreased tumor growth.

(A, B) ELISA data from 48 hour cell culture samples showing PGE_3 and CSF2 secretion from KPC (control) cells and subsequent knockout cell lines (n = 3/group). **(C, D)** Allograft tumor growth results from the various Csf2^{KO} and Ptgs2^{KO} cell lines. (n = 4-8/group)

4.3 Discussion

PDAC is a poorly immune responsive and highly treatment-refractory malignancy. Indeed, while immune checkpoint inhibitors have been a tremendous breakthrough for the treatment of various solid and hematological cancers, they have been ineffective as a PDAC therapy, likely due to a lack of infiltrating cytotoxic T cells (Kabacaoglu et al., 2018). One report found as few as 16% of resected patient PDAC samples exhibited classifiable levels of intertumoral CD4 and CD8 staining, yet this was an independent favorable prognostic factor (Fukunaga et al., 2004), truly emphasizing the scarcity and importance of these lymphocytic populations for patient survival. As such, PDAC is often classified as an immunologically "cold" cancer, and a great amount of research has focused on understanding why this is the case.

Although the classic model of tumor immune evasion involves a process of immunoediting, wherein cancer cells that survive selective pressure from the immune system are better able to escape elimination and thus give rise to immune-resistant populations (Mittal et al., 2014), studies indicate that PDAC may instead create an immune-privileged or immune-quiescent environment, circumventing this process all together. Analysis of the immune profile of spontaneous GEM tumors from KPC mice found immunosuppressive T_{regs}, MDSCs, and M2 macrophages began to accumulate early around preinvasive PanIN lesions, while CD8 positive T cells were rarely detected throughout disease progression and were found to be largely inactive (Clark et al., 2007). Furthermore, CD8 positive T cell depletion had no impact on spontaneous KPC tumor development (Evans et al., 2016), again indicating a lack of anti-tumor immunity during natural disease progression. The low mutational burden observed in PDAC, and resulting paucity of neoantigens, has been proposed as one reason for the frequent absence of PDAC immunogenicity (Evans et al., 2016) although the prevalence of neoantigens does not correlate with PDAC cytolytic T-cell activity (Balli et al., 2017). Instead, tumor cell intrinsic factors responsible for shaping the immunosuppressive microenvironment have been explored as a major influence on lymphocytic infiltration (Li et al., 2018). Consistent with this concept, the research described here outlines PDAC expression of PAR1 as a novel and critical modulator of anti-tumor immunity.

PAR1 ablation renders PDAC cells susceptible to immune clearance, and T cell depletion experiments indicate this is largely mediated by an adaptive CD8 T cell response. However, $PAR1^{KO}$ tumor cells only fully regained their tumor forming capacity when injected into severely immunocompromised NSG mice, indicating the involvement of additional immune cells in the

anti-tumor PAR1^{KO} immune reaction. Somewhat surprisingly given previous research and current theories on PDAC immune-privilege, control PAR1-expressing KPC cells also showed a positive increase in tumor growth following CD8 T cell depletion. This suggests that the control KPC cells used here are actively eliminated by an adaptive immune response, albeit one that they readily overcome. Indeed, KPC tumors overall displayed a scarcity of CD8a positive T cells especially when compared to PAR1^{KO} tumors. KPC tumors also had a significantly higher TAM population which could contribute to the generation of an immunosuppressive TME (Petty and Yang, 2017). However, a pilot study not shown here using liposomal clodronate to deplete macrophages from allograft tumors showed no change in tumor growth in either the KPC or PAR1^{KO} cells, seeming to indicate that this cell population is nonessential for maintain KPC tumor growth. Furthermore, no difference in myeloid derived MDSC's were detected between KPC and PAR1^{KO} tumors, though polymorphonuclear MDC's and/or neutrophils were present at a significantly higher level in KPC tumors. Whether these cells can suppress T cell activation remains to be assessed. Additionally, though not analyzed here, the presence of Tregs (Wang et al., 2017) and a scarcity of dendritic cells (DCs) (Deicher et al., 2018) have also been implicated as major contributing factors in PDAC immunosuppression and their levels in relation to PAR1 expression should be examined in future studies. Additionally, whether cancer cell expression of PAR1 is responsible for immune evasion in other tumor models is being actively explored starting with the B16 melanoma line which has been reported to express high levels of PAR1 (Niers et al., 2009).

RNA-Seq was used to identify PAR1-dependent changes in gene regulation that could contribute to anti-tumor immune evasion. It is worth noting that although this method provided an accurate representation of PAR1 downstream signaling, showing enrichment in categories known to be influenced by PAR1 activation and serves as a useful reference for querying the expression of known immunosuppressive factors, it may miss critical PAR1-dependent effects not regulated at the transcriptional level. Indeed, several previously reported physiological responses to PAR1 signaling could contribute to tumor immune evasion. For example, PAR1 activation can cause phosphorylation of focal adhesion kinase (FAK) (Even-Ram et al., 2001), which may be one of the reasons for the increased KPC migration observed following thrombin treatment. Importantly, high levels of phosphorylated FAK have been reported in PDAC and correlate with the presence of immunosuppressive TMEs. Additionally, inhibition of FAK caused a significant CD4/CD8 T cell-dependent decrease in tumor growth (Jiang et al., 2016a). Whether this same mechanism

contributes to PAR1-dependent immune evasion remains to be determined and should be investigated in future studies. Similarly, PAR1 can induce secretion of S1P through transient activation of sphingosine kinase 1 (SPHK1) (Rauch, 2014), and S1P has been linked to the accumulation of M2 macrophages and Tregs in the TME, though S1P also has proinflammatory functions that could theoretically inhibit tumor growth (reviewed in: (Rodriguez et al., 2016)). PAR1-dependent S1P secretion was never assessed in the KPC cells although *Sgpp2*, an S1P degrading phosphatase, did show PAR1-dependent upregulation in the RNA-Seq and in *in vivo* tumor samples, and this could potentially prolong S1P accumulation in the TME. Nevertheless, *Sgpp2* knockdown was unable to rescue $PAR1^{KO}$ tumor growth. Interestingly, $PAR1^{KO}$ cell transcripts for *Sgpp2* were already "reduced" prior to shRNA knockdown, displaying levels comparable to those observed in thrombin treated control cells. Moreover, if PAR1 is required for S1P synthesis and release, then reduction of *Sgpp2* would likely have no effect in $PAR1^{KO}$ cells. As a final example of transcription independent mechanisms of immune evasion, platelet activation by thrombin through PAR1 signaling causes phosphatidylserine (PS) externalization (Harper and Poole, 2011), and PS has immunosuppressive effects and can act as a ligand to the inhibitory immune checkpoint receptor TIM-3 (Birge et al., 2016).

Additional characterization of the TME and extra cellular matrix (ECM) composition from *in vivo* tumor samples should also be performed, as the presence and nature of fibroblasts and ECM proteins could contribute to immune evasion (Mushtaq et al., 2018). Interestingly, while morphologically similar in culture, the histological phenotype of $PAR1^{KO}$ tumors was distinct from KPC control tumors, displaying a more differentiated phenotype with clearly defined duct-like structures (see Figure 4.8C). This same finding was reported previously in a $Ptf1a^{Cre}$; *LSL-Kras;* $Trp53^{flox/flox}$ KPC PDAC model and was attributed to an increase in PAR1 driven epithelial-to-mesenchymal transition (EMT) (Tekin et al., 2018). The EMT regulators *Snai1, Snai2,* and *Zeb2* were upregulated upon PAR1 activation in our RNA-Seq, but no changes in *Cdh1* or *Vim* were detected, and no clear morphological changes were observed in culture after thrombin treatment. Of note, EMT and tumor-budding phenotypes are associated with highly immunosuppressive PDAC subtypes (Karamitopoulou, 2019), and EMT has been shown to impact tumor immune evasion through several mechanisms (Romeo et al., 2019). Whether the influence of PAR1 on PDAC EMT *in vivo* represents another component in the PAR1-dependent immune evasion pathway remains to be seen.

Analysis of the RNA-Seq found no changes in transcripts related to well-known inhibitory immune checkpoint proteins or *Fas/FasL*. However, several genes encoding antigen processing machinery components were downregulated upon thrombin activation. Surprisingly, this did not translate to changes in MHC-I presentation *in vitro* or *in vivo*. Unexpectedly, differences in the $PAR1^{KO}$ and control KPC cell responses to IFNγ *in vitro* became apparent based on analysis of MHC-I presentation and PDL1 induction. While the reason for this remains unclear, it does appear to be dependent on PAR1 expression, but not on PAR1 activation by thrombin, as results using the $PAR1^{KO/Tg}$ cells corroborated these initial findings. It is possible that basal activity of PAR1 occurs in culture, as KPC cells are typically passaged using trypsin, which is a known activator of PAR1. Additionally, the RNA-Seq detected transcripts for the noncanonical PAR1 activator *Mmp13*, its upstream activator *Mmp14*, and the *Mmp14* activator *Furin* though whether these factors are truly part of a functional cascade in culture is unknown. A decrease in transcripts for the IFNγ receptor *Ifngr2* was also detected by the RNA-Seq. Hypothetically, frequent PAR1 activation during cell passaging, or basal activity due to KPC generated proteases could cause a gradual shift in the expression of cell surface receptors, including the IFNγ receptor, resulting in distinct differences between the $PAR1^{KO}$ and control cell lines, including their IFNγ responsiveness, although this is strictly speculative and does not account for the ability to rescue tumor growth in the $Par1^{KO/Tg}$ cell line. Regardless, since no changes in MHC-I expression were detected between the $PAR1^{KO}$ and control cells isolated from *in vivo* tumor samples this does not appear to be a relevant mechanism of immune evasion.

An examination of transcript levels for secreted factors known to promote immunosuppression and/or tumor immune evasion was also performed and identified several gene targets for further investigation. Of those tested both *Ptgs2* and *Csf2* were capable of restoring tumor growth when expressed in $PAR1^{KO}$ cells. *Csf2* expression had a particularly profound effect on tumor growth in addition to causing sever splenomegaly, non-tumorigenic pulmonary lesions, and increased animal frailty. Notably, overexpression of CSF2 has been linked to muscle wasting in a previous study (Lang et al., 1987). Strangely, though immunosuppressive effects of CSF2 have been well demonstrated in PDAC (Bayne et al., 2012; Pylayeva-Gupta et al., 2012) and other cancers (Bronte et al., 1999; Sotomayor et al., 1991), CSF2 can also act as immunostimulant in some ways, including a critical role in dendritic cell differentiation. CSF2 has even shown promising results as a therapeutic component (Hong, 2016), including its use in vaccines generated

from irradiated CSF2 expressing tumor cells as a PDAC therapeutic, though this treatment method failed to improve patient survival (Le et al., 2019). Both *Ptgs2* and *Csf2* have been shown previously to be necessary for PDAC tumorigenesis via their ability to prevent T cell mediated anti-tumor immunity through the recruitment of suppressive immune cells such as MDSCs (Bayne et al., 2012; Markosyan et al., 2019; Pylayeva-Gupta et al., 2012). Whether this mechanism accounts for the improved tumor growth in $PAR1^{KO}$ cells requires further analysis to assess the presence of MDSC, however as stated earlier myeloid derived MDSCs were comparable in number between $PAR1^{KO}$ and KPC tumors, but the functionality of these cells requires further testing.

Despite the ability of *Ptgs2* and *Csf2* to restore $PAR1^{KO}$ tumor growth, results from the mixed $PAR1^{KO}$/KPC control allograft experiment indicate a cell autonomous immune evasive role for PAR1, as PAR1 expressing cells were preferentially capable of surviving an active anti-tumor adaptive immune response. Secretion of PGE_2 or CSF2 should theoretically produce systemic changes in the TME, resulting in an accumulation of suppressive cells that inhibit CTL activity, thus enhancing $PAR1^{KO}$ cell survival. Indeed similar experiments investigating the intrinsic capacity for PDAC cells to reshape the TME showed that cell lines capable of attracting immunosuppressive cell populations had a dominant influence over the TME when co-injected with PDAC cells known to accrue high levels of infiltrating T cells (Li et al., 2018). This was further supported by the tumor rechallenge assays which showed that PAR1 expressing KPC cells can survive in animals previously exposed to KPC antigens. A simple explanation for these results is that the $PAR1^{KO}$ cells simply express different neoantigens than the parental KPC cells and are therefore more readily targeted. However, the ability of $PAR1^{KO/Tg}$ cells to completely regain their tumor forming ability through the re-expression of PAR1 makes this an unlikely scenario.

These findings therefore point to a more direct mechanism of immune evasion. This can be best assessed using *in vitro* CTL assays to determine if PAR1 expression can prevent CTL mediated tumor cell lysis without the influence of the TME. Initial attempts to perform this assay showed a lack of specific cytotoxicity as evidenced by the low targeting efficiency and similar outcomes from both $PAR1^{KO}$ and B16 primed CTLs. Unfortunately, because the KPC antigen(s) recognized by the CTLs is unknown, and the population of T cells with receptors capable of recognizing these antigens is likely only a very small population prior to expansion, improved methods to prime and expand CTLs, such as DC loading strategies, may be necessary in future studies. Alternatively, specific targeting could be overcome through expression of ovalbumin

antigen in the KPC cells. CTLs isolated from OT-1 GEM could then be used to specifically target all KPC cells expressing the OVA transgene and provide a cleaner system for testing the influence of PAR1 on immune evasion.

Though further optimization of the CTL assay is necessary, preliminary findings indicated that $PAR1^{KO}$ cells were generally more susceptible to CTL mediated killing, even in a nonspecific manner. To gain more insight into this phenomenon the assay should be repeated using transwell inserts to physically separate the CTL and $PAR1^{KO}$ cells in order to determine if any CTL secreted factors can induce $PAR1^{KO}$ cytotoxicity, though it was already shown that IFNγ treatment did not cause increased cell death in the $PAR1^{KO}$ cells, even though they were generally more responsive to its influence. Similarly, analysis of $PAR1^{KO}$ tumor growth in perforin knockout mice would help determine if $PAR1^{KO}$ cells are primarily eliminated by the canonical perforin/granzyme mediated mechanism, or if alternate methods like those involving LTα or FasL should be more closely examined. In general, apoptosis resistance can provide a means of immune escape on its own (Igney and Krammer, 2002), and therefore the influence of PAR1 on cell survival and apoptosis resistance should also be assessed, especially in regard to the CTL assay results.

Taken together the findings outlined here identify PAR1 as a novel modulator of PDAC tumor immune evasion capable of promoting PDAC resistance to an adaptive CTL-driven immune response. Though further research is needed to fully understand the mechanism(s) of PAR1-mediated immune escape, PAR1 activation was shown to increase secretion of critical immunosuppressive factors that in turn restored tumor growth when re-introduced into $PAR1^{KO}$ cells. However, additional findings indicate that PAR1 expression enables PDAC cells to circumvent CTL killing through a more direct mechanism yet to be identified. As a particularly nonimmunogenic cancer, PDAC is particularly difficult to treat even with the growing arsenal of immune checkpoint inhibitors and immune oncology-based therapeutics. The data presented here show PAR1 to be a novel therapeutic candidate capable of influencing tumor differentiation, immune cell infiltration, and evasion of an adaptive immune response.

CHAPTER 5. SUMMARY AND FUTURE DIRECTIONS

Progress in developing effective pancreatic ductal adenocarcinoma (PDAC) therapeutics and improving patient prognoses has been slow and overall relatively stagnant. Despite strong research efforts and recent breakthroughs in immune-based cancer treatments, the vast majority of PDAC patients ultimately succumb to the disease within only a few years of diagnosis (American Cancer Society, 2019). Therefore, research into the mechanisms of PDAC progression and pathogenesis is pivotal in order to identify any proverbial chink in the armor of this devastating disease that might one day be used to design an effective therapeutic.

Genetically engineered mouse (GEM) models that mimic the earliest events in PDAC development revealed distinct changes in transcriptional programming that occur during disease progression, including the upregulation of the normally silenced developmental transcription factor SOX9. Further analysis confirmed a critical role for SOX9 in PDAC initiation, most clearly demonstrated by the complete ablation of precancerous lesion formation from mouse pancreatic acinar cells in which SOX9 was genetically deleted. Additional experiments corroborated this conclusion showing that forced ectopic expression of SOX9 drastically accelerated lesion formation in a PDAC mouse model. While these results clearly indicate that SOX9 is necessary for early events in PDAC initiation to occur, its involvement in later stages of PDAC progression and tumor maintenance are less certain. Though SOX9 knockdown in human Panc-1 cells reduced tumorigenic properties such as proliferation, soft agar colony formation, and most importantly xenograft tumor growth, similar experiments examining the effects of *Sox9* deletion in primary mouse PDAC cells showed no impact of SOX9 on allograft tumor growth, signifying that SOX9 is dispensable in many cases for PDAC tumorigenesis and maintenance. Analysis of SOX9-dependent changes in the gene regulation patterns of normal pancreatic acinar cells identified a relatively small number of differentially expressed genes, especially given SOX9's canonical function as a transcription factor, though, previously identified SOX9 regulated genes were present within the gene set validating its findings (Bi et al., 1999; Kadaja et al., 2014; Kolanczyk et al., 2011; Liu et al., 2017a; Shi et al., 2015; Wilhelm et al., 2007; Zalzali et al., 2008). Pathway analysis using multiple software programs highlighted similar categories of enrichment within the dataset including those related to cytoskeletal changes, cell adhesion, and angiogenesis. In agreement with

previous reports that SOX9 promotes acinar cell reprogramming and dedifferentiation (Kopp et al., 2012; Prévot et al., 2012), Enrichr analysis found significant commonalities between the SOX9 transcriptional network and that of a previously published *Mist1* knockout study wherein the acinar cell differentiation status was greatly impacted by loss of MIST1 expression (Direnzo et al., 2012). However, subtle but important differences exist between these findings and past reports, suggesting that SOX9 serves a more nuanced role. Indeed, ectopic expression of SOX9 alone, in the absence of oncogenic driver mutations, had little overall impact on acinar cell integrity unless additional perturbations were used, such as pancreatitis or ablation of MIST1, to initiate the dedifferentiation process, and even in these cases the effects were prevalent but somewhat mild overall. Taken as a whole, these results define a pivotal role for SOX9 at the tipping point of PDAC initiation, revealing it to be a crucial and necessary factor for precursor lesion development, but find it to be largely dispensable in established tumor cells.

In future studies, the generation of mouse models that enable temporal control of both oncogenic KRAS (Collins et al., 2013) and SOX9 expression could provide greater insight into the precise timing and influence of SOX9 on PDAC initiation. As our research shows, SOX9 is necessary for precancerous lesion formation *in vivo*. However, SOX9 has no detectable impact on tumor growth in established murine PDAC cell lines, indicating that SOX9 is necessary for early events in PDAC development but is superfluous in established tumor cells. Using a mouse model with inducible $Kras^{G12D}$ and *Sox9* expression, such that these genes can be turned both on and off, would enable the individual, and potentially synergistic, contributions of KRAS and SOX9 to be explored at various stages throughout PDAC development. Indeed, while studies find that SOX9 lies downstream of KRAS signaling (Chen et al., 2015b; Eberl et al., 2012; Hessmann et al., 2016), both SOX9 and oncogenic KRAS are necessary for PanIN formation. This was demonstrated by the lack of PanINs in both our KC/ΔSOX9 mice, which express oncogenic KRAS but not SOX9, and in our iSOX9 mice, which ectopically express SOX9 but not oncogenic KRAS, thus indicating that neither factor can induce lesion formation on its own. By controlling the temporal expression patterns of both KRAS and SOX9 it would be possible to determine if both factors are required throughout tumorigenesis, and as a result to determine if there is a tipping point in disease progression, past which point SOX9 becomes dispensable for tumorigenesis.

Additional transcriptomic analyses should also be conducted to further map the SOX9 gene regulatory network as it pertains to PDAC initiation. Based on the recent finding that SOX9 can

influence mRNA splicing (Girardot et al., 2018), our original RNA-Seq data and all future analyses should be examined for differential splicing events, as this may reveal important SOX9-dependent effects that were missed in our initial interpretation of the results. Furthermore, it is possible that our RNA-Seq experiment lacked the proper cellular context necessary to elicit SOX9's full effects. SOX9 is known to act in a context dependent manner (Kamachi et al., 2000), and in our study ectopic expression of SOX9 alone had no impact on PanIN formation or acinar cell homeostasis in the absence of oncogenic KRAS. An additional RNA-Seq designed to identify differences between KC and KC/ΔSOX9 pancreata just prior to lesion formation would provide a more appropriate sample set for this analysis, revealing transcriptional changes in pancreata destined to progress into PanINs (KC) compared to those returning to a healthy acinar state (KC/ΔSOX9) (see Figure 3.25A). To determine the importance of candidate SOX9-regulated genes in PanIN formation, adenoviral vectors encoding putative SOX9 targets could be directly injected into the pancreata of $Kras^{G12D}; Sox9^{fl/fl}$ mice. The presence of PanIN lesions could then be assessed after acute pancreatitis induction to see if the introduction of these vectors could promote PanIN formation even in the absence of SOX9, thus identifying necessary factors downstream of SOX9 critical for lesion formation.

Though SOX9 was shown to be dispensable in established PDAC tumor cells, further analysis of these cells uncovered a novel role for the thrombin receptor PAR1 in PDAC immune evasion. PAR1 is a uniquely activated G protein-coupled receptor important for hemostasis (Andersen et al., 1999) and previously shown to promote cancer cell proliferation, migration, and metastasis (Arora et al., 2007; Han et al., 2011). PAR1 was highly expressed in primary mouse PDAC cells and its activation resulted in several well characterized PAR1-dependent biological effects, including cytoskeletal reorganization, pERK signaling, and a significant increase in transwell migration. Surprisingly however, cell proliferation was not impacted by PAR1 activity. Utilizing PAR1 knockout PDAC cells it we previously demonstrated that PAR1 is required for allograft tumor growth when injected into syngeneic wild type mice, but the presence or absence of PAR1 had no impact on tumor growth when these same cells were injected into immunocompromised animals (Yang et al., 2019b), indicating a critical interplay between the anti-tumor immune response and PAR1 expression. To investigate this relationship in more detail a monoclonal antibody depletion strategy was employed to eliminate specific T cell subsets from wild type host animals and determine their impact on PAR1 knockout cell tumor growth. This

study revealed $CD8a^+$ T cells to be primarily responsible for preventing PAR1 knockout tumor growth, while NK1.1 and CD4 expressing cells had no effect. Thus, PAR1 expression protects PDAC tumor cells from an adaptive $CD8a^+$ cell mediated anti-tumor immune response. Additionally, experiments involving the co-injection of PAR1 knockout and control PDAC cells showed that PAR1 knockout cells were preferentially targeted and eliminated from these mixed tumors, while PAR1 expressing cells were able to survive this active immune response, seeming to indicate a PAR1-driven local, if not direct, mechanism of immune evasion, as opposed to the systemic creation of an immunosuppressive tumor microenvironment. Though several potential mechanisms of direct immune evasion were evaluated none were identified here, even though PAR1 knockout cells did display an increased susceptibility to nonspecific cytotoxic T cell mediated killing, a result which merits further investigation. Additional research to confirm the presence of a direct mechanism of PAR1-dependent immune evasion is therefore ongoing. Interestingly, and in agreement with previous studies (Rudroff et al., 2002; Tekin et al., 2018), PAR1 expression promoted an undifferentiated tumor phenotype, as evidenced by both tissue histology and downstream gene expression patterns. Whether this contributes to PAR1-dependent immune evasion requires further investigation. However, PAR1 expression has been shown to induce EMT (Otsuki et al., 2014; Tekin et al., 2018), which in turn can promote tumor immune evasion through various mechanisms (Chae et al., 2018; Terry et al., 2017).

A broader analysis of PAR1 downstream signaling identified several immunosuppressive factors that were upregulated upon PAR1 activation. Of these factors *Csf2* and *Ptgs2* were capable of restoring allograft tumor growth in PAR1 knockout cells and were shown to be critical for tumor growth in PAR1 expressing PDAC cells as well. Though earlier findings indicate that these factors are likely not major contributors to PAR1-dependent immune evasion, as presumably they would generate a systemically immunosuppressive environment which was not observed in the mixed cell study, they may indicate that PAR1 expression enhances multiple immunosuppressive and evasive mechanisms in PDAC cells.

PAR1's role in PDAC immune evasion is likely multifaceted and merits further investigation. While our *in vitro* analysis has focused on the role of thrombin in PAR1 signaling, other proteases, such as APC, could potentially be activating PAR1 *in vivo*. Importantly the downstream signaling events induced by alternative PAR1 activating proteases can differ from the canonical thrombin-mediated pathways (Zhao et al., 2014). The importance of different PAR1

activating proteases could be evaluated *in vivo* by generating doxycycline inducible PAR1 expression vectors with point mutations at the various protease cleavage sites along PAR1's cytoplasmic tail. Expression of these constructs in the $PAR1^{KO}$ cells could then determine whether each mutant could restore allograft tumor growth, and therefore promote immune evasion. A completely non-targetable PAR1 should also be included in this analysis, to ensure that PAR1 downstream signaling, and not simply the cell surface expression of PAR1, is actually required for PAR1-dependent immune evasion to occur. Similarly, mutations in the intracellular domains of PAR1 should also be employed to determine the necessity of the various downstream g-protein signaling pathways.

Our mixed tumor study and tumor rechallenge experiments indicate that PAR1 likely induces a cell autonomous mechanism of immune evasion. However, this conclusion requires further validation. Therefore, the rechallenge experiments should be repeated using the doxycycline inducible $PAR1^{KO/Tg}$ cell line, thus enabling both the initial PAR1-null challenge (-Dox) and PAR1-expressing rechallenge (+Dox) to be performed using the same cell line. This will eliminate any risk that our results were somehow caused by an inherent difference in the $PAR1^{KO}$ and KPC control cells not related to PAR1 expression. Furthermore, to determine if a PAR1-driven cell autonomous mechanism of immune evasion exists *in vitro* cytotoxic lymphocyte assays should also be performed. Though we made initial attempts at performing this assay, our data so far indicate that proper CTL specificity was not achieved. Alternative mechanisms of CTL priming, such as DC antigen loading, may therefore be necessary. Alternatively, ovalbumin expressing KPC cells could be generated in order to use the ovalbumin-specific, $CD8^+$ T cells (OT-I cells) (Clarke et al., 2000), which are frequently used for such assays.

Additionally, as mentioned earlier, our analysis thus far has focused primarily on transcriptional changes induced by PAR1 signaling *in vitro*. However, it is quite likely that transcription-independent events induced by PAR1 activation also contribute to the phenotypes we observed. Indeed, though quite an undertaking, to fully grasp the effects of PAR1 expression on tumor growth *in vivo*, single cell RNA-Seq combined with proteomics analysis of PAR1-expressing, $PAR1^{KO}$, and mixed PAR1-expressing/$PAR1^{KO}$ tumors should be performed. This would provide a comprehensive profile of the immune infiltrates and tumor cell status of each tumor and could be used to more clearly identify PAR1-dependent factors influencing the tumor microenvironment and anti-tumor immune reaction.

Taken as a whole, these findings highlight two key proteins, SOX9 and PAR1, that serve crucial roles at different stages of PDAC development. While SOX9 is essential for PDAC initiation and therefore provides an interesting target for preventive interventions, PAR1 plays a major role in tumor immune evasion and may provide a novel target for immune oncology. The work presented here expands on the general understanding of how these factors function in the context of disease progression, and although precise mechanisms of action are yet to be fully elucidated the data shown here provides valuable headway toward that end.

SUPPLEMENTAL WORK: EFFECTIVE AND EFFICIENT USE OF CRISPR/CAS12A IN CHINESE HAMSTER OVARY BIOTHERAPEUTIC PRODUCTION CELL LINE GENERATION

S.1 Introduction

S.1.1 A brief statement about this work

During the course of my PhD training I spent 6 months at Eli Lilly and Company as an academic intern, during which time I performed a brief evaluation of the utility of the recently identified CRISPR/Cas12a gene editing system for use in the generation of cell lines for biotherapeutic production. Outlined here are the results of this study. However, due to the sensitive nature of some aspects of this work several gene names and identifying aspects have been masked for this iteration of the work.

S.1.2 Background

Chinese hamster ovary (CHO) cells can produce high quantities of recombinant proteins with bioactivity in human hosts (Kim et al., 2012; Lalonde and Durocher, 2017). For this reason, the majority of biopharmaceuticals made today are generated using CHO cells (Jayapal et al., 2007; Walsh G, 2014). Decades of improvement in media composition and culturing techniques have enabled CHO cells to grow at higher densities and for longer periods, drastically increasing their protein output (Hacker et al., 2009). Now, cell line engineering through genome editing offers an additional avenue to enhance CHO cell productivity and product quality.

Complete sequencing of the CHO cell genome (Lewis et al., 2013; Xu et al., 2011) and advances in endonuclease based gene editing (Adli, 2018; Carroll, 2011) have simplified and expedited the CHO cell engineering process. Programmable nucleases such as zinc-finger nucleases (ZFN) and CRISPR/Cas can now be used with relative ease to generate cell lines with targeted gene knockouts (Lee et al., 2015). Specifically, these nucleases create double-strand breaks (DSB) at specified DNA sequences, activating the host cell DNA repair machinery and ultimately leading to random or targeted sequence modifications at the break site. Most commonly these DSBs are repaired by non-homologous end-joining (NHEJ), which is a naturally occurring

error prone process that often creates random insertions or deletions (indels) (Adli, 2018). Indels that alter the reading frame of a gene or create early stop codons prevent gene expression, creating knockouts. Alternatively, homology-directed repair (HDR), a second method of DSB repair, can be exploited to create targeted insertions of foreign DNA at the break site (Doudna and Charpentier, 2014).

ZFNs have been used previously to engineer CHO cell lines with improved selection stringency (Fan et al., 2012; Santiago et al., 2008), increased survival capabilities (Cost et al., 2010), and more potent antibody production (Malphettes et al., 2010). However, despite the success of ZFN mediated CHO cell engineering, ZFNs can be cumbersome to use. Many ZFNs fail, and because their DNA targeting specificity is based on their protein sequence, new ZFN proteins must be designed, cloned, and validated for each target loci (Carroll, 2011). While commercial services exist to produce custom ZFNs, the process can be costly and time consuming, often taking months.

The CRISPR/Cas system is a more flexible alternative to ZFNs that utilizes RNA based DNA targeting. Currently two Cas proteins have shown programmable genome editing capacity in eukaryotic cells: Cas9 (Cong et al., 2013; Jinek et al., 2012), and more recently Cas12a, previously known as Cpf1 (Zetsche et al., 2015). Both Cas proteins target DNA by forming a complex with a CRISPR RNA (crRNA), which in turn binds complementary regions of DNA enabling the Cas nuclease to induce a DSB (Swarts and Jinek, 2018). Because RNAs can be commercially synthesized quickly and cost-effectively the CRISPR/Cas system is easily adapted to new user defined targets. However, targeted DNA must contain a protospacer adjacent motif (PAM) to be recognized by the Cas nuclease, consisting of either 5'-NGG for Cas9, or 5'-TTTV for Cas12a (Swarts and Jinek, 2018). While this creates slight restrictions on the targeting capacity of CRISPR, PAM sites occur frequently in the genome and the recent addition of Cas12a as a gene editing tool has greatly increased the number of CRISPR targetable loci.

Cas9 has been used extensively since its debut as a genome editing tool, and has been shown to be effective for CHO cell engineering (Byrne et al., 2018; Lee et al., 2015; Wang et al., 2018), however, Cas12a is still a recent addition to the genome editing toolkit and differs from Cas9 in some important and advantageous ways. As mentioned above, Cas12a targets T-rich PAM sites, allowing it to target regions of DNA previously inaccessible by Cas9. Additionally, Cas12a generates staggered DSBs distal from its PAM site, potentially permitting multiple rounds of

targeting and the possibility for DNA with sticky ends to be integrated at the DSB (Zetsche et al., 2015). This differs from Cas9 which creates blunt end cuts proximal to its PAM site, often causing the PAM to be destroyed during NHEJ (Swarts and Jinek, 2018). Cas12a also uses shorter guide RNAs than Cas9 (42 nt vs 100 nt), which makes crRNA synthesis simpler and opens more possibilities for viral packaging or multiplexing using plasmid vectors (Swarts and Jinek, 2018). Finally, while Cas12a and Cas9 have shown similar activity in CHO-K1 cells (Schmieder et al., 2018), Cas12a is reported to have a higher specificity than Cas9 (Kim et al., 2016; Strohkendl et al., 2018; Swarts et al., 2017), decreasing the risk of unwanted off-target effects.

Despite the advantages offered by Cas12a, its utility in generating clonally derived CHO knockout cell lines has not been fully evaluated. In this study we demonstrate the use of Cas12a for the generation of high-producing CHO knockout cell lines. We find Cas12a editing efficiency to be crRNA dependent, highlighting the importance of screening multiple crRNAs for each gene target. We show that Cas12a can be successfully implemented at various stages in the production cell line generation process to generate knockout cell lines using small screens of 96-320 clonally derived cell lines. Together these results indicate that Cas12a is an effective and efficient means to generate engineered CHO mAb expressing cells.

S.2 Results

S.2.1 Cas12a shows crRNA dependent genome editing efficiency in CHO cells

Cas12a genome editing efficiency was first assessed in a parental CHO cell line, without mAb expression, by targeting Gene A. Because ZFNs are still used frequently in CHO cell engineering, ZFN targeting of Gene A was also analyzed for comparison. Following standard operating procedure, a single ZFN was designed and validated by Sigma-Aldrich's CompoZr custom ZFN service. Alternatively, four crRNAs targeting various regions of Gene A were designed using Benchling (https://www.benchling.com) and crRNAs with low off-target probabilities (Hsu et al., 2013) were selected (Figure S.1A). CHO cells were transfected with ZFN-mRNA or Cas12a and crRNA ribonucleoprotein (RNP) complexes, and bulk cultures were analyzed 4 days post transfection by SURVEYOR mutation detection assay (MDA) and capillary electrophoresis (CE) (Figure S.1B). crRNA-3 showed the highest indel frequency, 27% based on CE, outperforming the ZFN and remaining crRNAs. Of the four crRNAs tested, two failed to produce detectable indels, indicating that Cas12a editing efficiency is highly dependent on the crRNA used.

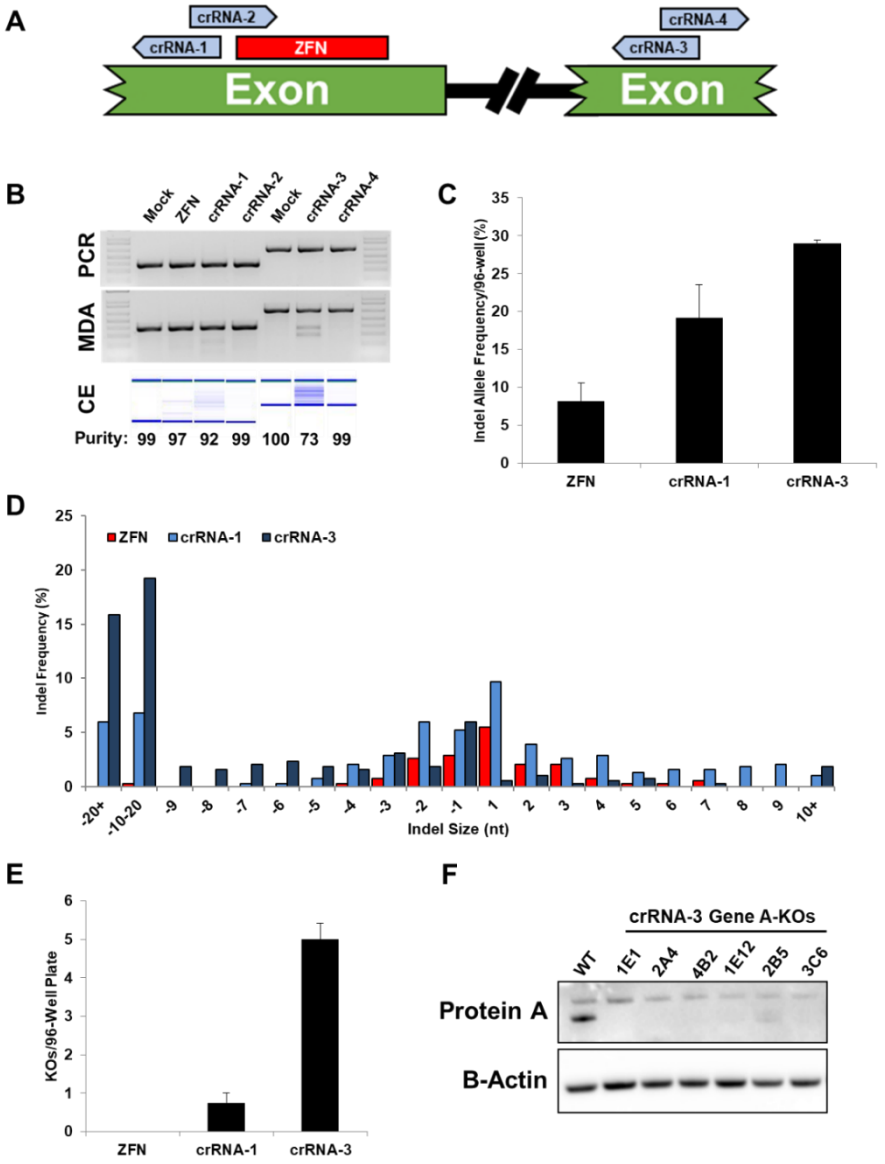

Figure S.1 Comparison of CRISPR/Cas12a and ZFN mediated genome engineering.

(A) Diagram showing the relative locations and orientations of the Cas12a crRNA and ZFN binding sites on Gene A. Arrows indicate crRNAs with homology to the sense strand (right arrow) or antisense strand (left arrow). **(B)** DNA was isolated from bulk cultures 4 days post transfection for analysis of indel frequencies. Upper, gel images showing the Surveyor mutation detection assay (MDA). Undigested PCR amplicons containing the Gene A targets are shown in the upper gel and Surveyor nuclease digested (MDA) amplicons are shown in the lower gel image. Lower, capillary electrophoresis (CE) results from the undigested PCR amplicons, purity scores are inversely proportional to the indel frequency. **(C)** Indel allele frequency based on IDAA of clonally derived cell lines (CDCLs). Four 96-well plates were analyzed per group. **(D)** Size distribution and frequency of indels identified in Figure 1C. **(E)** Number of Gene A knockouts identified per 96-well plate of CDCLs by IDAA. **(F)** Confirmation of Gene A knockout CDCLs by Western blot analysis of whole cell protein extracts. WT sample was isolated from the parental CHO cell line.

S.2.2 Effective generation of engineered CHO cell lines using Cas12a

To determine the frequency of Gene A knockouts (KOs), bulk cultures were sorted into single cell suspensions to create clonally derived cell lines (CDCLs). DNA was isolated by direct lysis and indels were identified using the indel detection by amplicon analysis (IDAA) method (Yang et al., 2015). The frequency of alleles with indels matched the pattern seen in the bulk culture analysis, with crRNA-3 producing a higher number of indels per plate compared to the ZFN (Figure S.1C). Analysis of indel size from the IDAA results showed that the ZFN produced relatively small indels mostly centered around ± 4 nucleotides, while the Cas12a crRNAs had a tendency to create large deletions of 10 nucleotides or greater (Figure S.1D). The IDAA results were then used to identify Gene A-KO CDCLs, defined as CDCLs with no detectable wild-type allele and indels that produced frameshift mutations. As expected, crRNA-3 produced the most knockouts, while crRNA-1 averaged less than one per 96-well plate (Figure S.1E). Notably, no Gene A-KOs were detected in the ZFN transfected group, as each CDCL had at least one wild type allele. The Gene A-KOs identified as having homozygous biallelic mutations by IDAA were further confirm by sanger sequencing (Table S.1). Importantly, the gene edits created by Cas12a remained stable over time with no new alterations in the Gene A sequence appearing after a 60-generation culture period (Table S.1). Finally, Western blot and shotgun proteomics analysis through LC-MS/MS confirmed the loss of Gene A protein in the engineered CDCLs (Figure S.1F, Table S.2).

Table S.1 Homozygous biallelic mutant indel size and stability over time

crRNA	CDCL	Generation 0 (Δnt)	Generation 60 (Δnt)
crRNA-1	1E1	-10	-10
	2A4	-8	-8
crRNA-3	1E12	-7	-7
	2B5	+2	+2
	3C6	-19	-19

Table S.2 Gene A-KO proteomics analysis

		Gene A-KOs	
Sample	**WT**	**2E5**	**3D3**
Detection of Gene A Protein by LC-MS/MS	**Yes**	**No**	**No**

S.2.3 Cas12a functions efficiently in antibody producing CHO cells

To determine if CRISPR/Cas12a performed similarly in mAb producing CHO cells, Gene A was targeted in an established mAb producing cell line (mAb-A producing cells). CHO cells were transfected with crRNA-3 and bulk cultures were sorted into CDCLs. Cas12a crRNA-3 showed similar targeting efficiency and indel size distribution to that found previously in the parental CHO cell line (Figure S.2AB). CDCLs with no detectable WT allele were screened by Western blot and two Gene A-KOs were identified based on Gene A protein expression (Figure S.3A). Because Gene A is known to impact a specific mAb attribute (Attribute 1), the effect of Gene A ablation could be directly measured by analysis of mAb titers. Indeed, while titers from the parental cells were > 90% positive for Attribute 1 based on LC-MS peptide mapping data, the attribute was almost completely absent from Gene A knockout CDCL titers (Figure S.3B). As before the genetic modifications created by Cas12a remained stable for 60 generations (data not shown). Taken together these results indicate that CRISPR/Cas12a operates with similar efficiency in both parental and antibody expressing CHO cells and can be used to alter aspects of mAb titers through specific gene targeting.

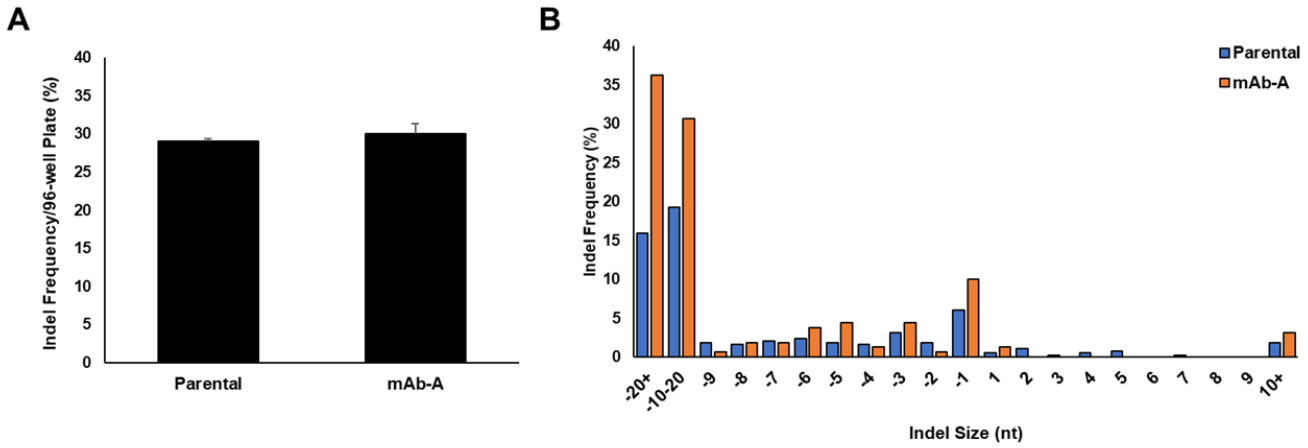

Figure S.2 Cas12a indel frequency and size distribution in CHO parental and mAb expressing cells.

(A) Comparison Gene A targeting Cas12a crRNA-3 efficiency in parental CHO cells (see Figure S.1) compared to CHO cells expressing a mAb. **(B)** Indel size distribution based on IDAA results from a parental CHO cell line (see Figure S.1) and a mAb expressing CHO cell line.

A

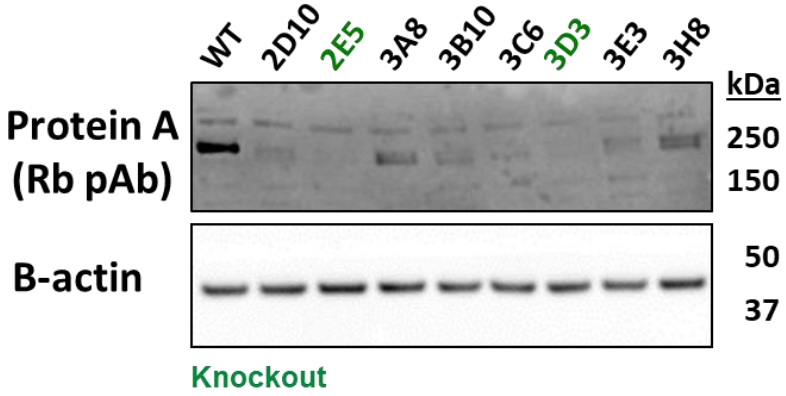

B

	Relative Percentage by LC-MS Peptide Mapping (%)		
Sample	WT	2E5	3D3
PQ Attribute 1	93.9	0.2	0.2

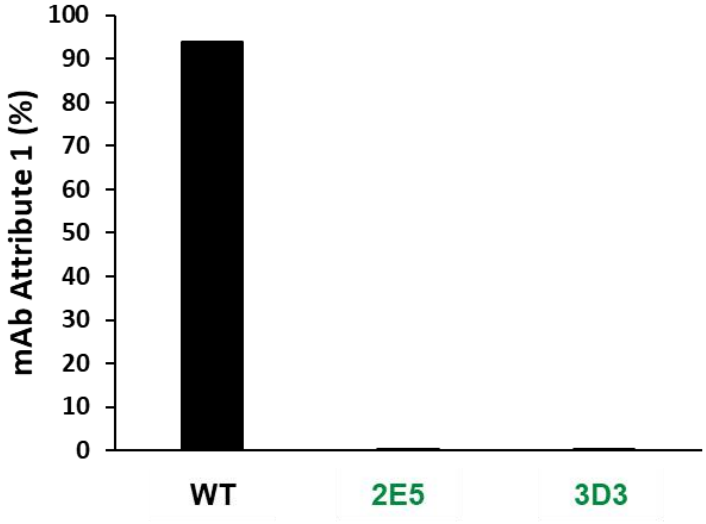

Figure S.3 Confirmation of Gene A knockouts and titer analysis.

(A) Western blot screen of Gene A protein expression. CDCLs shown had no detectable wild type allele based on IDAA. The "WT" sample represents the original mAb-A expressing CHO cell line. **(B)** LC-MS/MS analysis showing loss of Attribute 1 in titers from the Gene A knockout cells identified in (A).

S.2.4 Cas12a gene engineering can be used during mAb vector incorporation

Finally, we wanted to determine if Cas12a gene editing could be used during the generation of antibody producing cell lines. Therefore, we sought to create two distinct CHO production lines from parental cells: 1) mAb-B expressing Gene A knockouts and 2) mAb-C expressing Gene B knockouts. Gene A was again targeted using crRNA-3 as before, while new Cas12a crRNAs targeting Gene B were tested and screened for editing efficiency (Figure S.4). One crRNA showed highly effective targeting of Gene B, producing indels at a frequency of 70%, and was used for all future analysis. Multiple transfection strategies were evaluated, either varying the order of Cas12 and mAb vector delivery or transfecting both components simultaneously (Figure S.5A). Bulk culture recovery and titers were similar between all transfection methods (Figure S.5BC). Importantly, the use of CRISPR/Cas12a had no negative impact on mAb titers as CHO cells transfected with only the mAb expression vector had titers comparable to those transfected with Cas12a (Figure S.5C). Next, to identify high producing knockout cells, the bulk cultures were sorted into single cell suspensions and CDCLs were analyzed by IDAA. Interestingly, the transfection strategy had a profound impact on the number of knockouts identified (Figure S.5D). Simultaneous delivery of Cas12a RNPs and the mAb vector greatly increased the number of knockouts identified by IDAA, while sequential delivery of Cas12a RNPs followed by the mAb vector transfection and subsequent selection negatively impact the number of knockouts. Though the exact reason for this discrepancy is unknown, simultaneous transfection may have increased the proportion of cells that received both Cas12a and the mAb vector. Glutamine synthetase selection for mAb expressing cells may have therefore indirectly selected for Cas12a treated cells, leading to a higher level of gene editing in the simultaneously transfected group.

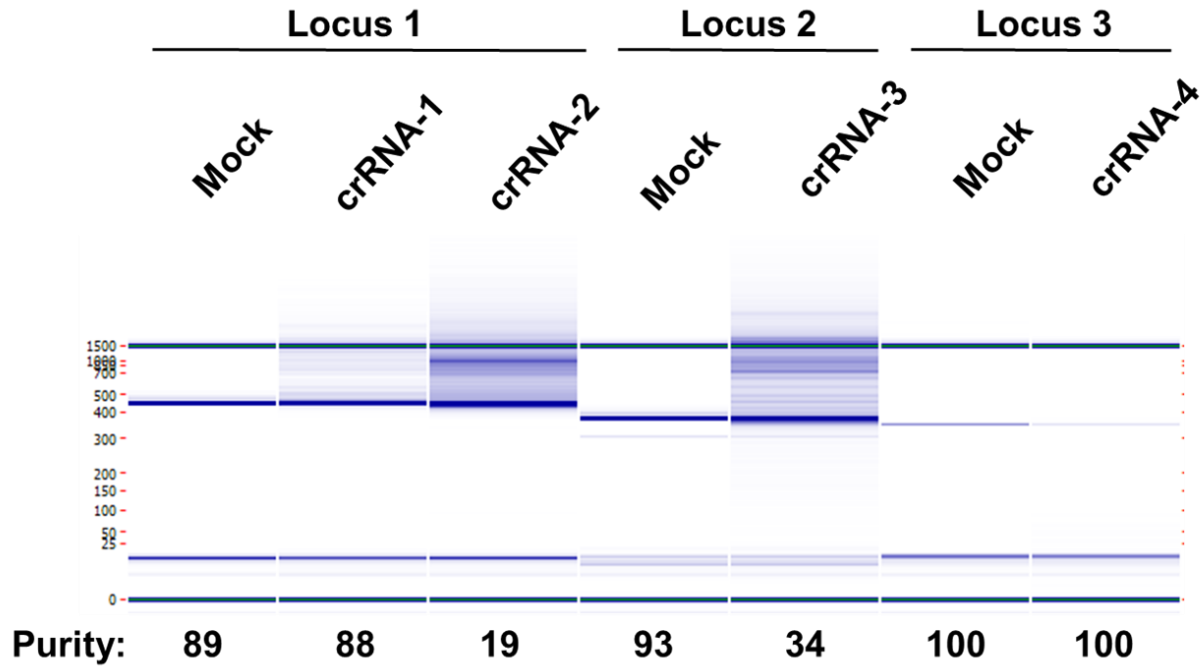

Figure S.4 Gene B Cas12a crRNA screen.

Capillary electrophoresis results from bulk cultures following transfection with crRNAs targeting three loci within Gene B. Mock samples did not receive Cas12a RNPs.

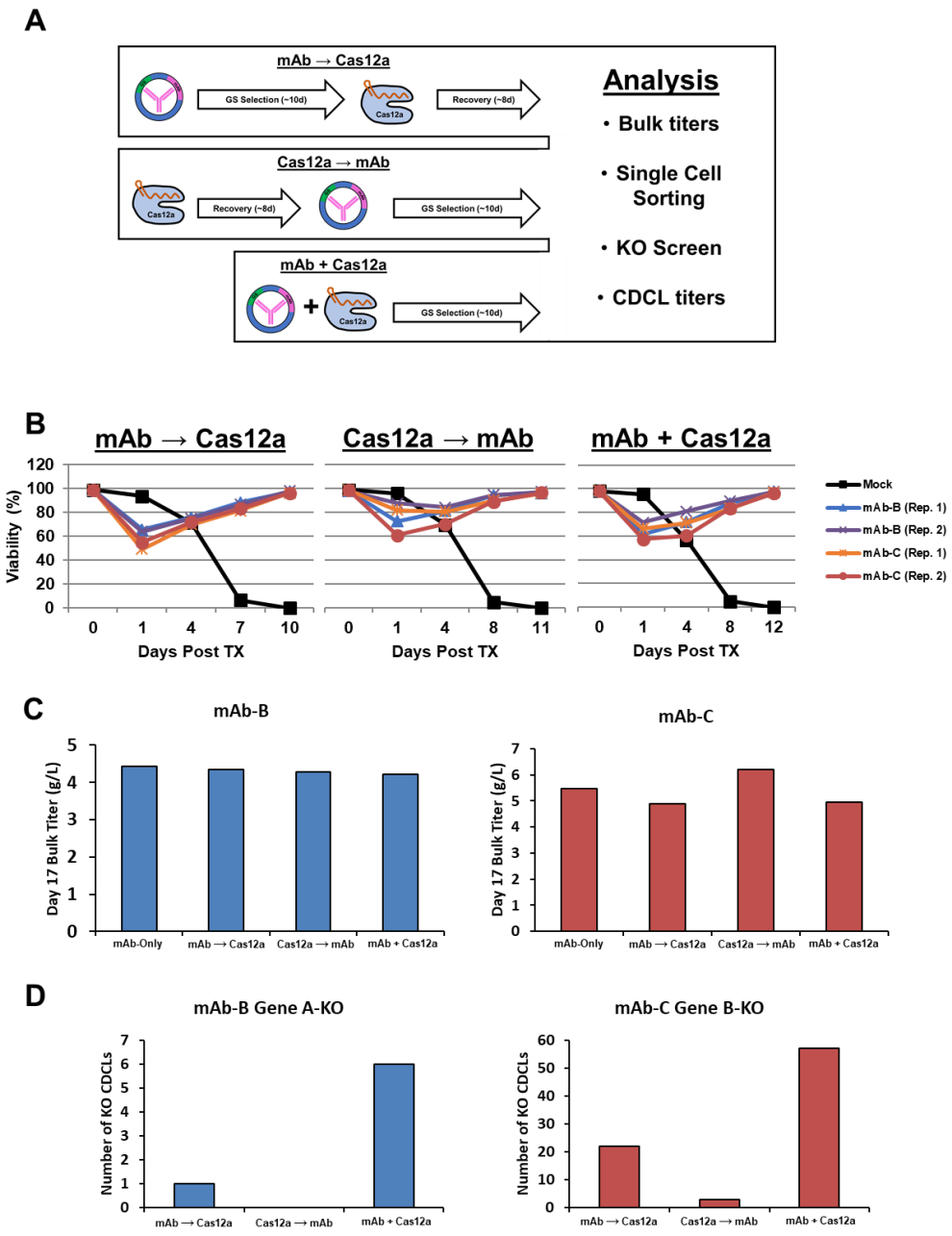

Figure S.5 CHO cell genome engineering and mAb expressing cell line generation.

(A) Diagram of the transfection strategies tested to combine CRISPR/Cas12a genetic engineering with the establishment of mAb vector expressing cells. Cas12a RNPs or mAb expression vectors were either delivered separately through sequential transfections (mAb → Cas12a; Cas12a → mAb), or simultaneously in a single cotransfection (mAb + Cas12a). **(B)** Cell viability during GS selection of bulk cultures was measured directly following mAb vector transfection for each group. **(C)** Analysis of 17-day bulk culture titers from the transfected groups, as well as a control group transfected with the mAb expression vector alone. **(D)** Graphs showing the total number of knockout cells identified by IDAA from each transfection strategy in a screen of 320 CDCLs for Gene A and 160 CDCLs for Gene B.

Further analysis identified several Gene B-KO CDCLs by IDAA that were verified by Western blot (Figure S.6A). Of particular note, a shake flask terminal study confirmed the presence of high producing (>4g/L) Gene B-KO CDCLs from a small screen of only 160 CDCLs (Figure S.6B). These results demonstrate that CRISPR/Cas12a gene editing can be performed during mAb vector integration and shows that simultaneous gene editing during bulk culture selection can increase the number of knockouts in the final CDCL screen, permitting for relatively small screen sizes depending on the crRNA efficiency.

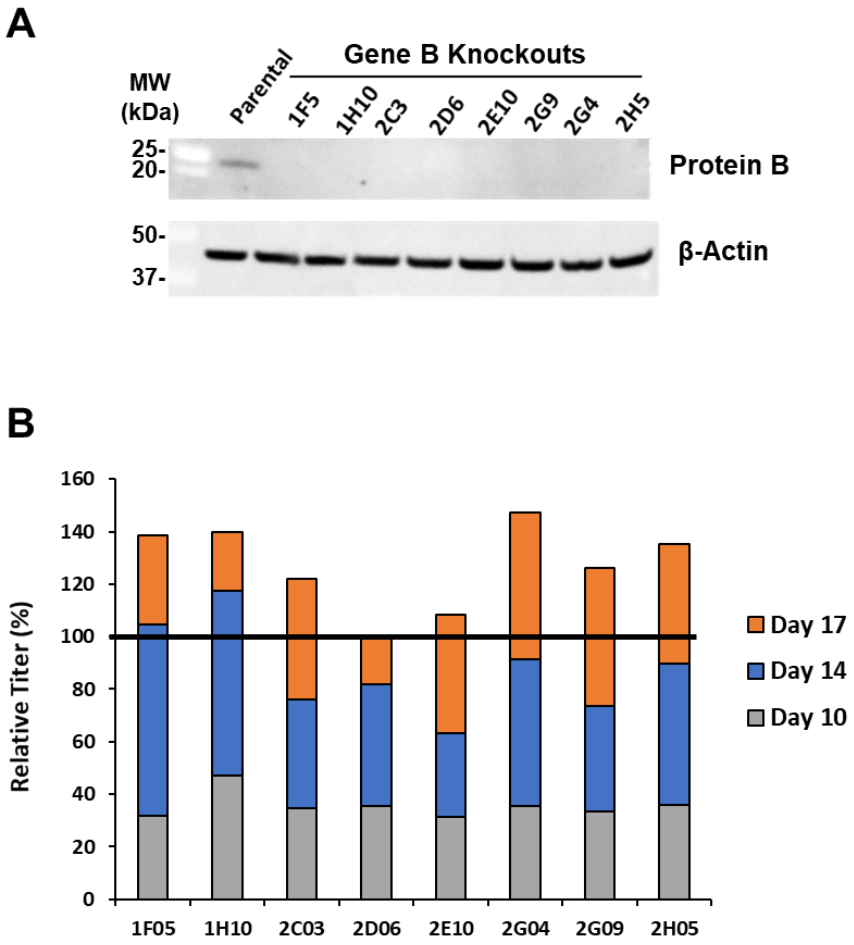

Figure S.6 Identification of high mAb producing Gene B knockouts.

(A) Western blot of Gene B protein (protein B) confirming the presence of Gene B knockout CDCLs from simultaneous transfection of Cas12a RNPs and a mAb expression vector.
(B) Seventeen-day titers from the Gene B knockouts shown in figure 4A. The horizontal black line represents historical titer value from mAb-C expressing CHO cells.

S.3 Discussion

ZFN and CRISPR/Cas9 mediate CHO cell line engineering has been well documented as a means to improve bioproduction (Byrne et al., 2018; Cost et al., 2010; Fan et al., 2012; Hu et al., 2016; Lee et al., 2015; Liu et al., 2010; Malphettes et al., 2010; Santiago et al., 2008; Wang et al., 2018). In this study, we demonstrate successful application of CRISPR/Cas12a for the generation of engineered CHO cell lines at multiple stages of the cell line generation process. In a direct comparison, Cas12a outperformed ZFN mediated gene disruption showing indel frequencies of 27% (crRNA-3) versus 3% respectively. This is consistent with previous reports of Cas12a (Schmieder et al., 2018) and ZFN (Cost et al., 2010) activity in CHO cells. Cas12a efficacy was highly dependent on the crRNA used, as only 2/4 Gene A and Gene B targeting crRNAs created detectable indels. This is roughly fitting with a recent report that found approximately 1/3 Cas12a crRNAs had indel efficiencies below 5% when examining 115 genomic targets in HEK293 cells (Bin Moon et al., 2018). While this highlights the importance of screening multiple crRNAs for each gene target, we were able to identify highly efficient (>20% indel frequency) crRNAs using small screens of only 4 crRNAs per gene. Additionally, as research to improve Cas12a activity (Bin Moon et al., 2018) and better on target prediction software (Kim et al., 2017) emerges, designing efficient Cas12a crRNAs should become easier.

In our analysis indels produced by Cas12a were typically larger than those from our ZFN, often consisting of deletions greater than 10 nucleotides. This is expected as Cas12a is thought to "re-target" and cut DNA multiple times, leading to larger deletions than those from other programmable nucleases (Swarts and Jinek, 2018). It is thought that this occurs because the target PAM site, which is located distal from the DSB, often remains intact after NHEJ repair, allowing for additional rounds Cas12a binding. In our analysis indels remained stable over time, and because Cas12a was transfected as a ribonucleoprotein (RNP) complex there was no risk of long term Cas12a expression or plasmid integration, which could otherwise be a concern for use in bioproduction.

Cas12a performed efficiently in both parental and mAb producing CHO cells and could even be used during mAb vector integration. We found that simultaneous delivery of Cas12a RNP and a mAb expression vector produced a greater number of CHO knockout CDCLs compared to sequential transfection strategies. We suspect this was due to an increased population of cells that

internalize both the mAb vector and Cas12a RNP by cotransfection, the effects of which were likely amplified by glutamine synthetase (GS) selection. GS selection was also likely responsible for the low number of engineered CDCLs found when Cas12a was transfected prior to the mAb vector. In this case knockout cells generated by Cas12a that did not uptake the mAb vector were eliminated by the GS selection and were therefore not present in the final CDCL screen. Importantly, Cas12a had no negative impact on bulk titers in any of the transfection strategies tested and high producing Gene B-KOs were identified in a small screen of only 160 CDCLs. Additionally, we demonstrate practical application of Cas12a by altering mAb titer attributes through ablation of Gene A expression in mAb-A expressing cells.

Taken together our results show that CRISPR/Cas12a offers a more flexible and efficient alternative to ZFNs for CHO cell engineering. Additionally, Cas12a crRNAs are smaller and easier to synthesize than those of Cas9, and the higher target specificity of Cas12a limits risk of off-target effects, making Cas12a a valuable alternative to Cas9 as well. Moreover, future analysis of CRISPR/Cas12a multiplex and HDR applications will likely expand its uses in CHO cell bioengineering, similar to those shown recently using CRISPR/Cas9 (Grav et al., 2015; Lee et al., 2016). In all, we show that CRISRP/Cas12a is a fast and effective system for CHO cell genome engineering and can generate knockout cell lines using small CDCL screens. We demonstrate that Cas12a can be used to alter specific mAb titer attributes through ablation of target gene expression, and we find no negative impact from Cas12a on mAb titers, even when bioengineering and production cell line generation are performed simultaneously. Taken together our results demonstrate that CRISPR/Cas12a is a useful tool for CHO cell engineering and offers an alternative system to ZFN and CRISPR/Cas9.

APPENDIX A. ISOX9 RNA-SEQ DIFFERENTIALLY EXPRESSED GENES

refseq ID	gene	logFC	FDR
NR_001463	Xist	9.15	2.4E-150
NM_001163626	Noxa1	6.31	5.6E-96
NM_177243	Slc26a9	5.98	1.1E-46
NM_026860	Gkn3	5.65	2.0E-51
NR_002844	Tsix	5.53	1.9E-28
NM_172862	Frem2	4.51	1.7E-61
NM_012006	Acot1	4.34	7.1E-59
NM_028093	Entpd8	3.30	2.3E-19
NM_011036	Reg3b	3.26	7.7E-40
NM_011448	Sox9	3.17	4.4E-43
NM_028176	Cda	2.94	1.5E-18
NM_030080	Creb3l4	2.91	7.4E-21
NM_011259	Reg3a	2.89	1.8E-30
NM_023455	Nat8	2.85	1.3E-30
NM_001136235	Kctd14	2.68	3.5E-29
NM_023493	Cml5	2.61	6.3E-12
NM_009692	Apoa1	2.54	2.2E-13
NM_001037842	Cml3	2.52	1.2E-18
NM_007603	Capn6	2.42	1.3E-22
NM_028004	Ttn	2.30	9.2E-12
NM_019395	Fbp1	2.21	1.5E-12
NM_009470	Umod	2.20	3.8E-16
NM_019563	Cited4	2.16	5.3E-20
NM_010766	Marco	2.15	4.5E-14
NM_011260	Reg3g	2.07	2.4E-14
NM_001110227	Kcnj13	2.03	2.6E-10
NR_001460	Rmrp	2.00	9.0E-08
NM_001164565	Acnat1	1.97	4.3E-15
NM_026785	Ube2c	1.91	4.0E-11
NM_178890	Abtb2	1.90	1.7E-14
NM_010870	Naip5	1.89	6.0E-13
NM_009844	Cd19	1.88	1.7E-08
NM_172523	Slc18a2	1.87	5.3E-11
NR_102723	Cd22	1.86	4.7E-07
NM_026976	Faim3	1.84	3.4E-06

NM_009043	Reg2	1.84	1.5E-12
NM_025750	4933417A18Rik	1.72	1.7E-08
NM_173870	Mgat4a	1.72	9.9E-14
NM_008963	Ptgds	1.69	7.0E-09
NM_001122683	Bdh1	1.69	2.0E-10
NM_009194	Slc12a2	1.66	6.3E-12
NM_009749	Bex2	1.65	1.5E-12
NM_028770	Krt80	1.65	4.5E-10
NM_013478	Azgp1	1.65	8.8E-12
NM_009037	Rcn1	1.64	1.1E-11
NM_008557	Fxyd3	1.62	2.2E-12
NM_021890	Fads3	1.62	6.5E-12
NM_008339	Cd79b	1.60	1.5E-07
NM_026947	Eci3	1.58	6.6E-11
NM_007914	Ehf	1.56	4.6E-10
NM_001190703	Dlk1	1.55	1.8E-05
NM_001109657	Gas7	1.54	1.6E-10
NM_019699	Fads2	1.53	1.7E-10
NM_028109	Tpx2	1.52	9.7E-06
NM_011693	Vcam1	1.50	1.7E-05
NM_026412	Knstrn	1.49	2.1E-05
NM_029338	Rsph9	1.48	2.8E-08
NM_023119	Eno1	1.48	1.3E-10
NM_001081363	Cenpf	1.47	3.0E-04
NM_145150	Prc1	1.46	6.5E-06
NR_046044	AI463170	1.44	3.0E-07
NM_001146318	Cnp	1.43	9.5E-10
NM_144556	Lgi4	1.42	4.9E-09
NM_010230	Fmn1	1.42	1.2E-04
NM_173379	Leprel1	1.40	5.3E-05
NM_001025388	Gm5506	1.39	8.4E-09
NM_007641	Ms4a1	1.37	6.3E-05
NM_009926	Col11a2	1.37	3.5E-04
NM_001271695	Kcnj15	1.36	9.0E-05
NM_033373	Krt23	1.35	2.3E-08
NM_177732	Slc35d1	1.34	5.9E-07
NM_026431	1810043G02Rik	1.30	1.5E-06
NM_001001880	Mpzl1	1.28	9.6E-06
NM_001037812	Tmem237	1.28	4.0E-05
NM_027988	Noxo1	1.28	2.2E-05
NM_001081117	Mki67	1.27	2.3E-06

NM_001102650	Nt5c3b	1.27	1.9E-07
NM_134127	Cyp4f15	1.26	2.3E-03
NM_019866	Spib	1.26	6.5E-04
NR_040491	1810053B23Rik	1.25	2.9E-07
NM_008256	Hmgcs2	1.25	5.9E-07
NM_010919	Nkx2-2	1.25	2.1E-06
NM_001199484	4931406C07Rik	1.24	1.2E-06
NM_178630	Agbl3	1.24	6.4E-04
NM_001243100	Gm11837	1.23	3.2E-04
NM_181401	Tmem64	1.23	8.3E-07
NM_009769	Klf5	1.21	2.2E-04
NM_010871	Naip6	1.21	4.9E-06
NM_009252	Serpina3n	1.20	1.2E-05
NM_001164640	Apol7a	1.20	7.4E-06
NM_197996	Tspan15	1.20	2.0E-05
NM_183187	Fam107a	1.20	3.5E-04
NM_175369	Ccdc122	1.19	1.0E-02
NR_027710	Ppargc1a	1.19	2.7E-04
NM_001038607	Kcnh1	1.16	5.9E-05
NM_019789	Kcnip3	1.16	2.1E-04
NM_023223	Cdc20	1.15	1.0E-03
NM_178886	Ldlrad3	1.15	1.7E-05
NM_020276	Nsmf	1.13	8.2E-06
NM_133754	Fblim1	1.13	7.1E-05
NM_007799	Ctse	1.13	1.1E-02
NM_178791	Vstm4	1.11	5.2E-04
NM_001164259	Fgfrl1	1.11	2.7E-05
NM_009413	Tpd52l1	1.11	1.0E-05
NM_011346	Sell	1.10	2.4E-02
NM_028333	Angptl1	1.09	6.3E-05
NM_021545	Naip7	1.09	9.9E-05
NM_001102660	Gm2663	1.08	4.7E-05
NM_033080	Nudt19	1.08	2.2E-05
NM_013538	Cdca3	1.07	1.2E-03
NM_001033500	Wdr72	1.07	2.3E-04
NM_023224	Cblc	1.06	6.2E-04
NM_030180	Usp54	1.06	6.5E-05
NM_001159620	Pigp	1.06	4.7E-04
NM_019811	Acss2	1.06	1.9E-04
NM_027927	Ints12	1.06	9.1E-05
NM_053123	Smarca1	1.05	5.2E-04

NM_019394	Mia	1.04	1.1E-04
NM_130863	Adrbk1	1.03	5.2E-05
NM_197990	1700025G04Rik	1.03	8.4E-04
NM_145448	9030617O03Rik	1.03	4.7E-04
NM_138584	Spg21	1.01	1.5E-04
NM_025520	Lsm5	1.01	5.4E-03
NM_028012	Xrcc4	1.01	8.0E-03
NM_009690	Cd5l	1.00	1.4E-02
NR_030769	Nkx2-2os	1.00	3.2E-03
NM_007885	Slc26a2	1.00	5.4E-03
NM_001081054	Qrsl1	1.00	3.3E-03
NM_021480	Tdh	1.00	1.4E-04
NM_001205057	Gm14295	0.99	3.7E-03
NM_001172472	Sphk1	0.99	3.5E-03
NR_024067	Snhg6	0.99	7.0E-04
NM_183270	Coa4	0.99	7.2E-03
NM_001038997	Gm5771	0.99	3.2E-04
NR_038157	2210019I11Rik	0.99	6.8E-03
NM_010696	Lcp2	0.98	1.8E-02
NM_134005	Enpp3	0.98	6.9E-04
NM_001039186	Ceacam1	0.97	2.3E-04
NM_007551	Cxcr5	0.97	3.1E-02
NM_001127330	Pparg	0.97	3.7E-03
NM_001025576	Ccdc141	0.97	6.9E-04
NM_153168	Lars2	0.96	1.8E-05
NR_003363	Gm6548	0.96	1.1E-02
NM_054057	Prosc	0.96	3.6E-04
NM_007994	Fbp2	0.95	9.2E-04
NM_012025	Racgap1	0.94	1.1E-02
NM_194355	Spire1	0.93	4.0E-03
NM_012026	Arhgef28	0.93	4.2E-04
NR_045883	4930413F20Rik	0.93	9.1E-03
NM_009609	Actg1	0.93	4.0E-04
NM_023543	Chn2	0.93	9.3E-04
NM_001243903	Gm14322	0.92	8.6E-03
NM_001160098	Cldn10	0.92	3.9E-04
NM_011623	Top2a	0.91	4.8E-03
NM_026316	Aldh3b1	0.90	2.1E-02
NM_178763	Zfp750	0.90	2.7E-03
NM_009423	Traf4	0.89	1.7E-03
NM_183310	Ccser1	0.89	6.9E-03

NM_011158	Prkar2b	0.89	1.7E-02
NM_008052	Dtx1	0.89	3.7E-04
NM_028072	Sulf2	0.89	1.3E-03
NM_177828	Arhgef37	0.88	1.5E-02
NM_206534	Churc1	0.88	3.3E-03
NM_023256	Krt20	0.88	2.7E-02
NM_001109045	Aqp8	0.88	2.5E-03
NM_008184	Gstm6	0.88	1.3E-02
NR_040589	6330410L21Rik	0.88	2.9E-02
NM_175116	Lpar6	0.88	1.5E-02
NM_172282	Tmco3	0.87	1.8E-03
NM_001111324	Nedd9	0.86	5.2E-03
NM_011863	Papss1	0.86	2.3E-03
NM_177876	Vps37b	0.86	3.5E-03
NM_001113368	Ceacam2	0.86	1.2E-02
NM_010067	Trdmt1	0.86	3.0E-02
NM_023824	Paqr4	0.86	1.2E-02
NR_033626	1810010D01Rik	0.86	9.6E-04
NM_008776	Pafah1b3	0.86	6.5E-03
NM_013697	Ttr	0.85	1.2E-03
NM_001271615	Fen1	0.85	1.6E-02
NM_001252108	Cadps2	0.85	3.6E-02
NM_144942	Csad	0.85	2.3E-03
NM_025286	Slc31a2	0.85	3.1E-03
NM_027009	Rfc3	0.84	1.3E-02
NM_176962	Zfp944	0.84	3.0E-02
NM_010436	H2afx	0.84	5.4E-03
NR_015536	1110038B12Rik	0.84	1.1E-02
NR_002840	Gas5	0.84	5.4E-03
NM_011943	Map2k6	0.83	2.9E-02
NR_037581	Magix	0.83	1.9E-02
NM_001099319	Gm12942	0.83	1.7E-02
NM_023058	Pkmyt1	0.83	3.3E-02
NM_025740	Ccdc104	0.82	5.3E-03
NM_173018	Myo9a	0.82	4.6E-03
NM_027999	Haus5	0.81	4.0E-02
NR_015531	Dancr	0.81	3.4E-02
NM_007428	Agt	0.81	2.0E-02
NM_009593	Abcg1	0.80	6.7E-03
NM_001012396	Ptpla	0.80	4.7E-03
NM_025939	Paics	0.80	5.8E-03

NM_026613	Ccdc34	0.79	3.1E-02
NM_011952	Mapk3	0.79	4.7E-03
NM_016957	Hmgn2	0.79	6.5E-03
NR_038153	1810044D09Rik	0.79	1.6E-02
NM_009466	Ugdh	0.78	1.2E-02
NM_026794	Deb1	0.78	7.5E-03
NM_001013375	Utp18	0.78	6.4E-03
NM_198860	Fam211b	0.78	1.1E-02
NM_007421	Adssl1	0.77	4.6E-02
NM_008812	Padi2	0.77	6.5E-03
NM_001161782	Trim32	0.77	2.4E-02
NM_011171	Procr	0.77	1.1E-02
NM_009121	Sat1	0.76	1.2E-02
NM_023258	Pycard	0.76	5.0E-02
NM_018866	Cxcl13	0.76	1.5E-02
NM_001040426	Thsd4	0.76	1.6E-02
NM_001162918	Ccdc90b	0.76	2.8E-02
NM_001033208	Myzap	0.76	2.5E-02
NM_027978	Coq2	0.76	1.2E-02
NM_173763	Ccbl2	0.75	1.1E-02
NM_010478	Hspa1b	0.75	4.2E-02
NM_011671	Ucp2	0.75	1.1E-02
NM_016772	Ech1	0.75	1.2E-02
NM_013812	Cdk2ap1	0.75	8.7E-03
NM_010135	Enah	0.74	2.0E-02
NM_177776	Smtnl2	0.73	3.9E-02
NM_007830	Dbi	0.73	1.1E-02
NM_025950	Cdc37l1	0.71	4.7E-02
NM_001033336	Abcc4	0.71	4.7E-02
NM_008982	Ptprj	0.71	2.4E-02
NM_133641	Rtkn	0.71	2.7E-02
NM_145422	D10Wsu52e	0.71	1.9E-02
NM_001270446	Ccdc30	0.70	2.9E-02
NM_007450	Slc25a4	0.70	2.2E-02
NM_029682	Stambpl1	0.70	4.5E-02
NM_001136240	Chdh	0.70	2.8E-02
NM_025563	2010012O05Rik	0.70	4.4E-02
NM_008251	Hmgn1	0.69	2.9E-02
NM_001163851	Tbc1d24	0.69	3.9E-02
NM_198113	Ssh3	0.69	3.1E-02
NM_011712	Wbp5	0.69	2.0E-02

NM_001017427	Rasef	0.69	4.8E-02
NM_053155	Clmn	0.69	3.0E-02
NM_178653	Sccpdh	0.69	3.8E-02
NM_013770	Slc25a10	0.69	1.9E-02
NM_026672	Gstm7	0.68	2.0E-02
NM_027925	Trnau1ap	0.68	3.5E-02
NR_030442	Mir677	0.68	4.6E-02
NM_001134791	Osbpl9	0.67	3.1E-02
NM_009128	Scd2	0.66	3.6E-02
NM_145413	Fam20b	0.66	4.4E-02
NM_008846	Pip5k1b	0.66	4.4E-02
NM_001190448	Ddc	0.66	3.7E-02
NM_133755	Tubgcp2	0.65	4.5E-02
NM_019427	Epb4.1l4b	0.65	3.7E-02
NM_031165	Hspa8	0.65	4.6E-02
NM_146101	Habp2	0.65	3.8E-02
NM_027976	Acsl5	0.64	4.7E-02
NM_144900	Atp1a1	0.64	4.6E-02
NM_010023	Eci1	0.64	4.6E-02
NM_013551	Hmbs	0.63	4.2E-02
NM_008817	Peg3	-0.60	4.5E-02
NM_001077495	Pik3r1	-0.61	4.7E-02
NM_010612	Kdr	-0.63	4.1E-02
NM_010295	Gclc	-0.63	3.5E-02
NM_052994	Spock2	-0.63	4.1E-02
NM_001123382	Il1r1	-0.64	4.7E-02
NM_026121	Bag4	-0.65	4.7E-02
NR_027651	Meg3	-0.66	3.5E-02
NM_138665	Sardh	-0.67	3.8E-02
NM_198114	Dagla	-0.67	4.7E-02
NM_001163336	Atp2a3	-0.67	3.1E-02
NM_009162	Scg5	-0.68	4.5E-02
NR_023846	Peg3os	-0.68	3.6E-02
NM_001177594	Slc8b1	-0.68	3.6E-02
NM_001252658	Ldlr	-0.68	3.9E-02
NM_153543	Aldh1l2	-0.68	2.5E-02
NM_133222	Eltd1	-0.69	3.7E-02
NM_138683	Rspo1	-0.69	3.6E-02
NM_147220	Abca9	-0.70	2.3E-02
NM_008719	Npas2	-0.70	3.7E-02
NM_025312	Sostdc1	-0.70	1.5E-02

NM_026122	Hmgn3	-0.70	4.1E-02
NM_009784	Cacna2d1	-0.71	3.1E-02
NM_011995	Pclo	-0.71	2.9E-02
NM_008340	Igfals	-0.71	4.1E-02
NM_025961	Gatm	-0.71	1.8E-02
NM_023913	Ern1	-0.71	1.5E-02
NM_001081268	Prss53	-0.71	2.7E-02
NM_133753	Errfi1	-0.71	1.9E-02
NM_178899	Hepacam2	-0.71	4.0E-02
NM_001276444	Gpr155	-0.72	4.6E-02
NM_030207	Sfi1	-0.72	1.6E-02
NM_001159486	Mcf2l	-0.72	2.4E-02
NM_145137	Mgl2	-0.72	2.9E-02
NM_008952	Pipox	-0.72	3.9E-02
NM_007679	Cebpd	-0.73	3.8E-02
NM_007694	Chgb	-0.73	1.7E-02
NM_008220	Hbb-bt	-0.73	1.3E-02
NM_016956	Hbb-b2	-0.73	1.3E-02
NR_040354	C630020P19Rik	-0.73	3.1E-02
NM_175473	Fras1	-0.74	1.7E-02
NM_001113384	Gnao1	-0.74	2.2E-02
NM_030725	Syt13	-0.74	1.8E-02
NM_001100449	Taf4b	-0.74	5.0E-02
NM_178727	D630039A03Rik	-0.74	2.2E-02
NM_001002927	Penk	-0.74	2.5E-02
NM_008135	Slc6a9	-0.75	1.1E-02
NM_144800	Mtss1	-0.75	1.5E-02
NM_013646	Rora	-0.75	2.7E-02
NM_172133	Adap2	-0.75	1.7E-02
NM_027309	Lysmd2	-0.75	4.1E-02
NM_146149	Fam151a	-0.76	2.2E-02
NM_001081017	Unc79	-0.76	2.6E-02
NM_011882	Rnasel	-0.76	3.7E-02
NM_175535	Arhgap20	-0.76	3.4E-02
NM_001252547	Sh2d3c	-0.76	4.6E-02
NM_011510	Abcc8	-0.77	8.5E-03
NM_022814	Svep1	-0.77	7.9E-03
NM_001102446	Alas2	-0.77	1.2E-02
NM_001081249	Vcan	-0.78	1.8E-02
NM_001012402	Hs3st6	-0.78	3.4E-02
NM_012008	Ddx3y	-0.78	1.5E-02

NM_026140	Ears2	-0.79	2.1E-02
NM_018777	Cldn6	-0.79	2.9E-02
NM_001083955	Hba-a2	-0.79	6.1E-03
NM_008218	Hba-a1	-0.79	6.1E-03
NM_007607	Car4	-0.79	2.7E-02
NM_011491	Stc2	-0.79	1.4E-02
NM_019945	Mast1	-0.80	1.0E-02
NM_029006	Kcnk16	-0.80	3.2E-02
NM_053166	Trim7	-0.80	3.0E-02
NM_031250	Ucn3	-0.80	1.7E-02
NM_010838	Mapt	-0.80	2.1E-02
NM_001081074	A1cf	-0.80	1.3E-02
NM_009308	Syt4	-0.80	5.0E-02
NM_013813	Epb4.1l3	-0.81	9.7E-03
NM_021355	Fmod	-0.81	5.4E-03
NM_008102	Gch1	-0.81	5.4E-03
NM_001024927	Pitpnm3	-0.81	2.9E-02
NM_001114332	Slc16a10	-0.82	1.0E-02
NM_175549	Robo2	-0.82	2.7E-02
NM_130887	Papln	-0.82	1.7E-02
NM_172309	Arntl2	-0.82	1.2E-02
NM_008387	Ins2	-0.83	3.3E-03
NM_198300	Cpeb3	-0.83	8.8E-03
NM_001024645	Lrrc16b	-0.83	1.0E-02
NM_011419	Kdm5d	-0.84	1.5E-02
NM_178743	Slc26a11	-0.84	3.5E-02
NR_031759	Syce2	-0.84	2.9E-02
NM_011857	Tenm3	-0.84	9.1E-03
NM_001081314	C2cd4b	-0.85	3.2E-03
NM_029466	Arl5b	-0.85	3.2E-03
NR_033538	Gm10421	-0.85	8.7E-03
NM_026301	Rnf125	-0.86	3.5E-02
NM_001159367	Per1	-0.86	2.5E-03
NM_016889	Insm1	-0.86	2.9E-02
NM_011670	Uchl1	-0.86	1.8E-02
NM_001278161	Hbb-b1	-0.87	1.4E-03
NM_001201391	Hbb-bs	-0.87	1.4E-03
NM_001166466	Spock1	-0.87	2.1E-02
NM_001109752	Dlg4	-0.88	5.2E-03
NM_080437	Celsr3	-0.88	6.7E-03
NM_031197	Slc2a2	-0.90	2.3E-03

NM_001024539	Shc2	-0.90	9.9E-03
NM_007731	Col13a1	-0.90	1.7E-02
NM_001099917	2210404O07Rik	-0.91	1.4E-03
NM_001033805	Tmem253	-0.91	3.5E-02
NM_021411	Rab37	-0.91	1.3E-02
NM_153542	Lrrc20	-0.91	1.3E-02
NM_001195006	Ndrg4	-0.92	9.0E-03
NR_003513	Neat1	-0.93	2.8E-04
NM_030707	Fcrls	-0.93	2.2E-02
NM_008386	Ins1	-0.93	4.3E-04
NM_178748	Egflam	-0.93	8.3E-03
NM_194350	Mafa	-0.94	2.3E-03
NM_170593	Disp2	-0.94	7.5E-04
NM_021391	Ppp1r1a	-0.94	1.6E-03
NM_008485	Lamc2	-0.94	5.4E-03
NM_148933	Slco4a1	-0.95	4.8E-03
NM_028618	Dmkn	-0.95	5.4E-03
NM_001039472	Kif21b	-0.96	2.8E-04
NM_001113204	Ncam1	-0.96	1.6E-02
NM_172479	Slc38a5	-0.96	2.7E-04
NM_007664	Cdh2	-0.96	1.9E-03
NM_183257	Hamp2	-0.97	2.2E-04
NM_008456	Klk1b5	-0.98	5.9E-05
NM_011832	Insrr	-0.98	1.9E-04
NM_001035509	Zcchc18	-0.99	4.6E-03
NM_001085376	Pappa2	-1.00	3.5E-04
NM_032610	Sptbn4	-1.01	4.1E-03
NM_001003664	Gm5409	-1.02	4.1E-04
NM_001102607	Col6a6	-1.03	3.4E-04
NM_019413	Robo1	-1.03	2.7E-03
NM_198627	Vstm2l	-1.04	7.5E-03
NM_178395	Zdhhc2	-1.05	1.0E-03
NM_175166	5430419D17Rik	-1.06	3.8E-04
NM_199201	Cd300lh	-1.06	2.8E-03
NM_001097623	Trerf1	-1.06	1.6E-03
NM_001277284	Ank1	-1.09	4.6E-03
NM_009895	Cish	-1.14	6.5E-06
NM_020013	Fgf21	-1.15	2.7E-04
NM_008177	Grpr	-1.15	8.4E-05
NM_130878	Cdhr1	-1.15	3.1E-04
NM_019445	Fmn2	-1.16	2.0E-04

NM_001081376	Chd5	-1.16	1.0E-03
NM_016801	Stx1a	-1.18	8.1E-06
NM_008827	Pgf	-1.18	1.9E-05
NM_028894	Lonrf3	-1.21	2.8E-04
NM_011866	Pde10a	-1.28	1.9E-04
NM_145378	Pla2g4b	-1.28	6.6E-05
NM_001081130	Ogdhl	-1.29	4.2E-05
NM_010867	Myom1	-1.30	1.0E-04
NM_001243837	C7	-1.35	2.2E-05
NM_028930	Tmc5	-1.41	2.0E-06
NM_009484	Uty	-1.44	2.0E-07
NR_045188	St18	-1.45	1.7E-07
NM_011856	Tenm2	-1.46	6.4E-06
NM_180960	Nnat	-1.48	5.9E-07
NM_010140	Epha3	-1.55	1.4E-06
NM_007470	Apod	-1.56	1.9E-07
NM_001177600	Adam23	-1.64	4.8E-07
NM_020277	Trpm5	-1.84	2.5E-10
NM_031368	Bglap3	-1.92	4.8E-10
NM_001034115	Shank1	-1.97	9.1E-16
NM_009943	Cox6a2	-2.10	1.1E-08
NM_007426	Angpt2	-2.11	3.8E-11
NM_001103153	Gm10334	-2.12	5.7E-20

APPENDIX B. ISOX9 OVERLAP WITH ADM AND PANIN: TRANSCRIPTOMIC ANAYSIS

	iSOX9		PanIN		ADM	
Gene	logFC	FDR	logFC	adj. P	FC	FDR
Gkn3	5.65	2.01E-51	5.58	2.17E-06	6.08	3.83e-60
Reg3b	3.26	7.70E-40	1.37	7.95E-04	2.76	6.58e-16
Sox9	3.17	4.44E-43	-	-	2.20	2.08e-26
Reg3a	2.89	1.75E-30	1.13	4.84E-03	1.66	3.08e-05
Apoa1	2.54	2.23E-13	5.81	3.89E-06	-	-
Capn6	2.42	1.26E-22	-	-	2.17	1.19E-03
Marco	2.15	4.53E-14	2.85	2.48E-05	4.64	1.15E-03
Reg3g	2.07	2.41E-14	2.07	1.71E-04	3.56	1.81e-36
Acnat1	1.97	4.33E-15	0.75	2.89E-02	2.43	2.06e-13
Cfap36	1.76	5.28E-03	-	-	0.64	2.12E-02
Fxyd3	1.62	2.24E-12	-	-	5.93	1.84e-16
Ehf	1.56	4.64E-10	1.43	1.09E-02	2.21	4.11e-24
Gas7	1.54	1.63E-10	0.66	1.71E-02	1.12	8.34e-05
Vcam1	1.50	1.68E-05	3.13	1.40E-05	1.49	3.05E-02
Rsph9	1.48	2.75E-08	-	-	3.57	2.46e-18
Eno1	1.48	1.30E-10	1.84	2.34E-03	-	-
Krt23	1.35	2.29E-08	-	-	0.84	2.22e-05
1810043G02Rik	1.30	1.47E-06	-	-	0.88	4.21E-02
Mpzl1	1.28	9.60E-06	1.00	4.53E-03	-	-
Mki67	1.27	2.25E-06	-	-	2.01	1.52E-02
Hmgcs2	1.25	5.93E-07	2.27	3.10E-05	4.00	1.41e-53
4931406C07Rik	1.24	1.15E-06	1.79	2.27E-04	0.75	5.61E-04
Klf5	1.21	2.16E-04	1.41	8.03E-04	1.44	7.65E-04
Serpina3n	1.20	1.19E-05	3.95	8.62E-06	2.09	8.09E-03
Tspan15	1.20	1.95E-05	1.75	4.28E-04	-	-
Kcnip3	1.16	2.10E-04	-	-	4.55	3.54e-16
Nsmf	1.13	8.16E-06	-	-	1.14	2.01e-10
Fblim1	1.13	7.13E-05	0.63	3.40E-02	1.65	5.92e-08
Ctse	1.13	1.10E-02	4.61	2.17E-06	-	-
Fgfrl1	1.11	2.71E-05	-	-	0.63	1.89E-02
Cdca3	1.07	1.21E-03	-	-	2.49	3.36E-03
Usp54	1.06	6.50E-05	-	-	1.06	4.47e-09
Pigp	1.06	4.67E-04	-	-	1.09	4.39E-03
Acss2	1.06	1.86E-04	0.69	2.14E-02	1.07	1.53E-03
Mia	1.04	1.10E-04	-	-	2.06	2.06e-12

9030617O03Rik	1.03	4.72E-04	-	-	1.19	9.92e-09
Cd5l	1.00	1.42E-02	2.27	1.26E-04	-	-
Lcp2	0.98	1.81E-02	1.68	5.01E-04	2.15	1.00E-02
Enpp3	0.98	6.91E-04	3.53	7.46E-06	-	-
Pparg	0.97	3.70E-03	1.23	2.87E-03	-	-
Fbp2	0.95	9.19E-04	2.58	1.74E-05	-	-
Actg1	0.93	3.96E-04	2.51	7.40E-05	-	-
Top2a	0.91	4.77E-03	0.61	2.96E-02	2.24	6.44E-03
Sulf2	0.89	1.27E-03	1.99	1.32E-04	1.09	5.63E-04
Churc1	0.88	3.32E-03	-	-	0.93	2.50E-03
Krt20	0.88	2.68E-02	3.45	1.97E-05	-	-
Lpar6	0.88	1.52E-02	1.69	6.50E-03	0.96	2.09E-02
Tmco3	0.87	1.75E-03	-	-	0.53	2.75E-02
Nedd9	0.86	5.19E-03	1.24	2.33E-03	1.34	1.6e-05
Paqr4	0.86	1.18E-02	-	-	1.23	1.88E-04
Pafah1b3	0.86	6.46E-03	1.30	4.08E-03	1.66	2.41E-04
Ttr	0.85	1.20E-03	-	-	5.44	5.36e-19
Gas5	0.84	5.37E-03	1.96	2.33E-04	-	-
Gm12942	0.83	1.66E-02	-	-	0.78	4.87E-02
Myo9a	0.82	4.57E-03	1.01	4.19E-03	-	-
Agt	0.81	2.04E-02	-	-	1.93	3.19E-04
Mapk3	0.79	4.67E-03	1.85	1.57E-03	-	-
Hmgn2	0.79	6.55E-03	1.52	9.28E-04	-	-
Ugdh	0.78	1.20E-02	2.50	2.54E-05	-	-
Trim32	0.77	2.38E-02	-	-	0.84	1.47E-03
Sat1	0.76	1.24E-02	1.82	1.04E-03	-	-
Pycard	0.76	5.00E-02	1.79	2.28E-04	-	-
Cxcl13	0.76	1.52E-02	2.80	7.23E-05	2.85	8.88E-03
Ccdc90b	0.76	2.81E-02	-	-	1.11	1.05E-03
Ucp2	0.75	1.10E-02	2.51	4.23E-05	1.81	3.08e-08
Ech1	0.75	1.22E-02	1.67	1.92E-04	1.15	6.94e-11
Dbi	0.73	1.10E-02	0.71	1.41E-02	1.54	6.31e-08
Rtkn	0.71	2.74E-02	-	-	0.64	9.07E-04
Slc25a4	0.70	2.19E-02	2.36	2.42E-04	0.74	3.92E-02
Chdh	0.70	2.79E-02	-	-	0.93	3.8e-05
Hmgn1	0.69	2.93E-02	-	-	0.97	2.01E-02
Clmn	0.69	3.01E-02	-	-	0.52	9.42E-03
Osbpl9	0.67	3.05E-02	1.15	2.59E-03	-	-
Scd2	0.66	3.59E-02	-	-	0.80	4.07E-03
Hspa8	0.65	4.60E-02	1.30	2.02E-03	0.84	1.89E-04
Acsl5	0.64	4.72E-02	2.76	6.06E-05	0.72	5.53E-04

Atp1a1	0.64	4.63E-02	1.66	3.09E-04	-	-
Sardh	-0.67	3.80E-02	-1.26	2.77E-03	-1.15	9.21e-07
Dagla	-0.67	4.66E-02	-1.33	1.20E-03	-2.52	1.32e-16
Aldh1l2	-0.68	2.54E-02	-2.62	7.19E-05	-2.10	8.49e-14
Sostdc1	-0.70	1.51E-02	-2.26	1.88E-04	-1.37	5.47e-08
Pclo	-0.71	2.86E-02	-	-	-0.48	3.61E-02
Gatm	-0.71	1.81E-02	-1.78	2.54E-04	-2.25	9.49e-09
Pipox	-0.72	3.95E-02	-	-	-2.31	1.03e-10
Slc6a9	-0.75	1.15E-02	-0.83	2.06E-02	-1.91	4.44e-08
Mtss1	-0.75	1.51E-02	-	-	-0.67	7.25E-04
Adap2	-0.75	1.65E-02	-	-	-1.19	1.11e-05
Unc79	-0.76	2.56E-02	-0.79	1.08E-02	-1.79	3.18e-09
Stc2	-0.79	1.43E-02	-	-	-2.75	1.81e-27
Trim7	-0.80	2.97E-02	-	-	-0.85	1.59E-02
Mapt	-0.80	2.08E-02	-0.83	6.47E-03	-2.41	2.75e-11
Gch1	-0.81	5.38E-03	-	-	-1.39	1.36e-09
Arntl2	-0.82	1.21E-02	-	-	-0.94	1.57E-02
Slco4a1	-0.95	4.79E-03	-	-	-2.16	1.43e-08
Slc38a5	-0.96	2.71E-04	-2.54	4.39E-05	-0.58	4.90E-02
Hamp2	-0.97	2.16E-04	-2.15	5.39E-04	-	-
Klk1b5	-0.98	5.91E-05	-2.80	2.68E-05	-1.99	2.75e-11
Gm5409	-1.02	4.15E-04	-0.95	6.80E-03	-1.56	2.92E-04
5430419D17Rik	-1.06	3.76E-04	-1.10	1.15E-02	-2.39	1.29e-08
Fgf21	-1.15	2.66E-04	-	-	-3.49	1.92e-10
Grpr	-1.15	8.43E-05	-1.56	2.47E-03	-	-
Pgf	-1.18	1.92E-05	-0.77	1.22E-02	-2.12	3.9e-08
Lonrf3	-1.21	2.82E-04	-	-	-1.31	1.57E-02
Bglap3	-1.92	4.78E-10	-	-	-1.80	5.62E-04
Shank1	-1.97	9.05E-16	-	-	-2.46	7.95e-16

REFEENCES

Abdulreda, M.H., Rodriguez-Diaz, R., Cabrera, O., Caicedo, A., and Berggren, P.-O. (2016). The Different Faces of the Pancreatic Islet. (Springer, Cham), pp. 11–24.

Adam, R.C., Yang, H., Rockowitz, S., Larsen, S.B., Nikolova, M., Oristian, D.S., Polak, L., Kadaja, M., Asare, A., Zheng, D., et al. (2015). Pioneer factors govern super-enhancer dynamics in stem cell plasticity an lineage choice. Nature.

Adams, G.N., Sharma, B.K., Rosenfeldt, L., Frederick, M., Flick, M.J., Witte, D.P., Mosnier, L.O., Harmel-Laws, E., Steinbrecher, K.A., and Palumbo, J.S. (2018). Protease-activated receptor-1 impedes prostate and intestinal tumor progression in mice. J. Thromb. Haemost. *16*, 2258–2269.

Adamska, A., Domenichini, A., and Falasca, M. (2017). Pancreatic Ductal Adenocarcinoma: Current and Evolving Therapies. Int. J. Mol. Sci. *18*, 1338.

Adli, M. (2018). The CRISPR tool kit for genome editing and beyond. Nat. Commun. *9*, 1–13.

Akiyama, H., Chaboissier, M.C., Martin, J.F., Schedl, A., and De Crombrugghe, B. (2002). The transcription factor Sox9 has essential roles in successive steps of the chondrocyte differentiation pathway and is required for expression of Sox5 and Sox6. Genes Dev. *16*, 2813–2828.

Amedei, A., Niccolai, E., and Prisco, D. (2014). Pancreatic cancer: Role of the immune system in cancer progression and vaccine-based immunotherapy. Hum. Vaccines Immunother.

American Cancer Society (2019). ACS cancer facts and figures. Am. Cancer Soc.

American Diabetes Association (2010). Diagnosis and Classification of Diabetes Mellitus. Diabetes Care *33*, S62–S69.

Ammann, R.W. (2006). Diagnosis and management of chronic pancreatitis: Current knowledge. Swiss Med. Wkly. *136*, 166–174.

Andersen, H., Greenberg, D.L., Fujikawa, K., Xu, W., Chung, D.W., and Davie, E.W. (1999). Protease-activated receptor 1 is the primary mediator of thrombin-stimulated platelet procoagulant activity. Proc. Natl. Acad. Sci. U. S. A. *96*, 11189–11193.

Apte, M. V, Pirola, R.C., and Wilson, J.S. (2006). Battle-scarred pancreas: Role of alcohol and pancreatic stellate cells in pancreatic fibrosis. J. Gastroenterol. Hepatol. *21*, S97–S101.

Apte, M. V, Pirola, R.C., and Wilson, J.S. (2010). Mechanisms of alcoholic pancreatitis. J. Gastroenterol. Hepatol. *25*, 1816–1826.

Arora, P., Ricks, T.K., and Trejo, J.A. (2007). Protease-activated receptor signalling, endocytic sorting and dysregulation in cancer. J. Cell Sci.

Arumugam, T., Ramachandran, V., Fournier, K.F., Wang, H., Marquis, L., Abbruzzese, J.L., Gallick, G.E., Logsdon, C.D., McConkey, D.J., and Choi, W. (2009). Epithelial to mesenchymal transition contributes to drug resistance in pancreatic cancer. Cancer Res.

Asokananthan, N., Graham, P.T., Fink, J., Knight, D.A., Bakker, A.J., McWilliam, A.S., Thompson, P.J., and Stewart, G.A. (2002). Activation of Protease-Activated Receptor (PAR)-1, PAR-2, and PAR-4 Stimulates IL-6, IL-8, and Prostaglandin E 2 Release from Human Respiratory Epithelial Cells . J. Immunol. *168*, 3577–3585.

Baghdadi, M., Wada, H., Nakanishi, S., Abe, H., Han, N., Putra, W.E., Endo, D., Watari, H., Sakuragi, N., Hida, Y., et al. (2016). Chemotherapy-Induced IL34 Enhances Immunosuppression by Tumor-Associated Macrophages and Mediates Survival of Chemoresistant Lung Cancer Cells.

Balli, D., Rech, A.J., Stanger, B.Z., and Vonderheide, R.H. (2017). Immune cytolytic activity stratifies molecular subsets of human pancreatic cancer. Clin. Cancer Res. *23*, 3129–3138.

Bansal, P., and Sonnenberg, A. (1995). Pancreatitis is a risk factor for pancreatic cancer. Gastroenterology *109*, 247–251.

Bayne, L.J., Beatty, G.L., Jhala, N., Clark, C.E., Rhim, A.D., Stanger, B.Z., and Vonderheide, R.H. (2012). Tumor-derived granulocyte-macrophage colony-stimulating factor regulates myeloid inflammation and T cell immunity in pancreatic cancer. Cancer Cell *21*, 822–835.

Beatty, G.L., and Gladney, W.L. (2015). Immune escape mechanisms as a guide for cancer immunotherapy. Clin. Cancer Res. *21*, 687–692.

Becker, A.E., Hernandez, Y.G., Frucht, H., and Lucas, A.L. (2014). Pancreatic ductal adenocarcinoma: risk factors, screening, and early detection. World J. Gastroenterol. *20*, 11182–11198.

Beer, R.L., Parsons, M.J., and Rovira, M. (2016). Centroacinar cells: At the center of pancreas regeneration. Dev. Biol. *413*, 8–15.

Bekkali, N.L.H., and Oppong, K.W. (2017). Pancreatic ductal adenocarcinoma epidemiology and risk assessment: Could we prevent? Possibility for an early diagnosis. Endosc. Ultrasound *6*, S58–S61.

Bellone, G., Turletti, A., Artusio, E., Mareschi, K., Carbone, A., Tibaudi, D., Robecchi, A., Emanuelli, G., and Rodeck, U. (1999). Tumor-associated transforming growth factor-beta and interleukin-10 contribute to a systemic Th2 immune phenotype in pancreatic carcinoma patients. Am. J. Pathol. *155*, 537–547.

Beres, T.M., Masui, T., Swift, G.H., Shi, L., Henke, R.M., and MacDonald, R.J. (2006). PTF1 is an organ-specific and Notch-independent basic helix-loop-helix complex containing the mammalian Suppressor of Hairless (RBP-J) or its paralogue, RBP-L. Mol. Cell. Biol. *26*, 117–130.

Bernard, P., Tang, P., Liu, S., Dewing, P., Harley, V.R., and Vilain, E. (2003). Dimerization of SOX9 is required for chondrogenesis, but not for sex determination. Hum. Mol. Genet. *12*, 1755–1765.

Bhagavan, N.V., Ha, C.-E., Bhagavan, N.V., and Ha, C.-E. (2015). Gastrointestinal Digestion and Absorption. In Essentials of Medical Biochemistry, (Academic Press), pp. 137–164.

Bi, W., Deng, J.M., Zhang, Z., Behringer, R.R., and De Crombrugghe, B. (1999). Sox9 is required for cartilage formation. Nat. Genet. *22*, 85–89.

Birge, R.B., Boeltz, S., Kumar, S., Carlson, J., Wanderley, J., Calianese, D., Barcinski, M., Brekken, R.A., and Huang, X. (2016). Phosphatidylserine is a global immunosuppressive signal in efferocytosis , infectious disease , and cancer. *23*, 962–978.

Blum, J.S., Wearsch, P.A., and Cresswell, P. (2013). Pathways of Antigen Processing. Annu. Rev. Immunol. *31*, 443–473.

Boire, A., Covic, L., Agarwal, A., Jacques, S., Sherifi, S., and Kuliopulos, A. (2005). PAR1 is a matrix metalloprotease-1 receptor that promotes invasion and tumorigenesis of breast cancer cells. Cell *120*, 303–313.

Bosman, F.T., Carneiro, F., Hruban, R.H., and Theise, N.D. (2010). WHO classification of tumours of the digestive system. WHO Classif. Tumours Dig. Syst.

Bouillaud, S., and Bouillaud, J. (1823). De l'Obliteration des veines et de son influence sur la formation des hydropisies partielles: consideration sur la hydropisies passive et general. Arch Gen Med *1*, 188–204.

Braganza, J.M., Lee, S.H., McCloy, R.F., and McMahon, M. (2011). Chronic pancreatitis. Gastrointest. Endosc. Clin. N. Am. *377*, 1184–1197.

Brembeck, F.H., Schreiber, F.S., Deramaudt, T.B., Craig, L., Rhoades, B., Swain, G., Grippo, P., Stoffers, D.A., Silberg, D.G., and Rustgi, A.K. (2003). The mutant K-ras oncogene causes pancreatic periductal lymphocytic infiltration and gastric mucous neck cell hyperplasia in transgenic mice. Cancer Res. *63*, 2005–2009.

Van den broeck, A., Sergeant, G., Ectors, N., Van Steenbergen, W., Aerts, R., and Topal, B. (2009). Patterns of recurrence after curative resection of pancreatic ductal adenocarcinoma. Eur. J. Surg. Oncol. *35*, 600–604.

Bronte, V., Chappell, D.B., Apolloni, E., Cabrelle, A., Wang, M., Hwu, P., and Restifo, N.P. (1999). Unopposed production of granulocyte-macrophage colony-stimulating factor by tumors inhibits CD8+ T cell responses by dysregulating antigen-presenting cell maturation. J. Immunol. *162*, 5728–5737.

Butenas, S. (2012). Tissue Factor Structure and Function. Scientifica (Cairo).

Byrne, G., O'Rourke, S.M., Alexander, D.L., Yu, B., Doran, R.C., Wright, M., Chen, Q., Azadi, P., and Berman, P.W. (2018). CRISPR/Cas9 gene editing for the creation of an MGAT1-deficient CHO cell line to control HIV-1 vaccine glycosylation. PLOS Biol. *16*, e2005817.

Canto, M.I., Almario, J.A., Schulick, R.D., Yeo, C.J., Klein, A., Blackford, A., Shin, E.J., Sanyal, A., Yenokyan, G., Lennon, A.M., et al. (2018). Risk of Neoplastic Progression in Individuals at High Risk for Pancreatic Cancer Undergoing Long-term Surveillance. Gastroenterology *155*, 740-751.e2.

Carrière, C., Young, A.L., Gunn, J.R., Longnecker, D.S., and Korc, M. (2009). Acute pancreatitis markedly accelerates pancreatic cancer progression in mice expressing oncogenic Kras. Biochem. Biophys. Res. Commun.

Carroll, D. (2011). Genome engineering with zinc-finger nucleases. Genetics *188*, 773–782.

Carstens, J.L., De Sampaio, P.C., Yang, D., Barua, S., Wang, H., Rao, A., Allison, J.P., Le Bleu, V.S., and Kalluri, R. (2017). Spatial computation of intratumoral T cells correlates with survival of patients with pancreatic cancer. Nat. Commun. *8*.

Case, R.M. (1978). Synthesis, intracellular transport and discharge of exportable proteins in the pancreatic acinar cell and other cells. Biol. Rev. Camb. Philos. Soc. *53*, 211–354.

Chae, Y.K., Chang, S., Ko, T., Anker, J., Agte, S., Iams, W., Choi, W.M., Lee, K., and Cruz, M. (2018). Epithelial-mesenchymal transition (EMT) signature is inversely associated with T-cell infiltration in non-small cell lung cancer (NSCLC). Sci. Rep. *8*, 1–8.

Chen, D.S., and Mellman, I. (2013). Oncology meets immunology: The cancer-immunity cycle. Immunity *39*, 1–10.

Chen, N.-M., Singh, G., Koenig, A., Liou, G.-Y., Storz, P., Zhang, J.-S., Regul, L., Nagarajan, S., Kühnemuth, B., Johnsen, S. a., et al. (2015a). NFATC1 Links EGFR Signaling to Induction of Sox9 Transcription and Acinar–Ductal Transdifferentiation in the Pancreas. Gastroenterology *148*, 1024-1034.e9.

Chen, N.M., Singh, G., Koenig, A., Liou, G.Y., Storz, P., Zhang, J.S., Regul, L., Nagarajan, S., Kühnemuth, B., Johnsen, S.A., et al. (2015b). NFATc1 links EGFR signaling to induction of sox9 transcription and acinar-ductal transdifferentiation in the pancreas. Gastroenterology *148*, 1024-1034.e9.

Cisowski, J., O'Callaghan, K., Kuliopulos, A., Yang, J., Nguyen, N., Deng, Q., Yang, E., Fogel, M., Tressel, S., Foley, C., et al. (2011). Targeting protease-activated receptor-1 with cell-penetrating pepducins in lung cancer. Am. J. Pathol. *179*, 513–523.

Clark, C.E., Hingorani, S.R., Mick, R., Combs, C., Tuveson, D. a., and Vonderheide, R.H. (2007). Dynamics of the immune reaction to pancreatic cancer from inception to invasion. Cancer Res. *67*, 9518–9527.

Clarke, S.Rm.K., Barnden, M., Kurts, C., Carbone, F.R., Miller, J.F., and Heath, W.R. (2000). Characterization of the ovalbumin-specific TCR transgenic line OT-I: MHC elements for positive and negative selection. Immunol. Cell Biol. *78*, 110–117.

Cleveland, M.H., Sawyer, J.M., Afelik, S., Jensen, J., and Leach, S.D. (2012). Exocrine ontogenies: On the development of pancreatic acinar, ductal and centroacinar cells. Semin. Cell Dev. Biol. *23*, 711–719.

Collins, M. a, Yan, W., Sebolt-Leopold, J.S., and Pasca di Magliano, M. (2013). Mapk Signaling is Required for Dedifferentiation of Acinar Cells and Development of Pancreatic Intraepithelial Neoplasia in Mice. Gastroenterology.

Collins, M. a, Yan, W., Sebolt-Leopold, J.S., and Pasca di Magliano, M. (2014). MAPK signaling is required for dedifferentiation of acinar cells and development of pancreatic intraepithelial neoplasia in mice. Gastroenterology *146*, 822-834.e7.

Collins, M.A., Bednar, F., Zhang, Y., Brisset, J.C., Galbán, S., Galbán, C.J., Rakshit, S., Flannagan, K.S., Adsay, N.V., and Pasca Di Magliano, M. (2012). Oncogenic Kras is required for both the initiation and maintenance of pancreatic cancer in mice. J. Clin. Invest. *122*, 639–653.

Cong, L., Ran, F.A., Cox, D., Lin, S., Barretto, R., Hsu, P.D., Wu, X., Jiang, W., and Marraffini, L.A. (2013). Multiplex Genome Engineering Using CRISPR/Cas Systems. Science (80-.). *339*, 819–823.

Conroy, T., Desseigne, F., Ychou, M., Bouché, O., Guimbaud, R., Bécouarn, Y., Adenis, A., Raoul, J.-L., Gourgou-Bourgade, S., de la Fouchardière, C., et al. (2011). FOLFIRINOX versus Gemcitabine for Metastatic Pancreatic Cancer. N. Engl. J. Med. *364*, 1817–1825.

Cost, G.J., Freyvert, Y., Vafiadis, A., Santiago, Y., Miller, J.C., Rebar, E., Collingwood, T.N., Snowden, A., and Gregory, P.D. (2010). BAK and BAX Deletion Using Zinc-Finger Nucleases Yields Apoptosis-Resistant CHO Cells. Biotechnol. Bioeng. *105*, 330–340.

Crippa, S., Salvia, R., Warshaw, A.L., Domínguez, I., Bassi, C., Falconi, M., Thayer, S.P., Zamboni, G., Lauwers, G.Y., Mino-Kenudson, M., et al. (2008). Mucinous cystic neoplasm of the pancreas is not an aggressive entity: Lessons from 163 resected patients. Ann. Surg.

Darido, C., Buchert, M., Pannequin, J., Bastide, P., Zalzali, H., Mantamadiotis, T., Bourgaux, J.-F., Garambois, V., Jay, P., Blache, P., et al. (2008). Defective Claudin-7 Regulation by Tcf-4 and Sox-9 Disrupts the Polarity and Increases the Tumorigenicity of Colorectal Cancer Cells. Cancer Res. *68*, 4258–4268.

David, J.M., Dominguez, C., Hamilton, D.H., and Palena, C. (2016). The IL-8/IL-8R axis: A double agent in tumor immune resistance. Vaccines *4*.

Deicher, A., Andersson, R., Tingstedt, B., Lindell, G., Bauden, M., and Ansari, D. (2018). Targeting dendritic cells in pancreatic ductal adenocarcinoma. Cancer Cell Int. *18*.

Deng, W., Vanderbilt, D.B., Lin, C.-C., Martin, K.H., Brundage, K.M., and Ruppert, J.M. (2015). SOX9 inhibits -TrCP-mediated protein degradation to promote nuclear GLI1 expression and cancer stem cell properties. J. Cell Sci. *128*, 1123–1138.

Direnzo, D., Hess, D.A., Damsz, B., Hallett, J.E., Marshall, B., Goswami, C., Liu, Y., Deering, T., MacDonald, R.J., and Konieczny, S.F. (2012). Induced Mist1 expression promotes remodeling of mouse pancreatic acinar cells. Gastroenterology *143*, 469–480.

Distler, M., Aust, D., Weitz, J., Pilarsky, C., and Grützmann, R. (2014). Precursor lesions for sporadic pancreatic cancer: PanIN, IPMN, and MCN. Biomed Res. Int. *2014*, 474905.

Domínguez-Muñoz, J.E. (2011). Pancreatic exocrine insufficiency: Diagnosis and treatment. J. Gastroenterol. Hepatol. *26*, 12–16.

Doudna, J.A., and Charpentier, E. (2014). The new frontier of genome engineering with CRISPR-Cas9. Science (80-.). *346*.

Eberl, M., Klingler, S., Mangelberger, D., Loipetzberger, A., Damhofer, H., Zoidl, K., Schnidar, H., Hache, H., Bauer, H.-C., Solca, F., et al. (2012). Hedgehog-EGFR cooperation response genes determine the oncogenic phenotype of basal cell carcinoma and tumour-initiating pancreatic cancer cells. EMBO Mol. Med. *4*, 218–233.

Ellis, C.A., Malik, A.B., Gilchrist, A., Hamm, H., Sandoval, R., Voyno-yasenetskaya, T., and Tiruppathi, C. (1999). Thrombin Induces Proteinase-activated Receptor-1 Gene Expression in Endothelial Cells via Activation of G i -linked Ras / Mitogen-activated Protein Kinase Pathway *. *274*, 13718–13727.

Eser, S., Schnieke, A., Schneider, G., and Saur, D. (2014). Oncogenic KRAS signalling in pancreatic cancer. Br. J. Cancer *111*, 817–822.

Evans, R.A., Diamond, M.S., Rech, A.J., Chao, T., Richardson, M.W., Lin, J.H., Bajor, D.L., Byrne, K.T., Stanger, B.Z., Riley, J.L., et al. (2016). Lack of immunoediting in murine pancreatic cancer reversed with neoantigen. JCI Insight *1*.

Even-Ram, S.C., Maoz, M., Pokroy, E., Reich, R., Katz, B.Z., Gutwein, P., Altevogt, P., and Bar-Shavit, R. (2001). Tumor Cell Invasion Is Promoted by Activation of Protease Activated Receptor-1 in Cooperation with the αvβ5Integrin. J. Biol. Chem. *276*, 10952–10962.

Falconi, M., Gabbrielli, A., Gaia, E., Graziani, R., Pezzilli, R., Uomo, G., Andriulli, A., Balzano, G., Benini, L., Calculli, L., et al. (2010). Italian consensus guidelines for chronic pancreatitis. Dig. Liver Dis. *42*, S381–S406.

Fan, L., Kadura, I., Krebs, L.E., Hatfield, C.C., Shaw, M.M., and Frye, C.C. (2012). Improving the Efficiency of CHO Cell Line Generation Using Glutamine Synthetase Gene Knockout Cells. Biotechnol. Bioeng. *109*, 1007–1015.

Farhood, B., Najafi, M., and Mortezaee, K. (2019). CD8+ cytotoxic T lymphocytes in cancer immunotherapy: A review. J. Cell. Physiol. *234*, 8509–8521.

Fauquette, V., Aubert, S., Groux-degroote, S., Hemon, B., Porchet, N., Van seuningen, I., and Pigny, P. (2007). Transcription factor AP-2α represses both the mucin MUC4 expression and pancreatic cancer cell proliferation. Carcinogenesis.

Fendrich, V., Esni, F., Garay, M.V.R., Feldmann, G., Habbe, N., Jensen, J.N., Dor, Y., Stoffers, D., Jensen, J., Leach, S.D., et al. (2008). Hedgehog signaling is required for effective regeneration of exocrine pancreas. Gastroenterology *135*, 621–631.

von Figura, G., Morris, J.P., Wright, C.V.E., and Hebrok, M. (2014). Nr5a2 maintains acinar cell differentiation and constrains oncogenic Kras-mediated pancreatic neoplastic initiation. Gut *63*, 656–664.

Fisher, D.T., Appenheimer, M.M., and Evans, S.S. (2014). The two faces of IL-6 in the tumor microenvironment. Semin. Immunol. *26*, 38–47.

El Fitori, J., Kleeff, J., Giese, N. a, Guweidhi, A., Bosserhoff, A.K., Büchler, M.W., and Friess, H. (2005). Melanoma Inhibitory Activity (MIA) increases the invasiveness of pancreatic cancer cells. Cancer Cell Int. *5*, 3.

Flandez, M., Cendrowski, J., Cañamero, M., Salas, A., del Pozo, N., Schoonjans, K., and Real, F.X. (2014). *Nr5a2* heterozygosity sensitises to, and cooperates with, inflammation in *KRas* ^{G12V} - driven pancreatic tumourigenesis. Gut *63*, 647–655.

Flaumenhaft, R., and De Ceunynck, K. (2017). Targeting PAR1: Now What? Trends Pharmacol. Sci. *38*, 701–716.

Forsmark, C.E., Swaroop Vege, S., and Wilcox, C.M. (2016). Acute Pancreatitis. N. Engl. J. Med. *375*, 1972–1981.

Friedlander, S.Y.G., Chu, G.C., Snyder, E.L., Girnius, N., Dibelius, G., Crowley, D., Vasile, E., DePinho, R.A., and Jacks, T. (2009). Context-Dependent Transformation of Adult Pancreatic Cells by Oncogenic K-Ras. Cancer Cell.

Fujimoto, D., Hirono, Y., Goi, T., Katayama, K., Matsukawa, S., and Yamaguchi, A. (2013). The activation of proteinase-activated receptor-1 (PAR1) promotes gastric cancer cell alteration of cellular morphology related to cell motility and invasion. Int. J. Oncol. *42*, 565–573.

Fukunaga, A., Miyamoto, M., Cho, Y., Murakami, S., Kawarada, Y., Oshikiri, T., Kato, K., Kurokawa, T., Suzuoki, M., Nakakubo, Y., et al. (2004). CD8+tumor-infiltrating lymphocytes together with CD4+tumor-infiltrating lymphocytes and dendritic cells improve the prognosis of patients with pancreatic adenocarcinoma. Pancreas *28*.

Gaisano, H.Y., and Gorelick, F.S. (2009). New Insights Into the Mechanisms of Pancreatitis. Gastroenterology *136*, 2040–2044.

Garcia-Lora, A., Algarra, I., and Garrido, F. (2003). MHC class I antigens, immune surveillance, and tumor immune escape. J. Cell. Physiol. *195*, 346–355.

Garside, V.C., Cullum, R., Alder, O., Lu, D.Y., Vander Werff, R., Bilenky, M., Zhao, Y., Jones, S.J.M., Marra, M.A., Underhill, T.M., et al. (2015). SOX9 modulates the expression of key transcription factors required for heart valve development. Development.

Geokas, M.C., and Rinderknecht, H. (1974). Free proteolytic enzymes in pancreatic juice of patients with acute pancreatitis. Am. J. Dig. Dis. *19*, 591–598.

Gill, R.M.S., Michael, A., Westley, L., Kocher, H.M., Murphy, J.I., and Dhoot, G.K. (2014). SULF1/SULF2 splice variants differentially regulate pancreatic tumour growth progression. Exp. Cell Res. *324*, 157–171.

Girardot, M., Bayet, E., Maurin, J., Fort, P., Roux, P., and Raynaud, P. (2018). SOX9 has distinct regulatory roles in alternative splicing and transcription. Nucleic Acids Res. *46*, 9106–9118.

Gloor, B., Müller, C.A., Worni, M., Martignoni, M.E., Uhl, W., and Büchler, M.W. (2001). Late mortality in patients with severe acute pancreatitis. Br. J. Surg. *88*, 975–979.

Goldstein, D., El-Maraghi, R.H., Hammel, P., Heinemann, V., Kunzmann, V., Sastre, J., Scheithauer, W., Siena, S., Tabernero, J., Teixeira, L., et al. (2015). nab-Paclitaxel Plus Gemcitabine for Metastatic Pancreatic Cancer: Long-Term Survival From a Phase III Trial. JNCI J. Natl. Cancer Inst. *107*, dju413–dju413.

Grady, T., Mah'Moud, M., Otani, T., Rhee, S., Lerch, M.M., and Gorelick, F.S. (1998). Zymogen proteolysis within the pancreatic acinar cell is associated with cellular injury. Am. J. Physiol. Liver Physiol. *275*, G1010–G1017.

Grapin-Botton, A. (2005). Ductal cells of the pancreas. Int. J. Biochem. Cell Biol. *37*, 504–510.

Grav, L.M., Lee, J.S., Gerling, S., Kallehauge, T.B., Hansen, A.H., Kol, S., Lee, G.M., Pedersen, L.E., and Kildegaard, H.F. (2015). One-step generation of triple knockout CHO cell lines using CRISPR/Cas9 and fluorescent enrichment. Biotechnol. J. *10*, 1446–1456.

Griffin, J.F., Poruk, K.E., and Wolfgang, C.L. (2015). Pancreatic cancer surgery: past, present, and future. Chinese J. Cancer Res. *27*, 332.

Grimont, A., Pinho, A. V, Cowley, M.J., Augereau, C., Mawson, A., Giry-Laterrière, M., Van den Steen, G., Waddell, N., Pajic, M., Sempoux, C., et al. (2014). SOX9 regulates ERBB signalling in pancreatic cancer development. Gut 1–10.

Grippo, P.J., Nowlin, P.S., Demeure, M.J., Longnecker, D.S., and Sandgren, E.P. (2003). Preinvasive pancreatic neoplasia of ductal phenotype induced by acinar cell targeting of mutant Kras in transgenic mice. Cancer Res. *63*, 2016–2019.

Grzesiak, J.J., Cao, H.S.T., Burton, D.W., Kaushal, S., Vargas, F., Clopton, P., Snyder, C.S., Deftos, L.J., Hoffman, R.M., and Bouvet, M. (2011). Knockdown of the β 1 integrin subunit reduces primary tumor growth and inhibits pancreatic cancer metastasis. Int. J. Cancer.

Guerra, C., Schuhmacher, A.J., Cañamero, M., Grippo, P.J., Verdaguer, L., Pérez-Gallego, L., Dubus, P., Sandgren, E.P., and Barbacid, M. (2007). Chronic Pancreatitis Is Essential for Induction of Pancreatic Ductal Adenocarcinoma by K-Ras Oncogenes in Adult Mice. Cancer Cell *11*, 291–302.

Guerra, C., Collado, M., Navas, C., Schuhmacher, A.J., Hernández-Porras, I., Cañamero, M., Rodriguez-Justo, M., Serrano, M., and Barbacid, M. (2011). Pancreatitis-induced inflammation contributes to pancreatic cancer by inhibiting oncogene-induced senescence. Cancer Cell *19*, 728–739.

Habbe, N., Shi, G., Meguid, R. a, Fendrich, V., Esni, F., Chen, H., Feldmann, G., Stoffers, D. a, Konieczny, S.F., Leach, S.D., et al. (2008). Spontaneous induction of murine pancreatic intraepithelial neoplasia (mPanIN) by acinar cell targeting of oncogenic Kras in adult mice. Proc. Natl. Acad. Sci. U. S. A. *105*, 18913–18918.

Hacker, D.L., De Jesus, M., and Wurm, F.M. (2009). 25 years of recombinant proteins from reactor-grown cells - Where do we go from here? Biotechnol. Adv. *27*, 1023–1027.

Hackert, T. (2018). Surgery for Pancreatic Cancer after neoadjuvant treatment. Ann. Gastroenterol. Surg. *2*, 413–418.

Hackert, T., and Büchler, M.W. (2013). Pancreatic Cancer: Advances in Treatment, Results and Limitations. Dig. Dis. *31*, 51–56.

Hale, M. a, Swift, G.H., Hoang, C.Q., Deering, T.G., Masui, T., Lee, Y.-K., Xue, J., and MacDonald, R.J. (2014). The nuclear hormone receptor family member NR5A2 controls aspects of multipotent progenitor cell-formation and acinar differentiation during pancreatic organogenesis. Development *4*, 1–11.

Han, N.A., Jin, K., He, K., Cao, J., and Teng, L. (2011). Protease-activated receptors in cancer : A systematic review. 599–608.

Hargadon, K.M., Johnson, C.E., and Williams, C.J. (2018). Immune checkpoint blockade therapy for cancer: An overview of FDA-approved immune checkpoint inhibitors. Int. Immunopharmacol. *62*, 29–39.

Harper, M.T., and Poole, A.W. (2011). PKC inhibition markedly enhances Ca 2+ signaling and phosphatidylserine exposure downstream of protease-activated receptor-1 but not protease-activated receptor-4 in human platelets. J. Thromb. Haemost. *9*, 1599–1607.

Hartwig, W., Werner, J., Jäger, D., Debus, J., and Büchler, M.W. (2013). Improvement of surgical results for pancreatic cancer. Lancet Oncol. *14*, e476–e485.

Hatziapostolou, M., Polytarchou, C., Panutsopulos, D., Covic, L., and Tsichlis, P.N. (2008). Proteinase-activated receptor-1-triggered activation of tumor progression locus-2 promotes actin cytoskeleton reorganization and cell migration. Cancer Res. *68*, 1851–1861.

Haurogné, K., Bach, J.M., and Lieubeau, B. (2007). Easy and rapid method of zygosity determination in transgenic mice by SYBR® Green real-time quantitative PCR with a simple data analysis. Transgenic Res. *16*, 127–131.

He, P., Yang, J.W., Yang, V.W., and Bialkowska, A.B. (2018). Krüppel-like Factor 5, Increased in Pancreatic Ductal Adenocarcinoma, Promotes Proliferation, Acinar-to-Ductal Metaplasia, Pancreatic Intraepithelial Neoplasia, and Tumor Growth in Mice. Gastroenterology *154*, 1494-1508.e13.

He, X., Ohba, S., Hojo, H., and McMahon, A.P. (2016). AP-1 family members act with Sox9 to promote chondrocyte hypertrophy. Development *1*, dev.134502.

Heinz, S., Benner, C., Spann, N., Bertolino, E., Lin, Y.C., Laslo, P., Cheng, J.X., Murre, C., Singh, H., and Glass, C.K. (2010). Simple Combinations of Lineage-Determining Transcription Factors Prime cis-Regulatory Elements Required for Macrophage and B Cell Identities. Mol. Cell *38*, 576–589.

Hermann, P.C., Huber, S.L., Herrler, T., Aicher, A., Ellwart, J.W., Guba, M., Bruns, C.J., and Heeschen, C. (2007). Distinct Populations of Cancer Stem Cells Determine Tumor Growth and Metastatic Activity in Human Pancreatic Cancer. Cell Stem Cell.

Herreros-Villanueva, M., Hijona, E., Bañales, J.M., Cosme, A., and Bujanda, L. (2013). Alcohol consumption on pancreatic diseases. World J. Gastroenterol. *19*, 638.

Hessmann, E., Zhang, J., Chen, N., Hasselluhn, M., Liou, G., Storz, P., Ellenrieder, V., Billadeau, D.D., and Koenig, A. (2016). NFATc4 Regulates Sox9 Gene Expression in Acinar Cell Plasticity and Pancreatic Cancer Initiation. Stem Cells Int.

Heuberger, D.M., and Schuepbach, R.A. (2019). Protease-activated receptors (PARs): mechanisms of action and potential therapeutic modulators in PAR-driven inflammatory diseases. Thromb. J. *17*, 4.

Hidalgo, M. (2010). Review Article: Medical Progress, Pancreatic Cancer. N Engl J Med *489*, 1605–1622.

Higashihara, T., Yoshitomi, H., Nakata, Y., Kagawa, S., Takano, S., Shimizu, H., Kato, A., Furukawa, K., Ohtsuka, M., and Miyazaki, M. (2017). Sex Determining Region y Box 9 Induces Chemoresistance in Pancreatic Cancer Cells by Induction of Putative Cancer Stem Cell Characteristics and Its High Expression Predicts Poor Prognosis. Pancreas *46*, 1296–1304.

Hingorani, S.R., Petricoin, E.F., Maitra, A., Rajapakse, V., King, C., Jacobetz, M. a, Ross, S., Conrads, T.P., Veenstra, T.D., Hitt, B. a, et al. (2003). Preinvasive and invasive ductal pancreatic cancer and its early detection in the mouse. Cancer Cell *4*, 437–450.

Hingorani, S.R., Wang, L., Multani, A.S., Combs, C., Deramaudt, T.B., Hruban, R.H., Rustgi, A.K., Chang, S., and Tuveson, D. a (2005). Trp53R172H and KrasG12D cooperate to promote chromosomal instability and widely metastatic pancreatic ductal adenocarcinoma in mice. Cancer Cell *7*, 469–483.

Hoang, C.Q., Hale, M.A., Azevedo-Pouly, A., Elsässer, H.P., Deering, T.G., Willet, S.G., Pan, F.C., Magnuson, M.A., Wright, C.V.E., Swift, G.H., et al. (2016). Transcriptional Maintenance of Pancreatic Acinar Identity, Differentiation and Homeostasis by PTF1A. Mol. Cell. Biol. *36*, MCB.00358-16.

Hofbauer, B., Saluja, A.K., Lerch, M.M., Bhagat, L., Bhatia, M., Lee, H.S., Frossard, J.L., Adler, G., and Steer, M.L. (1998). Intra-acinar cell activation of trypsinogen during caerulein-induced pancreatitis in rats. Am. J. Physiol. Liver Physiol. *275*, G352–G362.

Holmstrom, S.R., Deering, T., Swift, G.H., Poelwijk, F.J., Mangelsdorf, D.J., Kliewer, S.A., and MacDonald, R.J. (2011). LRH-1 and PTF1-L coregulate an exocrine pancreas-specific transcriptional network for digestive function. Genes Dev. *25*, 1674–1679.

Hong, I.S. (2016). Stimulatory versus suppressive effects of GM-CSF on tumor progression in multiple cancer types. Exp. Mol. Med. *48*, e242.

Hornyák, L., Dobos, N., Koncz, G., Karányi, Z., Páll, D., Szabó, Z., Halmos, G., and Székvölgyi, L. (2018). The role of indoleamine-2,3-dioxygenase in cancer development, diagnostics, and therapy. Front. Immunol. *9*.

Horsted, F., West, J., and Grainge, M.J. (2012). Risk of Venous Thromboembolism in Patients with Cancer: A Systematic Review and Meta-Analysis. PLoS Med. *9*, e1001275.

Hruban, R.H., Goggins, M., Parsons, J., and Kern, S.E. (2000). Progression model for pancreatic cancer. Clin. Cancer Res. *6*, 2969–2972.

Hruban, R.H., Adsay, N.V., Albores-Saavedra, J., Compton, C., Garrett, E.S., Goodman, S.N., Kern, S.E., Klimstra, D.S., Klöppel, G., Longnecker, D.S., et al. (2001). Pancreatic intraepithelial neoplasia: A new nomenclature and classification system for pancreatic duct lesions. Am. J. Surg. Pathol.

Hruban, R.H., Takaori, K., Klimstra, D.S., Adsay, N.V., Albores-Saavedra, J., Biankin, A. V, Biankin, S.A., Compton, C., Fukushima, N., Furukawa, T., et al. (2004). An Illustrated Consensus on the Classification of Pancreatic Intraepithelial Neoplasia and Intraductal Papillary Mucinous Neoplasms. Am. J. Surg. Pathol. *28*, 977–987.

Hruban, R.H., Maitra, A., and Goggins, M. (2008). Update on pancreatic intraepithelial neoplasia. Int. J. Clin. Exp. Pathol. *1*, 306–316.

Hsu, P.D., Scott, D.A., Weinstein, J.A., Ran, F.A., Konermann, S., Agarwala, V., Li, Y., Fine, E.J., Wu, X., Shalem, O., et al. (2013). DNA targeting specificity of RNA-guided Cas9 nucleases. Nat. Biotechnol. *31*, 827–832.

Hu, Z., Zhang, H., Haley, B., Macchi, F., Yang, F., Misaghi, S., Elich, J., Yang, R., Tang, Y., Joly, J.C., et al. (2016). Carboxypeptidase D is the only enzyme responsible for antibody C-terminal lysine cleavage in Chinese hamster ovary (CHO) cells. Biotechnol. Bioeng. *113*, 2100–2106.

Huang, C., Du, J., and Xie, K. (2014). FOXM1 and its oncogenic signaling in pancreatic cancer pathogenesis. Biochim. Biophys. Acta - Rev. Cancer *1845*, 104–116.

Huang, L., Wang, N., Mitchell, C.E., Brownlee, T., Maple, S.R., and Felippis, M.R. De (2017). A Novel Sample Preparation for Shotgun Proteomics Characterization of HCPs in Antibodies. Anal. Chem. *89*, 5436–5444.

Igney, F.H., and Krammer, P.H. (2002). Immune escape of tumors: apoptosis resistance and tumor counterattack. J. Leukoc. Biol. *71*, 907–920.

Ino, Y., Yamazaki-Itoh, R., Shimada, K., Iwasaki, M., Kosuge, T., Kanai, Y., and Hiraoka, N. (2013). Immune cell infiltration as an indicator of the immune microenvironment of pancreatic cancer. Br. J. Cancer *108*, 914–923.

Jain, D., Baldi, S., Zabel, A., Straub, T., and Becker, P.B. (2015). Active promoters give rise to false positive “Phantom Peaks” in ChIP-seq experiments. Nucleic Acids Res. *43*, 6959–6968.

Jakubison, B.L., Schweickert, P.G., Moser, S.E., Yang, Y., Gao, H., Scully, K., Itkin-Ansari, P., Liu, Y., and Konieczny, S.F. (2018). Induced PTF1a expression in pancreatic ductal adenocarcinoma cells activates acinar gene networks, reduces tumorigenic properties, and sensitizes cells to gemcitabine treatment. Mol. Oncol. *12*, 1104–1124.

Jayapal, K., Wlaschin, K., Hu, W., and Yap, G. (2007). Recombinant protein therapeutics from CHO cells-20 years and counting. Chem. Eng. Prog. *103*, 40–47.

Jeannot, P., Callot, C., Baer, R., Duquesnes, N., Guerra, C., Guillermet-guibert, J., Bachs, O., and Arnaud, B. (2015). Loss of p27 Kip1 promotes metaplasia in the pancreas via the regulation of Sox9 expression. Oncotarget *6*.

Jensen, J.N., Cameron, E., Garay, M.V.R., Starkey, T.W., Gianani, R., and Jensen, J. (2005). Recapitulation of elements of embryonic development in adult mouse pancreatic regeneration. Gastroenterology *128*, 728–741.

Jiang, H., Hegde, S., Knolhoff, B.L., Zhu, Y., Herndon, J.M., Meyer, M.A., Nywening, T.M., Hawkins, W.G., Shapiro, I.M., Weaver, D.T., et al. (2016a). Targeting focal adhesion kinase renders pancreatic cancers responsive to checkpoint immunotherapy. Nat. Med. *22*, 851–860.

Jiang, M., Azevedo-Pouly, A., Deering, T.G., Hoang, C.Q., DiRenzo, D., Hess, D.A., Konieczny, S.F., Swift, G.H., and MacDonald, R.J. (2016b). MIST1 and PTF1 Collaborate in Feed-forward Regulatory Loops that Maintain the Pancreatic Acinar Phenotype in Adult Mice. Mol. Cell. Biol. *36*, 2945–2955.

Jinek, M., Chylinski, K., Fonfara, I., Hauer, M., Doudna, J.A., and Charpentier, E. (2012). A Programmable Dual-RNA – Guided DNA Endonuclease in Adaptice Bacterial Immunity. Science *337*, 816–822.

Jo, A., Denduluri, S., Zhang, B., Wang, Z., Yin, L., Yan, Z., Kang, R., Shi, L.L., Mok, J., Lee, M.J., et al. (2014). The versatile functions of Sox9 in development, stem cells, and human diseases. Genes Dis. *1*, 149–161.

Jonckheere, N., Skrypek, N., and Van Seuningen, I. (2010). Mucins and pancreatic cancer. Cancers (Basel). *2*, 1794–1812.

Kabacaoglu, D., Ciecielski, K.J., Ruess, D.A., and Algül, H. (2018). Immune checkpoint inhibition for pancreatic ductal adenocarcinoma: Current limitations and future options. Front. Immunol. *9*.

Kadaja, M., Keyes, B.E., Lin, M., Pasolli, H. a., Genander, M., Polak, L., Stokes, N., Zheng, D., and Fuchs, E. (2014). SOX9: a stem cell transcriptional regulator of secreted niche signaling factors. Genes Dev. *28*, 328–341.

Kakkar, A.K., Lemoine, N.R., Scully, M.F., Tebbutt, S., and Williamson, R.C.N. (1995). Tissue factor expression correlates with histological grade in human pancreatic cancer. Br. J. Surg. *82*, 1101–1104.

Kamachi, Y., Uchikawa, M., and Kondoh, H. (2000). Pairing SOX off: With partners in the regulation of embryonic development. Trends Genet. *16*, 182–187.

Kanda, M., Matthaei, H., Wu, J., Hong, S.M., Yu, J., Borges, M., Hruban, R.H., Maitra, A., Kinzler, K., Vogelstein, B., et al. (2012). Presence of somatic mutations in most early-stage pancreatic intraepithelial neoplasia. Gastroenterology *142*, 730-733.e9.

Kanemaru, M., Maehara, N., Iwamura, T., and Chijiiwa, K. (2012). Thrombin stimulates integrin β1-dependent adhesion of human pancreatic cancer cells to vitronectin through protease-activated receptor (PAR)-1. Hepatogastroenterology. *59*, 1614–1620.

Karamitopoulou, E. (2019). Tumour microenvironment of pancreatic cancer: immune landscape is dictated by molecular and histopathological features. Br. J. Cancer *121*, 5–14.

Karki, A., Humphrey, S.E., Steele, R.E., Hess, D.A., Taparowsky, E.J., and Konieczny, S.F. (2015). Silencing Mist1 gene expression is essential for recovery from acute pancreatitis. PLoS One *10*, 1–24.

Kayed, H., Kleeff, J., Kolb, A., Ketterer, K., Keleg, S., Felix, K., Giese, T., Penzel, R., Zentgraf, H., Büchler, M.W., et al. (2006). FXYD3 is overexpressed in pancreatic ductal adenocarcinoma and influences pancreatic cancer cell growth. Int. J. Cancer *118*, 43–54.

Khorana, A.A., Ahrendt, S.A., Ryan, C.K., Francis, C.W., Hruban, R.H., Ying, C.H., Hostetter, G., Harvey, J., and Taubman, M.B. (2007). Tissue factor expression, angiogenesis, and thrombosis in pancreatic cancer. Clin. Cancer Res. *13*, 2870–2875.

Kim, D., Kim, J., Hur, J.K., Been, K.W., Yoon, S.H., and Kim, J.S. (2016). Genome-wide analysis reveals specificities of Cpf1 endonucleases in human cells. Nat. Biotechnol. *34*, 863–868.

Kim, H.K., Song, M., Lee, J., Menon, A.V., Jung, S., Kang, Y.M., Choi, J.W., Woo, E., Koh, H.C., Nam, J.W., et al. (2017). In vivo high-throughput profiling of CRISPR-Cpf1 activity. Nat. Methods *14*, 153–159.

Kim, J.Y., Kim, Y.G., and Lee, G.M. (2012). CHO cells in biotechnology for production of recombinant proteins: Current state and further potential. Appl. Microbiol. Biotechnol. *93*, 917–930.

Kim, S., Lahmy, R., Riha, C., Yang, C., Jakubison, B.L., Niekerk, J. Van, Staub, C., Wu, Y., Gates, K., Dong, D.S., et al. (2015). The Basic Helix-Loop-Helix Transcription Factor E47 Reprograms Human Pancreatic Cancer Cells to a Quiescent Acinar State With Reduced Tumorigenic Potential. *44*, 718–727.

Klöppel, G., and Maillet, B. (1992). The morphological basis for the evolution of acute pancreatitis into chronic pancreatitis. Virchows Arch. A Pathol. Anat. Histopathol. *420*, 1–4.

Kmieciak, M., Toor, A., Graham, L., Bear, H.D., and Manjili, M.H. (2011). Ex vivo Expansion of Tumor-reactive T Cells by Means of Bryostatin 1/Ionomycin and the Common Gamma Chain Cytokines Formulation 1. Isolation of Lymphocytes 5 2. Determine Fold Expansion of T Cells by Cell Counts and Flow Cytometry Analysis 5.

Knudsen, E.S., Vail, P., Balaji, U., Ngo, H., Botros, I.W., Makarov, V., Riaz, N., Balachandran, V., Leach, S., Thompson, D.M., et al. (2017). Biology of Human Tumors Stratification of Pancreatic Ductal Adenocarcinoma: Combinatorial Genetic, Stromal, and Immunologic Markers.

Kolanczyk, M., Mautner, V., Kossler, N., Nguyen, R., Kühnisch, J., Zemojtel, T., Jamsheer, A., Wegener, E., Thurisch, B., Tinschert, S., et al. (2011). MIA is a potential biomarker for tumour load in neurofibromatosis type 1. BMC Med. *9*, 82.

Koong, A.C., Mehta, V.K., Le, Q.T., Fisher, G.A., Terris, D.J., Brown, J.M., Bastidas, A.J., and Vierra, M. (2000). Pancreatic tumors show high levels of hypoxia. Int. J. Radiat. Oncol. Biol. Phys. *48*, 919–922.

Kopp, J.L., von Figura, G., Mayes, E., Liu, F.-F., Dubois, C.L., Morris, J.P., Pan, F.C., Akiyama, H., Wright, C.V.E., Jensen, K., et al. (2012). Identification of Sox9-dependent acinar-to-ductal reprogramming as the principal mechanism for initiation of pancreatic ductal adenocarcinoma. Cancer Cell *22*, 737–750.

Krah, N.M., O, J.D. La, Swift, G.H., Hoang, C.Q., Willet, S.G., Chen, F., Cash, G.M., Bronner, M.P., Wright, C.V.E., Macdonald, R.J., et al. (2015). The acinar differentiation determinant PTF1A inhibitis initiation of pancreatic ductal adenocarcinoma. Elife.

Krah, N.M., Narayanan, S.M., Yugawa, D.E., Straley, J.A., Wright, C.V.E., MacDonald, R.J., and Murtaugh, L.C. (2019). Prevention and Reversion of Pancreatic Tumorigenesis through a Differentiation-Based Mechanism. Dev. Cell *50*, 744-754.e4.

Krapp, A., Knöfler, M., Frutiger, S., Hughes, G.J., Hagenbüchle, O., and Wellauer, P.K. (1996). The p48 DNA-binding subunit of transcription factor PTF1 is a new exocrine pancreas-specific basic helix-loop-helix protein. EMBO J. *15*, 4317–4329.

Krapp, A., Knöfler, M., Ledermann, B., Bürki, K., Berney, C., Zoerkler, N., Hagenbüchle, O., and Wellauer, P.K. (1998). The bHLH protein PTF1-p48 is essential for the formation of the exocrine and the correct spatial organization of the endocrine pancreas. Genes Dev. *12*, 3752–3763.

Krebs, L., Gao, J., and Frye, C. (2015). Statistical Verification that One Round of Fluorescence-Activated Cell Sorting (FACS) Can Effectively Generate a Clonally-Derived Cell Line. Bioprocess. J. *13*, 6–19.

Kubisch, C.H., and Logsdon, C.D. (2008). Endoplasmic reticulum stress and the pancreatic acinar cell. Expert Rev. Gastroenterol. Hepatol. *2*, 249–260.

Kudo-Saito, C., Shirako, H., Ohike, M., Tsukamoto, N., and Kawakami, Y. (2013). CCL2 is critical for immunosuppression to promote cancer metastasis. Clin. Exp. Metastasis *30*, 393–405.

Kuleshov, M. V, Jones, M.R., Rouillard, A.D., Fernandez, N.F., Duan, Q., Wang, Z., Koplev, S., Jenkins, S.L., Jagodnik, K.M., Lachmann, A., et al. (2016). Enrichr: a comprehensive gene set enrichment analysis web server 2016 update. Nucleic Acids Res. *44*.

Kunovsky, L., Tesarikova, P., Kala, Z., Kroupa, R., Kysela, P., Dolina, J., and Trna, J. (2018). The Use of Biomarkers in Early Diagnostics of Pancreatic Cancer. Can. J. Gastroenterol. Hepatol. *2018*, 1–10.

de la Iglesia-Garcia, D., Vallejo-Senra, N., Iglesias-Garcia, J., López-López, A., Nieto, L., and Domínguez-Muñoz, J.E. (2018). Increased Risk of Mortality Associated With Pancreatic Exocrine Insufficiency in Patients With Chronic Pancreatitis. J. Clin. Gastroenterol. *52*, e63–e72.

De La O, J.-P., Emerson, L.L., Goodman, J.L., Froebe, S.C., Illum, B.E., Curtis, A.B., and Murtaugh, L.C. (2008). Notch and Kras reprogram pancreatic acinar cells to ductal intraepithelial neoplasia. Proc. Natl. Acad. Sci. U. S. A. *105*, 18907–18912.

Lalonde, M.E., and Durocher, Y. (2017). Therapeutic glycoprotein production in mammalian cells. J. Biotechnol. *251*, 128–140.

Lang, R.A., Metcalf, D., Cuthbertson, R.A., Lyons, I., Stanley, E., Kelso, A., Kannourakis, G., Williamson, D.J., Klintworth, G.K., and Gonda, T.J. (1987). Transgenic mice expressing a hemopoietic growth factor gene (GM-CSF) develop accumulations of macrophages, blindness, and a fatal syndrome of tissue damage. Cell *51*, 675–686.

Larsimont, J.-C., Youssef, K.K., Sánchez-Danés, A., Sukumaran, V., Defrance, M., Delatte, B., Liagre, M., Baatsen, P., Marine, J.-C., Lippens, S., et al. (2015). Sox9 Controls Self-Renewal of Oncogene Targeted Cells and Links Tumor Initiation and Invasion. Cell Stem Cell 1–14.

Le, D.T., Picozzi, V.J., Ko, A.H., Wainberg, Z.A., Kindler, H., Wang-Gillam, A., Oberstein, P., Morse, M.A., Zeh, H.J., Weekes, C., et al. (2019). Results from a phase IIb, randomized, multicenter study of GVAX pancreas and CRS-207 compared with chemotherapy in adults with previously treated metastatic pancreatic adenocarcinoma (ECLIPSE study). Clin. Cancer Res. *25*, 5493–5502.

Lee, M.G., and Muallem, S. (2008). Physiology of Duct Cell Secretion. In The Pancreas: An Integrated Textbook of Basic Science, Medicine, and Surgery: Second Edition, (Oxford, UK: Blackwell Publishing Ltd.), pp. 78–90.

Lee, A.Y.L., Dubois, C.L., Sarai, K., Zarei, S., Schaeffer, D.F., Sander, M., and Kopp, J.L. (2018). Cell of origin affects tumour development and phenotype in pancreatic ductal adenocarcinoma. Gut gutjnl-2017-314426.

Lee, J.S., Grav, L.M., Lewis, N.E., and Kildegaard, H.F. (2015). CRISPR/Cas9-mediated genome engineering of CHO cell factories: Application and perspectives. Biotechnol. J. *10*, 979–994.

Lee, J.S., Grav, L.M., Pedersen, L.E., Lee, G.M., and Kildegaard, H.F. (2016). Accelerated homology-directed targeted integration of transgenes in Chinese hamster ovary cells via CRISPR/Cas9 and fluorescent enrichment. Biotechnol. Bioeng. *113*, 2518–2523.

Lee, P.C., Taylor-Jaffe, K.M., Nordin, K.M., Prasad, M.S., Lander, R.M., and LaBonne, C. (2012). SUMOylated SoxE factors recruit Grg4 and function as transcriptional repressors in the neural crest. J. Cell Biol. *198*, 799–813.

Lefebvre, V., and Dvir-Ginzberg, M. (2017). SOX9 and the many facets of its regulation in the chondrocyte lineage. Connect. Tissue Res. *58*, 2–14.

Lefebvre, V., and Smits, P. (2005). Transcriptional control of chondrocyte fate and differentiation. Birth Defects Res. Part C Embryo Today Rev. *75*, 200–212.

Lefebvre, V., Huang, W., Harley, V.R., Goodfellow, P.N., and de Crombrugghe, B. (1997). SOX9 is a potent activator of the chondrocyte-specific enhancer of the pro alpha1(II) collagen gene. Mol. Cell. Biol. *17*, 2336–2346.

Lefebvre, V., Dumitriu, B., Penzo-Méndez, A., Han, Y., and Pallavi, B. (2007). Control of cell fate and differentiation by Sry-related high-mobility-group box (Sox) transcription factors. Int. J. Biochem. Cell Biol. *39*, 2195–2214.

Leone, P., Shin, E.-C., Perosa, F., Vacca, A., Dammacco, F., and Racanelli, V. (2013). MHC Class i Antigen Processing and Presenting Machinery: Organization, Function, and Defects in Tumor Cells. *105*.

Lerch, M.M., and Gorelick, F.S. (2000). Early trypsinogen activation in acute pancreatitis. Med. Clin. North Am. *84*, 549–563.

Leung, V.Y.L., Gao, B., Leung, K.K.H., Melhado, I.G., Wynn, S.L., Au, T.Y.K., Dung, N.W.F., Lau, J.Y.B., Mak, A.C.Y., Chan, D., et al. (2011). SOX9 governs differentiation stage-specific gene expression in growth plate chondrocytes via direct concomitant transactivation and repression. PLoS Genet. *7*, 1–16.

Lewis, N.E., Liu, X., Li, Y., Nagarajan, H., Yerganian, G., O'Brien, E., Bordbar, A., Roth, A.M., Rosenbloom, J., Bian, C., et al. (2013). Genomic landscapes of Chinese hamster ovary cell lines as revealed by the Cricetulus griseus draft genome. Nat. Biotechnol. *31*, 759–765.

Li, C., Heidt, D.G., Dalerba, P., Burant, C.F., Zhang, L., Adsay, V., Wicha, M., Clarke, M.F., and Simeone, D.M. (2007). Identification of pancreatic cancer stem cells. Cancer Res. *67*, 1030–1037.

Li, J., Byrne, K.T., Yan, F., Yamazoe, T., Chen, Z., Baslan, T., Richman, L.P., Lin, J.H., Sun, Y.H., Rech, A.J., et al. (2018). Tumor Cell-Intrinsic Factors Underlie Heterogeneity of Immune Cell Infiltration and Response to Immunotherapy. Immunity *49*, 178-193.e7.

Li, Q., Brown, J.B., Huang, H., and Bickel, P.J. (2011). Measuring reproducibility of high-throughput experiments. Ann. Appl. Stat. *5*, 1752–1779.

Li, Y., Kong, R., Chen, H., Zhao, Z., Li, L., Li, J., Hu, J., Zhang, G., Pan, S., Wang, Y., et al. (2019). Overexpression of KLF5 is associated with poor survival and G1/S progression in pancreatic cancer. Aging (Albany. NY). *11*, 5035–5057.

Lindkvist, B., Fajardo, I., Pejler, G., and Borgström, A. (2006). Cathepsin B activates human trypsinogen 1 but not proelastase 2 or procarboxypeptidase B. Pancreatology *6*, 224–231.

Ling, J., Kang, Y., Zhao, R., Xia, Q., Lee, D.F., Chang, Z., Li, J., Peng, B., Fleming, J.B., Wang, H., et al. (2012). KrasG12D-induced IKK2/beta/NF-kappaB activation by IL-1alpha and p62 Supp. Cancer Cell *21*, 105–120.

Liou, G.-Y., Doppler, H., Necela, B., Krishna, M., Crawford, H.C., Raimondo, M., and Storz, P. (2013). Macrophage-secreted cytokines drive pancreatic acinar-to-ductal metaplasia through NF- B and MMPs. J. Cell Biol. *202*, 563–577.

Liu, B., Qu, L., and Yan, S. (2015). Cyclooxygenase - 2 promotes tumor growth and suppresses tumor immunity. Cancer Cell Int. 2–7.

Liu, C.-F., Angelozzi, M., Haseeb, A., and Lefebvre, V. (2018). SOX9 is dispensable for the initiation of epigenetic remodeling and the activation of marker genes at the onset of chondrogenesis. Development *145*, dev164459.

Liu, J.A., Rao, Y., Cheung, M.P.L., Hui, M.N., Wu, M.H., Chan, L.K., Ng, I.O.L., Niu, B., Cheah, K.S.E., Sharma, R., et al. (2017a). Asymmetric localization of DLC1 defines avian trunk neural crest polarity for directional delamination and migration. Nat. Commun. *8*, 1–17.

Liu, P.Q., Chan, E.M., Cost, G.J., Zhang, L., Wang, J., Miller, J.C., Guschin, D.Y., Reik, A., Holmes, M.C., Mott, J.E., et al. (2010). Generation of a triple-gene knockout mammalian cell line using engineered zinc-finger nucleases. Biotechnol. Bioeng. *106*, 97–105.

Liu, X., Yu, J., Song, S., Yue, X., and Li, Q. (2017b). Protease-activated receptor-1 (PAR-1): a promising molecular target for cancer. Oncotarget *8*, 107334–107345.

Long, J., Zhang, Y., Yu, X., Yang, J., Lebrun, D.G., Chen, C., Yao, Q., and Li, M. (2011). Overcoming drug resistance in pancreatic cancer. Expert Opin. Ther. Targets.

Lonowski, L.A., Narimatsu, Y., Riaz, A., Delay, C.E., Yang, Z., Niola, F., Duda, K., Ober, E.A., Clausen, H., Wandall, H.H., et al. (2017). Genome editing using FACS enrichment of nuclease-expressing cells and indel detection by amplicon analysis. Nat. Protoc. *12*, 581–603.

Looi, C.K., Chung, F.F.L., Leong, C.O., Wong, S.F., Rosli, R., and Mai, C.W. (2019). Therapeutic challenges and current immunomodulatory strategies in targeting the immunosuppressive pancreatic tumor microenvironment. J. Exp. Clin. Cancer Res. *38*.

Lu, L., and Zeng, J. (2017). Evaluation of K-ras and p53 expression in pancreatic adenocarcinoma using the cancer genome atlas. PLoS One *12*.

Macfarlane, S.R., Seatter, M.J., Kanke, T., Hunter, G.D., and Plevin, R. (2001). Proteinase-Activated Receptors. *53*, 245–282.

Macherla, S., Laks, S., Naqash, A.R., Bulumulle, A., Zervos, E., and Muzaffar, M. (2018). Emerging Role of Immune Checkpoint Blockade in Pancreatic Cancer. Int. J. Mol. Sci. *19*.

di Magliano, M.P., and Logsdon, C.D. (2013). Roles for KRAS in Pancreatic Tumor Development and Progression. Gastroenterology *29*, 997–1003.

Makohon-Moore, A.P., Matsukuma, K., Zhang, M., Reiter, J.G., Gerold, J.M., Jiao, Y., Sikkema, L., Attiyeh, M.A., Yachida, S., Sandone, C., et al. (2018). Precancerous neoplastic cells can move through the pancreatic ductal system. Nature.

Malphettes, L., Freyvert, Y., Chang, J., Liu, P., Chan, E., Miller, J.C., Zhou, Z., Nguyen, T., Tsai, C., Snowden, A.W., et al. (2010). Highly Efficient Deletion of FUT8 in CHO Cell Lines Using Zinc-Finger Nucleases Yields Cells That Produce Completely Nonfucosylated Antibodies. Biotechnol. Bioeng. *106*, 774–783.

Markosyan, N., Li, J., Sun, Y.H., Richman, L.P., Lin, J.H., Yan, F., Quinones, L., Sela, Y., Yamazoe, T., Gordon, N., et al. (2019). Tumor cell-intrinsic EPHA2 suppresses antitumor immunity by regulating PTGS2 (COX-2). J. Clin. Invest. *129*, 3594–3609.

Martin, C.B., Mahon, G.M., Klinger, M.B., Kay, R.J., Symons, M., Der, C.J., and Whitehead, I.P. (2001). The thrombin receptor, PAR-1, causes transformation by activation of Rho-mediated signaling pathways. Oncogene *20*, 1953–1963.

Martinelli, P., Cañamero, M., del Pozo, N., Madriles, F., Zapata, A., and Real, F.X. (2013). Gata6 is required for complete acinar differentiation and maintenance of the exocrine pancreas in adult mice. Gut *62*, 1481–1488.

Martinelli, P., Madriles, F., Cañamero, M., Pau, E.C.S., Pozo, N. Del, Guerra, C., and Real, F.X. (2016). The acinar regulator Gata6 suppresses KrasG12V-driven pancreatic tumorigenesis in mice. Gut *65*, 476–486.

Martinez-Bosch, N., Vinaixa, J., and Navarro, P. (2018). Immune evasion in pancreatic cancer: From mechanisms to therapy. Cancers (Basel). *10*.

Matheu, A., Collado, M., Wise, C., Manterola, L., Cekaite, L., Tye, A.J., Canamero, M., Bujanda, L., Schedl, A., Cheah, K.S.E., et al. (2012). Oncogenicity of the developmental transcription factor Sox9. Cancer Res. *72*, 1301–1315.

Mazur, P.K., Einwächter, H., Lee, M., Sipos, B., Nakhai, H., Rad, R., Zimber-Strobl, U., Strobl, L.J., Radtke, F., Klöppel, G., et al. (2010). Notch2 is required for progression of pancreatic intraepithelial neoplasia and development of pancreatic ductal adenocarcinoma. Proc. Natl. Acad. Sci. U. S. A. *107*, 13438–13443.

McCarthy, D.M., Brat, D.J., Wilentz, R.E., Yeo, C.J., Cameron, J.L., Kern, S.E., and Hruban, R.H. (2001). Pancreatic intraepithelial neoplasia and infiltrating adenocarcinoma: Analysis of progression and recurrence by DPC4 immunohistochemical labeling. Hum. Pathol.

McLean, C.Y., Bristor, D., Hiller, M., Clarke, S.L., Schaar, B.T., Lowe, C.B., Wenger, A.M., and Bejerano, G. (2010). GREAT improves functional interpretation of cis-regulatory regions. Nat. Biotechnol. *28*, 495–501.

Mead, T.J., Wang, Q., Bhattaram, P., Dy, P., Afelik, S., Jensen, J., and Lefebvre, V. (2013). A far-upstream (-70 kb) enhancer mediates Sox9 auto-regulation in somatic tissues during development and adult regeneration. Nucleic Acids Res. gkt140-.

Mertin, S., McDowall, S.G., and Harley, V.R. (1999). The DNA-binding specificity of SOX9 and other SOX proteins. Nucleic Acids Res. *27*, 1359–1364.

Mihara, K., Ramachandran, R., Renaux, B., Saifeddine, M., and Hollenberg, M.D. (2013). Neutrophil elastase and proteinase-3 trigger G proteinbiased signaling through proteinase-activated receptor-1 (PAR1). J. Biol. Chem. *288*, 32979–32990.

Miliotou, A.N., and Papadopoulou, L.C. (2018). CAR T-cell Therapy: A New Era in Cancer Immunotherapy. Curr. Pharm. Biotechnol. *19*, 5–18.

Mitchell, R.M.S., Byrne, M.F., and Baillie, J. (2003). Pancreatitis. Lancet *361*, 1447–1455.

Mittal, D., Gubin, M.M., Schreiber, R.D., and Smyth, M.J. (2014). New insights into cancer immunoediting and its three component phases-elimination, equilibrium and escape. Curr. Opin. Immunol. *27*, 16–25.

Moini, J. (2019). The Pancreas and Classifications of Insulin. In Epidemiology of Diabetes, (Elsevier), pp. 11–23.

Molero, X., Vaquero, E.C., Flández, M., González, A.M., Ortiz, M.Á., Cibrián-Uhalte, E., Servitja, J.-M., Merlos, A., Juanpere, N., Massumi, M., et al. (2012). Gene expression dynamics after murine pancreatitis unveils novel roles for Hnf1α in acinar cell homeostasis. Gut *61*, 1187–1196.

Bin Moon, S., Lee, J.M., Kang, J.G., Lee, N.-E., Ha, D.-I., Kim, D.Y., Kim, S.H., Yoo, K., Kim, D., Ko, J.-H., et al. (2018). Highly efficient genome editing by CRISPR-Cpf1 using CRISPR RNA with a uridinylate-rich 3′-overhang. Nat. Commun. *9*, 3651.

Morris, J.P., Wang, S.C., and Hebrok, M. (2010a). KRAS, Hedgehog, Wnt and the twisted developmental biology of pancreatic ductal adenocarcinoma. Nat. Rev. Cancer *10*, 683–695.

Morris, J.P.I., Cano, D.A., Sekine, S., Wang, S.C., and Hebrok, M. (2010b). β -catenin blocks Kras-dependent reprogramming of acini into pancreatic cancer precursor lesions in mice. *120*.

Murchison, J.T., Wylie, L., and Stockton, D.L. (2004). Excess risk of cancer in patients with primary venous thromboembolism: A national, population-based cohort study. Br. J. Cancer *91*, 92–95.

Murtaugh, L.C., and Keefe, M.D. (2015). Regeneration and Repair of the Exocrine Pancreas. Annu. Rev. Physiol. *77*, 229–249.

Mushtaq, M.U., Papadas, A., Pagenkopf, A., Flietner, E., Morrow, Z., Chaudhary, S.G., and Asimakopoulos, F. (2018). Tumor matrix remodeling and novel immunotherapies: The promise of matrix-derived immune biomarkers. J. Immunother. Cancer *6*, 1–14.

Neoptolemos, J.P., Stocken, D.D., Dunn, J.A., Almond, J., Beger, H.G., Pederzoli, P., Bassi, C., Dervenis, C., Fernandez-Cruz, L., Lacaine, F., et al. (2001). Influence of resection margins on survival for patients with pancreatic cancer treated by adjuvant chemoradiation and/or chemotherapy in the ESPAC-1 randomized controlled trial. In Annals of Surgery, p.

Neoptolemos, J.P., Palmer, D.H., Ghaneh, P., Psarelli, E.E., Valle, J.W., Halloran, C.M., Faluyi, O., O'Reilly, D.A., Cunningham, D., Wadsley, J., et al. (2017). Comparison of adjuvant gemcitabine and capecitabine with gemcitabine monotherapy in patients with resected pancreatic cancer (ESPAC-4): a multicentre, open-label, randomised, phase 3 trial. Lancet *389*, 1011–1024.

Nieman, M.T. (2016). Protease-activated receptors in hemostasis. Blood *128*, 169–177.

Niers, T.M.H., Brüggemann, L.W., Klerk, C.P.W., Muller, F.J.M., Buckle, T., Reitsma, P.H., Richel, D.J., Spek, C.A., Van Tellingen, O., and Van Noorden, C.J.F. (2009). Differential effects of anticoagulants on tumor development of mouse cancer cell lines B16, K1735 and CT26 in lung. Clin. Exp. Metastasis *26*, 171–178.

Nitori, N., Ino, Y., Nakanishi, Y., Yamada, T., Honda, K., Yanagihara, K., Kosuge, T., Kanai, Y., Kitajima, M., and Hirohashi, S. (2005). Prognostic significance of tissue factor in pancreatic ductal adenocarcinoma. Clin. Cancer Res. *11*, 2531–2539.

Noble, S., and Pasi, J. (2010). Epidemiology and pathophysiology of cancer-associated thrombosis. Br. J. Cancer *102*, S2–S9.

Nøjgaard, C., Bendtsen, F., Becker, U., Andersen, J.R., Holst, C., and Matzen, P. (2010). Danish Patients With Chronic Pancreatitis Have a Four-Fold Higher Mortality Rate Than the Danish Population. Clin. Gastroenterol. Hepatol. *8*, 384–390.

Nomi, T., Sho, M., Akahori, T., Hamada, K., Kubo, A., Kanehiro, H., Nakamura, S., Enomoto, K., Yagita, H., Azuma, M., et al. (2007). Clinical significance and therapeutic potential of the programmed death-1 ligand/programmed death-1 pathway in human pancreatic cancer. Clin. Cancer Res. *13*, 2151–2157.

Ohba, S., He, X., Hojo, H., and McMahon, A.P. (2015). Distinct Transcriptional Programs Underlie Sox9 Regulation of the Mammalian Chondrocyte. Cell Rep. *12*, 1–15.

Olson, S.H., and Kurtz, R.C. (2013). Epidemiology of pancreatic cancer and the role of family history. J. Surg. Oncol. *107*, 1–7.

Ortiz-Stern, A., Deng, X., Smoktunowicz, N., Mercer, P.F., and Chambers, R.C. (2012). PAR-1-dependent and PAR-independent pro-inflammatory signaling in human lung fibroblasts exposed to thrombin. J. Cell. Physiol. *227*, 3575–3584.

Ossovskaya, V.S., and Bunnett, N.W. (2004). Protease-Activated Receptors: Contribution to Physiology and Disease. Physiol. Rev. *84*, 579–621.

Otsuki, T., Fujimoto, D., Hirono, Y., Goi, T., and Yamaguchi, A. (2014). Thrombin conducts epithelial-mesenchymal transition via protease-activated receptor-1 in human gastric cancer. Int. J. Oncol. *45*, 2287–2294.

Paing, M.M., Johnston, C.A., Siderovski, D.P., and Trejo, J. (2006). Clathrin Adaptor AP2 Regulates Thrombin Receptor Constitutive Internalization and Endothelial Cell Resensitization. Mol. Cell. Biol. *26*, 3231–3242.

Pan, F.C., and Wright, C. (2011). Pancreas organogenesis: From bud to plexus to gland. Dev. Dyn. *240*, 530–565.

Pandol, S.J. (2010). The Exocrine Pancreas (Morgan & Claypool Life Sciences).

Paniccia, A., and Schulick, R.D. (2017). Pancreatic Physiology and Functional Assessment. In Blumgart's Surgery of the Liver, Biliary Tract and Pancreas, 2-Volume Set, (Content Repository Only!), pp. 66-76.e3.

Passeron, T., Valencia, J.C., Namiki, T., Vieira, W.D., Passeron, H., Miyamura, Y., and Hearing, V.J. (2009). Upregulation of SOX9 inhibits the growth of human and mouse melanomas and restores their sensitivity to retinoic acid. J. Clin. Invest. *119*, 954–963.

Pasut, A., Oleynik, P., and Rudnicki, M.A. (2012). Isolation of muscle stem cells by fluorescence activated cell sorting cytometry. Methods Mol. Biol. *798*, 53–64.

Patra, K.C., Bardeesy, N., and Mizukami, Y. (2017). Diversity of Precursor Lesions for Pancreatic Cancer: The Genetics and Biology of Intraductal Papillary Mucinous Neoplasm. Clin. Transl. Gastroenterol.

Pei, Y. fei, Yin, X. min, and Liu, X. qiang (2018). TOP2A induces malignant character of pancreatic cancer through activating β-catenin signaling pathway. Biochim. Biophys. Acta - Mol. Basis Dis. *1864*, 197–207.

Pekala, K.R., Ma, X., Kropp, P.A., Petersen, C.P., Hudgens, C.W., Chung, C.H., Shi, C., Merchant, N.B., Maitra, A., Means, A.L., et al. (2014). Loss of HNF6 expression correlates with human pancreatic cancer progression. Lab. Invest. *94*, 517–527.

Petty, A.J., and Yang, Y. (2017). Tumor-associated macrophages: Implications in cancer immunotherapy. Immunotherapy *9*, 289–302.

Pezzilli, R., Andriulli, A., Bassi, C., Balzano, G., Cantore, M., Fave, G.D., Falconi, M., Frulloni, L., and Group, the E.P.I. collaborative (EPIc) (2013). Exocrine pancreatic insufficiency in adults: A shared position statement of the Italian association for the study of the pancreas. World J. Gastroenterol. *19*, 7930.

Pin, C.L., Rukstalis, J.M., Johnson, C., and Konieczny, S.F. (2001). The bHLH transcription factor Mist1 is required to maintain exocrine pancreas cell organization and acinar cell identity. J. Cell Biol. *155*, 519–530.

Pittman, M.E., Rao, R., and Hruban, R.H. (2017). Classification, Morphology, Molecular Pathogenesis, and Outcome of Premalignant Lesions of the Pancreas. Arch. Pathol. Lab. Med. *141*, 1606–1614.

Prévostel, C., and Blache, P. (2017). The dose-dependent effect of SOX9 and its incidence in colorectal cancer. Eur. J. Cancer *86*, 150–157.

Prévot, P.-P., Simion, A., Grimont, A., Colletti, M., Khalaileh, A., Van den Steen, G., Sempoux, C., Xu, X., Roelants, V., Hald, J., et al. (2012). Role of the ductal transcription factors HNF6 and Sox9 in pancreatic acinar-to-ductal metaplasia. Gut *61*, 1723–1732.

Provenzano, P.P., Cuevas, C., Chang, A.E., Goel, V.K., Von Hoff, D.D., and Hingorani, S.R. (2012). Enzymatic targeting of the stroma ablates physical barriers to treatment of pancreatic ductal adenocarcinoma. Cancer Cell *21*, 418–429.

Puccini, J., Dorstyn, L., and Kumar, S. (2013). Genetic background and tumour susceptibility in mouse models. Cell Death Differ. *20*, 964.

Puri, S., Folias, A.E., and Hebrok, M. (2014). Plasticity and Dedifferentiation within the Pancreas : Development , Homeostasis , and Disease. Stem Cell *16*, 18–31.

Pylayeva-Gupta, Y., Lee, K.E., Hajdu, C.H., Miller, G., and Bar-Sagi, D. (2012). Oncogenic Kras-induced GM-CSF production promotes the development of pancreatic neoplasia. Cancer Cell *21*, 836–847.

Queiroz, K.C.S., Shi, K., Duitman, J., Aberson, H.L., Wilmink, J.W., Van Noesel, C.J.M., Richel, D.J., and Spek, C.A. (2014). Protease-activated receptor-1 drives pancreatic cancer progression and chemoresistance. Int. J. Cancer *135*, 2294–2304.

Raimondi, S., Lowenfels, A.B., Morselli-Labate, A.M., Maisonneuve, P., and Pezzilli, R. (2010). Pancreatic cancer in chronic pancreatitis; Aetiology, incidence, and early detection. Best Pract. Res. Clin. Gastroenterol. *24*, 349–358.

Rakshit, S., Chandrasekar, B.S., Saha, B., Victor, E.S., Majumdar, S., and Nandi, D. (2014). Interferon-gamma induced cell death: Regulation and contributions of nitric oxide, cJun N-terminal kinase, reactive oxygen species and peroxynitrite. Biochim. Biophys. Acta - Mol. Cell Res. *1843*, 2645–2661.

Rauch, B.H. (2014). Sphingosine 1-Phosphate as a Link between Blood Coagulation and Inflammation. Cell. Physiol. Biochem. *34*, 185–196.

Ray, K.C., Bell, K.M., Yan, J., Gu, G., Chung, C.H., Washington, M.K., and Means, A.L. (2011). Epithelial tissues have varying degrees of susceptibility to Kras(G12D)-initiated tumorigenesis in a mouse model. PLoS One *6*, e16786.

Razak, N.B.A., Jones, G., Bhandari, M., Berndt, M.C., and Metharom, P. (2018). Cancer-associated thrombosis: An overview of mechanisms, risk factors, and treatment. Cancers (Basel). *10*.

Reichert, M., and Takano, S. (2013). The Prrx1 homeodomain transcription factor plays a central role in pancreatic regeneration and carcinogenesis. Genes … 288–300.

Robinson, M.D., McCarthy, D.J., and Smyth, G.K. (2010). edgeR: a Bioconductor package for differential expression analysis of digital gene expression data. Bioinformatics *26*, 139–140.

Rodriguez, Y.I., Campos, L.E., Castro, M.G., Aladhami, A., Oskeritzian, C.A., and Alvarez, S.E. (2016). Sphingosine-1 phosphate: A new modulator of immune plasticity in the tumor microenvironment. Front. Oncol. *6*.

Romeo, E., Caserta, C.A., Rumio, C., and Marcucci, F. (2019). The Vicious Cross-Talk between Tumor Cells with an EMT Phenotype and Cells of the Immune System. Cells *8*, 460.

Rose, S.D., Swift, G.H., Peyton, M.J., Hammer, R.E., and MacDonald, R.J. (2001). The Role of PTF1-P48 in Pancreatic Acinar Gene Expression. J. Biol. Chem. *276*, 44018–44026.

Ruan, H., Hu, S., Zhang, H., Du, G., Li, X., Li, X., and Li, X. (2017). Upregulated SOX9 expression indicates worse prognosis in solid tumors: A systematic review and meta-analysis. Oncotarget *8*, 113163–113173.

Rudroff, C., Seibold, S., Kaufmann, R., Cu Zetina, C., Reise, K., Schäfer, U., Schneider, A., Brockmann, M., Scheele, J., and Neugebauer, E.A.M. (2002). Expression of the thrombin receptor PAR-1 correlates with tumour cell differentiation of pancreatic adenocarcinoma in vitro. Clin. Exp. Metastasis *19*, 181–189.

Ryan, A.E., Shanahan, F., O'Connell, J., and Houston, A.M. (2005). Addressing the "Fas counterattack" controversy: Blocking fas ligand expression suppresses tumor immune evasion of colon cancer in vivo. Cancer Res. *65*, 9817–9823.

Sakikubo, M., Furuyama, K., Horiguchi, M., Hosokawa, S., Aoyama, Y., Tsuboi, K., Goto, T., Hirata, K., Masui, T., Dor, Y., et al. (2018). Ptf1a inactivation in adult pancreatic acinar cells causes apoptosis through activation of the endoplasmic reticulum stress pathway. Sci. Rep. *8*, 15812.

Salah, Z., Haupt, S., Maoz, M., Baraz, L., Rotter, V., Peretz, T., and Haupt, Y. (2008). p53 controls hPar1 function and expression. 6866–6874.

De Santa Barbara, P., Bonneaud, N., Boizet, B., Desclozeaux, M., Moniot, B., Sudbeck, P., Scherer, G., Poulat, F., and Berta, P. (1998). Direct interaction of SRY-related protein SOX9 and steroidogenic factor 1 regulates transcription of the human anti-Müllerian hormone gene. Mol. Cell. Biol. *18*, 6653–6665.

Santiago, Y., Chan, E., Liu, P.Q., Orlando, S., Zhang, L., Urnov, F.D., Holmes, M.C., Guschin, D., Waite, A., Miller, J.C., et al. (2008). Targeted gene knockout in mammalian cells by using engineered zinc-finger nucleases. Proc. Natl. Acad. Sci. U. S. A. *105*, 5809–5814.

Sarkar, A., and Hochedlinger, K. (2013). The Sox family of transcription factors: Versatile regulators of stem and progenitor cell fate. Cell Stem Cell *12*, 15–30.

Sarner, M., and Cotton, P.B. (1984). Classification of pancreatitis. Gut *25*, 756–759.

Schindelin, J., Arganda-Carreras, I., Frise, E., Kaynig, V., Longair, M., Pietzsch, T., Preibisch, S., Rueden, C., Saalfeld, S., Schmid, B., et al. (2012). Fiji: An open-source platform for biological-image analysis. Nat. Methods *9*, 676–682.

Schmieder, V., Bydlinski, N., Strasser, R., Baumann, M., Kildegaard, H.F., Jadhav, V., and Borth, N. (2018). Enhanced Genome Editing Tools For Multi-Gene Deletion Knock-Out Approaches Using Paired CRISPR sgRNAs in CHO Cells. Biotechnol. J. *13*, 1–10.

Schultz, M.J., Holdbrooks, A.T., Chakraborty, A., Grizzle, W.E., Landen, C.N., Buchsbaum, D.J., Conner, M.G., Arend, R.C., Yoon, K.J., Klug, C.A., et al. (2016). The Tumor-Associated Glycosyltransferase ST6Gal-I Regulates Stem Cell Transcription Factors and Confers a Cancer Stem Cell Phenotype. Cancer Res. *76*, 3978–3988.

Scott, C.E., Wynn, S.L., Sesay, A., Cruz, C., Cheung, M., Gomez Gaviro, M.-V., Booth, S., Gao, B., Cheah, K.S.E., Lovell-Badge, R., et al. (2010). SOX9 induces and maintains neural stem cells. Nat. Neurosci. *13*, 1181–1189.

Sellick, G.S., Barker, K.T., Stolte-Dijkstra, I., Fleischmann, C., J Coleman, R., Garrett, C., Gloyn, A.L., Edghill, E.L., Hattersley, A.T., Wellauer, P.K., et al. (2004). Mutations in PTF1A cause pancreatic and cerebellar agenesis. Nat. Genet. *36*, 1301–1305.

Seufferlein, T., and Ettrich, T.J. (2019). Treatment of pancreatic cancer-neoadjuvant treatment in resectable pancreatic cancer (PDAC). Transl. Gastroenterol. Hepatol. *4*, 21.

Seymour, P. a (2014). Sox9: a master regulator of the pancreatic program. Rev. Diabet. Stud. *11*, 51–83.

Seymour, P.A., Freude, K.K., Dubois, C.L., Shih, H.P., Patel, N.A., and Sander, M. (2008). A dosage-dependent requirement for Sox9 in pancreatic endocrine cell formation. Dev. Biol. *323*, 19–30.

Sharma, B.K., Flick, M.J., and Palumbo, J.S. (2019). Cancer-Associated Thrombosis : A Two-Way Street. Semin Thromb Hemost *45*, 559–568.

Shi, C., and Hruban, R.H. (2012). Intraductal Papillary Mucinous Neoplasm. Hum. Pathol. *43*, 1–16.

Shi, C., Pan, F.C., Kim, J.N., Washington, M.K., Padmanabhan, C., Meyer, C.T., Kopp, J.L., Sander, M., Gannon, M., Beauchamp, R.D., et al. (2019). Differential Cell Susceptibilities to Kras in the Setting of Obstructive Chronic Pancreatitis. Cell. Mol. Gastroenterol. Hepatol.

Shi, G., Zhu, L., Sun, Y., Bettencourt, R., Damsz, B., Hruban, R.H., and Konieczny, S.F. (2009). Loss of the Acinar-Restricted Transcription Factor Mist1 Accelerates Kras-Induced Pancreatic Intraepithelial Neoplasia. Gastroenterology *136*, 1368–1378.

Shi, G., DiRenzo, D., Qu, C., Barney, D., Miley, D., and Konieczny, S.F. (2013). Maintenance of acinar cell organization is critical to preventing Kras-induced acinar-ductal metaplasia. Oncogene *32*, 1950–1958.

Shi, Z., Chiang, C.I., Labhart, P., Zhao, Y., Yang, J., Mistretta, T.A., Henning, S.J., Maity, S.N., and Mori-Akiyama, Y. (2015). Context-specific role of SOX9 in NF-Y mediated gene regulation in colorectal cancer cells. Nucleic Acids Res. *43*, 6257–6269.

Shih, H.P., Kopp, J.L., Sandhu, M., Dubois, C.L., Seymour, P. a, Grapin-Botton, A., and Sander, M. (2012). A Notch-dependent molecular circuitry initiates pancreatic endocrine and ductal cell differentiation. Development *139*, 2488–2499.

Shih, H.P., Seymour, P.A., Patel, N.A., Xie, R., Wang, A., Liu, P.P., Yeo, G.W., Magnuson, M.A., and Sander, M. (2015). A Gene Regulatory Network Cooperatively Controlled by Pdx1 and Sox9 Governs Lineage Allocation of Foregut Progenitor Cells. Cell Rep. 1–11.

Shimaya, Y., Shimada, M., Shutto, Y., Fujita, T., Murakami, R., Nakamura, N., Yamabe, H., and Okumura, K. (2012). Thrombin Stimulates Synthesis of Macrophage Colony-Stimulating Factor, Granulocyte-Macrophage Colony-Stimulating Factor and Granulocyte Colony-Stimulating Factor by Human Proximal Tubular Epithelial Cells in Culture. Nephron Extra *2*, 1–8.

Shpacovitch, V., Feld, M., Hollenberg, M.D., Luger, T.A., and Steinhoff, M. (2008). Role of protease-activated receptors in inflammatory responses, innate and adaptive immunity. J. Leukoc. Biol. *83*, 1309–1322.

Siegel, R.L., Miller, K.D., and Jemal, A. (2019). Cancer statistics, 2019. CA. Cancer J. Clin. *69*, 7–34.

Da Silva Xavier, G. (2018). The Cells of the Islets of Langerhans. J. Clin. Med. *7*.

Simeone, D.M., Ji, B., Banerjee, M., Arumugam, T., Li, D., Anderson, M. a, Bamberger, A.M., Greenson, J., Brand, R.E., Ramachandran, V., et al. (2007). CEACAM1, a novel serum biomarker for pancreatic cancer. Pancreas *34*, 436–443.

Soh, U.J., Dores, M.R., Chen, B., and Trejo, J. (2010). Signal transduction by protease-activated receptors. Br. J. Pharmacol. *160*, 191–203.

Sotomayor, E.M., Fu, Y.X., Lopez-Cepero, M., Herbert, L., Jimenez, J.J., Albarracin, C., and Lopez, D.M. (1991). Role of tumor-derived cytokines on the immune system of mice bearing a mammary adenocarcinoma. II. Down-regulation of macrophage-mediated cytotoxicity by tumor-derived granulocyte-macrophage colony-stimulating factor. J. Immunol. *147*, 2816–2823.

Steer, M.L., Waxman, I., and Freedman, S. (1995). Chronic Pancreatitis. N. Engl. J. Med. *332*, 1482–1490.

Steinhoff, M., Buddenkotte, J., Shpacovitch, V., Rattenholl, A., Moormann, C., Vergnolle, N., Luger, T.A., and Hollenberg, M.D. (2005). Proteinase-activated receptors: Transducers of proteinase-mediated signaling in inflammation and immune response. Endocr. Rev. *26*, 1–43.

Storz, P. (2017). Acinar cell plasticity and development of pancreatic ductal adenocarcinoma. Nat. Rev. Gastroenterol. Hepatol.

Strohkendl, I., Saifuddin, F.A., Rybarski, J.R., Finkelstein, I.J., and Russell, R. (2018). Kinetic Basis for DNA Target Specificity of CRISPR-Cas12a. Mol. Cell *71*, 816-824.e3.

Struyvenberg, M.R., Martin, C.R., and Freedman, S.D. (2017). Practical guide to exocrine pancreatic insufficiency – Breaking the myths. BMC Med. *15*, 29.

Sun, L., Mathews, L. a, Cabarcas, S.M., Zhang, X., Yang, A., Zhang, Y., Young, M.R., Klarmann, K.D., Keller, J.R., and Farrar, W.L. (2013). Epigenetic regulation of SOX9 by the NF-κB signaling pathway in pancreatic cancer stem cells. Stem Cells *31*, 1454–1466.

Swarts, D.C., and Jinek, M. (2018). Cas9 versus Cas12a/Cpf1: Structure – function comparisons and implications for genome editing. WIREs RNA *9*, 1–19.

Swarts, D.C., van der Oost, J., and Jinek, M. (2017). Structural Basis for Guide RNA Processing and Seed-Dependent DNA Targeting by CRISPR-Cas12a. Mol. Cell *66*, 221-233.e4.

Takeda, Y., Saiura, A., Takahashi, Y., Inoue, Y., Ishizawa, T., Mise, Y., Matsumura, M., Ichida, H., Matsuki, R., Tanaka, M., et al. (2017). Asymptomatic Pancreatic Cancer: Does Incidental Detection Impact Long-Term Outcomes? J. Gastrointest. Surg. *21*, 1287–1295.

Tan, T.M., and Bloom, S.R. (2013). Pancreatic Polypeptide. In Handbook of Biologically Active Peptides, (Academic Press), pp. 1294–1299.

Tanaka, M., Fernández-Del Castillo, C., Adsay, V., Chari, S., Falconi, M., Jang, J.Y., Kimura, W., Levy, P., Pitman, M.B., Schmidt, C.M., et al. (2012). International consensus guidelines 2012 for the management of IPMN and MCN of the pancreas. In Pancreatology, (Elsevier), pp. 183–197.

Tantivejkul, K., Loberg, R.D., Mawocha, S.C., Day, L.L., St. John, L., Pienta, B.A., Rubin, M.A., and Pienta, K.J. (2005). PAR1-mediated NFκB activation promotes survival of prostate cancer cells through a Bcl-xL-dependent mechanism. J. Cell. Biochem. *96*, 641–652.

Tekin, C., Shi, K., Dallhuisen, J.B., ten Brink, M.S., Bijlsma, M.F., and Spek, A. (2018). PAR1 signaling on tumor cells limits tumor growth by maintaining a mesenchymal phenotype in pancreatic cancer. Cancer Res. *78*, 5225–5225.

Tellez, C., McCarty, M., Ruiz, M., and Bar-Eli, M. (2003). Loss of Activator Protein-2α Results in Overexpression of Protease-activated Receptor-1 and Correlates with the Malignant Phenotype of Human Melanoma. J. Biol. Chem. *278*, 46632–46642.

Tempia-Caliera, A.A., Horvath, L.Z., Zimmermann, A., Tihanyi, T.T., Korc, M., Friess, H., and Büchler, M.W. (2002). Adhesion molecules in human pancreatic cancer. J. Surg. Oncol. *79*, 93–100.

Terry, S., Savagner, P., Ortiz-Cuaran, S., Mahjoubi, L., Saintigny, P., Thiery, J.P., and Chouaib, S. (2017). New insights into the role of EMT in tumor immune escape. Mol. Oncol. *11*, 824–846.

Thomas, M.M., Zhang, Y., Mathew, E., Kane, K.T., Maillard, I., and Di Magliano, M.P. (2014). Epithelial Notch signaling is a limiting step for pancreatic carcinogenesis. BMC Cancer *14*.

Thomsen, M.K., Ambroisine, L., Wynn, S., Cheah, K.S.E., Foster, C.S., Fisher, G., Berney, D.M., Møller, H., Victor, E., Scardino, P., et al. (2011). High Level of SOX9 in the prostate contributes to increased proliferation and can cooperate with PTEN loss to accelerate neoplasia formation. Cancer Res *70*, 979–987.

Trousseau, A. (1865). Phlegmasia alba dolens. Clin Med Hotel. Paris *3*, 654–712.

Tsai, S.Q., Wyvekens, N., Khayter, C., Foden, J. a, Thapar, V., Reyon, D., Goodwin, M.J., Aryee, M.J., and Joung, J.K. (2014). Dimeric CRISPR RNA-guided FokI nucleases for highly specific genome editing. Nat. Biotechnol. *32*, 569–576.

Tsuda, M., Fukuda, A., Roy, N., Hiramatsu, Y., Leonhardt, L., Kakiuchi, N., Hoyer, K., Ogawa, S., Goto, N., Ikuta, K., et al. (2018). The BRG1/SOX9 axis is critical for acinar cell–derived pancreatic tumorigenesis. J. Clin. Invest. *128*, 3475–3489.

Tumeh, P.C., Harview, C.L., Yearley, J.H., Shintaku, I.P., Taylor, E.J.M., Robert, L., Chmielowski, B., Spasic, M., Henry, G., Ciobanu, V., et al. (2014). PD-1 blockade induces responses by inhibiting adaptive immune resistance. Nature *515*, 568–571.

Vasen, H., Ibrahim, I., Robbers, K., Van Mil, A.M., Potjer, T., Bonsing, B.A., Bergman, W., Wasser, M., Morreau, H., De Vos Tot Nederveen Cappel, W.H., et al. (2016). Benefit of surveillance for pancreatic cancer in high-risk individuals: Outcome of long-term prospective follow-up studies from three European expert centers. J. Clin. Oncol.

Vigano, S., Alatzoglou, D., Irving, M., Ménétrier-Caux, C., Caux, C., Romero, P., and Coukos, G. (2019). Targeting adenosine in cancer immunotherapy to enhance T-Cell function. Front. Immunol. *10*.

Vijayan, D., Young, A., Teng, M.W.L., and Smyth, M.J. (2017). Targeting immunosuppressive adenosine in cancer. Nat. Rev. Cancer *17*, 709–724.

Wakita, H., Furukawa, F., and Takigawa, M. (1997). Thrombin and trypsin induce granulocyte-macrophage colony-stimulating factor and interleukin-6 gene expression in cultured normal human keratinocytes. Proc. Assoc. Am. Physicians *109*, 190–207.

Walsh G (2014). Biopharmaceutical benchmarks 2014. Nat. Biotechnol. *32*, 992–1000.

Wang, J., Sun, J., Liu, L.N., Flies, D.B., Nie, X., Toki, M., Zhang, J., Song, C., Zarr, M., Zhou, X., et al. (2019a). Siglec-15 as an immune suppressor and potential target for normalization cancer immunotherapy. Nat. Med. *25*, 656–666.

Wang, L., Yang, H., Zamperone, A., Diolaiti, D., Palmbos, P.L., Abel, E. V, Purohit, V., Dolgalev, I., Rhim, A.D., Ljungman, M., et al. (2019b). ATDC is required for the initiation of KRAS-induced pancreatic tumorigenesis. Genes Dev. *33*, 641–655.

Wang, W., Zheng, W., Hu, F., He, X., Wu, D., Zhang, W., Liu, H., and Ma, X. (2018). Enhanced Biosynthesis Performance of Heterologous Proteins in CHO-K1 Cells Using CRISPR-Cas9. ACS Synth. Biol. *7*, 1259–1268.

Wang, X., Lang, M., Zhao, T., Feng, X., Zheng, C., Huang, C., Hao, J., Dong, J., Luo, L., Li, X., et al. (2017). Cancer-FOXP3 directly activated CCL5 to recruit FOXP3 + Treg cells in pancreatic ductal adenocarcinoma. Oncogene *36*, 3048–3058.

Wei, S.C., Duffy, C.R., and Allison, J.P. (2018). Fundamental mechanisms of immune checkpoint blockade therapy. Cancer Discov. *8*, 1069–1086.

Whitcomb, D.C., Gorry, M.C., Preston, R.A., Furey, W., Sossenheimer, M.J., Ulrich, C.D., Martin, S.P., Gates, L.K., Amann, S.T., Toskes, P.P., et al. (1996). Hereditary pancreatitis is caused by a mutation in the cationic trypsinogen gene. Nat. Genet. *14*, 141–145.

Wilhelm, D., Hiramatsu, R., Mizusaki, H., Widjaja, L., Combes, A.N., Kanai, Y., and Koopman, P. (2007). SOX9 regulates prostaglandin D synthase gene transcription in vivo to ensure testis development. J. Biol. Chem. *282*, 10553–10560.

Witkiewicz, A.K., McMillan, E.A., Balaji, U., Baek, G., Lin, W.-C., Mansour, J., Mollaee, M., Wagner, K.-U., Koduru, P., Yopp, A., et al. (2015). Whole-exome sequencing of pancreatic cancer defines genetic diversity and therapeutic targets. Nat. Commun. *6*, 6744.

Wojtukiewicz, M.Z., Rucinska, M., Zacharski, L.R., Kozlowski, L., Zimnoch, L., Piotrowski, Z., Kudryk, B.J., and Kisiel, W. (2001). Localization of blood coagulation factors in situ in pancreatic carcinoma. Thromb. Haemost.

Wu, B.U., Johannes, R.S., Sun, X., Tabak, Y., Conwell, D.L., and Banks, P.A. (2008). The early prediction of mortality in acute pancreatitis: a large population-based study. Gut *57*, 1698–1703.

Xiao, A., Cheng, Z., Kong, L., Zhu, Z., Lin, S., Gao, G., and Zhang, B. (2014). CasOT: a genome-wide Cas9/gRNA off-target searching tool. Bioinformatics *30*, 1180–1182.

Xie, D., and Xie, K. (2015). Pancreatic cancer stromal biology and therapy. Genes Dis. *2*, 133–143.

Xie, W.F., Zhang, X., Sakano, S., Lefebvre, V., and Sandell, L.J. (1999). Trans-activation of the mouse cartilage-derived retinoic acid-sensitive protein gene by Sox9. J. Bone Miner. Res. *14*, 757–763.

Xu, X., Nagarajan, H., Lewis, N.E., Pan, S., Cai, Z., Liu, X., Chen, W., Xie, M., Wang, W., Hammond, S., et al. (2011). The genomic sequence of the Chinese hamster ovary (CHO)-K1 cell line. Nat. Biotechnol. *29*, 735–741.

Xue, Y.-Z., Sheng, Y.-Y., Liu, Z.-L., Wei, Z.-Q., Cao, H.-Y., Wu, Y.-M., Lu, Y.-F., Yu, L.-H., Li, J.-P., and Li, Z.-S. (2013). Expression of NEDD9 in pancreatic ductal adenocarcinoma and its clinical significance. Tumour Biol. *34*, 895–899.

Xuequn Chen, P.D. (2018). Protein Composition and Biogenesis of the Pancreatic Zymogen Granules. Pancreapedia Exocrine Pancreas Knowl. Base.

Yadav, D., O'Connell, M., and Papachristou, G.I. (2012). Natural History Following the First Attack of Acute Pancreatitis. Am. J. Gastroenterol. *107*, 1096–1103.

Yang, E., Boire, A., Agarwal, A., Nguyen, N., O'Callaghan, K., Tu, P., Kuliopulos, A., and Covic, L. (2009). Blockade of PAR1 signaling with cell-penetrating pepducins inhibits Akt survival pathways in breast cancer cells and suppresses tumor survival and metastasis. Cancer Res. *69*, 6223–6231.

Yang, J., Yan, J., and Liu, B. (2018). Targeting VEGF/VEGFR to modulate antitumor immunity. Front. Immunol. *9*.

Yang, L., Pang, Y., and Moses, H.L. (2010). TGF-β and immune cells: an important regulatory axis in the tumor microenvironment and progression. Trends Immunol. *31*, 220–227.

Yang, X., Liang, R., Liu, C., Liu, J.A., Cheung, M.P.L., Liu, X., Man, O.Y., Guan, X.Y., Lung, H.L., and Cheung, M. (2019a). SOX9 is a dose-dependent metastatic fate determinant in melanoma. J. Exp. Clin. Cancer Res. *38*, 17.

Yang, Y., Stang, A., Schweickert, P.G., Lanman, N.A., Paul, E.N., Monia, B.P., Revenko, A.S., Palumbo, J.S., Mullins, E.S., Elzey, B.D., et al. (2019b). Thrombin signaling promotes pancreatic adenocarcinoma through PAR-1–dependent immune evasion. Cancer Res. *79*, 3417–3430.

Yang, Z., Steentoft, C., Hauge, C., Hansen, L., Thomsen, A.L., Niola, F., Vester-Christensen, M.B., Frödin, M., Clausen, H., Wandall, H.H., et al. (2015). Fast and sensitive detection of indels induced by precise gene targeting. Nucleic Acids Res. *43*.

Zalzali, H., Naudin, C., Bastide, P., Quittau-Prévostel, C., Yaghi, C., Poulat, F., Jay, P., and Blache, P. (2008). CEACAM1, a SOX9 direct transcriptional target identified in the colon epithelium. Oncogene *27*, 7131–7138.

Zetsche, B., Gootenberg, J.S., Abudayyeh, O.O., Slaymaker, I.M., Makarova, K.S., Essletzbichler, P., Volz, S.E., Joung, J., Van Der Oost, J., Regev, A., et al. (2015). Cpf1 Is a Single RNA-Guided Endonuclease of a Class 2 CRISPR-Cas System. Cell *163*, 759–771.

Zhang, Y., Morris IV, J.P., Yan, W., Schofield, H.K., Gurney, A., Simeone, D.M., Millar, S.E., Hoey, T., Hebrok, M., and Di Magliano, M.P. (2013). Canonical Wnt signaling is required for pancreatic carcinogenesis. Cancer Res. *73*, 4909–4922.

Zhao, P., Metcalf, M., and Bunnett, N.W. (2014). Biased signaling of protease-activated receptors. Front. Endocrinol. (Lausanne). *5*.

Zhou, F. (2009). Molecular mechanisms of IFN-γ to up-regulate MHC class i antigen processing and presentation. Int. Rev. Immunol. *28*, 239–260.

Zhou, Q., and Melton, D.A. (2018). Pancreas regeneration. Nature *557*, 351–358.

Zhou, H., Qin, Y., Ji, S., Ling, J., Fu, J., Zhuang, Z., Fan, X., Song, L., Yu, X., and Chiao, P.J. (2017). SOX9 activity is induced by oncogenic Kras to affect MDC1 and MCMs expression in pancreatic cancer. Oncogene 1–12.

Zhu, A.-J., Shi, J.-S., and Sun, X.-J. (2003). Organ failure associated with severe acute pancreatitis. World J. Gastroenterol. *9*, 2570–2573.

Zhu, L., Shi, G., Schmidt, C.M., Hruban, R.H., and Konieczny, S.F. (2007). Acinar Cells Contribute to the Molecular Heterogeneity of Pancreatic Intraepithelial Neoplasia. Am. J. Pathol. *171*, 263–273.

Zhu, X., Xu, Y., Yu, S., Lu, L., Ding, M., Cheng, J., Song, G., Gao, X., Yao, L., Fan, D., et al. (2014). An efficient genotyping method for genome-modified animals and human cells generated with CRISPR/Cas9 system. Sci. Rep. *4*, 1–8.

Zigler, M., Kamiya, T., Brantley, E.C., Villares, G.J., and Bar-eli, M. (2011). PAR-1 and Thrombin : The Ties That Bind the Microenvironment to Melanoma Metastasis. 6561–6567.

VITA

Patrick graduated from Jefferson High School in 2006 and went on to pursue a Bachelor of Science degree at Indiana University with a focus in biology and minors in chemistry and psychology. After graduating from Indiana University in 2010, Patrick was hired as a laboratory technician at Purdue University, working for both Dr. Erik Barton and Dr. Stephen Konieczny. In August 2013 Patrick joined the biology graduate program at Purdue with Dr. Stephen Konieczny as his advisor. During his time at Purdue Patrick worked collaboratively on several research projects with a primary focus on the study of gene regulatory networks related to pancreatic ductal adenocarcinoma initiation, differentiation, and immune evasion. In the summer of 2017 Patrick left Purdue's campus and began work fulltime as an academic intern at Eli Lilly in Indianapolis, Indiana under the mentorship of Dr. Zhuo Cheng. Over the next six months he conducted studies on the efficacy of various gene editing strategies for applications related to the production of biotherapeutics. In the winter of 2018 Patrick returned to Purdue University to finish his graduate studies. Patrick earned his doctorate in May 2020 and accepted a position as a research scientist at Arcus Biosciences in Hayward, California where he will help develop best-in-class cancer therapies.

PUBLICATIONS

Schweickert, P. G., Yang, Y., White, E., Cresswell, G. M, Elzey, B. D., Ratliff, T. L., Flick, M. J., Konieczny, S. F. (2020). PAR1 expression protects pancreatic ductal adenocarcinoma cells from antitumor immunity, influences the inflammatory microenvironment, and mediates expression of immunosuppressive genes. *Submitted.*

Schweickert, P. G., Wang, N., Sandefur, S. L., Lloyd, M. E., Konieczny, S. F., Frye, C., Cheng, Z. (2020) Effective and efficient integration of CRISPR/Cas genome engineering at multiple stages of CHO production cell line generation. *Manuscript in preparation.*

Schweickert, P. G. and Cheng, Z. (2019). Application of genetic engineering in biotherapeutics development. Journal of Pharmaceutical Innovation, https://doi.org/10.1007/s12247-019-09411-6

Yang, Y., Stang, A., **Schweickert, P. G**., Lanman, N. A., Paul, E. N., Monia, B. P., Revenko, A. S., Palumbo, J. S., Mullins, E. S., Elzey, B. D., Janssen, E. M., Konieczny, S. F., Flick, M. J. (2019). Thrombin signaling promotes pancreatic adenocarcinoma through PAR-1-dependent immune evasion. Cancer Research 79, 3417-3430

Jakubison, B. L., **Schweickert, P. G**., Moser, S. E., Yang, Y., Gao, H., Scully, K., Itkin-Ansari, P., Liu, Y., Konieczny, S. F. (2018). Induced PTF1a expression in pancreatic ductal adenocarcinoma cells activates acinar gene networks, reduces tumorigenic properties, and sensitizes cells to gemcitabine treatment. Molecular Oncology 12, 1104-1124

Morman, R. E., **Schweickert, P. G**., Konieczny, S. F., and Taparowsky, E. J. (2018). BATF regulates the expression of Nfil3, Wnt10a, and miR155hg for efficient induction of antibody class switch recombination in mice. European Journal of Immunology 48, 1492-1505

Liu, X., Pitarresi, J. R., Cuitino, M. C., Kladney, R. D., Woelke, S. A., Sizemore, G. M. Nayak, S. G., Egriboz, O., **Schweickert, P. G**., Yu, L., Trela, S., Schilling, D. J., Halloran, S. K., Li, M., Dutta, S., Fernandez, S. A., Rosol, T. J., Lesinski, G. B., Shakya, R., Ludwig, T., Konieczny, S. F., Leone, G., Wu, J., and Ostrowski, M. C. (2016). Genetic ablation of Smoothened in pancreatic fibroblasts increases acinar-ductal metaplasia. Genes & Development 30, 1–13.

Li, J., Wang, R., **Schweickert, P. G**., Karki, A., Yang, Y., Kong, Y., Ahmad, N., Konieczny, S. F., and Liu, X. (2016). Plk1 inhibition enhances the efficacy of gemcitabine in human pancreatic cancer. Cell Cycle 15, 711-719.

Lee, H., Kim, Y., **Schweickert, P. G**., Konieczny, S. F., and Won, Y. Y. (2014). A photo-degradable gene delivery system for enhanced nuclear gene transcription. Biomaterials 35, 1040-1049.